Contributions to the fracture mechanics of thermoplastic composite materials at high temperature : experimental and numerical analyzes

Manel Chabchoub

Normandie Université

THESE

Pour obtenir le diplôme de doctorat

Spécialité Mécanique des matériaux

Préparée au sein de l'Institut National des Sciences Appliquées de Rouen
En cotutelle avec l'École Nationale d'Ingénieurs de Sfax

Contributions à la mécanique de la rupture des matériaux composites thermoplastiques à haute température : analyses expérimentales et numériques

Présentée et soutenue par
Manel CHABCHOUB

Thèse soutenue publiquement le 15 décembre 2017 devant le jury composé de		
Mr / Alain THIONNET	Professeur des Universités à l'Université de Bourgogne, France	Président
Mr / Christophe BOUVET	Professeur à ISAE-Supaéro Toulouse, France	Rapporteur
Mr / Mohamed SOULA	Professeur à l'Ecole Nationale Supérieure d'Ingénieurs de Tunis,Tunisie	Rapporteur
Mr / Lassaad WALHA	Professeur à l'Ecole Nationale d'Ingénieurs de Sfax, Tunisie	Examinateur
Mr / Benoit VIEILLE	Maître de Conférences (HDR) à l'INSA Rouen Normandie, France	Directeur de thèse
Mr / Mohamed TAKTAK	Maître de Conférences à la Faculté des Sciences de Sfax, Tunisie	Directeur de thèse
Mr / Lakhdar TALEB	Professeur des Universités à l'INSA Rouen Normandie, France	Co-encadrant
Mr / Mohamed HADDAR	Professeur à l'Ecole Nationale d'Ingénieurs de Sfax, Tunisie	Co-encadrant

Thèse dirigée par Benoit VIEILLE (laboratoire GPM) et Mohamed TAKTAK (laboratoire LA2MP)

INSA INSTITUT NATIONAL DES SCIENCES APPLIQUÉES ROUEN NORMANDIE

SPMI ECOLE DOCTORALE

GPM Groupe de Physique des Matériaux

Acknowledgement

This PhD dissertation represents not only my efforts, but also the time, energy, support, and encouragement of my supervisors, colleagues, friends and family. I am grateful for this opportunity to acknowledge all those who made this thesis possible. First and foremost, I thank my supervisor at INSA Rouen, Mr. Benoit Vieille, a person who is exceptional in all ways, scientifically, professionally and especially on the human side, for sharing his vision and experience, for putting me on track in various fields. The joy and enthusiasm he has for his research was contagious and motivational for me, even during tough times in the Ph.D. pursuit.

I would like to thank all the members of the jury for the attention they have paid to my work and for their constructive remarks and questions. More precisely, I thank: Mr. Alain Thionnet who made me the honor of being the president of this jury, Mr. Christophe Bouvet and Mr. Mohamed Soula who have accepted the difficult task of being my reporters and Mr. Lassad Walha who has examined carefully this manuscript.

I would also like to thank my supervisor at ENIS, Mr. Mohamed Taktak, for giving me the freedom to explore my own ideas and for the support he showed during my three-years PhD trip.

I also wish to express my sincere gratitude to my co-supervisors Professor Lakhdar Taleb at INSA Rouen and Professor Mohamed Haddar at ENIS for the confidence they showed in me and the encouragement they gave me during my three-years PhD trip.

I am also grateful to Mr. Rostand Moutou Pitti for providing me with CH_THETA and M_THETA procedures which helped me immensely to move forward on the numerical part.

I cannot forget all the people with whom I spend many hours and which are much more than colleagues. Without their collective efforts and cooperation, this thesis could not have been completed as it stands. I would like to convey my regards and express my gratitude to all of them. I would especially like to thank David Bouscarrat for his help in the implementation of the Acoustic Emission device and Christophe Gautrelet for his help in using high-speed camera.

I owe special thanks to my family. My mom and dad, I am grateful to you for your love, prayers, caring and sacrifices for educating and preparing me for my future. I love you very much. My brother Amin, my sisters Nadia and Wafa and my sisters in law Saoussen and Farah, thank you for supporting me for everything and encouraging me throughout this experience. My nephews Habib, Omar and Karim and my nieces Mariem, Zeineb and Malek, thank you for bringing me so much happiness. I also thank my parents in law for their support and for attending my dissertation defense.

Finally, I would like to thank Omar, my husband. for his endless love, patience, and support all along these last years. He was always there cheering me up and stood by me through the good times and bad.

Résumé

Depuis une quarantaine d'années, les matériaux composites, reconnus pour leurs propriétés mécaniques spécifiques élevées (ramenées à leur masse volumique), sont largement privilégiés dans l'industrie aéronautique. Au cours de cette période, les innovations se sont principalement focalisées sur le développement de composites à matrice thermodurcissable (TD), qui dominent encore aujourd'hui très largement le marché. Les industriels se posent néanmoins la question : quels matériaux pour les avions de demain ?

La généralisation des matériaux composites (50% de taux massique) dans les structures aéronautiques pose des problèmes à différents niveaux : conception, fabrication, assemblage et maîtrise de la fiabilité en service. Ainsi, l'exploitation croissante des composites a mis en évidence les limites des matériaux à résine thermodurcissable (TD) utilisés majoritairement depuis plus de 40 ans. En effet, le drapage manuel de pré-imprégnés thermodurcissables est un procédé bien maîtrisé, mais long et coûteux. Ainsi, plusieurs procédés offrent une alternative au drapage manuel des préimprégnés TD : RTM, Infusion, Moulage par compression de thermoplastiques. Les contraintes associées aux TD ont ainsi favorisé l'émergence de nouveaux matériaux composites à base de fibres de carbone et de résine thermoplastique (TP) haute performance présentant un meilleur compromis. Si ce type de polymère a longtemps été délaissé en raison de propriétés mécaniques médiocres à haute température (soit environ 120°-200°C pour des composites à matrice polymère), le développement de résines haute performance (PEEK, PES, PI, PPS) dans les années 90, a ouvert la voie à des composites structuraux associant fibres de carbone et matrice TP haute performance. Cependant, l'utilisation des composites à matrice organique (CMO) TP soulève plusieurs problématiques quant à leur exploitation à grande échelle dans le secteur aéronautique, en termes de fabrication (Estampage, Resin Transfer Molding, Sheet Molding Compound, soudage par interpénétration des couches superficielles...), de comportement (sous chargement monotone ou cyclique) et de propriétés dans des conditions critiques et en particulier, son comportement à la rupture à haute température.

Concernant la tolérance au dommage, les stratifiés à matrice TP haute performance sont caractérisés par des valeurs de résistance à la rupture élevées par rapport aux composites à matrice thermodurcissable. De plus, la plupart des études disponibles dans la littérature

traitent le délaminage des composites à matrice TP au moyen des éprouvettes DCB (Double Cantilever Beam), et très peu d'auteurs ont étudié l'influence de la température.

Ce travail s'articule autour de deux axes (expérimental et numérique) concernant le comportement à la rupture des stratifiés C/PPS à haute température (HT) ($T > T_g$).

Du point de vue expérimental, le but était d'étudier l'énergie de rupture translaminaire en mode I des stratifiés tissés C/PPS soumis à des essais de traction à $T > T_g$ (température de transition vitreuse) lorsque la ténacité de la matrice est significativement élevée dans deux cas différents : des stratifiés C/PPS quasi-isotropes dont le comportement est gouverné par les fibres et des stratifiés C/PPS à plis orientés dont le comportement est gouverné par la matrice, c'est-à-dire fortement ductile à haute température. Les éprouvettes quasi-isotropes (QI) à simple entaille (SEN) sont caractérisées par un comportement élastique-fragile résultant de la fissuration transverse de la matrice et de la rupture des fibres près de l'extrémité de l'entaille. Du point de vue macroscopique, l'initiation et la propagation des fissures se produisent en même temps correspondant à la rupture finale, ce qui rend difficile l'évaluation du taux de restitution d'énergie correspondant. Les valeurs obtenues à l'initiation de la propagation instable ont été déterminées en utilisant trois techniques différentes : (i) la méthode CTOD (Crack Tip Opening Displacement) basée sur la mesure de champs par CIN - (ii) jauges de fissuration liées à la surface externe - (iii) surveillance de l'activité d'émission acoustique (AE) associée aux mécanismes d'endommagement importants (fissuration matricielle transverse et rupture des fibres). Dans le cadre de la mécanique linéaire élastique de la rupture (LEFM), la ténacité à l'initiation $K_{I\ init}$ et la ténacité critique K_{Ic} en mode I ont été calculées à partir du taux de restitution d'énergie G_I dans le cas de stratifiés quasi-isotropes. En comparant les résultats obtenus avec les valeurs calculées à partir des solutions empiriques développées pour les matériaux isotropes, la capacité de ces méthodes à fournir les valeurs ductiles et précises a été bien validée. La technique d'EA s'est montrée particulièrement pertinente car elle fournit une approche fiable pour quantifier le taux de restitution d'énergie à l'initiation et à la propagation de la fissure. Afin d'étudier la corrélation entre l'énergie acoustique cumulée et le taux de restitution d'énergie, les coefficients du modèle ont été identifiés à partir des données expérimentales pour un rapport a/W donné. Il apparaît donc que l'énergie acoustique cumulative peut être utilisée comme critère d'endommagement pour déterminer la tolérance aux dommages (évaluer le taux de restitution d'énergie) d'un matériau composite à matrice thermoplastique. Enfin, la correspondance entre l'évolution de

l'endommagement donnée par les données acoustiques expérimentales à l'échelle microscopique et une variable de dommages cumulée basée sur les mesures de rigidité à l'échelle macroscopique valide la capacité des deux approches à quantifier le degré d'endommagement des CMOs renforcés d'un tissu de fibres de carbone et à identifier un seuil critique de l'initiation de la propagation instable de la fissure.

Dans le cas des stratifiés à plis croisés (AP) caractérisés par un comportement ductile à haute température, la mécanique linéaire élastique de la rupture ne peut être appliquée et il faut faire appel aux concepts de la mécanique élastoplastique de la rupture. Ainsi, afin de déterminer le taux de restitution d'énergie J, une attention particulière a été portée sur la détermination des paramètres η_{el} et η_{pl} qui sont des éléments clés dans la détermination du taux de restitution d'énergie J. η_{el} a été classiquement déterminé en utilisant la méthode de complaisance. η_{pl} a été obtenu à partir de la méthode de séparation des charges. En se basant sur les paramètres S_{ij}, l'évolution de la longueur d'entaille a été déterminé. Ainsi, les courbes JR ont été obtenues pour différents rapports a/W. Les résultats obtenus ont montré que le taux de restitution d'énergie critique est beaucoup plus important lorsque la longueur d'entaille initiale est faible. Autrement dit, la ténacité n'est pas une caractéristique du matériau mais elle dépend de la géométrie de l'éprouvette.

Afin de mieux comprendre l'influence de la ductilité et la ténacité de la matrice sur le taux de restitution d'énergie et la mécanique de la rupture dans les stratifiés à matrice TP à haute température, deux orientations d'entaille ont été étudiées : une entaille transverse à 0° (non inclinée) et une entaille inclinée à 45°. Selon l'orientation initiale de l'entaille (0° ou 45°), le mode de rupture est un mode I ou un mode mixte (I et II). Cette stratégie a montré que le taux de restitution d'énergie est plus important dans le cas d'une entaille inclinée caractérisée par un mode de rupture mixte et dans le cas des stratifiés AP car on est majoritairement en présence des phénomènes plastiques à haute température.

Concernant le volet numérique de la thèse, une brève revue bibliographique a montré que très peu de références font état de la modélisation de la propagation de fissure dans le cas d'un matériau orthotrope élastique ou viscoélastique en 2D et aucune référence s'intéresse à la détermination numérique du taux de restitution d'énergie en 3D dans le cas des matériaux composites caractérisés par un comportement visco-élasto-plastique à haute température.

Le comportement ductile marqué des stratifiés à matrice TP à haute température a été représenté par un modèle viscoélastique spectral associé à un modèle viscoplastique de Norton généralisé. Ensuite, une optimisation du maillage a été réalisée afin d'obtenir des champs mécaniques précis au voisinage de l'entaille. Un maillage rayonnant a été sélectionné pour calculer le taux de restitution d'énergie en utilisant la méthode G_θ. L'évolution du taux de restitution d'énergie en fonction de la force appliquée et de la croissance de la fissure a été obtenue pour $a/W = 0.2$ et $a/W = 0.3$ dans le cas des stratifiés AP et QI. En revanche, certaines divergences entre les résultats expérimentaux et numériques ont été observées en raison de différents phénomènes qui n'ont pas été pris en compte dans le modèle tels que l'endommagement et l'instabilité des fissures.

Dans la dernière partie de cette thèse, un modèle physique simple « Critical Damage Growth » dérivé des critères de la mécanique de la rupture a été appliqué aux stratifiés QI C/PPS pour prédire leur résistance à la rupture à haute température. Les paramètres d'entrée de ce modèle sont la résistance du stratifié non entaillé et la ténacité à la rupture du stratifié. La ténacité à la rupture translaminaire a été calculée en utilisant la méthode de la complaisance dans le cas des stratifiés QI troués pour différents rapports d/W. Le modèle « Critical Damage Growth » a montré sa capacité à prédire la résistance à la rupture de stratifiés QI troués à haute température lorsque la ductilité et la ténacité de la matrice PPS sont exacerbées.

Table of contents

List of figures

List of tables

Nomenclature

G_i	Strain energy release rate in elastic material in mode i ($i = I, II\ or\ III$)
G_{i_init}	Initiation strain energy release rate
G_{i_c}	Critical strain energy release rate
K_i	Stress intensity factor in mode i ($i = I, II\ or\ III$)
K_{i_init}	Initiation stress intensity factor
K_{i_c}	Critical stress intensity factor
a	Crack length
a_0	Initial crack length
W	Specimen width
G_θ	G_θ-integral
σ_{max}	Maximum stress at the notch tip
K_t	Stress concentration factor
σ_{nom}	Nominal stress
σ_y	Yield strength
ν	Poisson's ratio
J	Strain energy release in elastic-plastic material
J_c	Critical strain energy release in elastic-plastic material
$J_{elastic}$	Elastic component of J

$J_{plastic}$	Plastic component of J
J_{totol}	J-integral
$G\left(\frac{a}{W}\right)$	Geometry-dependent function
$H\left(\frac{\Delta_{pl}}{W}\right)$	Deformation-dependent function
Ψ	Potential energy
A	Crack surface area
F	Applied load
B	Specimen thickness
δ	Crack opening displacement
F_{max}	Maximum load at failure
C	Compliance
E_x	Longitudinal stiffness
σ	Remote applied stress
$F(a/W)$	Finite-width-correction factor
$f(x)$	Sentry function
$E_s(x)$	Mechanical energy
$E_a(x)$	Acoustic energy
W_{AE}	Cumulative acoustic energy
$\beta(c_L^2)$	Proportionality constant
E_i	Energy absorbed during the elastic-plastic deformation

Δa	Crack extension
$d(N)$	Macroscopic cumulated damage variable
U_P	Potential energy for the crack body
A_{el}	Elastic part of the area under load-displacement record
A_{pl}	Plastic part of the area under load-displacement record
b	Length of the uncracked ligament
$G(a/W)$	Geometry dependent function
$H(\Delta_{pl}/W)$	Deformation dependent function
Δ_{pl}	Plastic displacement
Δ_{el}	Elastic displacement
$F(a_i)$	Applied load to a tested specimen (i) with a crack length a_i
$F(a_j)$	Applied load to a reference specimen (j) with a crack length a_j
S_{ij}	Separation parameter
A' and A''	Two constants
E_x	Longitudinal modulus
σ_x^u	Ultimate strength
ε_x^u	Ultimate strain
σ_{ij}	Components of stress tensor
ε_{ij}	Components of strain tensor
w	Strain energy density

$\vec{\theta}$	Virtual displacement field
$(\sigma_{ij}^{(u)}, u)$	Real stress and displacement fields
$(\sigma_{ij}^{(v)}, v)$	Virtual stress and displacement fields
$\left(\sigma_{ij}^{(k)}(u), u_i{}^{(k)}\right)$	Real stress and displacement in the k$^{\text{th}}$ spring
$\left(\sigma_{ij,k}^{(v)}(v), v_i{}^{(k)}\right)$	Virtual stress and displacement in the k$^{\text{th}}$ spring
N	Number of springs
$\underline{\varepsilon}^{e}$	Elastic strain
$\underline{\varepsilon}^{ve}$	Viscoelastic strain
$\underline{\varepsilon}^{vp}$	Viscoplastic strain
$\underline{\xi}_{\text{i}}$	Elementary mechanisms
n_b	Total number of mechanisms
μ_i	Relaxation mechanisms weights
τ_i	Relaxation time
n_i	ith relaxation mechanism
Δ	Time interval separating two relaxation times
n_0	Standard deviation of the spectrum
n_c	Average value of the spectrum
$\underline{\underline{S}}^{ve}$	Viscoelastic compliances tensor
G_{12}	Shear modulus

β_{44}	Material viscosity parameter
$\underline{\underline{M}}$	Describes the viscoplastic flow anisotropy associated with the PPS matrix in shear loading
$\underline{X}$	Thermodynamic force
δ_m	Material parameter associated with the linear kinematic hardening
$\dot{\lambda}_{vp}$	Lagrange viscoplastic multiplier
TF	Stress triaxiality ratio
p	Hydrostatic pressure
$\overline{\sigma}$	Von Mises equivalent stress
ε_X	Longitudinal strains obtained from a blade-extensometer.
F^u	Maximum force borne by the specimen at failure
K_T^∞	Concentration factor at the edge of a hole
d	Hole diameters
c_0	Critical damage zone size
Y_1 and Y_2	FWC factors
F_0	Correction factor

Introduction

Composite materials logically imposed in lots of applications over the past forty years because of their exceptional mechanical properties (relative to their density) and their predisposition to a customized design. During this period, the innovations have focused mainly on the development of thermosetting matrix (TS) composites, which still today dominate the market. Almost 40 years of evolution and innovation have passed, but one question remains open: what composite materials for tomorrow?

The generalization of composite materials (50% mass ratio) in aeronautical structures poses problems at various levels: design, manufacture, assembly and control of service. Thus, the increasing use of composites has highlighted the limits of thermosetting resin materials predominantly used in aeronautics. In addition, manual draping of thermosetting prepregs is a well-controlled, but long and expensive process. Thus, several processes offer an alternative to manual draping of TS prepregs: RTM, Infusion, Compression molding of thermoplastics. The constraints associated with TS have thus promoted the emergence of new materials Carbon fiber composites and high performance thermoplastic resin (TP) with a better compromise. If this type of polymer has been neglected for a long time due to poor mechanical properties at high temperature (i.e. about 120°-200°C for polymer matrix composites), the development of high performance resins (PEEK, PES, PI, PPS) in the 1990s, opened the door to structural composites combining carbon fibers and high-performance TP matrices. However, the use of polymer matrix composites (PMC) raises several problems concerning their large-scale exploitation in the aeronautics sector in terms of manufacturing (Stamping, Resin Transfer Molding, Sheet Molding Compound, interpenetration welding of surface layers, etc.), behavior (under monotonic or cyclic loading), properties under critical conditions and more particularly their fracture behavior at high temperature.

When it comes to damage tolerance, high-performance TP matrix laminates are characterized by high values of fracture toughness compared to thermosetting-based composites. In addition, potential advantages of using woven-ply laminates as opposed to UD-ply laminates are discussed in the literature as woven-ply composites have higher values of interlaminar critical strain energy release rates G_{IC}. Most of the studies available in the literature deal with

the mode I delamination of TP based composites by means of double cantilever beam tests, and very few authors have investigated the influence of temperature.

This work involves around two numerical and experimental axes concerning the fracture behavior in C/PPS laminates at high temperature (HT) ($T>T_g$).

This study proposed a literature review on composite materials and their mechanical behavior as well as a few important concepts on fracture mechanics in heterogeneous (brittle or ductile) materials.

In chapter II, the Crack Tip Opening Displacement (CTOD) method, AE technique and cracking gauges were used in order to detect the crack initiation, whereas the compliance-based method was considered to determine the strain energy release rate corresponding to crack propagation for in quasi-isotropic SEN specimens with different ratio a/w. Then, the AE technique was used to investigate the damage evolution in thermoplastic based composites and to define a damage initiation criterion.

For angle-ply laminates, the J-integral was calculated using compliance and load separation methods in order to obtain J-R curves of highly ductile composite systems at $T>T_g$ for different initial crack length over specimen width ratios (a/W).

In addition, the influence of matrix ductility on the thermomechanical behavior of SEN structures was evaluated in QI laminates (fiber-dominated behavior) or AP laminates (matrix-dominated behavior) by combining the loading conditions (orientation of initial notch), the location of defect and the material heterogeneity (presence of matrix-rich regions at the crimp area in woven-ply laminates).

The third chapter presents a brief background about numerical methods for determining the strain energy release rate. A time dependent model was used to take into account the high ductile behavior of TP based laminates at high temperature. Then, a mesh optimization was carried out to obtain accurate mechanical fields in the vicinity of the crack tip. The selected mesh was used to compute the strain energy release rate using G_θ method.

Finally, the purpose of the last chapter is to study the capability of a Critical Damage Growth model derived from fracture mechanics to predict the notched strength of QI laminates at high temperature.

Chapter I. Background

Nowadays, composite materials represent an alternative to metallic materials in many primarily and secondary industrial applications such as aeronautical industry.

After a brief reminder on composite materials and the principal damage mechanisms that may arise within a composite material as well as their industrial interests, a few concepts about fracture mechanics in brittle or ductile materials will be presented. Then, the main objectives of this thesis will be underlined.

Chapter I outline

I.1 Composite materials

In its most basic form, a composite material is composed of two or more materials assembled on a macroscopic scale to form a third heterogeneous material. The advantage of such material is that, if well designed, it usually exhibits the best qualities of its constituents and often some qualities that neither component possesses. Among the properties that can be improved by forming a composite material, one can cite: strength, stiffness, weight, temperature-dependent behavior...

Composite material is a heterogeneous material that is different from common heterogeneous materials. Currently composite materials refer to materials having strong fibers (continuous or noncontinuous) surrounded by a weaker matrix material.

The matrix acts as a binder, allowing the transfer of loads within the material and the preservation of the desired shape to the final product as well as the protection against harsh environments. The reinforcement is a material having high mechanical characteristics in terms of stiffness and / or strength. In some cases, to obtain a good interface between the two components, a binding agent may be used. In order to improve certain characteristics of the composite (impact resistance, UV resistance, fire resistance, etc.), additives or fillers can be added.

I.1.1 The reinforcement

The reinforcement of the composite material plays an important role in increasing the mechanical properties of the neat matrix system. The latter is generally of fibrous nature, thus giving the material a directional character. Besides its shape (long or short fibers or particles), the reinforcement is also defined by its nature (organic or mineral) and its architecture. Glass, carbon and aramid are the most frequently used reinforcements.

The long fibers consist of thousands of filaments, each filament having a diameter of few tens of micrometers. Different architectures of fibrous reinforcements can be obtained according to the spatial arrangement of the fiber bundles (see Figure 1):

- The mats patterns present a random assembly of noncontinuous fibers oriented in different directions, held in place by a binder. They have many advantages such as easy processing and possibility to produce complex geometries possessing identical

properties in the plane. However, they present inferior mechanical properties compared to composites reinforced by fiber fabrics because they are characterized by low fiber content [Apolinario Testoni, 2015].

- The unidirectional fibers (UD) are the most common architecture of fibrous composites. It is an assembly of continuous fibers, oriented in the same direction, awarding them good axial properties to composites.
- The fabric is a bi-directional assembly where the fibers are oriented generally in two perpendicular directions (0° and 90°), defining the warp and weft directions. The most used weavings are taffeta, twill and satin.

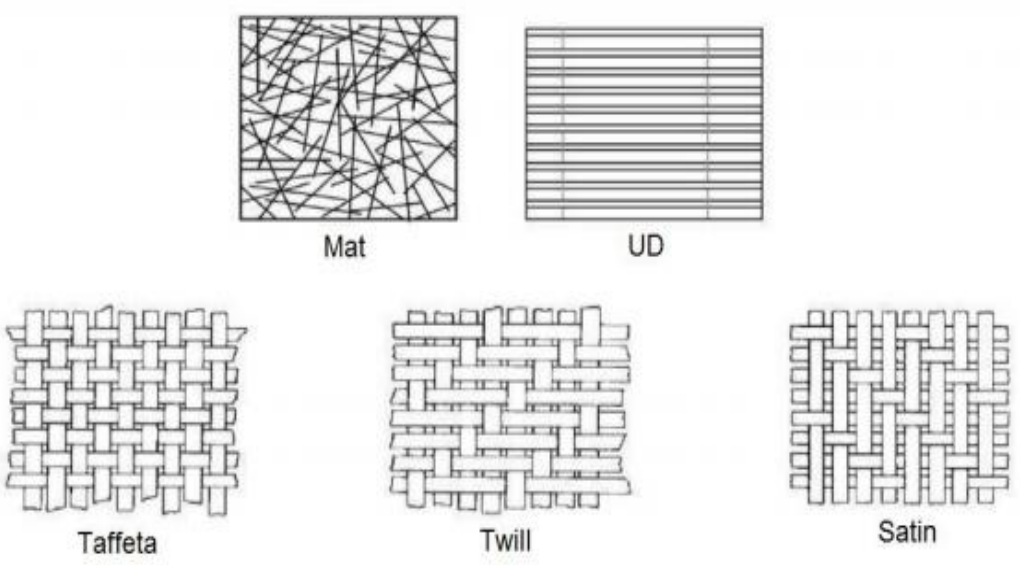

Figure 1. *Typical fiber weavings [Perrot, 2006]*

I.1.2 The matrix

The matrix is the binder material. The purpose of the matrix is manifold: transmit stress between fibers, fixation the desired geometric shape, protection of the fibers from the potentially aggressive environment (chemical, moisture, resistance to fire ...) ...

Composite materials are classified according to the nature of their matrix:

- Organic matrix composites (OMCs): the term organic matrix composite is generally assumed to include two classes of composites, namely Polymer Matrix Composites (PMCs) and carbon matrix composites commonly referred to as carbon/carbon composites. The organic matrix composites are extensively used in aeronautical applications as they can be

processed easily, possess lightweight, and desirable mechanical properties. However, this type of composite can be used over limited range of temperature (it should not exceed 300°C).

- Metal matrix composites (MMCs): they can withstand important temperature (up to 1000°C) in corrosive environment compared to polymer composites. The metal matrix offers to the composite additional properties such as resistance to abrasion, creep, thermal conductivity and dimensional stability. Their main shortcomings are their price and their very high density.

- Ceramic matrix composites (CMMs): They are mainly used in the aerospace sector; due to their high thermomechanical performances at high temperature (may exceed 1000°C). They possess excellent specific properties (stiffness and resistance). However, ceramic matrix composites are characterized by a brittle behavior.

I.1.3 Damage mechanisms in composite materials

Damage is a physical discontinuity in the material on the micro, meso- or macroscale. It can take place either during manufacturing or service stage and can impair normal functioning of the material. Damage location, evolution or size can be evaluated using numerical, analytical and experimental methods. Fracture can be seen as the separation of the material into two or more pieces under mechanical loading.

Before studying the fracture behavior of the composite in the presence of a notch, let's recall the primary damage mechanisms which can appear within composite materials, during loading, until its final failure.

Figure 2 represents the typical response of a TP-based composite under monotonic tensile loading. Actually, the thermo-mechanical response and the damage chronology strongly depend on the architecture of the reinforcement (UD- or woven-ply) [Gao, 1999] [Pandita, 2001] [Osada, 2003] [Daggumati, 2011].

The main damage mechanisms in composite laminates are in the chronological order: matrix cracking, fiber-matrix debonding, delamination and fiber breakage (see Figure 3).

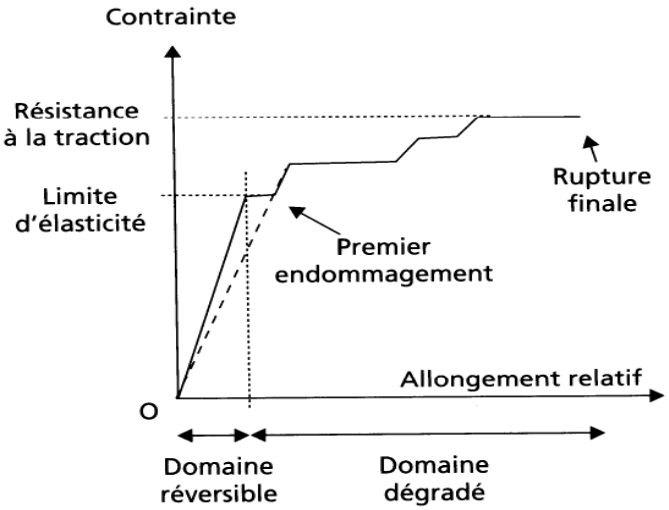

Figure 2. *Typical stress vs strain curve of thermoplastic based composite under tensile loading*

Even though fabric laminates are more resistant to splitting and delamination than UD laminates [De Azevedo Soriano, 1999], most of the research effort has been devoted to investigate the damage mechanisms in UD-ply laminates. The low strength in the transverse direction promotes the splitting in UD laminates, while delamination is facilitated by both Poisson's ratio and shear coupling mismatch. However, in balanced fabric laminates, delamination due to shear coupling mismatch is limited [Lagace, 1986].

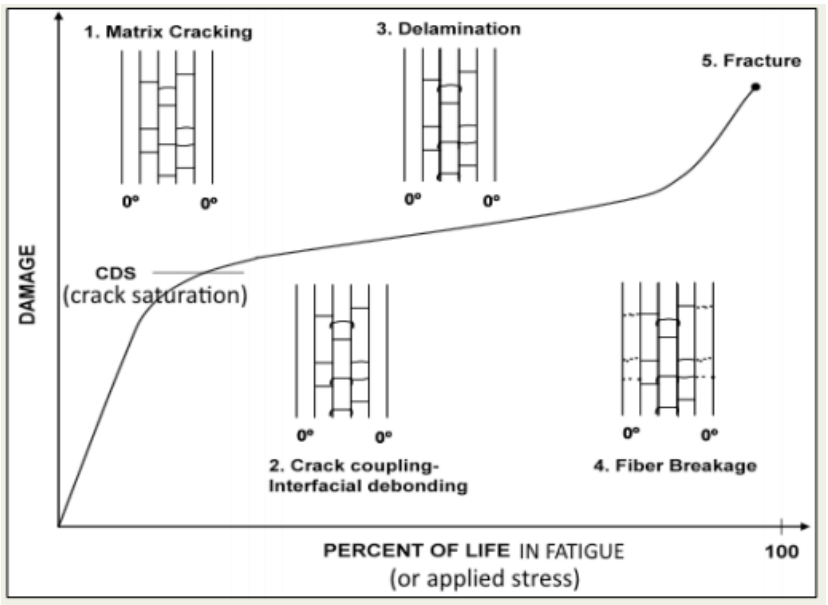

Figure 3. *Damage mechanisms in composite laminates [Talreja, 2012]*

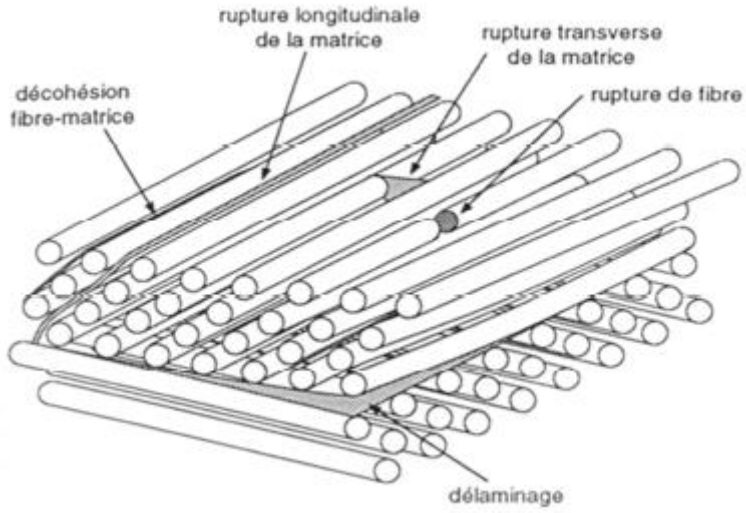

Figure 4. *Schematic representation of the main damage mechanisms in UD laminates [Berthelot, 2005]*

Recently, [Albouy et al., 2014] have investigated the thermomechanical response and the corresponding damage mechanisms of woven-ply C/PPS $[\pm 45]_7$ laminates subjected to load-unload tensile tests at 120°C. This test makes possible to gradually increase the imposed mechanical load and to take into account the contribution of the viscous effects on the damage behavior. They found that pull-out of 45° oriented fibers, intra-bundles splitting as well as an extensive fiber/matrix debonding and fiber rotation (10°) can be observed (see Figure 5). The highly ductile behavior of C/PPS comes along with the initiation and the propagation of interlaminar cracks, particularly at the crimps, where the weft fiber bundles undulate over the warp fiber bundles.

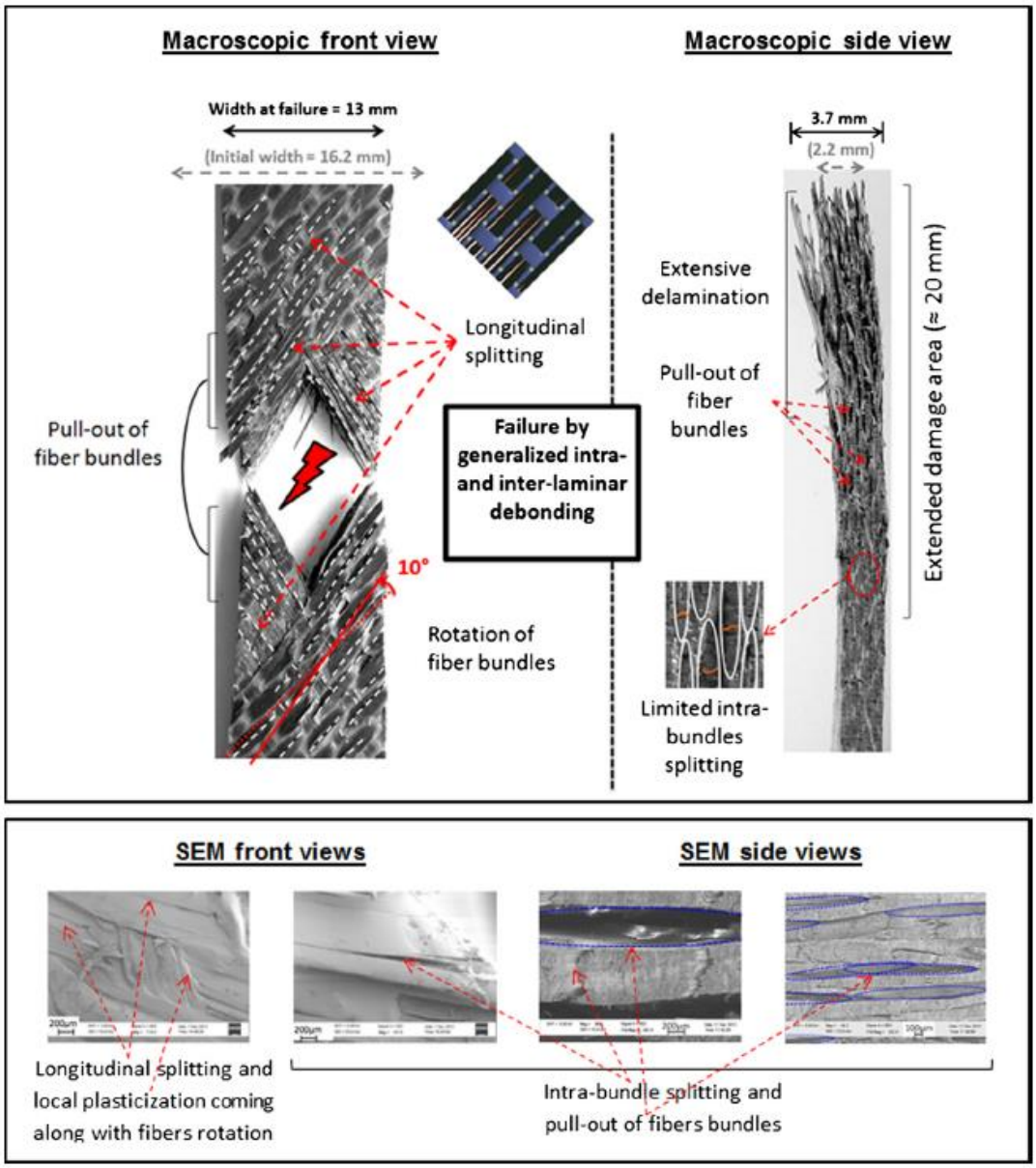

Figure 5. *Analysis of fracture surface in angle-ply C/PPS laminates subjected to a load–unload tensile test at 120°C: macroscopic views and SEM views [Albouy, 2014]*

I.2 General problematic: Organic Matrix Composites (OMC's)

Industrial interest

Thanks to their low density, organic matrix composites have been extensively used since the aeronautics early days. For airlines companies, fuel represents 30% of the operating cost, 40 to 50% for a low-cost company. Faced with the increasing scarcity of fossil fuels and the increase in air traffic, the reduction of kerosene consumption and the emission of polluting

particles is one of the challenges facing the aircraft industry. This reduction can be achieved by decreasing aircraft weight. Figure 6 shows the fuel consumption according to the gross weigh for an airliner at constant speed.

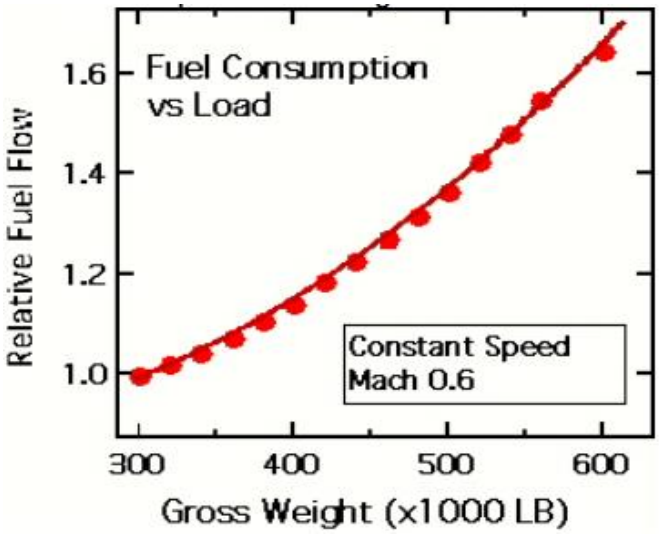

Figure 6. *Fuel consumption according to the load for an airplane traveling at a constant speed [Anderson, 2015]*

At the beginning of 2007, the aircraft consisted of approximately 20% composite materials and 80% aluminum alloys (35% heavier). In 2015, the airbus A350 developed by E.A.D.S was made from 52% composites (see Figure 7). There are strong indications everywhere that their importance will continue to be underlined in the future.

Figure 8 shows that aircraft energy consumption decreased by up to four times per passenger and per km from 1960 to 2015.

Other advantages of OMCs that may interest the manufacturers:

- Good fatigue resistance resulting in a better service life, thus, a decrease in the long-term cost of the product.
- Good corrosion resistance which involves in saving on maintenance cost.

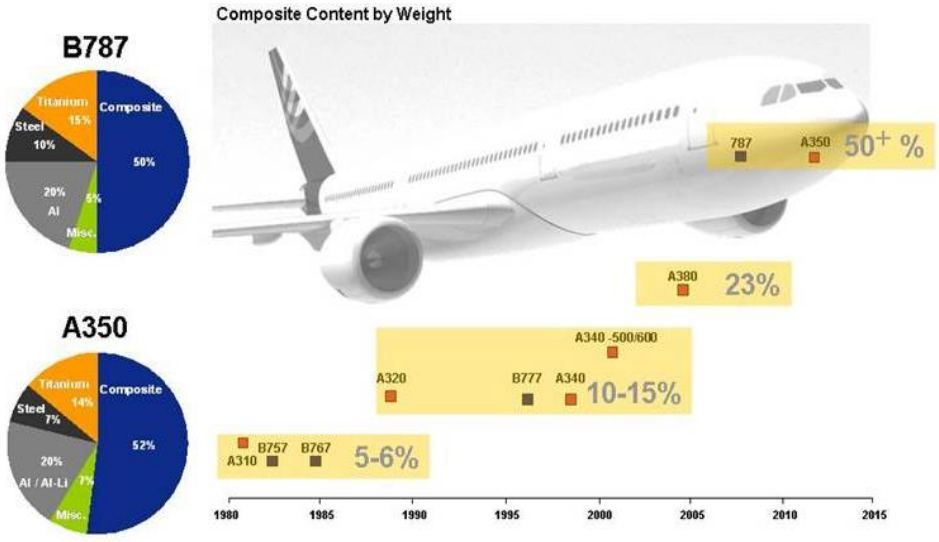

Figure 7**.** *Evolution of the percentage by weight in modern civil aircraft*

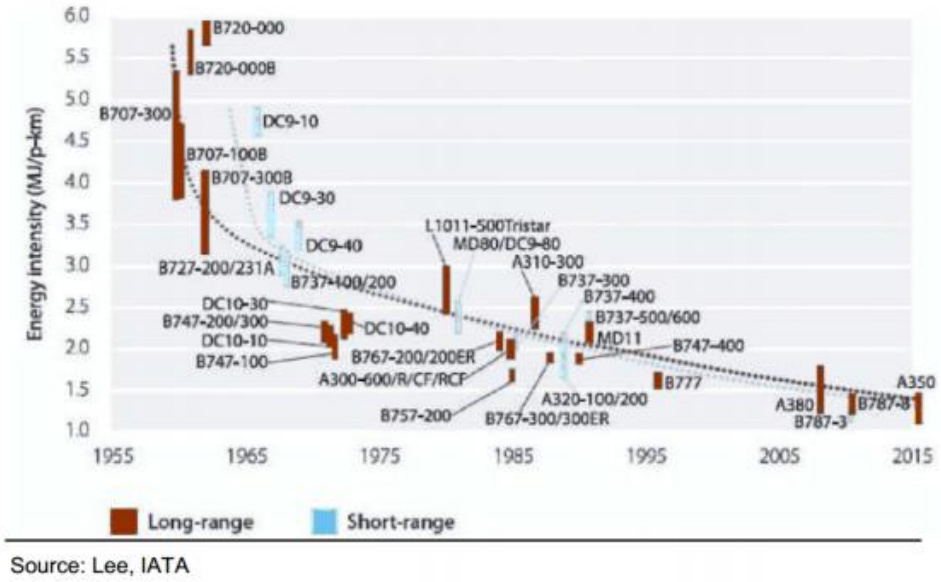

Figure 8. *Aircraft energy consumption from 1955 to 2015*

Currently, in a global market monopolized by TS matrix composites, TP matrix composites represent only 20% of composites. However, their development is considered to be twice that of TS matrix composites. Most TPs have poor mechanical properties at high temperatures and 90% of applications of thermoplastic matrix composites concern short fiber reinforced TPs (PA, PP, PC, PET, PPO). Nevertheless, the use of fiber-reinforced TPs is not new since, as early as the 1970s; Glass Mat Thermoplastics (GMT) emerged with the development of a new stamping technique for automobile industry. In the 1980s, high performance TP resins (e.g.

PEEK, PES, PI, PEI, PPS) were combined with long carbon fibers for aeronautical and military applications. Thus, these materials have been widely studied in the 1990s as evidenced by the relative richness of the literature, particularly on the behavior of PEEK matrix carbon composites. After falling back into a relative anonymity in the early 2000s, TP resins come to the forefront with the development of the A380 which integrates several pieces of TP composites including the leading edge of the wings (see Figure 7).

The renewal of composites is launched so that in 2004, the journal Industrie et Technologies titled: " Dare the thermoplastic composites! ".

The experimental and numerical activities developed in recent years revolve around TP matrix composites, from the perspective of aeronautical applications, and more particularly in aircraft engine nacelles which are exposed to high temperature (see Figure 9).

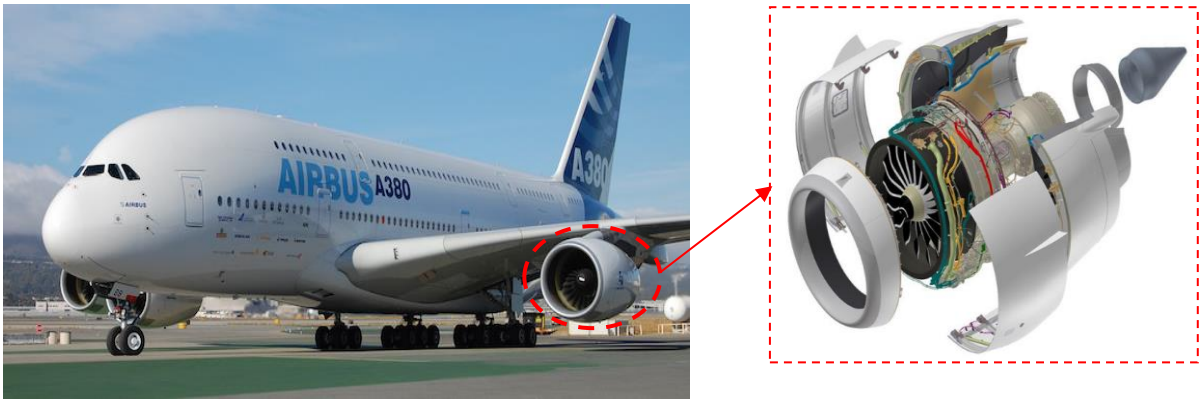

Figure 9. *Airbus A380 Nacelle Systems*

I.3 Structural effects and stress concentration

For joining purposes using mechanical fasteners and open cut-outs for access, it is often necessary to drill the composite material which causes an inhomogeneous stress distribution and a stress concentration in the vicinity of the notch (see Figure 10). The severity of the stress concentration is depending on the geometry of the notch configuration, generally referred to as the shape of the notch. In addition, notches significantly affect the growth of damaged zones as it damages both fibers and matrix around the crack tip. It has also a significant impact on the mechanical properties of the composite laminates. That's the reason

why designers should reduce stress concentrations as much as possible [Pilkey, 2008] [Schijve, 2001].

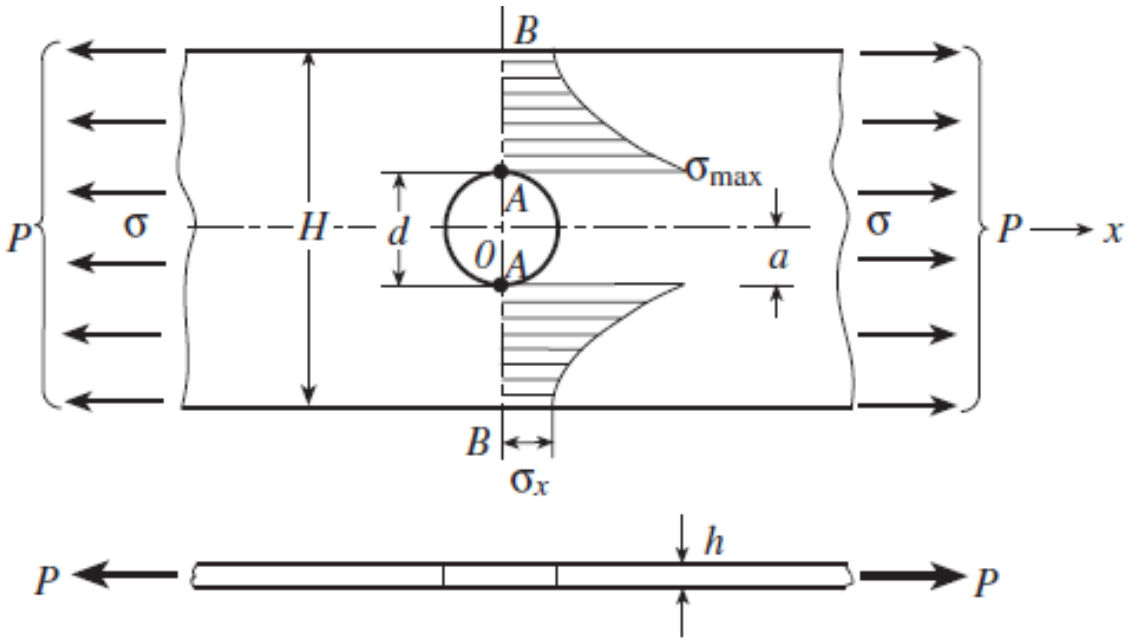

Figure 10. *Distribution of the stress concentration in a specimen with a central hole under tensile loading [Pilkey, 2008]*

Among the theories of elasticity analytical solutions for stress concentrations, Figure 10 shows elliptical hole in a specimen under tension. It appears that the stress decreases approximately exponentially from the location of the maximum stress (in the vicinity of the hole) to the nominal value far from the hole, with an important rate of decay near the maximum stress. Actually, the stress concentration profile depends on the mechanical behavior of the material. For a ductile material with a V-shaped notch subjected to tensile loading (see Figure 11). If the yield strength is higher than the maximum stress at the notch tip $\sigma_y > \sigma_{max}$, the stress distribution in the vicinity of the notch appear such in curves 1 and 2 in Figure 11. The maximum stress can be expressed as:

$$\sigma_{max} = K_t . \sigma_{nom} \quad (1)$$

When σ_{max} exceeds σ_y, the maximum stress increases slightly but the strain at the notch tip continues to increase. Then, the stress distributions take the form of curves 3 and 4 (see Figure 11). In this case, Equation (1) can no longer be applied. For higher values of σ_{nom}, the stress distribution in the vicinity of the notch tends to be more uniform.

For brittle materials whose behavior can be considered as elastic, the stress and strain retain their typical linear relationship until damage appears.

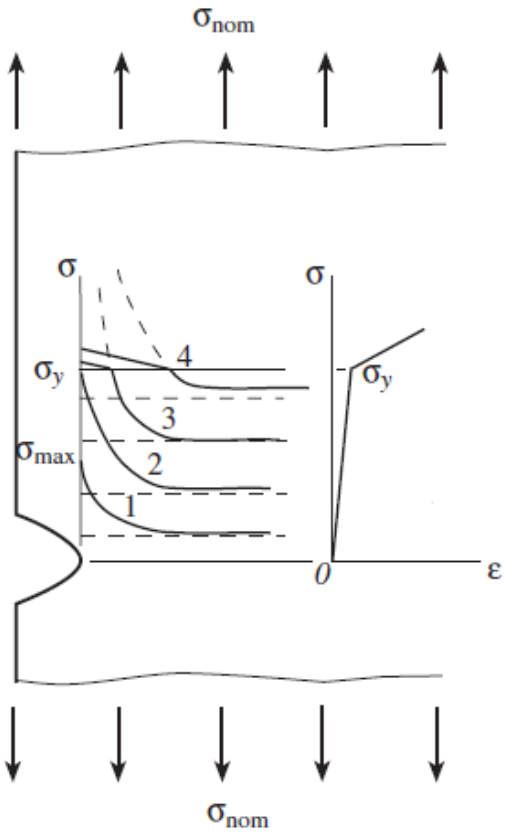

Figure 11. *Stress distribution near a notch for a ductile material [Pilkey, 2008]*

I.4 Fracture mechanics in composite materials

Fiber breakage, matrix cracking, interface debonding and delamination are the principal failure modes observed at the laboratory scale level. The complexity of the progressive failure process in a composite material makes impossible to analytically describe each successive stage. In order to bridge the gap between composite testing and design, methods of analysis procedures are needed. In this way, using fracture toughness and strength data obtained from small-scale laboratory tests, reliable estimates of the allowable stresses expected in service can be made. Because of the material anisotropy and inhomogeneity interacting with the complexity of cracks, this capability still doesn't exist. As an alternative, the fracture mechanics is the best tool to use for this purpose.

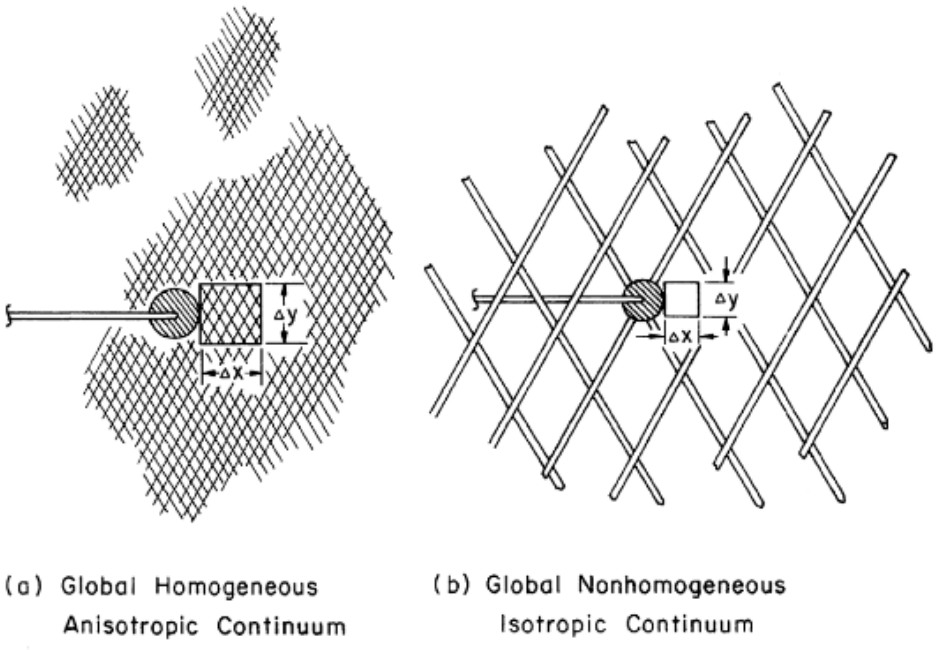

Figure 12. *Scaling of the continuum element with reference to crack size and microstructure of the composite [Sih, 2012]*

Before going to fracture mechanics, it's interesting to recall some basic principles about scaling the defect size and microstructure of a composite material.

In the literature, there are two main approaches [Sih, 2012]:

The first approach considers that the crack extends in an idealized global anisotropic homogeneous continuum. In other words, it doesn't take into account the local damages occurring at the crack tip such as fiber breakage and matrix cracking, etc.

The second assumes a global nonhomogeneous anisotropic body. In this case, at a given instance, the crack tip with a given radius of curvature is localized in a well-defined phase of the composite material (fiber, matrix or at the interface fiber/matrix).

The validity of these approaches depends of course on how the specimen dimensions are scaled with respect to the allowable stress level and size of the cracks or damage zone. The reason is that failure modes are dictated by the rate and amount of energy dissipated which depends on specimen size and the kind and rate of loading. The sequential order of discrete failure modes can also greatly influence the life of composite laminates. This is known as the stacking sequence effect.

In order to study the crack behavior, [Irwin, 1954] have introduced three different modes of fracture depending on the applied loading (see Figure 13):

- Mode I (Opening mode): Principal load is applied to the crack plane.
- Mode II (Sliding mode): In-plane shear loading tends to slide one crack face according to the other face in its plane.
- Mode III (Tearing mode): Out-of-plane shear loading tends to slide one crack face to according the other face out of plane.

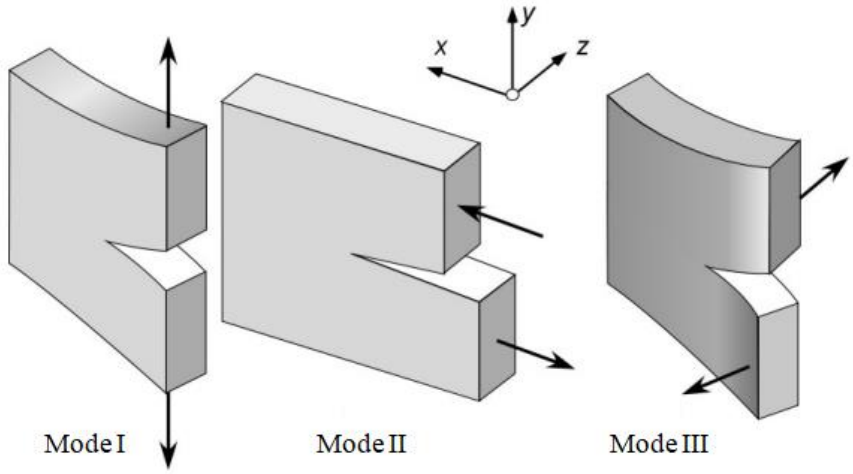

Figure 13. *Fracture modes [Brocks, 2012]*

I.4.1 General approach in heterogeneous fibrous composites

Damage tolerance is classically the property of a material to sustain defects safely until repair can be conducted. Fracture toughness is the ability of a material containing a crack to resist fracture. It is one of the most important properties for structural design applications. The fracture mechanics viewpoint is that all failure modes initiate from a preexisting defect (e.g. a pre-crack with different lengths). The strain energy release (in kJ/m^2) associated with the crack growth is classically defined as the energy dissipated during fracture per unit of newly created fracture surface area. Thus, the measurement of the energy required to grow a crack that must be balanced by the amount of energy dissipated due to the formation of new surfaces and other dissipative processes such as plasticity.

Edge cracks can initiate from notches at the surface of composite laminates due to processing (consolidation, machining) or stress concentrations due to the geometry of composite structures (see Figure 14).

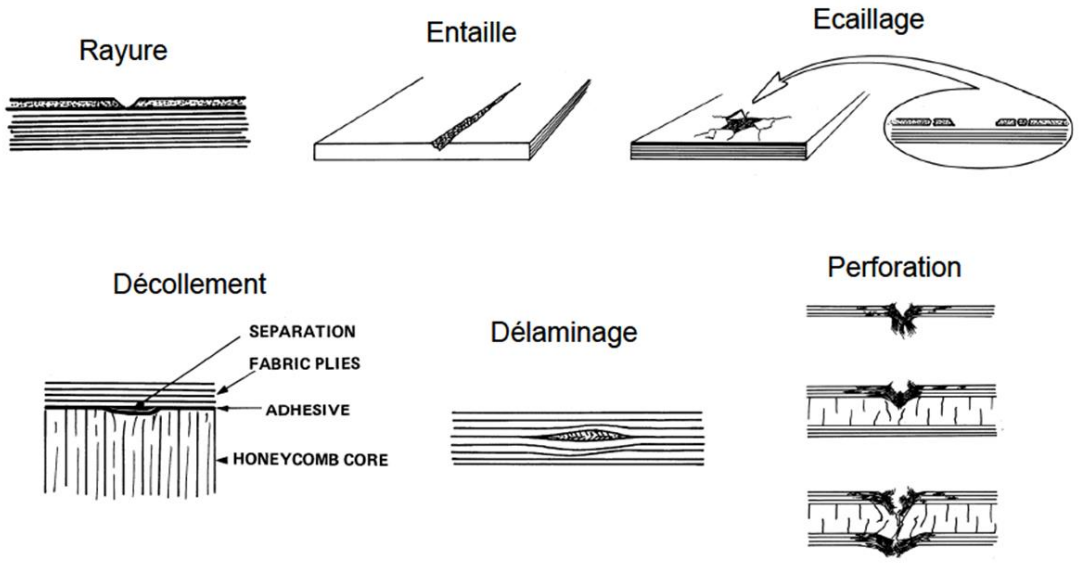

Figure 14. *Different type of defects in composites [Torres, 1986]*

They may result in the failure of composite structures subjected to monotonic or cyclic loadings. It is therefore necessary to evaluate the influence of prominent factors (notch length and orientation, stacking sequence, matrix ductility, service temperature) on the overstress distribution at the notch tip in order to better understand the subsequent damage mechanisms and failure modes. The stress concentration resulting from the presence of a notch or a crack is therefore closely associated with the material behavior (elastic-brittle or elastic-ductile), as is illustrated in the longitudinal stress profile in the vicinity of the crack tip in SEN laminates loaded in opening mode (see Figure 15).

In orthotropic or quasi-isotropic composite laminates, transverse matrix cracking and fibers breakage (also known as translaminar failure modes) are usually the primary damage mechanisms occurring in the early phase of mechanical loading. The micro-structural mechanisms of damage [Davies, 2003], including fiber breakage and matrix cracking, fiber/matrix debonding, transverse- ply cracking, delamination, and void growth, form a discrete but complex damage zone (See Figure 16). The onset of damages within composite laminates is associated with the critical stress intensity factor (SIF) denoted K_C (MPa.$\sqrt{m}$) from which a crack in the material begins to grow.

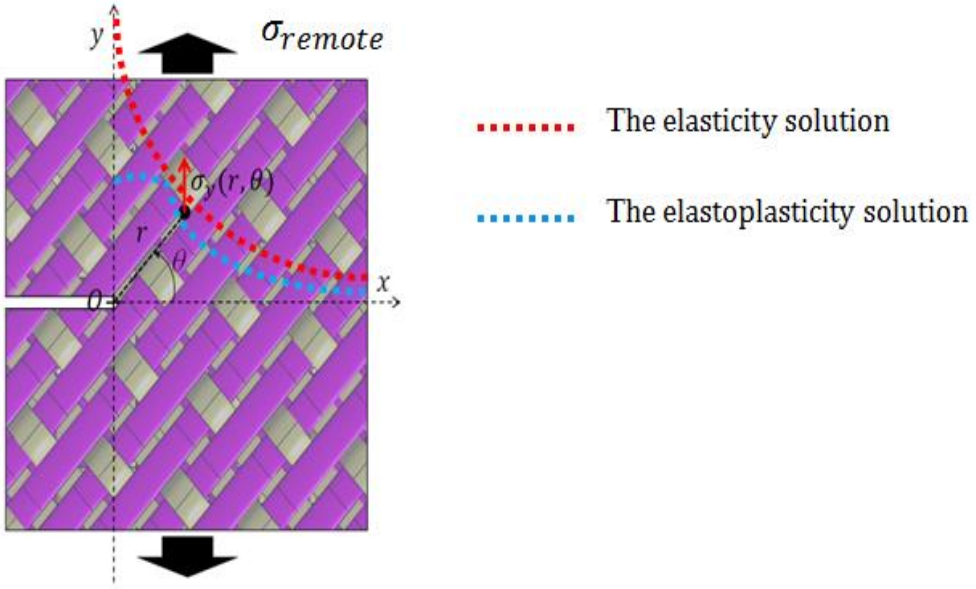

Figure 15. *Longitudinal stress profile in the vicinity of the crack tip in SEN laminates loaded in opening mode*

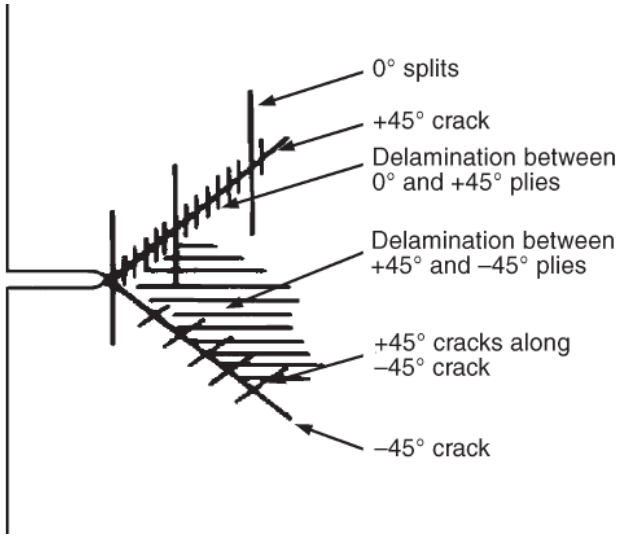

Figure 16. *Typical damage zone at a sharp crack in composite laminates subjected to mode I loading [Davies, 2003]*

Thus, the fracture toughness of FRPs is associated with their crack-stopping ability, which results from their inhomogeneity on a fine scale (the fiber/matrix interface) and on a gross scale (laminated structure) makes it difficult in many cases to generalize a fracture mechanics approach to FRPs with different reinforcements (UD- or woven-ply) and various stacking sequences [Reifsnider, 1991]. In UD-ply composite laminates, stress concentrating effects of

notches and holes may be almost completely eliminated by large-scale splitting in the 0º and 45º plies and by delamination between the plies, the net result often being disintegration of the composite. By contrast, in woven-ply, the scale of this damage is limited by the woven structure of the composite, and cracks and notches will often propagate in a more self-similar fashion (see Figure 17), especially in wide plates [Harris, 2003].

Depending on the matrix nature and the laminates' stacking sequence, the fracture mechanics analysis usually depends on the type of the fracture response (brittle or ductile) observed in composite laminates [Vieille, 2016]. In elastic brittle composite materials, fracture is usually analyzed by using the Linear Elastic Fracture Mechanics (LEFM) parameters: R-curve analysis, critical strain energy release rate G_{Ic}, stress intensity factor K_{Ic}.

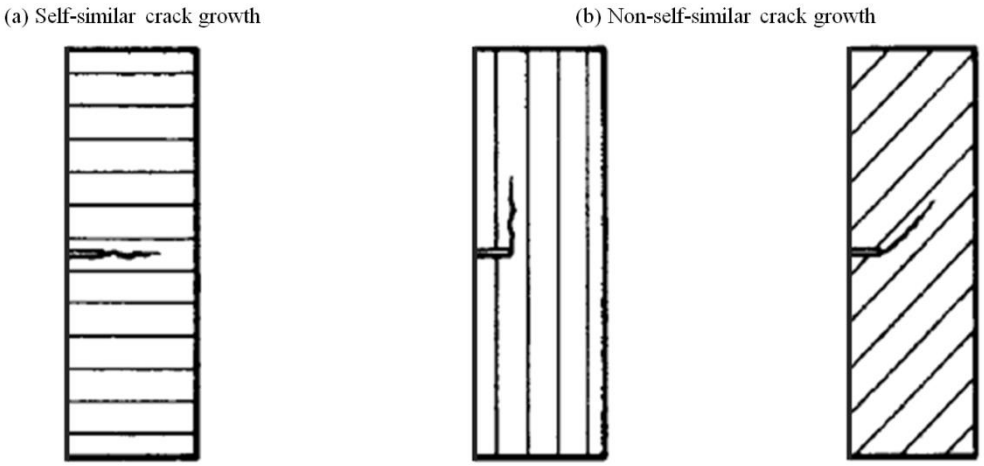

Figure 17. *Crack growth in Single-Edge-Notch laminates: (a) Self-similar – (b) Non-self-similar [Jones, 1999]*

In elastic-ductile composite materials, fracture analysis is done by means of J-integral, crack opening displacement (COD) or J-R curves. The use of LEFM to describe damage as the propagation of a single dominant crack may be not always self-similar in heterogeneous composite materials depending on its stacking sequence. In quasi-isotropic brittle laminates, the translaminar crack growth resulting from an initial transverse notch is usually self-similar. In angle-ply ductile laminates, a self-similar crack growth may be expected in materials that have very strong matrix materials with either of the following two conditions: (i) The strain to fatigue failure in the matrix is close to the strain required to fail the fiber; (ii) the matrix and the fiber/matrix interface are sufficiently strong to enable a matrix crack stress concentration

to fail the fibers. Thus, this idealization of a damage zone, which extends in a self-similar manner, allows a global analysis based on a global strain energy release-rate that can be calculated solely on the applied tensile loading.

The total elastic energy made available per unit increase in crack surface area (one side of the crack surface) is denoted by G for the linear-elastic case whereas the non-linear counterpart is denoted by J [Tada, 2000]. As it is defined by [Tada, 2000], G and J may be viewed physically as the energy made available for the crack extension processes at the crack tip as a result of the work from displacements of loadings forces and/or reductions in strain energy in a body accompanying a unit increase in crack area. Alternatively, G and J can be regarded as "generalized forces" based on the potential energy change per unit forward displacement of a unit length of crack front, which results in G and J defined as "crack extension forces".

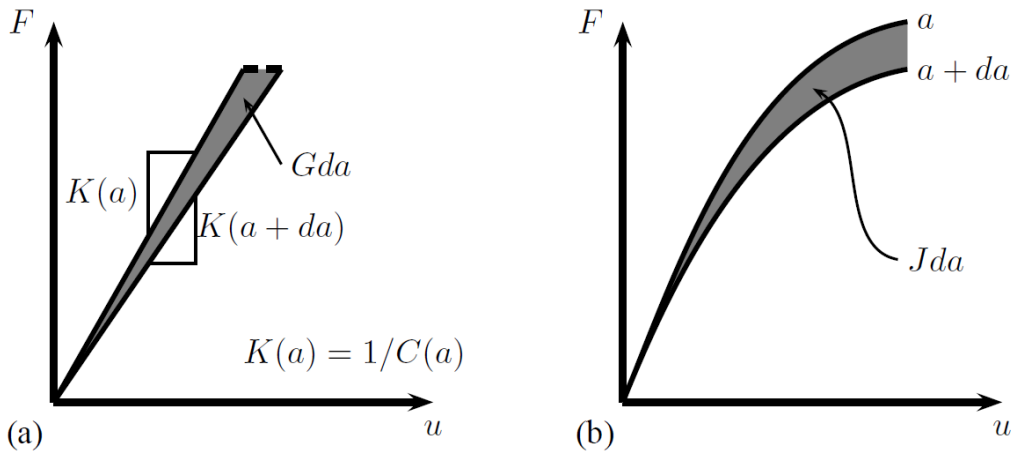

Figure 18. *Determination of strain energy release rate from load-displacement curves: (a) linear behavior – (b) nonlinear behavior*

I.4.2 Fracture analysis in brittle materials

Early in the sixties, Sih et al. examined the nature of the local crack-tip stress field in anisotropic bodies [Sih, 1965]. They proposed a method to determine the stress-intensity factors K_i which can be related to the energy release rates G_i (i=1,2,3). As was introduced by Sih et al., the stress-intensity factors or the fracture toughness K_i represent physically the intensity of the linear-elastic stress distribution, due to the introduction of a crack into the body, surrounding a crack-tip. It is therefore assumed that small amounts of nonlinearity (e.g. plastic deformation) at the crack-tip are embedded within the field, and do not significantly disturb it [Tada, 2000] [Vieille, 2016]. In the case of SEN specimens, the strain energy release

rate can be evaluated directly from the application of double cantilever beam method to the mechanical tests data:

$$G_I(X,A) = -\frac{\partial \Psi}{\partial A} = \frac{12F^2a^2}{EB^2h^3} = \frac{3\delta F}{2aB} \quad (2)$$

Where Ψ is the potential energy, A is the crack surface area, δ is the crack opening displacements, F is the applied load, B is the specimen thickness, h is the specimen width, a is the notch length evolution and E is the axial stiffness. The crack opening displacements δ is defined as the total separation of the crack faces and can be measured directly by in-situ Digital Image Correlation from gradually loaded SEN specimens.

Among the different methods developed over the years to quantify the fracture toughness of materials, the compliance method has been successfully applied to fiber-reinforced polymer composites [Sih, 1965]. The compliance C is defined by the slope of the load-displacement curve. LEFM requires a linear load-displacement behavior and much localized plastic deformation at the crack tip. When the mechanical response of composite materials is quasi elastic-brittle, the relationship between the compliance C and the crack length a can be classically associated with the calculation of the critical strain energy release rate G_{Ic} as follows:

$$G_{Ic} = \frac{F_{max}^2}{2B}\frac{dC}{da} \quad (3)$$

Where F_{max} is the maximum load at failure. Then, based on LEFM, the fracture toughness K_I was calculated from the following expression established for plane stress conditions [Belmonte, 2004], the latter assumption being verified in the case of thin laminates:

$$K_I = \sqrt{E_x\, G_I} \quad (4)$$

where E_x is the longitudinal stiffness.

In addition, different approximations have been proposed for K_I in the literature [Tada, 2000], and the stress intensity factor can be classically expressed as follows for SEN specimens:

$$K_I = \sigma\sqrt{\pi a}.F(a/w) \quad (5)$$

where σ is the remote applied stress, a denotes the length of the initial crack and w is the specimen width. $F(a/w)$ is a finite-width-correction (FWC) factor calculated from the ratio a/w and empirical formulas. By definition, this FWC factor is a scale factor applied to multiply the notched infinite-plate solution to obtain the notched finite-plate result [Tan, 1994]. For example, [Gross, 1964] have proposed the following expression for SENT specimens, whose precision is 0.5% for $a/w \leq 0.6$:

$$F(a/w) = 1.122 - 0.231 * (a/w) + 10.550 * (a/w)^2 - 21.710 * (a/w)^3 + 30.382 * (a/w)^4 \quad (6)$$

If the material is orthotropic with the crack in one plane of symmetry, the three basic modes are conveniently independent. In the case of plane stress conditions, if the first two modes are present together then:

$$G_{Total} = G_I + G_{II} \quad (7)$$

Where the strain energy release rates in mode I and II are defined plane stress conditions by:

$$G_I = \pi K_I^2 \sqrt{\frac{C_{11}C_{22}}{2}} \sqrt{\sqrt{\frac{C_{22}}{C_{11}}} + \frac{2C_{12} + C_{66}}{2C_{11}}} = C_I . K_I^2$$

$$G_{II} = \pi K_{II}^2 \frac{C_{11}}{\sqrt{2}} \sqrt{\sqrt{\frac{C_{22}}{C_{11}}} + \frac{2C_{12} + C_{66}}{2C_{11}}} = C_{II} . K_{II}^2$$

Where C_{ij} are the components of the compliance tensor.
These expressions can also be given in terms of engineering constants:

$$G_I = C_I . K_I^2 \text{ and } G_{II} = C_{II} . K_{II}^2$$

With $C_I = \pi \sqrt{\frac{1}{2E_x E_y}} \sqrt{\sqrt{\frac{E_x}{E_y}} - \nu_{xy} + \frac{E_x}{2G_{xy}}}$ and $C_{II} = \pi \frac{1}{E_x \sqrt{2}} \sqrt{\sqrt{\frac{E_x}{E_y}} - \nu_{xy} + \frac{E_x}{2G_{xy}}}$

I.4.2.1 Correlation between AE energy and mechanical energy

To characterize damage mechanisms and investigate their evolution in FRPs, many *in situ* and non-destructive evaluation techniques have been implemented. Acoustic Emission (AE) techniques are often used to detect the onset and growth of microscopic failure in composite

materials [Albouy el al., 2014] [Dickinson et al., 2009] [Ben Ammar et al., 2014], and many attempts have been made to distinguish between different types of failure [Sause et al., 2014] [Sause et al., 2009] [Giordano et al., 1998] [Bohse, 2000] [Huguet et al., 2002] [Hamdi et al., 2013]. Among the different approaches developed Modal Acoustic Emission (MAE) and peak frequency analysis of generated AE waveforms, proved to be very effective to characterize damage types as it was shown recently by [Baker et al., 2015] who have studied the initiation and propagation of cracks in CFR epoxy laminates using MAE and waveform energies, coupled with peak frequency data correlated to matrix crack density in the transverse direction. During mechanical loading, the degree of damage and the fracture events sequence can be extracted from an exponential damage evolution profile obtained in terms of AE counts rate and cumulative AE counts as it was shown in [Bussiba et al., 2008]. Using wavelet transforms to process AE signals, [Bussiba et al., 2008] obtained both frequencies and time information on the main failure mechanisms and the sequential events during fracture process. In order to investigate the mode I interlaminar fracture in UD glass/epoxy, a similar approach was applied to Double Cantilever Beam specimens to indicate the damage initiation from microscopic and macroscopic (delamination) standpoints by means of longitudinal and transverse strain gages combined with an AE transducer [Davies et al., 1989]. It is therefore possible to correlate the strain energy release rate in mode I (interlaminar fracture) with the effective crack length. Very recently, [Ivanov et al., 2017] have demonstrated the correspondence between AE cumulative energy in the warp direction and crack appearance in the weft yarns. They also conclude that the effect of transverse cracks in the matrix on the onset and growth of delamination(s) needs further investigation. It is also worth noticing that strain gages can be usefully replaced by full-field measurements to estimate the transverse crack propagation, as well as the opening of the crack tip (CTOD). Still considering the interlaminar fracture mode, a few authors have implemented the sentry function in the case of UD-ply and woven-ply glass fiber reinforced polyester laminates [Oskouei et al., 2012] [Fotouhi et al., 2011]. The sentry function $f(x)$ is defined from as the logarithm of the ratio between mechanical $E_s(x)$ and acoustic $E_a(x)$ energies, and it can be formulated as follows:

$$f(x) = ln\left[\frac{E_s(x)}{E_a(x)}\right] \tag{8}$$

Where x denotes the Crack Tip Opening Displacement.

On the one hand, the relationship between the sentry function and the first visible crack propagation is based on the fact that the sentry function simultaneously takes into account the strain energy storing capability (E_s) and the release of the internal energy (E_a) due to damage. On the other hand, it is possible to obtain classically the evolution of the mode-I strain energy release rate G_I and the crack length as a function of the CTOD. [Sause et al., 2014] have recently showed that the quantification of matrix cracking, interfacial failure and fiber breakage in UD-ply orthotropic carbon/epoxy laminates can be evaluated by interpretation of the obtained distributions of acoustic emission signals types in terms of fracture mechanics. Considering the idea initially proposed by [Ndiaye et al., 2000], the cumulative acoustic energy W_{AE} of an AE-signal can be associated with the critical strain energy release rate G_{Ic} in the case of stable mode I crack growth as follows [Sause et al., 2009]:

$$W_{AE} = \beta(c_L^2).G_{Ic}.\Delta A \tag{9}$$

where the proportionality constant $\beta(c_L^2)$ is a linear function of the cracked materials squared longitudinal sound velocity c_L^2, and ΔA represents the crack surface area. In other words, it means that the release of acoustic emission energy in FRPs is expected to be proportional to the mechanical energy release when damage grows within the materials. To confirm the correlation between the types of acoustic emission signals and the respective failure mechanisms and to assess the validity of the acoustic emission method to describe mechanical failure, the micro-mechanical fracture energies released during mechanical loading were calculated based on microscopic measurements of the crack progress utilizing scanning electron microscopy and scanning acoustic microscopy [Sause et al., 2009]. In a study validating the use of cluster analysis of AE for identification of damage modes in plain weave glass fiber reinforced epoxy laminates subjected to tensile loading, [Li et al., 2015] have correlated direct in-situ observations of the matrix cracking to positions and time of AE events, therefore succeeding in associating an AE event with the corresponding damage mechanism. However, such an approach is limited to glass fibers reinforced composites, as damage evolution can be observed during mechanical loading by means of backlighting.

I.4.3 Fracture analysis in ductile materials

LEFM strictly applies only when the material behavior is dominantly elastic and the fracture response, brittle. Thus, LEFM provides conservative fracture analyses for these conditions, with the net result that designs are penalized by not taking advantage of the material's full

load carrying capabilities [Kumar et al., 1981]. Many works in elastic-plastic fracture mechanics have demonstrated that more realistic measures of fracture behavior and design margin can be obtained through the use of elastic-plastic analyses [Rice et al., 1973] [Begley et al., 1972] [Hutchinson et al., 1979] [Dowling et al., 1976]. As it is underlined by [Kumar et al., 1981], fracture analysis in the elastic-plastic regime involves a number of complications not present in the elastic. Foremost are the inherent nonlinearities in the material deformation and large geometry changes. A further complication is the fact that there is a significant amount of crack tip blunting prior to initiation and stable crack extension prior to final fracture. This contrasts sharply with the brittle mode of fracture in which the crack initiation and rapid crack propagation events are essentially coincident. In materials experiencing both elastic and plastic deformation (Figure 18b), the fracture toughness can be determined by using the J-integral [Hertzberg et al., 1996]. The characterization of near tip stress and strain fields by the J-integral is analogous to the use of the stress intensity factor K as the characterizing parameter in linear elastic fracture mechanics. In ductile materials, J becomes a measure of the intensity of the entire elastic-plastic stress-strain field that surrounds the crack tip (see Figure 19). Analogous to K_{Ic} which represents the material's resistance to crack extension, one may define the value J_{Ic} which characterizes then material's toughness [Hertzberg et al., 1996].

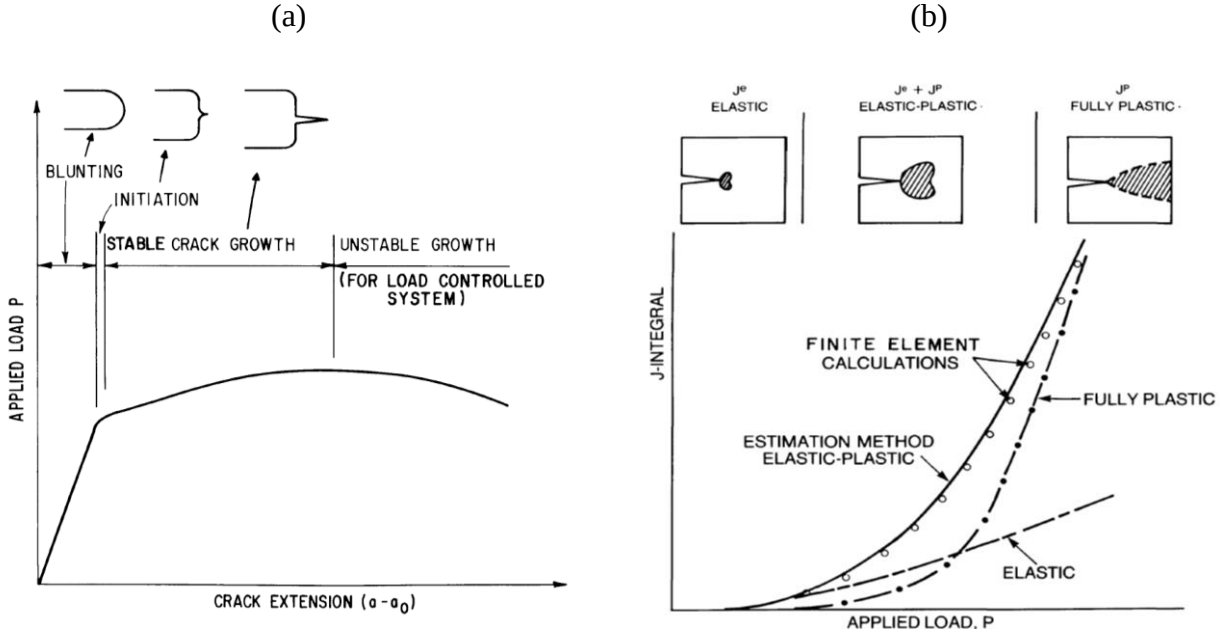

Figure 19. *Elastic-plastic fracture analysis [Kumar et al., 1981]: (a) Typical crack growth behavior of ductile materials – (b) Illustration of the elastic-plastic estimation procedure*

In literature, J_{Ic} appears to be equal to G_{Ic} values obtained for predominantly elastic behaviors associated with sudden failure without prior crack extension:

$$J_I = G_{Ic} \tag{10}$$

Rice et al developed a simple method for the determination of the plastic component $J_{i_{pl}}$ of J_i in isotropic materials (in accordance with ASTM standard E813-89):

$$J_i = J_{i_{el}} + J_{i_{pl}} = \frac{K_i^2}{E}(1-\mu^2) + \frac{\eta E_i}{B(w-a_0)} \tag{11}$$

Where $\mu = \nu$ in plane strain and $\mu = 0$ in plane stress, $\eta = 2 + 0.522 * (b/w)$ for a compact tension specimen and $\eta = 2$ for a three-point bend specimen, E_i is the energy absorbed during the elastic-plastic deformation, and is represented by the area under the load P_i vs displacement δ curve, B is the specimen thickness, $b = w - a_0$ is the length of the remaining unbroken ligament (w specimen width and a_0 initial precrack length).

This, in turn, can also be written for orthotropic materials using the following expression:

$$J_i = J_{i_{el}} + J_{i_{pl}} = C.K_i^2 + \frac{\eta E_i}{B(w-a_0)} \tag{12}$$

With $C = \pi\sqrt{\frac{1}{2E_xE_y}}\sqrt{\sqrt{\frac{E_x}{E_y}} - \nu_{xy} + \frac{E_x}{2G_{xy}}}$

In elastic-ductile composite materials, factor η can be evaluated by the load separation criterion and methodology developed by [Sharobeam et al., 1993]. This criterion allows the load to be represented as the multiplication of two separate functions: a material deformation function and a crack geometry function. Load separation implies a method for J-integral evaluating using only a single load-displacement record. The original method for evaluating J, proposed by [Begley et al., 1972] in the case of isotropic materials, used the energy rate interpretation of Rice which requires several load-displacement records for identical specimens with varying crack lengths. The load separation method will be implemented in chapter II section 4.2 so as to determine the strain energy release rate J in angle-ply (AP) thermoplastic-based laminates whose mechanical behavior is mainly matrix-dominated by matrix behavior resulting in highly ductile behaviors at high temperature (120°C>Tg).

In addition, specimens with SEN geometry are often used to determine the ductile fracture toughness, though it requires a correction due to the rotation of specimens along with the opening of the crack [Cravero et al., 2007] [Ruggieri, 2012]. More specifically, the specimen compliance needed to determine the crack length may not reflect changes in specimen geometry due to large rotations as the applied load increases, particularly in SEN specimens.

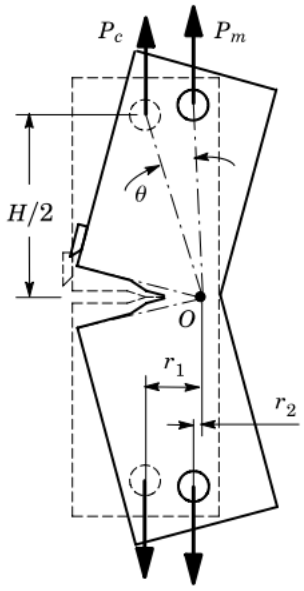

Figure 20. *Scheme of the rotation correction for the compliance of the SE(T) specimen [Cravero et al., 2007]*

Numerically, many tools have been developed providing the mechanical field characterization in the vicinity of the crack tip for ductile materials. Among them, the energy methods based on unvarying integrals such as *J*- or G_θ-integrals [Bouchard, 2000] provide the strain energy release rate in accordance with a thermodynamic approach. Particularly, the G_θ-integral method applied to elastic, viscoelastic and viscoplastic fractures [Dubois et al., 1999], provides a way to determine the strain energy release rate by using a surface integral. The G_θ-integral can be computed by means of the procedure G_THETA available in the finite element code cast3m®. More details about *J*- and G_θ-integrals are presented in section III.2.

I.5 Objectives of the thesis

Experimentally, the main objectives were to:

- Study the contribution of matrix ductility and toughness to the fracture mechanisms in TP-based composites subjected to high temperature service conditions ($T>T_g$).
- Understand the different damage mechanisms which are likely to occur in woven ply thermoplastic composites with angle ply (AP) (matrix-dominated behavior) and quasi-isotropic (QI) (fiber-dominated behavior) stacking sequences.
- Investigate the relation between the acoustic activity associated with the cracking mechanism and the strain energy release rate.
- Determine the evolution of the strain energy release rate according to the crack propagation (J-R curves) in angle ply laminates characterized by a highly ductile behavior at 120°C.

From the numerical simulation standpoint, the purpose was twofold:

- To validate the capability of a viscoelastic-viscoplastic model implemented in the FE code Cast3m to accurately predict the stress/strain fields and the overstress profile in the vicinity of the crack tip.
- To combine these constitutive laws with the G-THETA procedure available in Cast3m to compute the strain energy release rate using the G_θ-integral.

I.6 Conclusion

To conclude, the purpose of this chapter was to present the overall context and objectives of this work which focuses on the fracture mechanics in high performance thermoplastic based composites at temperature higher than their transition temperature. The few reminders presented in this chapter concerning the damage mechanisms and fracture mechanics in composite materials will help to study and understand the fracture behavior of this material under several condition tests.

Chapter II. Experimental investigation on translaminar failure at high temperature

Chapter II outline

II.1 Introduction

This chapter aims to experimentally investigate the translaminar failure in woven ply PPS thermoplastic laminates with quasi-isotropic and angle-ply stacking sequences. In the first part of this chapter, a brief background about translaminar fracture toughness measurement in fiber reinforced PMCs is presented. In the second part, the test conditions (materials and experimental set-up) are detailed. Then, the main experimental results are presented. Firstly, the fracture behavior of quasi-isotropic laminates was investigated by means of different methods (EA, COD, cracking gage). Thereafter, the J-integral and J-R curves are obtained for angle-ply laminates characterized by highly ductile behavior at high temperature. Finally, the influence of the architecture of reinforcement and the properties of the constituents on the fracture behavior of C/PPS laminates was studied.

II.2 Translaminar fracture toughness measurement

Fracture mechanics is usually characterized by many parameters (e.g. fracture toughness) that can be obtained from different experimental techniques applied to various testing conditions (tensile or bending loadings) and specific specimens' geometry. Depending on the fracture behavior of the materials (e.g. brittle or ductile), a relevant fracture mechanics approach should be adopted. Thus, the assessment of fracture toughness for structural integrity can be achieved by many methods requiring a single-point value [Zhu X-K, 2012]. Basically, the fracture behavior of fiber-reinforced PMCs is described as ductile, brittle or quasi-brittle. Brittle or quasi-brittle fracture is associated with a rapid and unstable crack extension resulting from transverse matrix cracking and the sudden breakage of 0° oriented fibers.

From the macroscopic response standpoint (stress vs strain curve), a brittle fracture failure is characterized by a well-defined point of crack initiation, corresponding to a sudden drop in load, and provides a measurement of initiation fracture toughness K_{Init}. The critical value of fracture toughness K_C can be identified from the unstable crack propagation which can be identified from the *R*- or *J*- resistance curves. For design purposes, the *R*- or *J*-curves represent the increasing resistance of the material (in terms of strain energy release (G or J)) for an increasing load, as the crack length grows (see Figure 21). After the onset of crack

extension, the initial part of *R*-or *J*-curves is associated with a stable crack growth prior unstable crack growth.

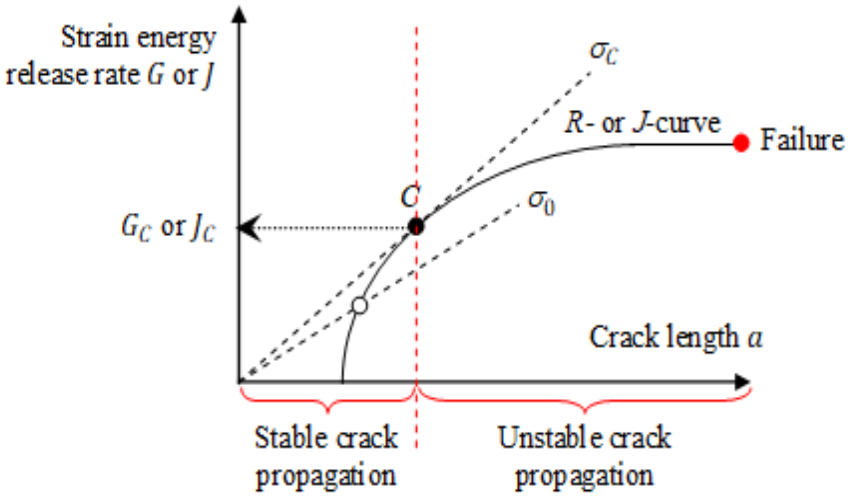

Figure 21. *Determination of the critical fracture toughness from R- or J-curves*

From the microscopic standpoint, the crack extension Δa is associated with different damage mechanisms depending on testing conditions (e.g. applied stress level, loading rate and temperature), the nature of constitutive elements (fibers + matrix), and the laminates stacking sequence. In the early stages of damage (at low stress levels), these micro-mechanisms absorb a small portion of the mechanical energy. As stress increases, damage grows and contributes to the dissipation of a larger portion of mechanical energy which can be measured by means of the strain energy release rate in standardized specimens, through the evaluation of the crack length (hence the created crack surface).

In laminates consisting of a ductile matrix system, ductile fracture is associated with a slow and stable crack extension. This type of fracture is characterized by a continuous extension of damage coming along with a ductile deformation rather than a point fracture. Such a fracture mode can also be quantified from *J*-resistance curves, which may result in some uncertainty due to the difficulty in localizing the fracture point due to plastic deformations. Ductile fracture initiation toughness K_{I_init} can still be obtained from a typical point defined near the onset of stable crack growth and deduced from the *J*-resistance curve near the transition from initial crack blunting to crack extension which can be identified by a distinct change in the

slope of the *J*-resistance curve [Zhu X-K, 2012]. Similarly to brittle fracture, the critical value of fracture toughness K_C can be identified from the unstable crack propagation. In ductile materials, instability of the crack propagation corresponds to the development of the plastic zone at the crack tip. Graphically, when the remote stress reaches a critical value σ_C, unstable crack propagation occurs as the crack driving force (represented by dJ/da) is higher than the slope of the J-resistance curve at the intersection point (see Figure 21).

In orthotropic or quasi-isotropic composite laminates, transverse matrix cracking and fibers breakage (also known as translaminar failure modes) are usually the primary damage mechanisms occurring in the early phase of mechanical loading. A comprehensive review of techniques for the experimental characterization of the fracture toughness is given in [Zhu X-K, 2012], and in [Laffan et al., 2012] when it comes to the translaminar failure mode of FRPs. When it comes to evaluate the mode I fracture toughness of FRPs, the translaminar fracture toughness can be estimated by means of Single-Edge-Notch structures [Laffan et al., 2011] [Woo et al., 2007]. However, translaminar fracture has received relatively little attention from the scientific community until now [Pinho et al., 2006].

II.2.1 Fracture toughness and damage mechanisms in fiber-reinforced plastics

Fracture toughness is utmost important for structural applications as it represents the material capability to resist to fracture. The toughness of a polymeric matrix depends on several factors: the amount of amorphous phase (in semi crystalline polymers such as PPS), the size and size distribution of crystals, the amount of rigid amorphous phase, the glass transition temperature (T_g), the strain at failure. In fiber-reinforced plastics, fibers are usually tougher than the polymer matrix [Kassapoglou, 2015], and the various origins of fracture toughness in composites may be characterized by considering the sequence of microscopic fracture events that lead to crack propagation macroscopically under monotonic increasing loads. The cracks in composites can propagate preferentially along the fiber-matrix and laminar interfaces (i.e. longitudinal splitting) or transversely right through the fiber and matrix (i.e. transverse cracking), depending on the properties of the interface relative to the fiber and matrix (see Figure 22). When a crack present in the matrix approaches an isolated fiber, the following failure mechanisms may be expected to take place [Kim et al., 1998]: (1) matrix cracking - (2)

fiber-matrix interface debonding - (3) post-debonding friction - (4) fiber fracture - (5) stress redistribution - (6) fiber pullout.

The non-conservative deformation processes have been discussed in details in the literature [Reifsnider, 1991]. In highly anisotropic composites with high fiber content, a crack normal to the fibers will often refuse to propagate in mode I, but will be diverted into a splitting mode. In unidirectional (UD) carbon-fiber reinforced plastics, this may result in a brittle, end-to-end splitting failure which simply eliminates the crack. By contrast, in fibers-reinforced plastic laminates containing woven-roving or chopped-strand mat reinforcement, crack-tip damage may remain localized by the complex geometry of the fiber array in the Fracture Process Zone (FPZ), and the crack may proceed through this damaged zone in a fashion analogous to the propagation of a crack in a plastically deformable metal [Harris, 2003]. The crack-stopping ability of composites, which results from their inhomogeneity on a fine scale (the fiber/ matrix interface) and on a gross scale (laminated structure) makes it difficult in many cases to generalize a fracture mechanics approach to fiber-reinforced composites with different reinforcements (UD- or woven-ply) and various stacking sequences. In UD-ply composite laminates, stress concentrating effects of notches and holes may be almost completely eliminated by large-scale splitting in the 0° and 45° plies and by delamination between the plies, the net result often being disintegration of the composite. By contrast, in woven-ply, the scale of this damage is limited by the woven structure of the composite, and cracks and notches will often propagate in a more self-similar fashion, especially in wide plates [Harris, 2003]. It also appears that woven-ply laminates are characterized by matrix-rich regions at the crimps (where warp fiber bundles undulate over weft fiber bundles), and the potential benefit of these matrix-rich regions is the development of plastic yield zones at the cracks tip as intra- and inter-ply cracks propagate [Albouy et al., 2014]. Depending on matrix toughness and ductility, the localized matrix plasticization is instrumental in ruling damage mechanism, as these matrix-rich regions may act as cracks barriers and subsequent propagation in unnotched laminates, as well as in notched laminates [Vieille et al., 2016b]. It is therefore expected this mechanism to reflect on material toughness measurements either in fiber-dominated laminates (quasi-isotropic) or matrix-dominated laminates (angle-ply). Toughness is therefore an intrinsic property of a material and it is the ability of a material to dissipate deformation energy without propagation of a crack. The design of tough microstructures in structural materials demands a compromise between resistance to intrinsic damage mechanisms ahead of the tip of a crack (intrinsic toughening) and the formation of crack-tip shielding

mechanisms, which act behind the tip to reduce the effective "crack-tip driving force" (extrinsic toughening) [Low, 2017]. The introduction of soft regions into fiber-reinforced composites to provide barriers to crack growth depends on matrix ductility, resulting in raising the intrinsic toughness of the material [Vieille et al., 2016] [Fernando, 2003]. As far the crack propagation is concerned, it is therefore potentially interesting to associate woven fabrics with highly ductile TP matrices [Kawai et al., 1996], the effect of which is even more noticeable when service temperature is higher than the material glass transition temperature [Kim et al., 1992], even in QI laminates whose behavior is fiber-dominated. However, as underlined by [Sih et al., 2012], the material in the immediate vicinity of the crack front is highly stressed and its behavior is not exactly known, therefore the fracture mechanics analysis must necessarily be restricted to regions outside of a small zone surrounding the crack tip.

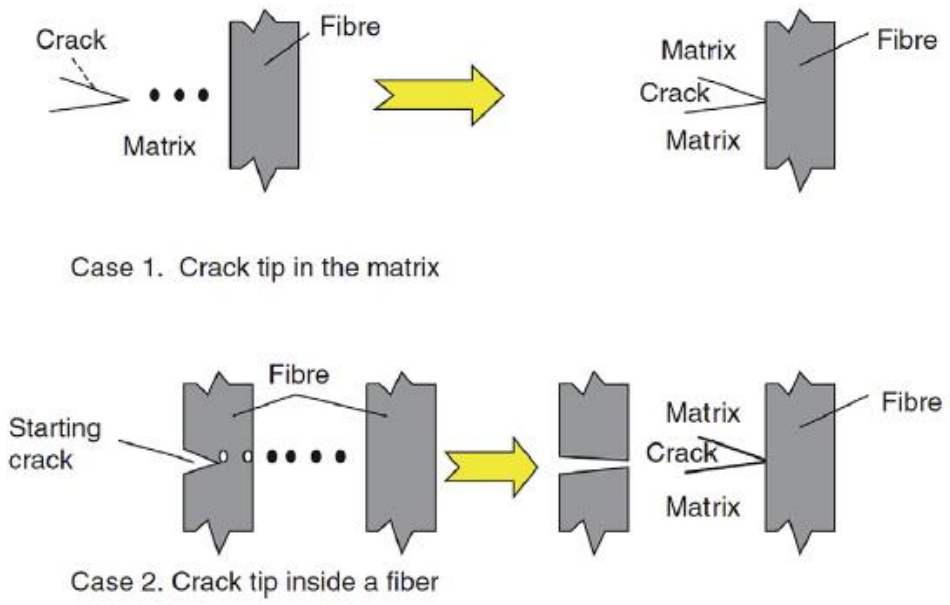

Figure 22. *Different cases of a crack in a composite laminate [Kassapoglou, 2015]*

II.2.2 Fiber/matrix interface-related fracture toughness

During fracture, the local response of the fiber-matrix interface within the composite is utmost important. [Kim et al., 1998] proposed a comprehensive review on the influence of interfaces on fracture toughness of fiber reinforced composites in both transverse and interlaminar fractures, as well as their consequences on the mechanical properties in various failure modes and loading configurations. In the present thesis, the discussion is restricted to transverse

fracture. In the literature, a weak interface bond is detrimental to some mechanical properties (longitudinal compressive strength and transverse tensile strength). At the same time, it allows these failure mechanisms to occur more readily and extensively with enhanced stability in crack growth. The ability of a composite material to arrest cracks through longitudinal splitting contributes to the overall improvement in energy absorption capability and thus its fracture toughness. Significant research efforts have been directed towards the development of techniques to enhance the fracture toughness of fibers-reinforced composites without impairing other mechanical properties. These techniques can be classified into two major approaches: (i) one relies on the improvement of the intrinsic properties of the composite constituents (reinforcement or matrix) - (ii) the other depends on the control of interface and/or interlaminar properties. In both cases, the energy absorption capability of fibers-reinforced composites can be improved significantly by promoting interface debonding and fiber pull-out, while maintaining a ductile interphase. On the one hand, IGIS (Interlaminar Graded Interphase Strength) laminates are a new class of hybrid laminates essentially concerning modifications of the matrix rather than of the reinforcement configuration [Simeoli et al., 2014] [Sorrentino et al., 2015] [Sorrentino et al., 2017]. [Boccardi et al., 2016] studied the effects of interface strength gradation on impact damage mechanisms in PP/woven glass fabric composites. By means of low velocity impact tests, they concluded that grading the matrix/fibers interface strength can be an effective way to retain good mechanical properties while allowing significant increases in the impact damage tolerance by maximizing the energy dissipation through different mechanisms.

On the other hand, if the fibers are coated with an appropriate coating material (e.g. TP resin), it results in regions characterized by weak interfacial bonds. Thus, high transverse fracture toughness can be achieved without deteriorating the composite mechanical properties [Kim et al., 1998]. The principal effect of altering the interfacial properties by coating is to modify the mode of failure and thus the potential energy absorption capacity which promotes the fracture toughness of composites. The TP coatings have advantages over other coatings in that they form a ductile layer at the interface acting as a crack arrester, allowing large debonding and fiber pullout to take place. Thus, the fiber/matrix interface region tends to be yielded in preference to clear-cut debonding.

II.3 Materials and experimental set up

II.3.1 Materials and specimens

The composite materials studied in this work are carbon fabric reinforced PPS prepreg laminate plates. Each ply has a thickness of 0.315mm. They consist of five harness satin weave fabrics supplied by SOFICAR and made using the T300 3K 5HS carbon fiber and Fortron 0214 high performance TP (PPS), whose volume fraction is 50%, supplied by Ticona company [Vieille et al., 2015] [Vieille et al., 2011] [Vieille et al., 2013] [Vieille et al., 2014] [Albouy et al., 2014]. The properties of the studied composite and its constituents are summarized in Table 1. The PPS matrix is characterized by a glass transition temperature of 96°C. The prepreg C/PPS plates are stacked by two different lay-ups: [(0;90),(+45;-45),(0;90),(+45;-45),(0;90),(+45;-45),(0;90)] and $[+45/-45]_7$). The first one can virtually be considered as quasi-isotropic (QI) and is characterized by an elastic brittle response. However, angle-ply (AP) laminates $[+45/-45]_7$ are characterized by a highly ductile behavior at temperatures higher than T_g [Vieille et al., 2012] [Albouy et al., 2013].

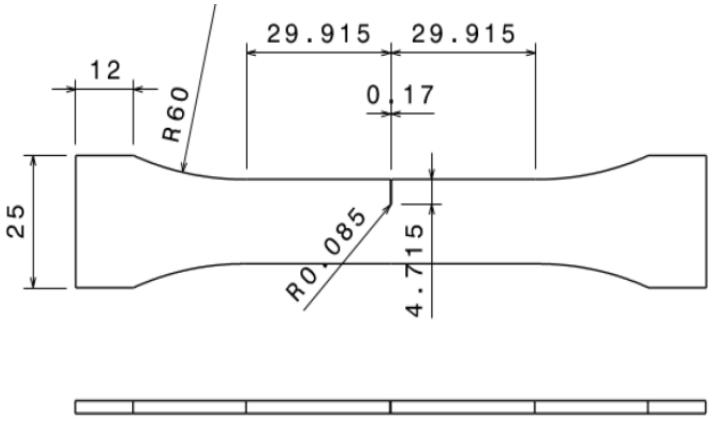

Figure 23. *Geometry of Single Edge Notched (SEN) specimens*

Table 1. *Properties of the studied composite and its constituents [Albouy, 2013]*

Characteristics of carbon fibers	
Average diameter (µm)	7
Traction modulus (GPa)	230
Ultimate tensile strength (GPa)	3.53
Ultimate strain (%)	1.5
Density (g/cm^3)	1.77

Characteristics of PPS resins	
Glass transition temperature (°C)	96
Traction modulus (GPa)	2.3
Ultimate tensile strength (MPa)	93
Ultimate strain (%)	15
Density (g/cm^3)	1.34
Degree of cristallinity (%)	38

Characteristics of C/PPS prepreg	
Ply thickness (mm)	0.317
Fiber volume content (%)	50
Resin volume content (%)	50
Fiber mass content (%)	57
Resin mass content (%)	43
Laminate density (g/cm^3)	1.56

Mechanical properties of the C/PPS ply	
E_l (GPa)	56.5
E_t (GPa)	56.5
G_{lt} (GPa)	4.08
υ_{lt}	0.04
X (Ultimate longitudinal strength) (MPa)	702
Y (Ultimate transverse strength) (MPa)	718
S (Ultimate shear strength) (MPa)	115

Dog-bone specimens with single edge notch are used. The idea to use SEN geometry in TP-based composites was twofold: (i) to estimate the value of mode I fracture toughness – (ii) to induce stress concentration at the crack tip and promote translaminar failure in order to reduce the coexisting damage mechanisms.

The machining of the Single-Edge Notches was done by means of a precision endless diamond wire saw whose radius is 0.085 mm (see Figure 23).

II.3.2 Methods

Mechanical testing

All the thermo-mechanical tests were performed using a 100 kN capacity load cell of an MTS 810 servo-hydraulic testing machine (see Figure 24). The temperature control system, which includes an oven and a temperature controller, provided a stable temperature environment during the test. In order to measure the axial displacement as load is applied, an extensometer is used and has fixed gage length l_0=25mm.

All the results presented in this thesis correspond to a test temperature T=120°C. Such a temperature was chosen because advanced aeronautics structures, and particularly nacelles are subjected to high temperatures up to about 120°C which is higher than the glass transition temperature of C/PPS composite $T_{g_{|C/pps}} = 95°C$.

Single-Edge Notch (SEN) specimens were subjected to monotonic tensile loadings at 120°C. SEN specimens have a given ratio a/w representing the ratio of the initial crack length over the specimen width. In addition, damage mechanisms have been discussed by means of fractographic analyses: microscopic observations by means of an optical microscope and scanning electron microscope (SEM) observations with a Leo 1530 Gemini Zeiss microscope as well as a 3D digital microscope VHX-5000 by Keyence. The average specimen's thickness (2.2mm) is small compared to the specimens' length and width. As a result, SEN specimens can be considered as thin structures in which a plane stress state prevails.

Figure 24. *MTS 810 servo-hydraulic testing machine*

Full-field measurements

SEN geometry leads to local damage within the laminates, resulting in singularities in the strain field on the outer surface (see Figure 26a). 2D Digital Image Correlation (DIC) technique is an appropriate tool to continuously track the influence of tensile loading on damage onset and growth. This method is based on the measurement of the displacement field between a reference time (stress-free state) and a given time of the loading (deformed state). This method requires painting one side of the specimen with a black and white speckle to obtain different shades of grey (see Figure 25) [Vieille et al., 2011]. Therefore, the Green-Lagrange strain field can be derived from the 2D displacement field by means of the VIC-2D correlation software (provided by the company Correlated Solutions). The 2D DIC technique was applied during tensile loading to investigate the early deformation mechanisms, but also to detect the onset of local damage events (transverse matrix cracking and breakage of 0° fibers) from the measurements of CTOD. During tensile tests, the onset and growth of macroscopic transverse crack at the outer surface of the laminates comes along with the Crack Tip Opening Displacement which can be evaluated from the DIC analysis. For QI laminates, where the crack propagates in the transverse direction, the crack onset was detected and the crack tip was localized when a discontinuity is observed on the curve displaying the longitudinal displacement field as a function of the axial position (see Figure 26b), because such discontinuity indicates that the displacement of the upper part is higher than the lower part's one [Vieille et al., 2011]. For AP laminates, the crack propagates along 45° oriented

fibers, making difficult the determination of crack length using COD tool. Thus, the calibration tool of the VIC-2D software, which is based on a reference image to determine the number of pixels in a one unit of length (Figure 28), was used.

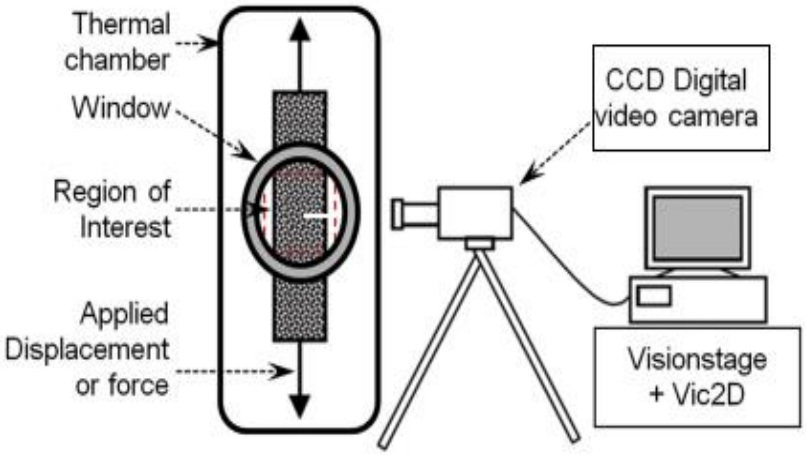

Figure 25. *Digital Image Correlation (DIC) set-up*

(a) (b)

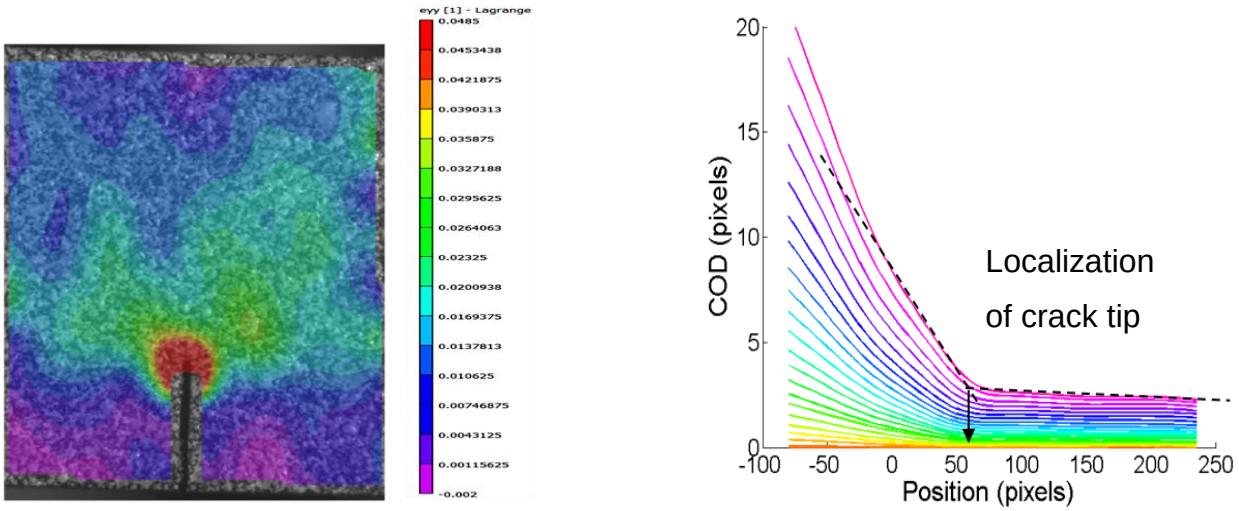

Figure 26. *Estimation of Crack Tip Opening Displacement δ obtained by Digital Image Correlation applied to quasi-isotropic C/PPS laminates at 120°: (a) longitudinal strain field – (b) Identification of the crack tip length from the discontinuity in the longitudinal displacement field*

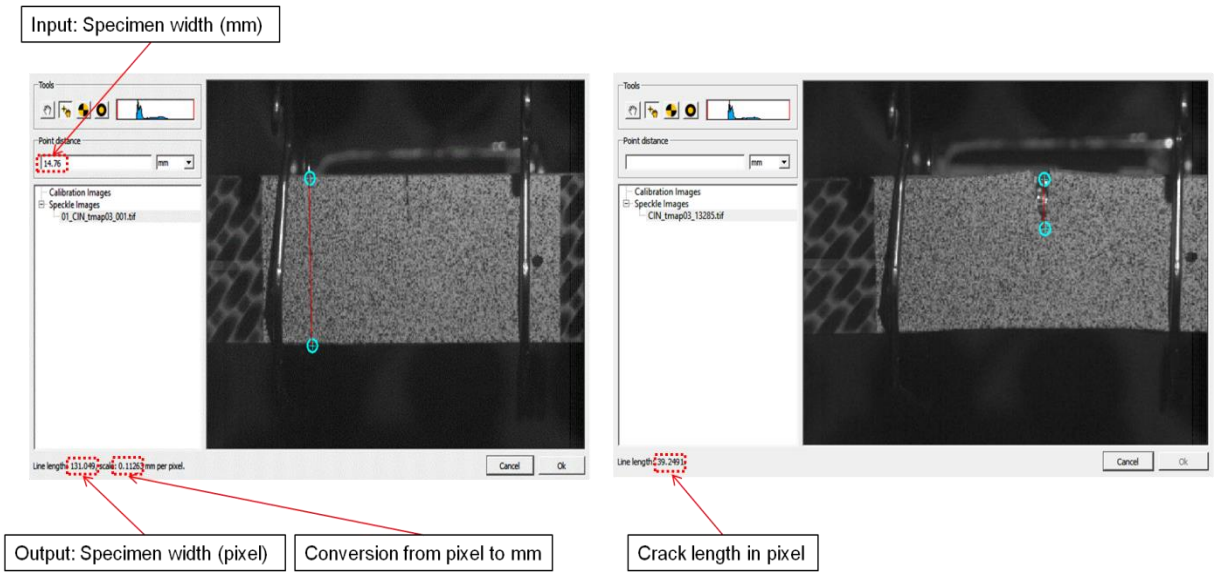

Figure 27. *Determination of the macroscopic crack length in SEN AP laminates at 120°C*

Acoustic Emission

The acoustic emission activity was monitored during load–unload and monotonic tensile tests. The AE signals were detected using two sensors of PAC micro80 type in linear arrangement and a PCI-2 data acquisition card. All signals were amplified by 20 dB using a 2/4/6 preamplifier and recorded with 45 dB threshold and 30/100/300 ls settings for Peak-Definition-Time/Hit-Definition-Time/Hit-Lockout-Time using the software AEwin with 10 MHz sampling rate. For all configurations, a band pass filter from 20 kHz to 1 MHz was used. From the sudden changes in the cumulated acoustic energy as a function of time, it is possible to identify the stress level corresponding to damage onset at both microscopic and macroscopic scales [Albouy et al., 2014].

Cracking gauge

The specimens were instrumented on one side by a crack propagation gauge (HBM crack gauge-type RDS22) which covers the whole bonding length and monitor crack initiation and propagation during the mechanical test. The crack gauges included 50 parallel links with a pitch of 0.1mm. As the macroscopic transverse crack initiates and propagates on the outer surface under the crack propagation gauges, the links were progressively broken and the electrical resistance of the gauge was increased. From the changes in the electrical resistance, it is therefore possible to calculate the changes in the crack length, and then to evaluate the stress level corresponding to the onset of transverse failure at the macroscopic scale.

II.4 Experimental determination of strain energy release rate in C/PPS at high temperature

II.4.1 QI laminates (Fiber-dominated behavior) [Vieille et al., 2017b] [Chabchoub et al., 2017b]

The purpose of this section is to investigate the mode I translaminar fracture energy for initiation and propagation and damage evolution in a 5-harness satin weave carbon fabric reinforced PolyPhenylene Sulphide (PPS) with quasi-isotropic stacking sequence. Based on the Linear Elastic Fracture mechanics (LEFM), the initiation K_{I_init} mode I fracture toughness were determined by means of three different technics: (i) the Crack Tip Opening Displacement (CTOD) method based on the outer surface full-field measurements – (ii) cracking gauges bonded to the outer surface – (iii) Monitoring of the Acoustic Emission (AE) activity associated with the prominent damage mechanisms (transverse matrix cracking and fibers breakage) and critical K_{Ic} mode I fracture toughness was determined using compliance method. Acoustic Emission (AE) activity was monitored to examine the reliability of this approach to quantify the strain energy release rate G_I as a function of the cumulative acoustic energy W_{AE}. In order to examine the correlation between AE energy and fracture energy, the coefficients of the model have been identified from the set of experimental data for one given ratio a/W. To investigate the fracture sequence and the damage kinetics, a macroscopic damage variable based on stiffness measurements and the evolution of the AE data (cumulative events and energy) were compared. The correspondence in damage evolution given by the experimental AE data at microscopic scale and a cumulated damage variable at macroscopic scale validates the ability of both approaches to quantify the damage degree in fiber-reinforced PMCs, and to identify a critical threshold for damage initiation.

II.4.1.1 Macroscopic tensile response of QI SEN specimens

The tested notched specimens are characterized by an elastic-brittle response (see Figure 28) as the tensile thermo-mechanical behavior of quasi-isotropic laminates is mostly driven by the tensile response of 0° oriented fibers. The elastic-brittle mechanical response primarily results from the transverse matrix cracking and fiber breakage near the notch tip (see Figure 29). In quasi-isotropic specimens, transverse crack initiation and propagation virtually occur at the same time corresponding to ultimate failure [Vieille et al., 2016]. It is also worth noticing that

the tensile response of SEN specimens depends on the testing conditions, as the thermomechanical behavior is significantly different when specimens are subjected to monotonic loadings or gradual load-unloads until failure (see Figure 28b).

(a)

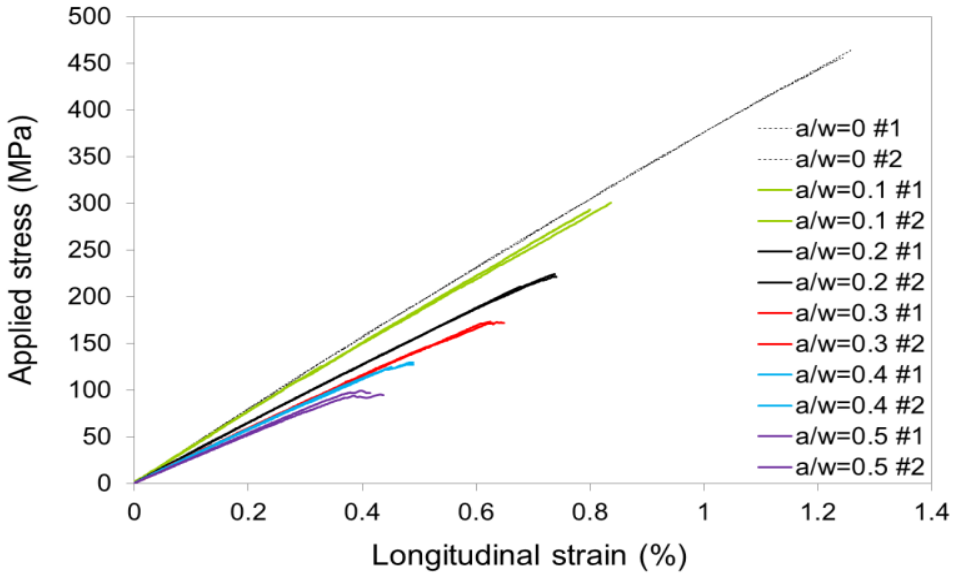

(b)

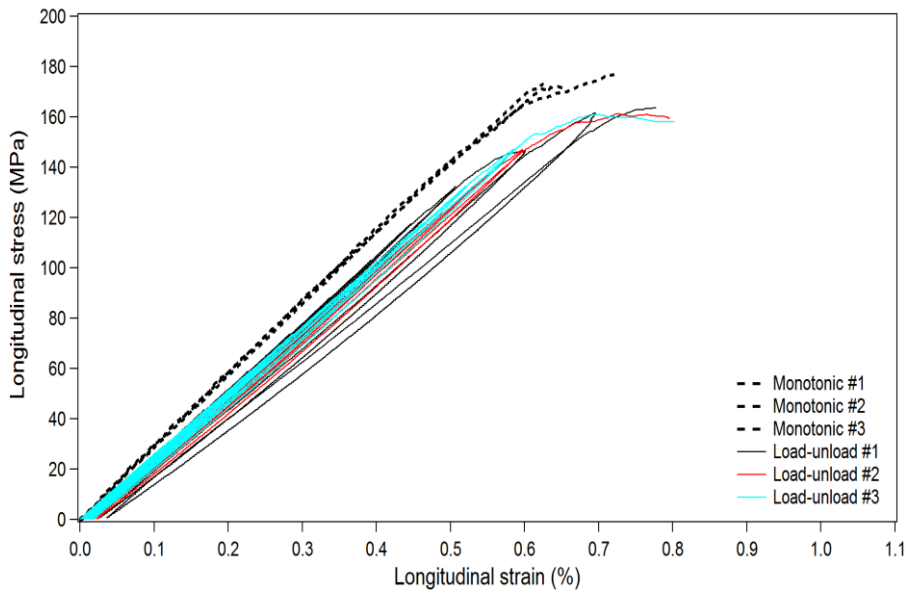

Figure 28. *Tensile responses of QI SEN C/PPS specimens at 120°C: (a) influence of the ratio a/W of the initial crack length over the specimen width on the monotonic behavior – (b) influence of loading conditions*

More specifically, a ductile-type fracture can be observed for high stress levels (around 140MPa). The corresponding damage mechanisms will be further discussed in the sequel. Even though the ultimate strengths are virtually the same, the strain at failure is about 30% as

high in gradually loaded specimens with respect to monotonically loaded one, with 0.77% vs 0.6% respectively (see Figure 28b). These results suggest that plastic deformations may develop along with a given degree of damage when a local maximum is reached during gradual load/unload tensile tests, what cannot be observed in the monotonic case as tensile loading continuously increases and promotes further damage without significant plastic deformation. Furthermore, the interest of conducting gradual tensile loadings will be discussed in section II.4.1.6 as the unload phase provides a measurement of the longitudinal stiffness which can be used to assess a damage variable at the macroscopic scale. In addition, in the thin specimens investigated in this work, the outer plies have 0° oriented fibers, and the longitudinal strain distribution obtained at the outer surface from DIC analysis conducted on monotonic loading data (see Figure 26a) suggests that plastic deformations are reduced at the crack tip. As a result, the LEFM relationships (see section I.4.2) will be applied in the case of a plane stress state in the section II.4.1.6.

II.4.1.2 Damage mechanisms in QI SEN specimens

The observation of fracture surfaces also show a few bare fiber bundles in the ±45° direction along specimens' free edges, due to fiber-matrix debonding and even fiber bundles pull-out (see Figure 29). The microscopic observations of the edges in QI laminates show a large number of matrix-rich regions, resulting from the non-planar inter-ply structure of woven plies [Vieille et al., 2014]. As far the translaminar fracture is concerned, these plain matrix regions play an important role on the evolution of damage depending on the testing temperature, as PPS matrix ductility increases with temperature. Damage is initiated at the crack tip under the form of inter/intra laminar cracking and transverse splitting (see Figure 29).

After initiation, cracks will propagate until they meet with the matrix-rich regions, resulting in a substantial crack growth resistance of the material (see Figure 30). Indeed, those regions will endure a localized plasticity at 120°C in PPS-based laminates, delaying the onset of cracks, due to the enhanced ductility of the PPS matrix at temperatures higher than materials' glass transition temperature. Consequently matrix-rich regions act as barrier to cracks, and this phenomenon seems to increase the material's toughness (see Figure 30).

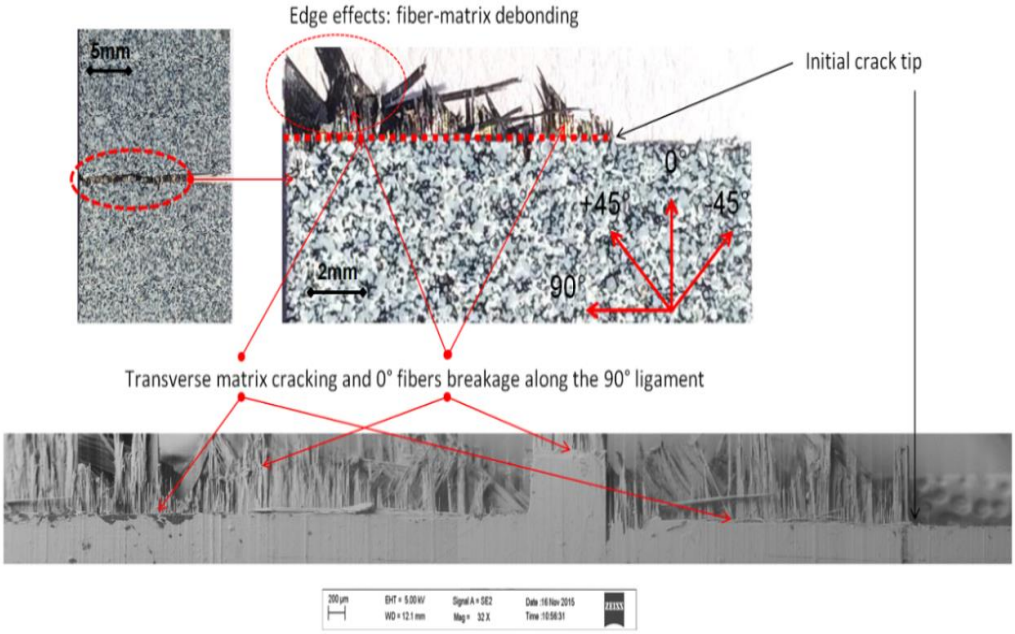

Figure 29. *Macroscopic and SEM observations of fracture surface in QI SEN C/PPS specimens subjected to tensile loadings at 120°C*

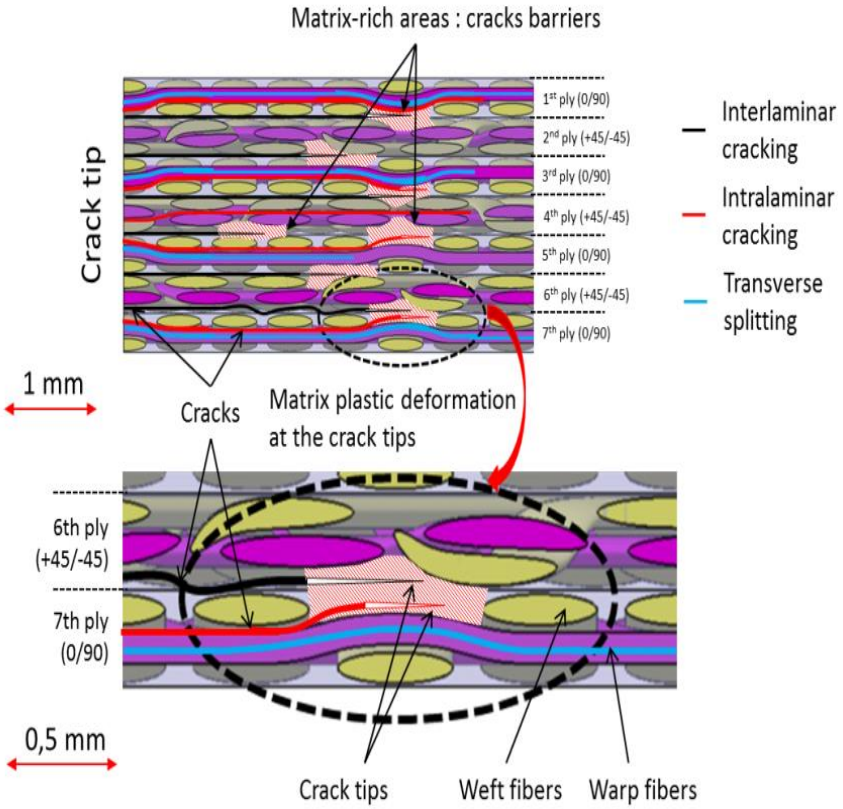

Figure 30. *Schematic representation of damage evolution in QI SEN C/PPS specimens subjected to tensile loadings at 120°C*

II.4.1.3 Evolution of the crack growth

The early crack growth observed in Figure 31 at low stress levels significantly depend on the location of the notch tip as it must lie either in the fiber bundle, in the matrix or at the interface between both constituents. Whether or not a pre-existing crack in a composite will propagate under the action of a tensile loading therefore depends upon the nature of the composite (and therefore the testing temperature), the laminates stacking sequence, but also the type of reinforcement (UD- or woven-ply). The reason is that fracture type is dictated by the rate and amount of energy dissipated (see Figure 28b) which depends on matrix ductility, but also on the rate and kind (monotonic or cyclic) of loading (see Figure 31). The sequential order of discrete failure modes can also greatly influence the life of composite laminates. This is known as the stacking sequence effect [Sih, 1981]. Thus, in UD-ply composites, stress concentrating effects of notches may be almost completely eliminated by large-scale splitting in the 0° and 45° plies and by delamination between the plies, the result often being disintegration of the composite [Reifsnider, 1991]. By contrast, in woven fabrics-reinforced composites, crack-tip damage may remain localized by the complex geometry of the fiber array and the crack may proceed through this damaged zone in a fashion analogous to the propagation of a crack in a plastically deformable metal [Harris et al., 2003]. Potential advantages of using woven fabrics as opposed to cross-ply UD prepreg tapes are observed [Vieille et al., 2013]: woven-fabric laminates exhibit much higher G_{Ic} values (often more than 4–5 times) than the UD counterparts. The unique features and advantageous failure mechanisms are identified: inherent roughness of the fabric; the availability of matrix-rich regions between the fabrics; crack propagation along the undulating pattern of the yarns creating a large fracture surface area. Thus, the crack-stopping ability of composites is significantly driven by the ductility and the toughness of the matrix in fabrics reinforced composites. The effect can be either localized at the crimp in matrix-rich areas of the laminates, or widespread depending on the lay-up. Hence, the macroscopic fracture may appear as quasi-brittle though the fracture at microscopic scale is rather ductile. Regarding the dependency of crack growth to the matrix nature, all fracture processes may be considered as transitions from stable to unstable crack propagation [Durelli, 1981]. In particular, the commonly observed phenomenon of ductile fracture in angle-ply laminates is characterized by slow and stable cracking prior to rapid crack propagation [Albouy et al., 2014]. This is associated with a nonlinear response on the load versus deformation curve and is attributed to progressive crack growth and material deformation beyond the elastic limit. In quasi-isotropic

laminates, as suggested by the crack growth in specimens subjected to gradual load-unload (see Figure 31), the localized matrix plasticization in matrix-rich areas governs the damage mechanisms, as it may delay the cracks onset and subsequent propagation [Albouy W., 2014].

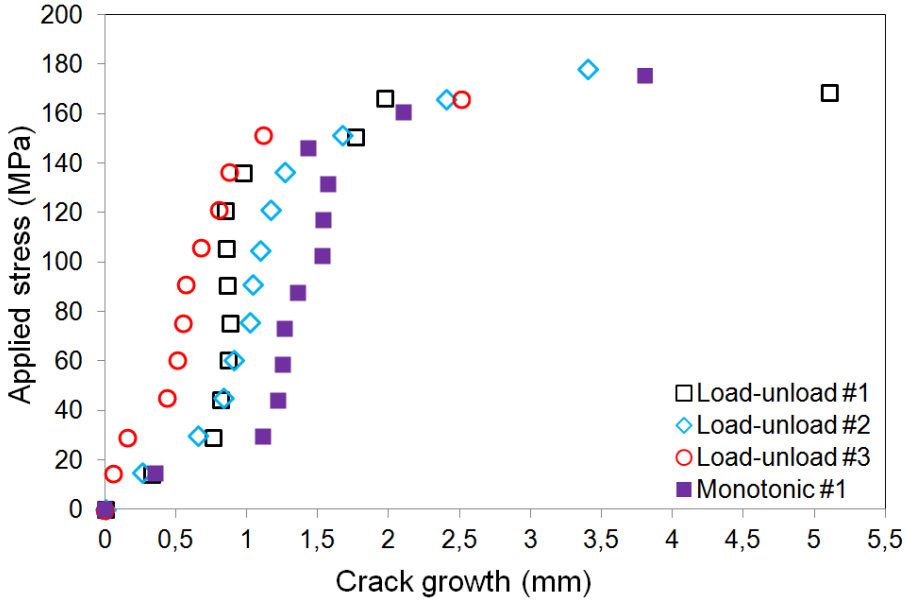

Figure 31. *Evolution of crack growth in QI SEN C/PPS specimens depending on testing conditions*

II.4.1.4 Damage initiation

As was introduced in section II.2, an accurate assessment of the fracture toughness for structural integrity can be achieved by many methods requiring a single-point value [Zhu X-K, 2012]. Depending on the type of fracture behavior, the visual determination of both the initiation point of crack growth and the exact crack length is experimentally difficult [Gross et al., 1964]. Besides, the detection of the initiation point is operator dependent and may be prone to significant statistical variations.

In the present case, CTOD and crack length can be classically measured from DIC in order to estimate the strain energy release rate at damage onset. The CTOD method also provides an estimation of the remote applied stress (143±8 MPa – see Table 2) at crack onset as both the crack length and the CTOD suddenly increase once crack is initiated (see Figure 32). In addition, for materials that exhibit stable crack growth prior to failure, the CTOD method provides toughness values for cracks initiation as the crack is driven stably into the fracture process zone caused by an increase in the applied stress (see Figure 32a).

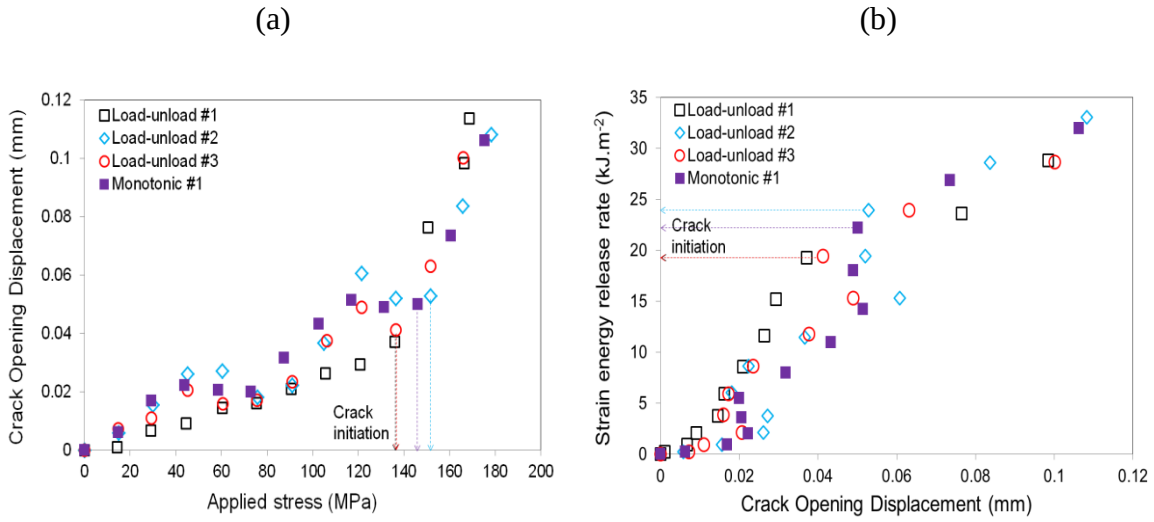

Figure 32. *Determination of crack initiation from CTOD measurements obtained from DIC applied to QI SEN C/PPS specimens at 120°: (a) Evolution of CTOD as a function of the remote applied stress – (b) Evolution of the strain energy release rate as a function of crack opening displacement*

According to Eq. (2), G_I can be computed from the values of the crack length a and the crack opening displacement δ obtained from DIC. From Figure 32b, it is also possible to determine the corresponding values G_{I_init} and therefore K_{I_init} from Eq. (4). Thus, the values for fracture toughness $K_{I\ init}$ at crack initiation were determined from the identified stress for a ratio $a/w = 0.3$: 28.14 MPa.m$^{1/2}$ from DBM method and 29.28 MPa.m$^{1/2}$ from semi-empirical expression (Eq. 5) given by Tada for isotropic materials respectively (see Table 2), hence proving the capacity of CTOD method to determine initiation fracture toughness values K_{I_init} for quasi-isotropic laminates at 120°C (see Table 2).

Crack propagation gauges are also commonly used to quantitatively investigate the onset and propagation of transverse cracks. For QI SEN specimens with a ratio $a/w = 0.3$, the length of crack starts to increase at 150 MPa (mean value) corresponding to crack initiation (see Figure 33). From (Eq. 5), the fracture toughness value was determined as 30.91 MPa.m$^{1/2}$ (see Table 2).

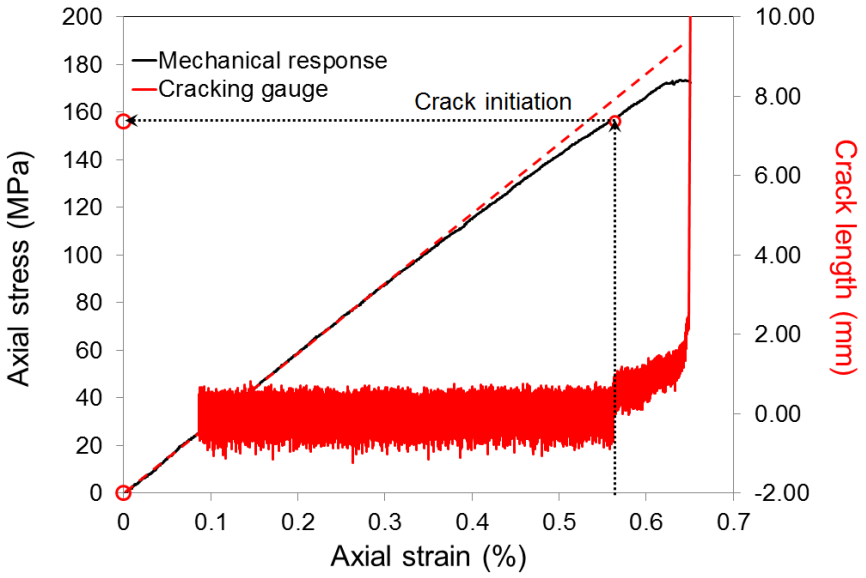

Figure 33. *Tensile response of QI SEN C/PPS at 120°C and identification of the remote applied stress at crack initiation using a cracking gauge*

Considering that the initiation of cracking is associated with a sudden increase in the cumulative AE energy [Sause et al., 2014] [Sih, 1981] [Reifsnider, 1991], the Acoustic Emission technique is an efficient tool to detect the stress at crack onset (see Figure 34). From the monitoring of the AE activity, the jumps in the cumulative AE energy provide reproducible values for σ_{init} and K_{I_init} (see Table 2).

Finally, the values obtained from these different techniques can be compared (see Table 2), and it appears that they are more or less accurate if one considers that the information given by the AE monitoring is the most relevant to identify the stress corresponding to crack onset. As a result, the value obtained with the cracking gauge data is slightly higher as it provides an estimation of the crack onset at the macroscopic scale whereas the COD and AE data rather give an approximation at the microscopic scale. From the macroscopic tensile response standpoint, it is also worth noticing that the ductile-type fracture observed in gradually loaded specimens (see Figure 28b) is initiated at a stress level around 140MPa.

(a)

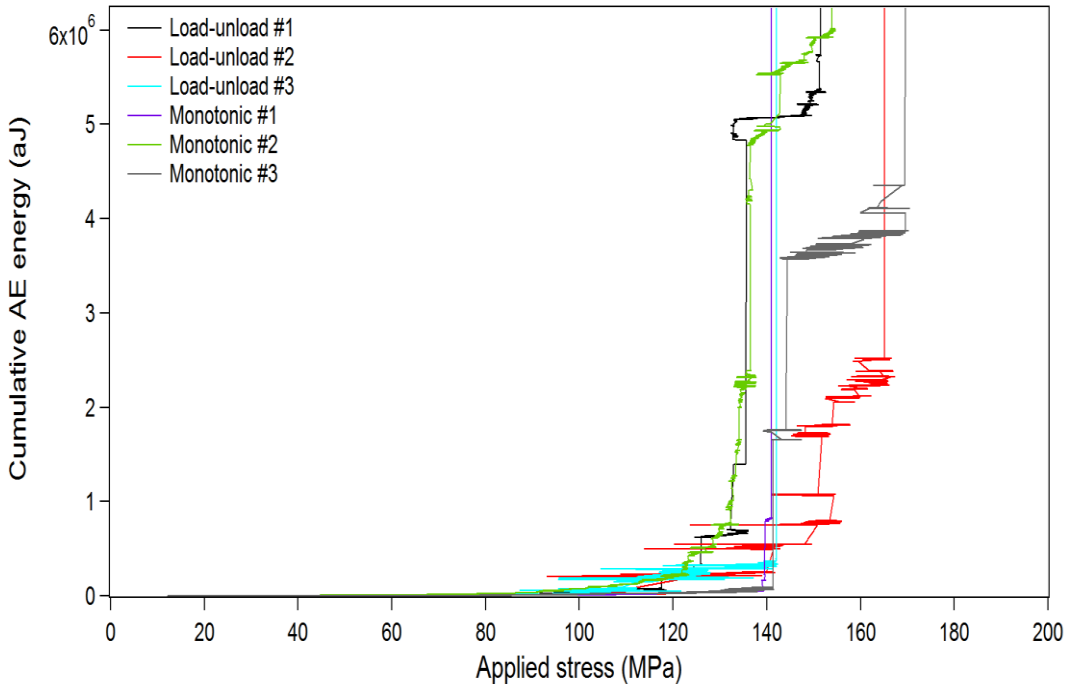

(b)

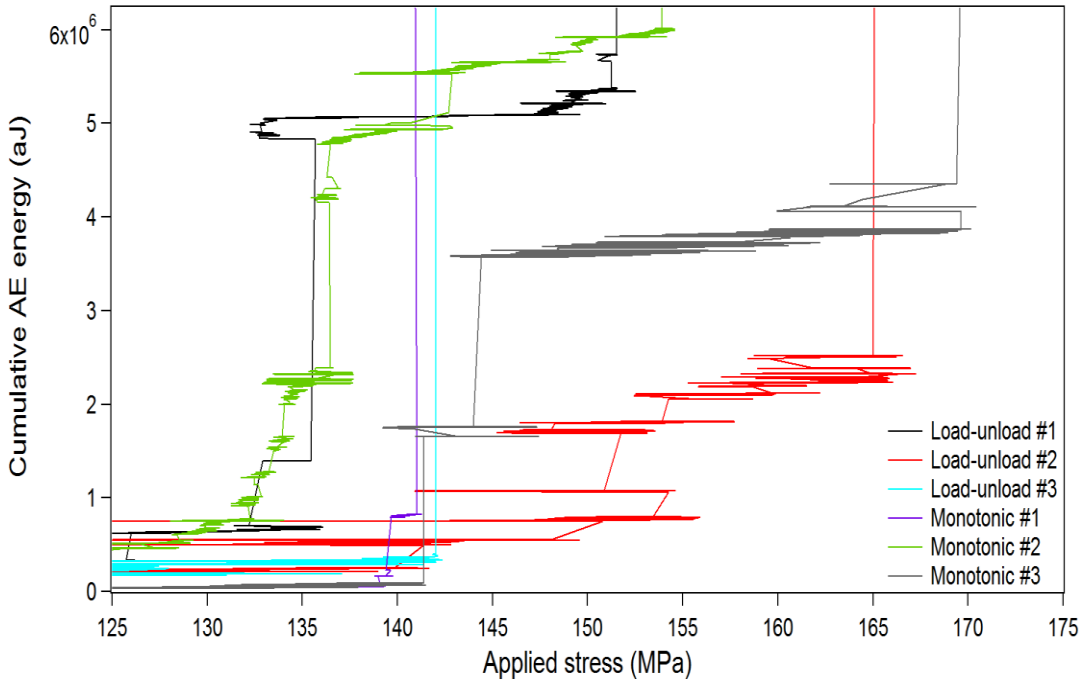

Figure 34. *Detection of the stress at crack onset from the evolution of the cumulated AE energy: (a) Influence of loading conditions – (b) Zoom on the early acoustic activity associated with damage initiation*

Table 2. *Comparison of the estimated stress levels σ_{init} and fracture toughness K_{I_init} at crack initiation*

	CTOD data (DIC)	Cracking gauge data	Acoustic Emission data
σ_{init} (MPa)	143±8	150±8	139±4
K_{I_init} (MPa.m$^{1/2}$)	29.28±1.56 Tada (Eq. 5) 28.14±0.28 Double beam method (Eq. 2) + (Eq. 4)	30.91±1.59 Tada (Eq. 5)	28.55±0.81 Tada (Eq. 5)

II.4.1.5 Damage propagation

In order to calculate the translaminar fracture toughness for crack propagation, the experimental responses of QI SEN specimens with different ratio a/w subjected to tensile loadings at 120°C (see Figure 28a) have been considered to apply the compliance method (see Figure 35a). From (Eq. 3), it is possible to compute the critical strain energy release rate in mode I and from (Eq. 4), to deduce the fracture toughness K_{IC}. As ratio a/w increases from 0.1 to 0.4, it appears that the fracture toughness linearly increases to reach a maximum value at about 37 MPa.m$^{1/2}$ where it starts decreasing (see Figure 35b). It might be explained by mixed failure modes resulting from important edge effects (fiber/matrix debonding and fiber bundles pull-out) in specimens with high initial crack lengths. At the same time, the residual tensile strength decreases.

For a ratio $a/w = 0.3$, the crack propagation fracture toughness has been estimated as about 35 MPa.m$^{1/2}$. In addition, the fracture toughness values calculated for quasi-isotropic laminates can be compared to the values obtained for isotropic materials (see Figure 35b),

from semi-empirical expressions established by different authors [Tada et al., 2000], as defined by (Eq. 5) in Section I.4.2. From Table 3, it can be observed that the average values obtained by the compliance method and Tada's formula are virtually the same (about 34 MPa.m$^{1/2}$).

(a) (b)

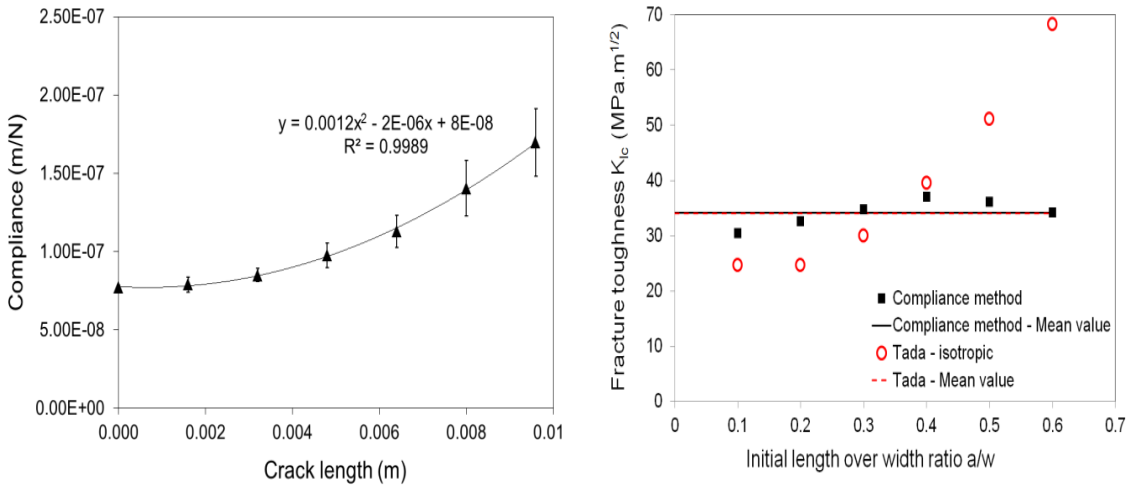

Figure 35. *Values of critical fracture toughness K_{IC} as a function of the ratio a/W for QI C/PPS laminates at 120°C [Vieille et al., 2016]: (a) Compliance method – (b) Comparison with the semi-empirical formula proposed for SEN isotropic specimen*

Table 3. *Comparison of the critical fracture toughness K_{IC} values obtained by different methods*

	CTOD data ($a/w = 0.3$)	Compliance method (Average value for $a/w = 0.1$ to 0.6)	Tada method (Average value for $a/w =$ 0.1 to 0.6)
K_{Ic} (MPa.m$^{1/2}$)	35.33±1.17 (Eq. 5)	34.15±2.39	33.99±17.25

II.4.1.6 Correlation between the mode I strain energy release rate G_I and the cumulative AE emission

Classically, the cumulative AE energy and events can be used to investigate damage evolution within composite materials depending on the applied stress (see Figure 36).

(a)

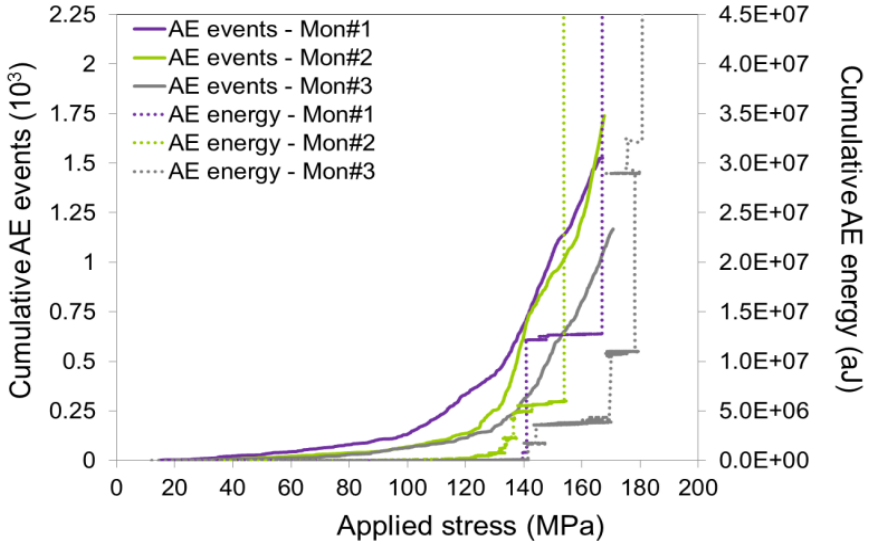

(b)

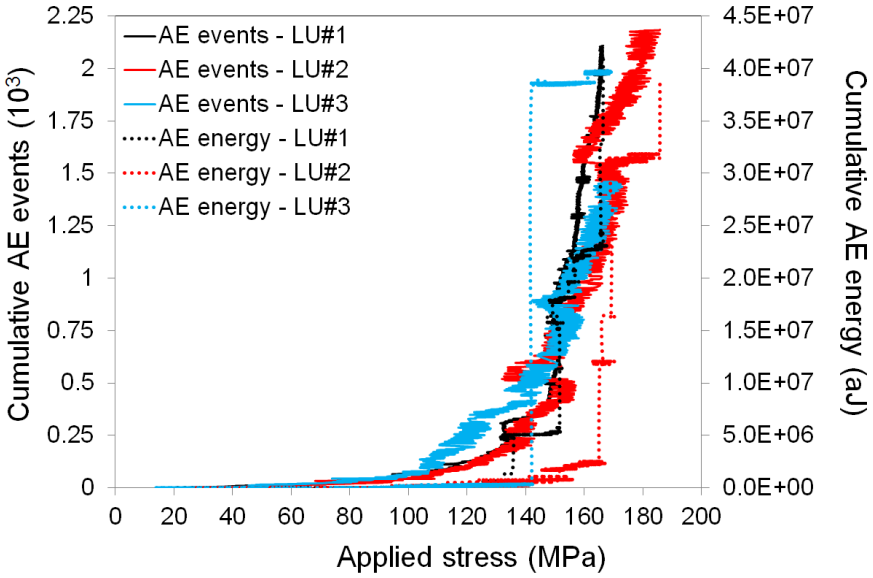

Figure 36. *Correlation between the cumulative AE energy and events in QI SEN C/PPS specimens subjected to tensile tests at 120°C: (a) Monotonic loading – (b) Gradual load-unload*

Considering the conclusions from a few studies in the literature, it is possible to correlate the strain energy release rate in mode I G_I with the cumulative AE energy (as introduced section I.4.2.1). For stable crack propagation, proportionality between the AE emission energy release rate and the associated failures micro-mechanical energy release rate has been reported in PMCs [Sause et al., 2009].

Following the approach initially developed by [Ndiaye et al., 2000], Oskouei et al observed that a linear correlation can be established between G_I and W_{AE} [Oskouei et al., 2010] [Oskouei et al., 2012] [Sih et al., 1965]:

$$G_I = \alpha . W_{AE} + \beta \tag{13}$$

Where α and β are materials parameters which can be identified from a tensile test on SEN specimens with a given ratio a/w. This result implies that macroscopic failure activity is directly linked to microscopic activity. The slope α of this linear function depends on matrix toughness. Thus, this correlation between AE energy and fracture energy can be useful to determine the damage tolerance of a composite material by using AE energy as a damage criterion.

What is also interesting to underline in the work of [Ndiaye et al., 2000] is the influence of test temperature on the value of the critical strain energy release rate G_{Ic}, which is expected to reflect on composite toughness as matrix toughness is higher at high temperature. Indeed, they concluded that specimens tested at temperatures (e.g. T=275°C) higher than the glass transition temperature (T_g=200°C) of the epoxy resin have higher values of G_{Ic}. The same effect is also expected in the present study as the PPS-based laminates were tested at test temperatures T>Tg, though the influence of temperature is not specifically investigated here.

From the application of (Eq. 5) to the experimental data, the values of G_I can be computed to plot the curves representing G_I vs the crack opening displacement on the one hand (see Figure 37a), and the curves showing correlation between G_I and the cumulative AE energy (see Figure 37b).

(a)

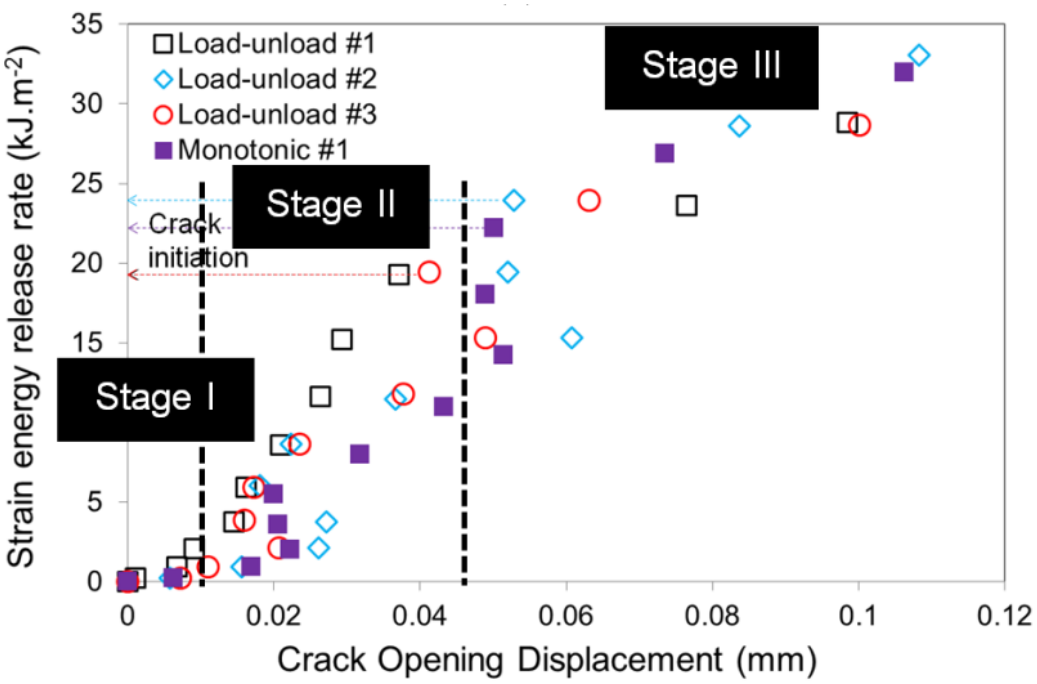

(b)

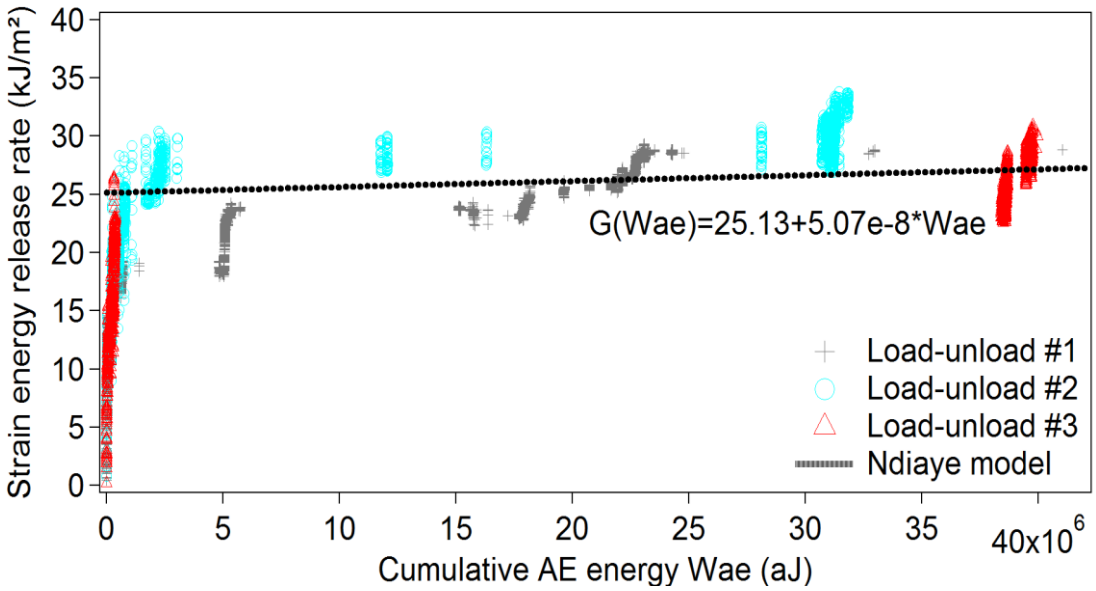

Figure 37. *Evolution of the strain energy release rate in QI SEN C/PPS specimens subjected to tensile loadings at 120°C: (a) G_I vs CTOD - (b) Correlation between G_I and the cumulative AE energy*

On the one hand, these curves are useful to determine the mean value G_{I_init} corresponding to crack initiation. According to (Eq. 13), the materials parameters α and β can be identified from the least square method applied to the set of experimental points:

$$G_I(W_{AE}) = 25.13 + 5.07 * 10^{-8}.W_{AE} \quad (14)$$

This relationship can be relevant to define a criterion to predict the failure of studied materials based on the knowledge of the cumulative AE energy. First of all, this expression gives the mean value of $G_{I\_init} = 25.13 kJ/m^2$ corresponding to the value at the origin (see Figure 37b). Second of all, from the mean value of the cumulative AE energy at failure, it is possible to estimate the critical value $G_{Ic} = 27.04 kJ/m^2$, and then the critical fracture toughness $K_{Ic} = 33.09 MPa.\sqrt{m}$. This value can be compared to the value $K_{Ic} = 34.15 MPa.\sqrt{m}$ obtained by means of the compliance method applied to different ratio a/w [Vieille et al., 2016].

On the other hand, the curves representing G_I vs CTOD can also be used to study damage chronology (see Figure 37a), as well as the evolution profile of the cumulative AE events (see Figure 38). From these curves, three primary stages can be clearly identified. At low stress levels (Stage I), a few AE events can be observed (see Figure 39) and may be associated with random micro-damages while 0° fibers are gradually loaded. Stage II is characterized by a linear evolution of the cumulative AE events which tend to localize at the crack tip. Finally, the beginning of stage III corresponds to the initiation of macroscopic crack growth. From all the experimental data representing the cumulative AE events vs applied stress, a power law can be identified as follows (see Figure 38):

$$Cumulative\ AE\ events\ (\sigma) = 5.6 * 10^{-4} + 1.1 * 10^{-14} * \sigma^{6.35} \quad (15)$$

(a)

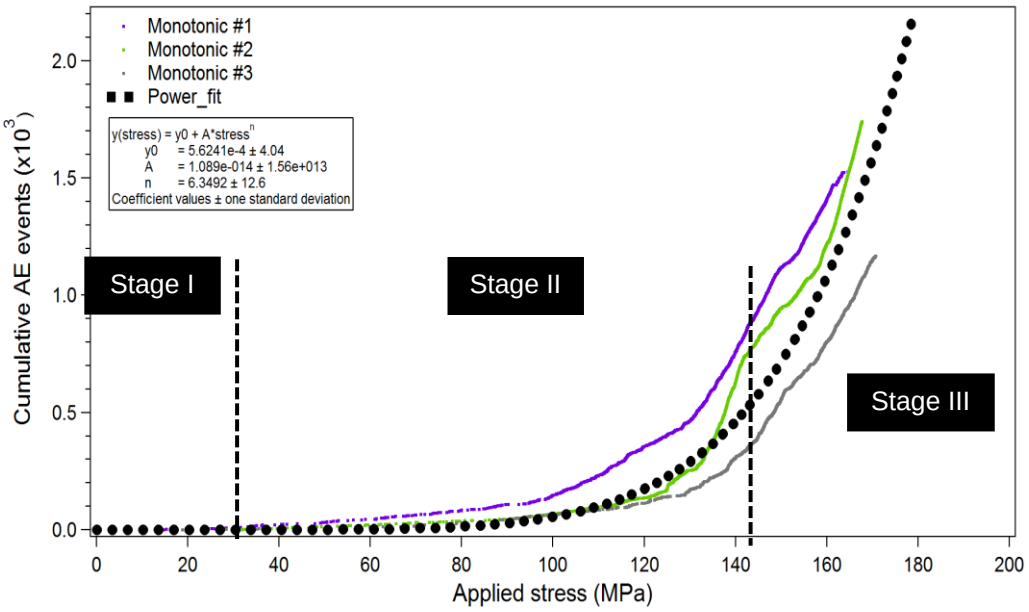

(b)

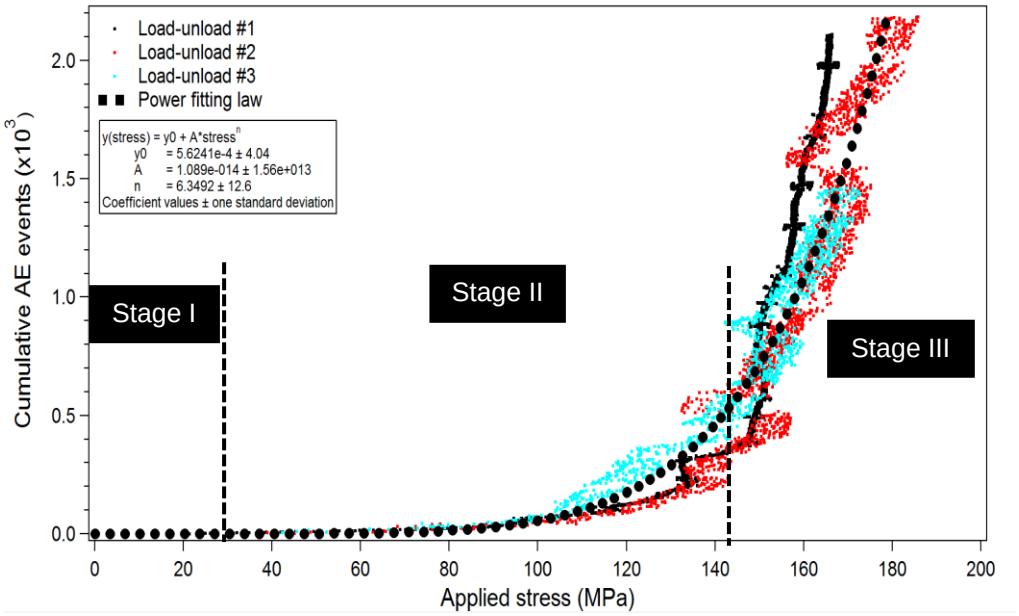

Figure 38. *Evolution of the cumulative AE events in QI SEN C/PPS specimens subjected to tensile loadings at 120°C: (a) Monotonic loading – (b) Gradual load-unload*

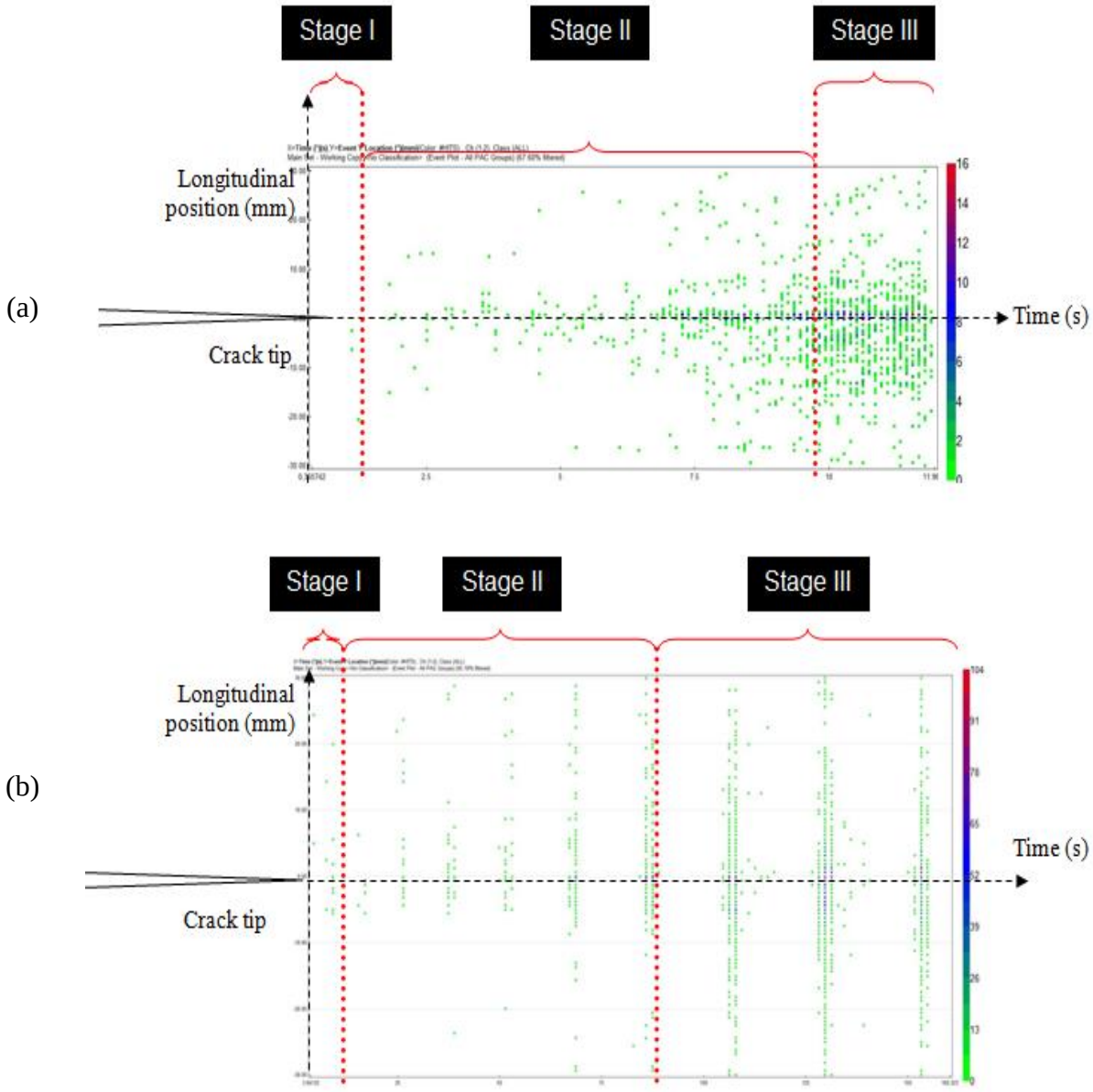

Figure 39. *Localization of the AE events density vs time in QI SEN C/PPS specimens subjected to: (a) monotonic tensile tests at 120°C – (b) gradual load/unload tensile tests at 120°C*

II.4.1.7 Macroscopic and microscopic analyses of translaminar failure

For structural design, AE techniques provide much information (cumulative energy, cumulative events, events rate) to account for the degree of damage during service at microscopic scale. Indeed, through the prediction of the transverse crack density, micromechanical models (e.g. shear-lag damage analysis) have been developed to estimate

the damage degree in PMCs [Nguyen et al., 2007] [Henaff-Gardin et al., 1996] [Gao et al., 1999] [Gao et al., 1999].

The question here is to compare the damage evolution profiles during loading at both microscopic and macroscopic scales. At microscopic scale, the monitoring of AE signals also provides in-situ and real time information to localize the AE events in the area near the crack tip during loading (see Figure 39). From a discrete steps tensile loading, it is possible to evaluate the density of AE events as a function of maximum local stresses applied to specimens. As stress increases, damage occurs not only along the crack tip where significant stress concentrations operate, but also in its surroundings. The density of AE events confirms that transverse cracking coming along with fibers breakage are the primary damage mechanisms, and indicates that there are also secondary micro-damages above and below the macroscopic transverse crack. Until the initiation of the crack, the evolution is virtually independent from the type of loading (see Figure 40a), but the degree of damage significantly differs afterwards. Gradual load/unload tensile tests lead to more damage, as the cumulative AE events is about three times as high at failure. The correspondence of crack onset point on the curves is in agreement with the values determined by others techniques in section II.4.1.6. The interest to use a gradual load/unload tensile test also consists in measuring the residual longitudinal stiffness after each unloading. Indeed, from the macroscopic standpoint, it appears that the longitudinal stiffness gradually decreases as the maximum stress level increases (see Figure 34a).

In order to estimate the macroscopic cumulated damage in QI composite materials subjected to cyclic loading, the changes in longitudinal stiffness $E(N)$ measured at each cycle N are an excellent indicator of the damage development $d(N)$ [Albouy et al., 2014] [Ladevèze et al., 1992] [Stinchcomb, 1986] [Poursartip et al., 1989] [Rotem, 1989]:

$$d(N) = \frac{E_0 - E(N)}{E_0 - E_f} \tag{16}$$

where E_0 is the initial longitudinal stiffness value of the undamaged material, and E_f is the longitudinal stiffness at cycle before failure.

(a)

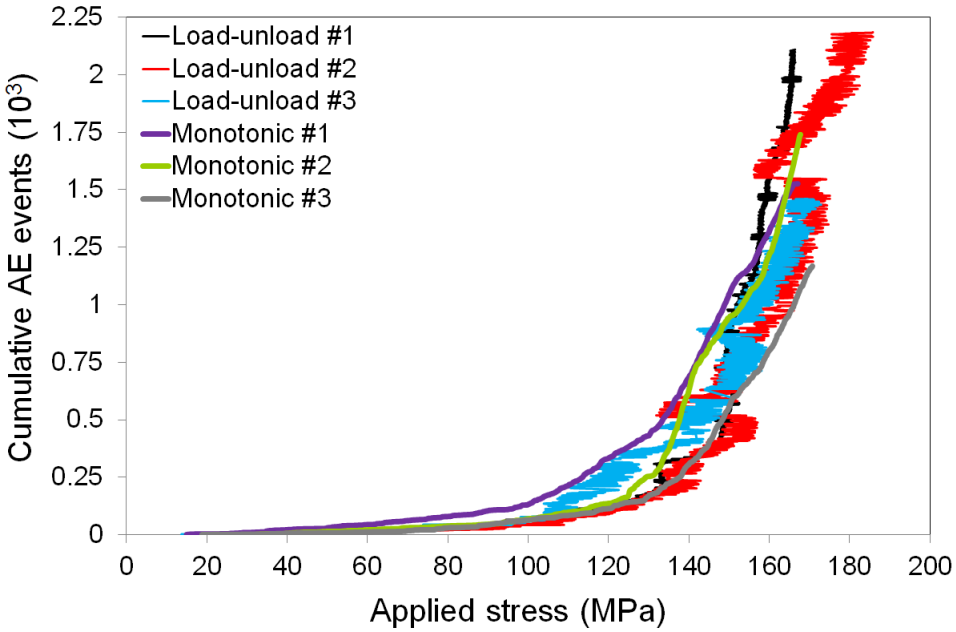

(b)

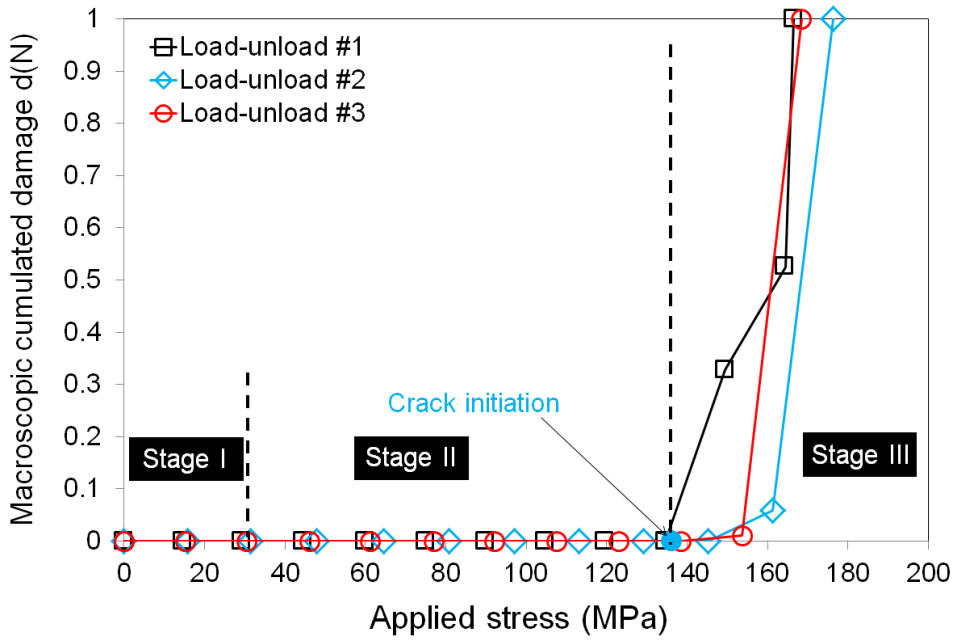

Figure 40. *Profiles of damage evolution: (a) Comparison of the cumulative AE events evolution depending on the type of loading – (b) Comparison of damage profiles obtained from AE data (microscopic scale) and a macroscopic cumulated damage variable based on stiffness measurements*

#LU1

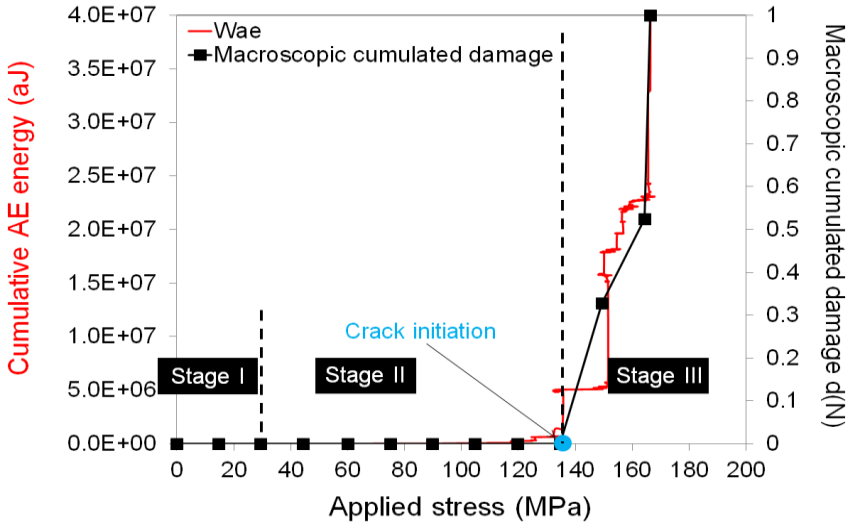

#LU2

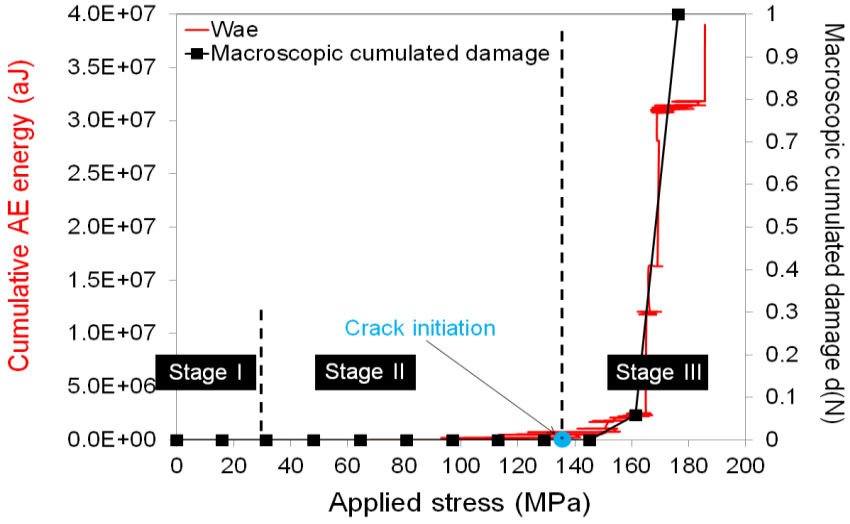

#LU3

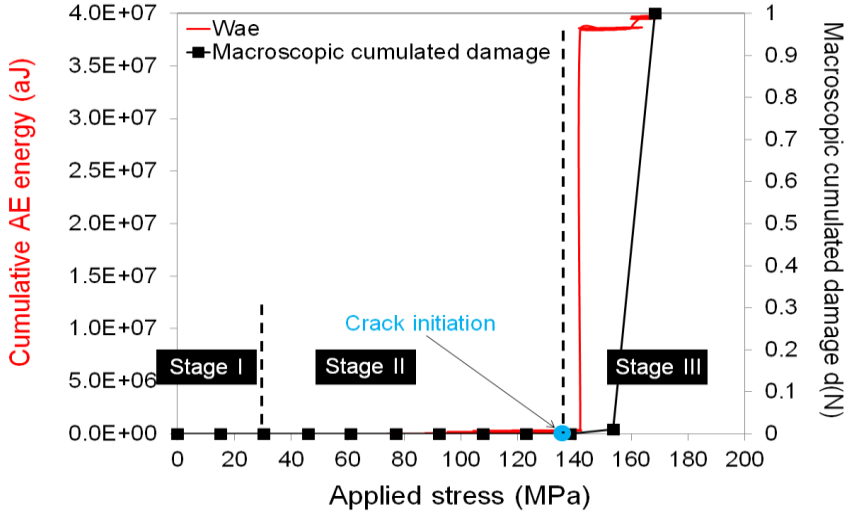

Figure 41. *Correlation between the macroscopic cumulated damage variable and the cumulative AE energy during load-unload tensile tests at 120°C on QI SEN C/PPS specimens*

From the previous definition, damage evolution can be classically investigated through the measurement of the laminates' stiffness in discrete steps (every 5% of the ultimate tensile strength) during gradual load/unload tensile tests.

At macroscopic scale, it is therefore possible to investigate the influence of matrix toughness on cumulated damage depending on the applied stress level (see Figure 40b). Thus, the similarity between the evolutions given by the cumulative AE energy at microscopic scale and a macroscopic damage variable based on stiffness measurements (see Figure 41) validates the ability of both approaches to quantify the damage degree in fiber-reinforced PMCs [Baker et al., 2015]. Finally, the existing of clearly identifiable mechanical thresholds (stress or CTOD) indicates that no damage occurs under these thresholds, a proof which is very important for structures where no damage is allowed during service.

II.4.2 **AP laminates (Matrix-dominated behavior)** [Chabchoub el al. 2017a]

The purpose of the present section is to determine the strain energy release rate J in angle-ply (AP) thermoplastic-based laminates whose mechanical behavior is mainly matrix-dominated by matrix behavior resulting in highly ductile behaviors at high temperature (120°C>T_g). For this purpose, a particular attention is paid to determine η_{el}- and η_{pl}-factors. On the one hand, the compliance method is applied to identify η_{el}-factor. On the other hand, the load separation criterion is used to evaluate η_{pl}-factor using plastic and total displacement. Then, the real initial crack length values and those calculated from η_{pl}-factor using plastic and total displacement are compared. Finally, in order to investigate the influence of the initial notch lengths (hence the stress intensity factor) on J-R curves, the separation method and a Digital Image Correlation technique are applied to evaluate the crack growth.

II.4.2.1 About J-integral estimation procedures

In brittle materials, fracture mechanics is often studied using LEFM framework through the stress intensity factor K or the strain energy release rate G. For materials characterized by a small plastic zone around the crack tip, it is possible to make a correction when calculating the stress intensity factor K. However, for large plastic zones, it becomes no longer possible to use the LEFM framework [Viswanathan, 1993]. Consequently, the J-integral and the crack opening displacement (COD) methods have been considered as efficient crack initiation parameters, as part of the elastic-plastic fracture mechanics (EPFM) procedure [Viswanathan, 1993] [Ruggieri, 2012]. For ductile fracture, the crack tip is dominated by plastic

deformation. Therefore, the toughness is often studied using the J-resistance curve (J-R curve) as the resistance of the material to fracture increases as the crack length grows [Vieille et al., 2016] [Zhu X-K, 2012] [Bernal et al., 1995].

The J-integral is essentially an energy criterion. Initially proposed by [Rice, 1968] to characterize the intensity of the elastic-plastic stress-strain fields at the crack tip, this method can be applied to elastic and elasto-plastic behaviors. In fact, the critical value of J_C obtained reduces to the strain energy release rate or Griffith G_C value in the case of elastic brittle materials.

Researchers have proposed many techniques to determine the J-integral. One of the earliest methods used for the evaluation of J-integral is the multispecimen technique. This method introduced by [Begley et al., 1972] and based on the energy rate interpretation form initially proposed by [Rice et al., 1973] as an equivalent to the curve integral form [Chabchoub et al., 2016] [Bouchard, 2000]. According to the technique proposed by [Sharobeam et al., 1991], it requires multiple load-displacement records for the same specimens but for different initial crack lengths.

[Rice, 1968] showed that the J-integral essentially consists in determining the energy release rate or work done on a nonlinear elastic material containing a crack per unit fracture surface area:

$$J = -\frac{1}{B}\frac{dU_p}{da} \tag{17}$$

where U_p is the potential energy for the cracked body, B denotes the specimen thickness and a is the crack length.

[Rice et al., 1973] have proposed to separate J into elastic and plastic components:

$$J = J_{elastic} + J_{plastic} \tag{18}$$

with $J_{elastic} = G$.

[Sumpter et al., 1976] modified this form to be:

$$J = \eta_{el}.\frac{A_{el}}{B.b} + \eta_{pl}.\frac{A_{pl}}{B.b} \tag{19}$$

where A_{el} and A_{pl} denote the elastic and plastic parts of the area under the load-displacement record respectively. η_{el} and η_{pl} are functions of crack length over specimen width ratio a/W, loading conditions and specimen geometry. b is the length of the uncracked ligament.

According to [Turner, 1980] and [Roos et al., 1986], η_{el} and η_{pl} are not equal and should be calculated separetely. η_{el} can be determined from the elastic compliance [Turner, 1973] using the following expression:

$$\eta_{el} = \frac{b}{C}.\frac{dC}{da} \tag{20}$$

where C is the compliance.

The use of the η-factor significantly simplifies the determination of J-integral [Zhu X-K, 2012], and Eq. (19) present a very convenient way for evaluating *J* experimentally for any fracture specimen from a simple load–displacement record, provided that the η_{el} and η_{pl} factors are determined a priori for that specimen, hence, the growing interest for the determination of η_{pl} [Cassanelli et al., 2003] [Cassanelli et al., 2001] [Kim et al., 2001] [Bernal et al., 1996] [Sharobeam et al., 1991].

The early approaches used for determining the η_{pl}-factor were based on the plastic limit analysis. [Clarke et al., 1979] gave an approximate fitted function of the η_{pl} factor in the case of compact tension specimens with deep cracks as:

$$\eta_{pl} = 2 + 0.522(\frac{b}{W}) \tag{21}$$

[Sumpter, 1987] obtained an approximation of the η_{pl} factor for specimens in pure bending conditions according to crack sizes as:

$$\eta_{pl} = \begin{cases} 2, & if\ \frac{a}{W} > 0.282 \\ 0.32 + 12\left(\frac{a}{W}\right) - 49.5(\frac{a}{W})^2 + 99.8(\frac{a}{W})^3, & if\ a/W \leq 0.282 \end{cases} \tag{22}$$

In order to obtain more accurate values of η_{pl}-factor, finite element methods can be used [Kirk et al., 1993] [Nevalainen et al., 1995].

The load separation method

Unlike other methods used for determining J-integral, the load separation method has been widely accepted and used because it allows us to evaluate J from a single load-displacement record for each crack length. Firstly performed by [Ernst et al., 1979] and adapted by [Sharobeam et al., 1993] in the case of ductile materials, this method assumes that the applied load F can be expressed as a product of two independent functions: a geometry-dependent function $G\left(\frac{a}{W}\right)$ and a deformation-dependent function $H\left(\frac{\Delta_{pl}}{W}\right)$. Therefore, it is possible to write:

$$F = G\left(\frac{a}{W}\right).H\left(\frac{\Delta_{pl}}{W}\right) \tag{23}$$

where Δ_{pl} denotes the plastic displacement.

In order to investigate the separation in different configurations, the separation parameter S_{ij} can be used [Sharobeam et al., 1991]. They suggested that, in the separable region, S_{ij} can be defined as the load ratio between two different records at constant plastic displacement (see Figure 42):

$$S_{ij} = \frac{F(a_i)}{F(a_j)}\Big|_{\Delta_{pl}} = \frac{G(\frac{a_i}{W}).H(\frac{\Delta_{pl}}{W})}{G(\frac{a_j}{W}).H(\frac{\Delta_{pl}}{W})} = \frac{G(\frac{a_i}{W})}{G(\frac{a_j}{W})} \tag{24}$$

where $F(a_i)$ represents the applied load to a tested specimen (i) with a crack length a_i and $F(a_j)$ represents the applied load to a reference specimen (j) with a crack length a_j.

From the above equation, S_{ij} is independent from the plastic displacement or the deformation properties as it depends only on the crack lengths a_i and a_j. In addition, as it's often difficult to separate the plastic displacement component from the total displacement when trying to fit the initial displacement with a linear function in order to define the first point of plastic displacement, [Cassanelli et al., 2003] proposed to study the separation parameter using total displacement:

$$S_{ij} = \frac{F(a_i)}{F(a_j)} \Big|_{\Delta_{total}} = \frac{G(\frac{a_i}{W}).H(\frac{\Delta_{total}}{W})}{G(\frac{a_j}{W}).H(\frac{\Delta_{total}}{W})} = \frac{G(\frac{a_i}{W})}{G(\frac{a_j}{W})} \quad (25)$$

According to the conclusion done in [Sharobeam et al., 1991], it is finally possible to assume that for a given material in the separable region, the separation parameter S_{ij} is given by a power law as follow:

$$S_{ij} = \frac{G\left(\frac{b_i}{W}\right)}{G\left(\frac{b_j}{W}\right)} |_{\Delta_{pl}} = A_1 \left(\frac{b_i}{W}\right)^m |_{\Delta_{pl}} \quad (26)$$

where $A_1 = \left(\frac{b_j}{W}\right)^{-m}$

Comparing the energy rate interpretation and the modified test record area form of J_{pl}, η_{pl} becomes:

$$\eta_{pl} = \frac{-\frac{\partial U_{pl}}{\partial a} |_{\Delta_{pl}}}{\frac{A_{pl}}{b}} \quad (27)$$

using the separable form (see Eq. (23)), an alternative expression could be obtained:

$$\eta_{pl} = -\frac{G'\left(\frac{a}{W}\right)}{G\left(\frac{a}{W}\right)} \frac{b}{W} \quad (28)$$

where $G'\left(\frac{a}{W}\right)$ is the derivative of $G\left(\frac{a}{W}\right)$ with respect to $\frac{a}{W}$.

Introducing $G\left(\frac{b_i}{W}\right)$ in Eq. (28) results in:

$$\eta_{pl} = \left(\frac{b_i}{W}\right) \frac{m\left(\frac{b_i}{W}\right)^{m-1}}{\left(\frac{b_j}{W}\right)^m} = m \quad (29)$$

Eq. (29) is particularly relevant as it will enable us to determine η_{pl} and then calculate the strain energy release rate for an elastic-plastic material.

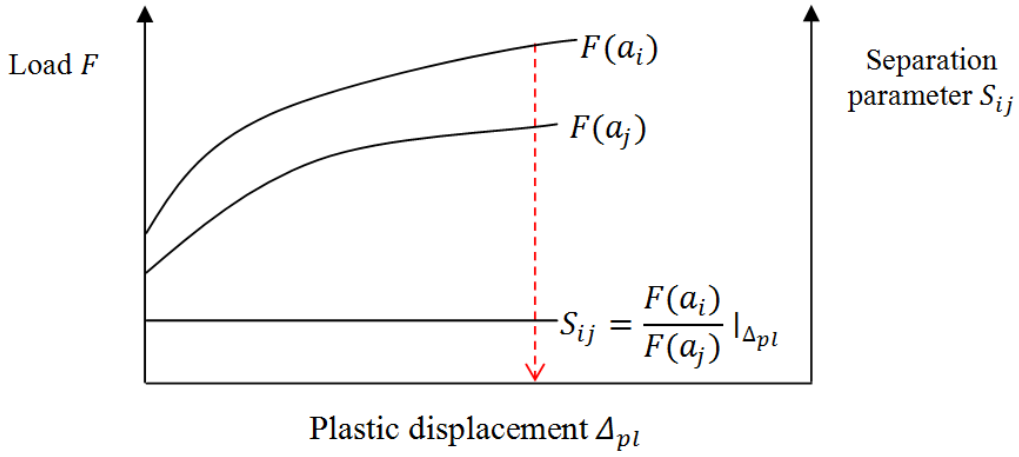

Figure 42. *Determination of the separation parameter from two load-displacement record*

II.4.2.2 Macroscopic tensile response of AP SEN specimens

The tested notched laminates are characterized by a highly ductile behavior at 120°C because the thermomechanical response of AP laminates is mainly dominated by the matrix behavior (see Figure 43a). The evolution of the damage in AP laminates is accompanied by a gradual plasticization of the matrix carrying along with the rotation of fiber bundles, and a necking of specimens [Vieille et al., 2011] [Albouy et al, 2014]. It's worth noting that, in the case of TP based composites, these deformation mechanisms are enhanced as temperature increases. In addition, woven-ply laminates have a periodic distribution of matrix-rich areas in their microstructure resulting from the undulation at the crimp between warp and weft fibers [Vieille et al., 2013]. These matrix-rich areas are instrumented in dissipating the mechanical energy brought to the specimen into local plastic deformations.

The observation of fracture surfaces (see Figure 44a) suggests that, after initiation, cracks will propagate along 45° oriented fibers. In fact, the tensile loading at 45° with respect to the fiber direction induces an in-plane shear effect in the weft and warp direction at the crack tip. In particular, this effect is amplified at the crimp. As weft fibers undulate over warp fiber bundles, weft fibers are curved and overstressed and usually fail first. Therefore, the crack will propagate along the warp direction which requires the least energy.

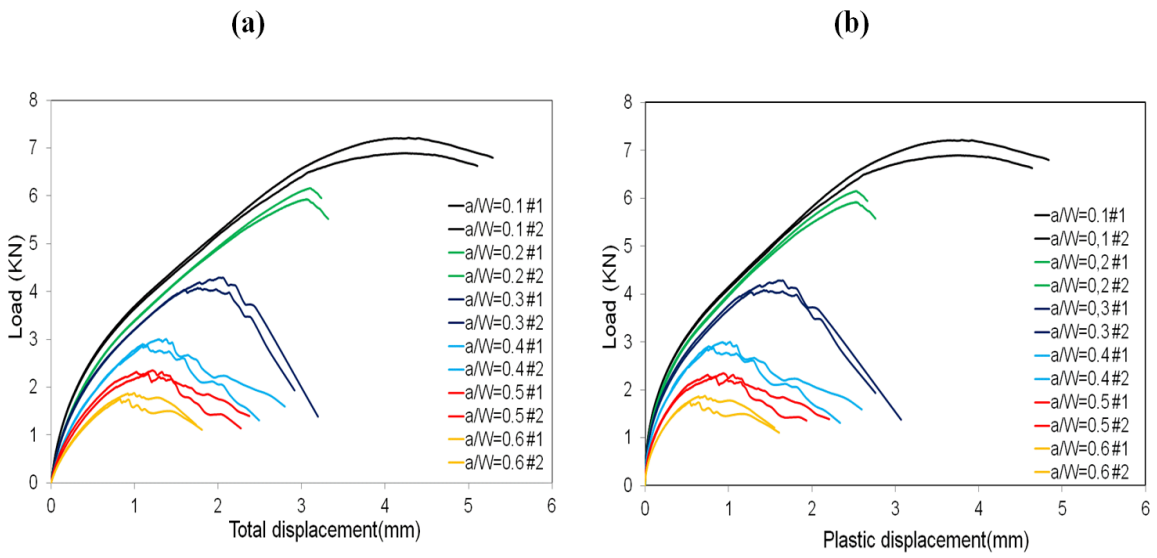

Figure 43. *(a) Load versus total displacement in SEN AP C/PPS specimens at 120°C: influence of the ratio a/W of the initial crack length over the specimen width on the monotonic behavior, and (b) Load versus plastic displacement of SEN AP C/PPS specimens at 120°*

As PPS matrix ductility increases at high temperature, leading to local plasticization, the ability of the matrix to transmit load to fibers impaired at high temperature, hence these fibers tend to rotate and stress concentration zones appear at the crimp. In C/PPS laminates, when matrix can no longer plastically deforms, matrix cracking and splitting take place along the 45° fiber direction as well as an extensive delamination and pull out of fibers bundles resulting from fiber-matrix debonding along the edges (see Figure 44 and Figure 45).

From the macroscopic standpoint, the large plastic deformations lead to a significant dissipation of mechanical energy in specimens with small initial notches (e.g. *a/W=0.1* or *0.2*) (see Figure 43). This result can be explained by the increase of the crack length coming along with large fiber rotations as applied stress increases. Thus, the neighboring fibers cannot support the tensile loading once cracks propagate. However, as ratio *a/W* increases, the cracks propagate more gradually and without an important fiber rotation. In other words, contrary to specimens with larger initial notches, specimens with small crack length are able to store sufficient strain energy during mechanical loading to cause catastrophic failure [Agarwal et al., 1983].

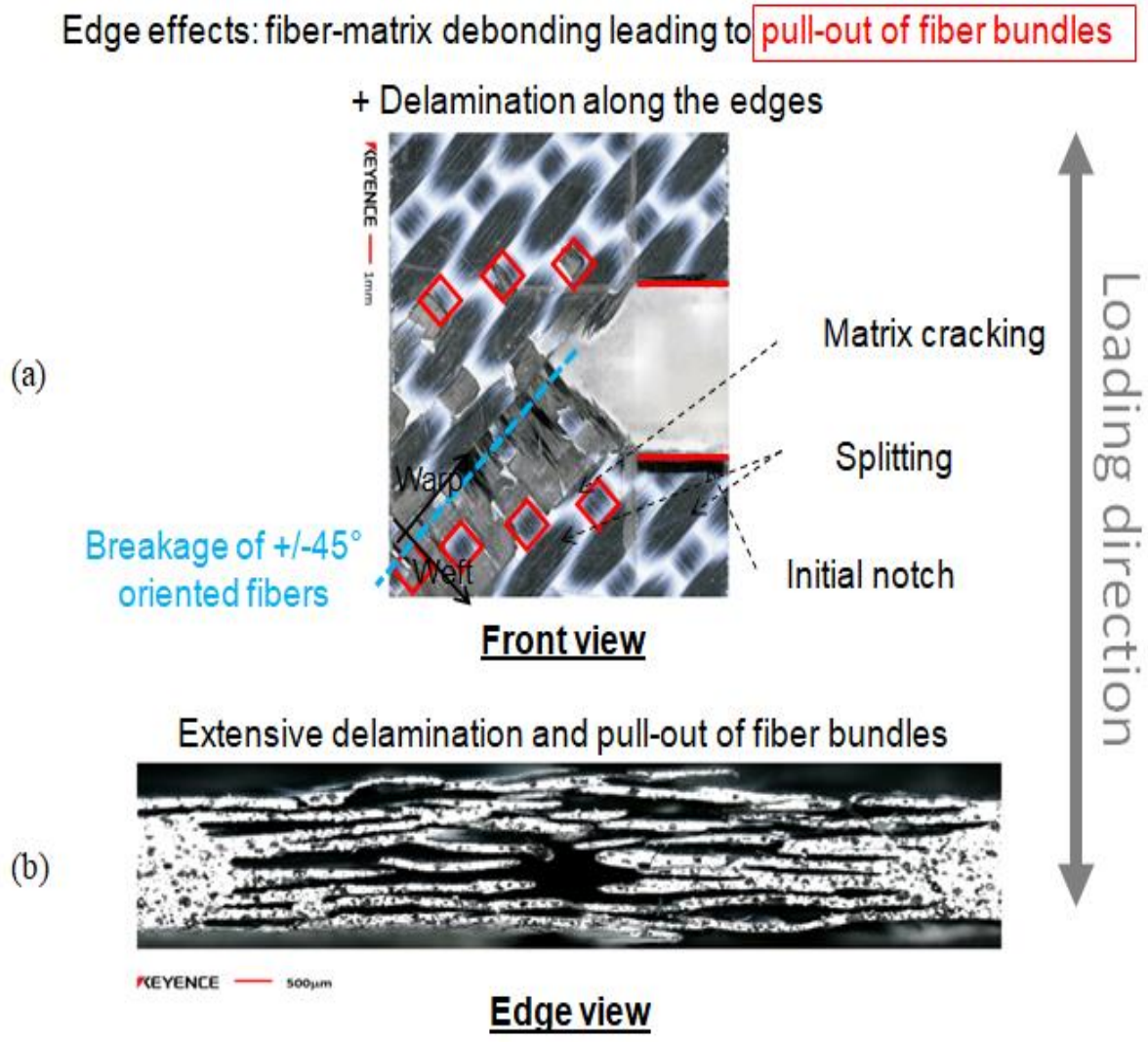

Figure 44. *Observations of fracture surface in SEN AP C/PPS specimens subjected to tensile loadings at 120 °C: (a) Front view-(b) Edge view*

Figure 43b shows the load vs plastic displacement curves for AP laminates obtained after subtracting the elastic displacements from the load vs displacement curves. This definition includes both the plastic phenomena and the damage phenomena which may appear especially when the initial notch is larger. Indeed, for specimens with small initial notches, where plastic phenomena are predominant (the notch gradually opened and blunted without crack propagation prior to peak load). All the mechanical energy dissipated in this form is then not devoted to transverse breakage or damage. Thus, there is no loss of stiffness.

The elastic displacements were measured using the compliance obtained from the initial slope of the load-displacement curves.

In addition, one can notice that the load increases with the plastic displacement to reach a maximum where the load borne by the specimen decreases due to the onset of transverse propagation. Hence the assumption of stationary crack can no longer be valid [Bernal et al., 1996].

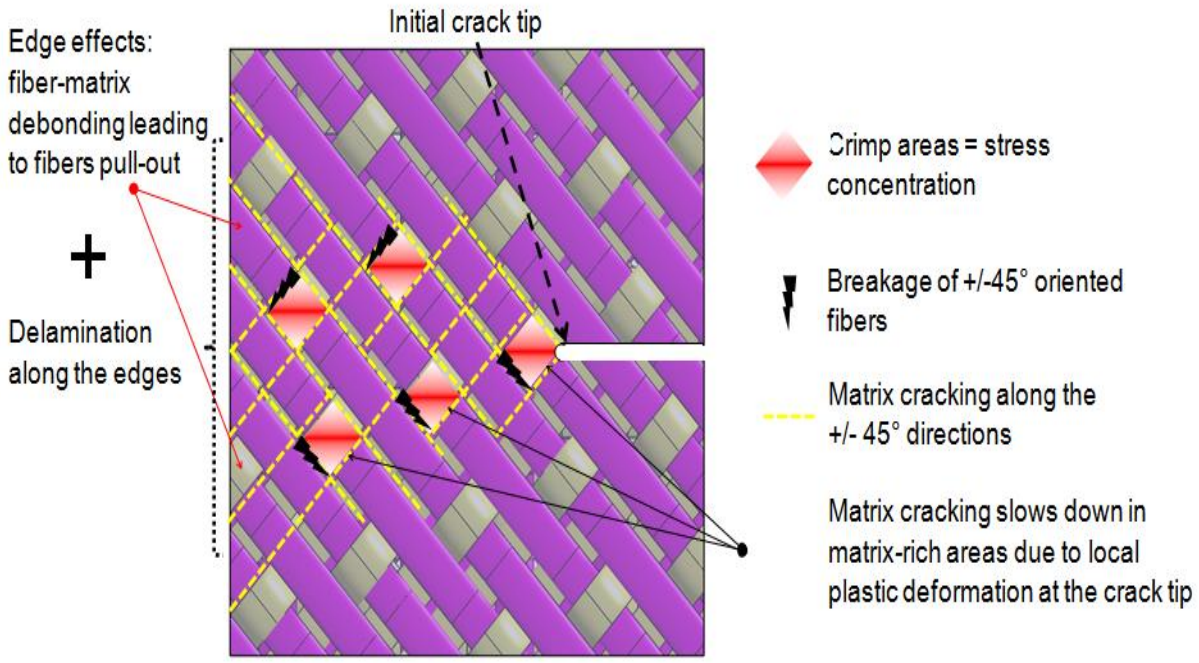

Figure 45. *Illustration of the damage mechanisms in SEN AP C/PPS specimens subjected to tensile loadings at 120 °C*

II.4.2.3 η-factor in SEN AP specimens

The separation parameters were determined from plastic and total displacement for different a_i/W values (0.1 - 0.2 - 0.3 - 0.5 - 0.6) with respect to an arbitrary a_j/W=0.4 reference value (see Figure 47 and Figure 48). The separation parameter S_{ij} was considered as a constant assuming a S_{ij} tolerance of ±0.01, corresponding to a crack length estimation uncertainty of ±0.05 mm. According to Figure 44 and Figure 45, three different regions can be distinguished: an unseparable zone at the beginning of the mechanical response where the plastic pattern has not been fully developed, a separable zone characterized by a constant separation parameter, proving the validity of the separability property in terms of both plastic and total displacement and corresponds to the initial crack length, and a third one where the separation parameter decreases when crack starts propagating. The load separation hypothesis is only valid in the two latter regions which are independent of the displacement but vary

according to the crack length (see Figure 46). It's important to underline that the unseparable region is slightly larger in the case where S_{ij} is determined using total displacement.

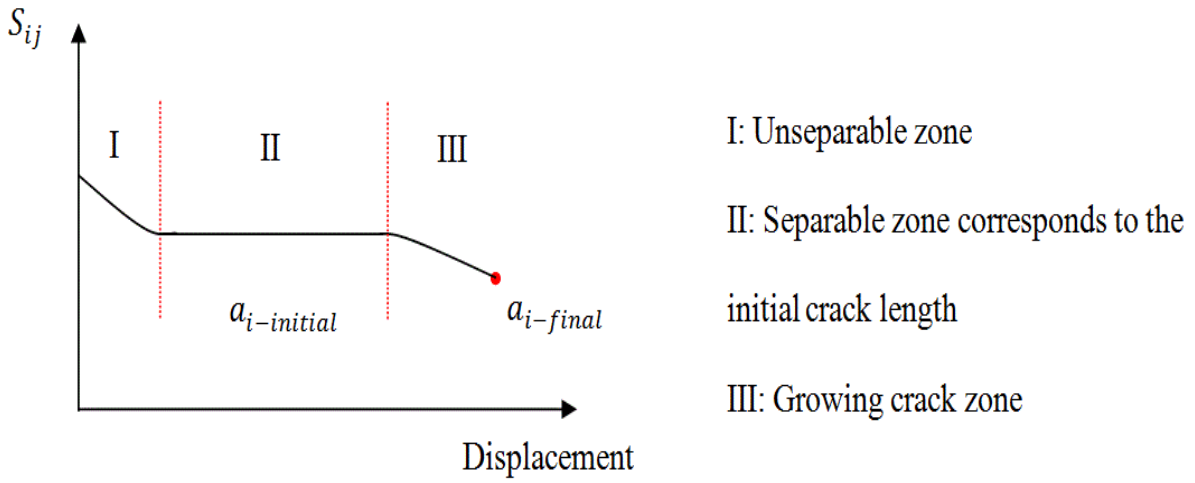

Figure 46. *Illustration of the S_{ij} vs Displacement curve*

Figure 47 and Figure 48 show the changes in the S_{ij} parameter as a function of b_i/W for the different specimens. The results obtained were fitted by a power law (see Figure 49 and Figure 50). Finally, η_{pl}-factors were determined in both cases from (Eq. 26). Thus, in order to validate the accuracy of the results, the initial crack lengths were computed from the η_{pl}-factors values.

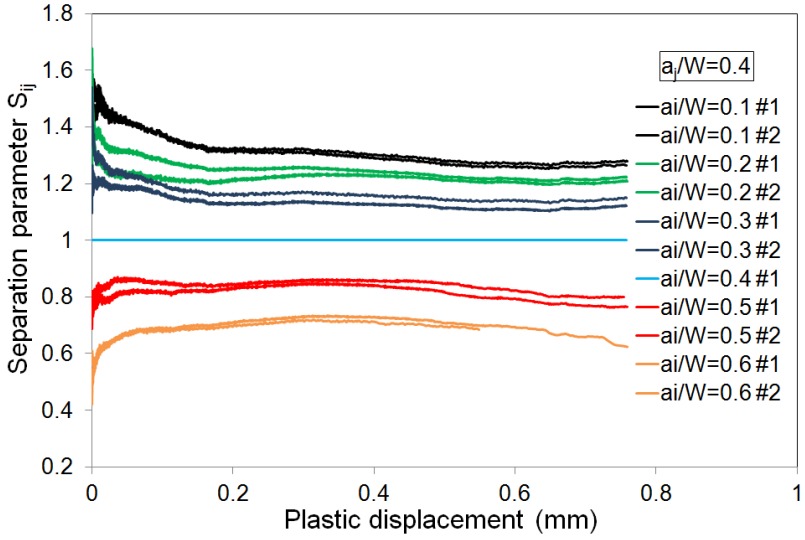

Figure 47. *Changes in the separation parameter vs the plastic displacement. (The reference record is a_j/W =0.4)*

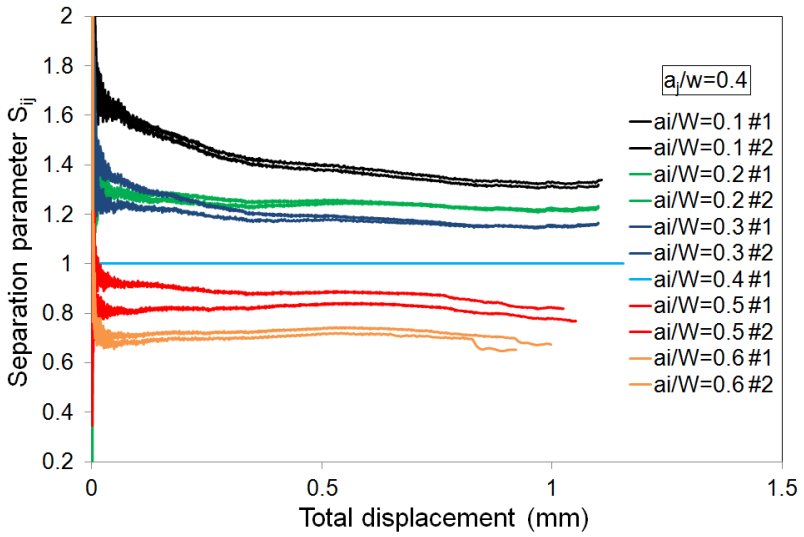

Figure 48. *Changes in the separation parameter vs the total displacement. (The reference record is a_j/W =0.4)*

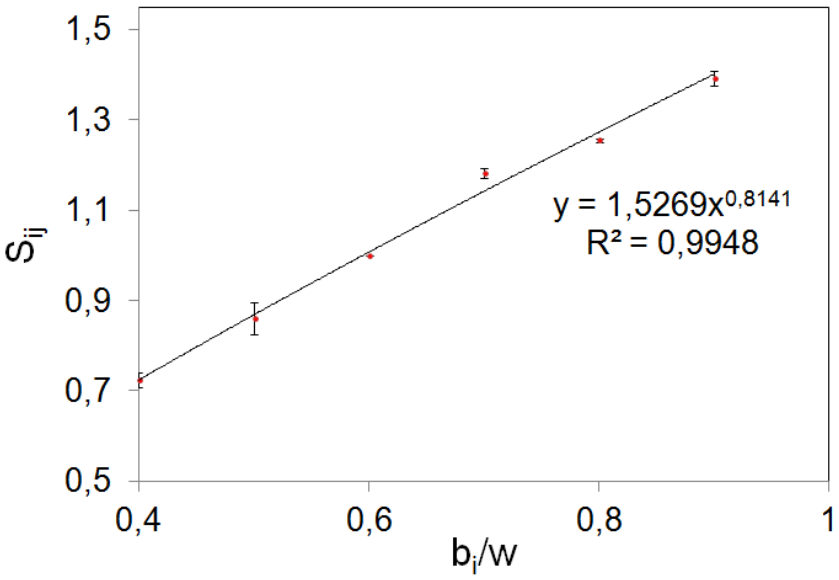

Figure 49. *Power law fit for the SEN AP C/PPS laminates separation data for reference $b_i/W = 0.6$ using total displacement*

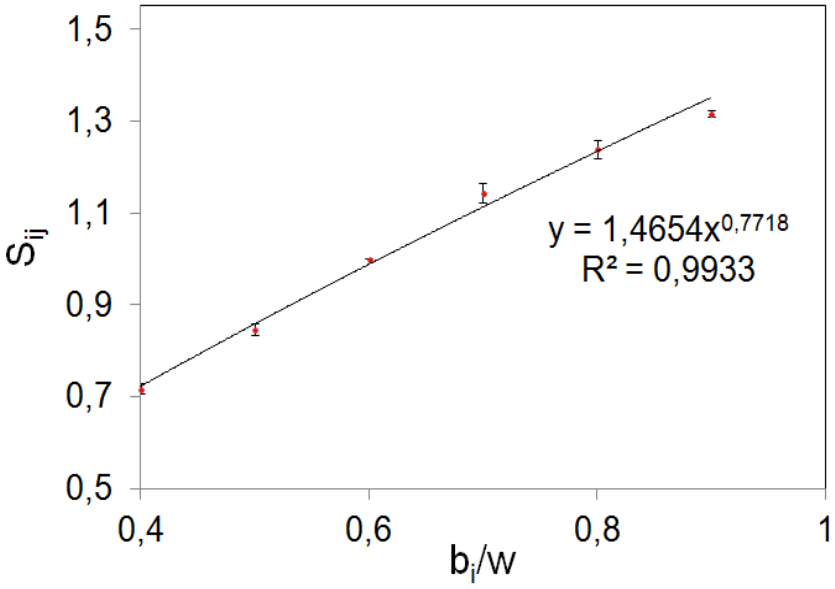

Figure 50. *Power law fit for the SEN AP C/PPS laminates separation data for reference* $b_i/W = 0.6$ *using plastic displacement*

Actually, for constant b_i/W, the separation parameter can be expressed as follow [Wainstein et al., 2004] [Wainstein et al., 2003]:

$$S_{ij} = A'.G(\frac{a_j}{W}) \tag{30}$$

Then, independently of the conditions at the crack tip, the geometry function becomes:

$$G(\frac{a_i}{W}) = A''.\left(\frac{b_i}{W}\right)^m \tag{31}$$

where A' and A'' are two constants.

Therefore, the separation parameter S_{ij} can be expressed as a function of the crack length as follow:

$$S_{ij} = \frac{G(\frac{a_i}{W})}{G(\frac{a_j}{W})} = \frac{A''.\left(\frac{b_i}{W}\right)^m}{A''.\left(\frac{b_j}{W}\right)^m} = \left(\frac{W-a_i}{W-a_j}\right)^m \tag{32}$$

Rearranging (Eq 32), the crack length results:

$$a_i = W - S_{ij}^{\frac{1}{m}}(W - a_j) \tag{33}$$

Table 4 summarizes the η_{pl}-values obtained and the corresponding initial crack lengths calculated using Eq. (33) in the separable zone. On the one hand, the difference observed between the η_{pl}-factors obtained from total and plastic displacement was about 5%. On the other hand, the comparison between the real initial crack length and the computed ones shows that the use of a deformation function with total displacement provides more accurate results.

Table 4. *Comparison between a_{real} and $a_{calculated}$ using total and plastic displacement*

a/W	a_{real}	Total displacement		Standard deviation (mm)	Plastic displacement		Standard deviation (mm)
		η_{pl}	$a_{\text{calculated}}$ (mm)		η_{pl}	$a_{calculated}$ (mm)	
0.1	1.48	0.8141	1.46	0.01	0.7718	2.13	0.46
0.2	2.96		3.05	0.06		3.07	0.08
0.3	4.44		3.89	0.39		4.32	0.08
0.4	5.92		5.92	0.00		6.4	0.00
0.5	7.4		7.42	0.01		7.64	0.17
0.6	8.88		8.81	0.05		9.75	0.09

In order to generalize the η_{pl}-factor obtained using total displacement from $a_j/W = 0.4$ reference record, the load separation method was applied for different reference record (see Figure 51 and Figure 52 and Figure 53 and Figure 54 and Figure 55). According to Table 5, it is possible to observe that a good agreement is obtained between the different η_{pl}-factors computed for different reference record.

Finally, the η_{el}-factor has been determined as $\eta_{el} = 0.8674$ from the compliance method.

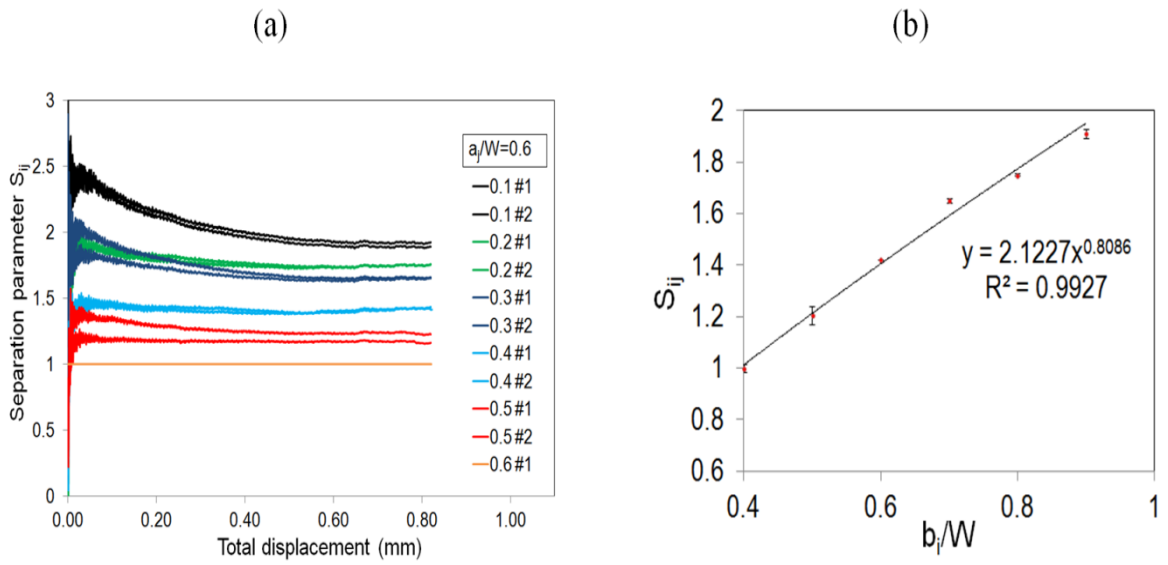

Figure 51. *S_{ij} vs total displacement plot and the corresponding power law fit (a_j/W =0.6 reference record)*

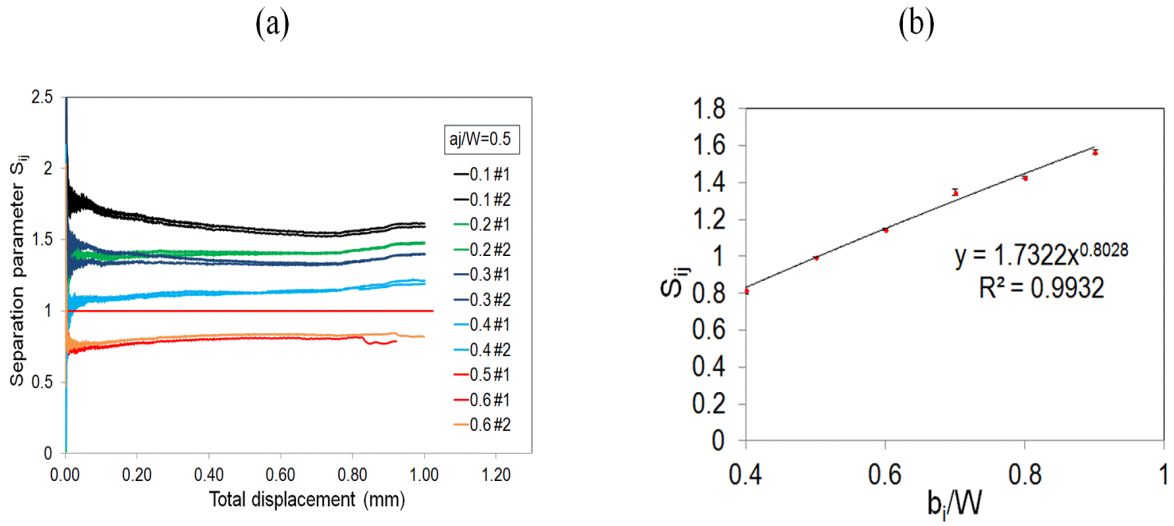

Figure 52. *S_{ij} vs total displacement plot and the corresponding power law fit (a_j/W =0.5 reference record)*

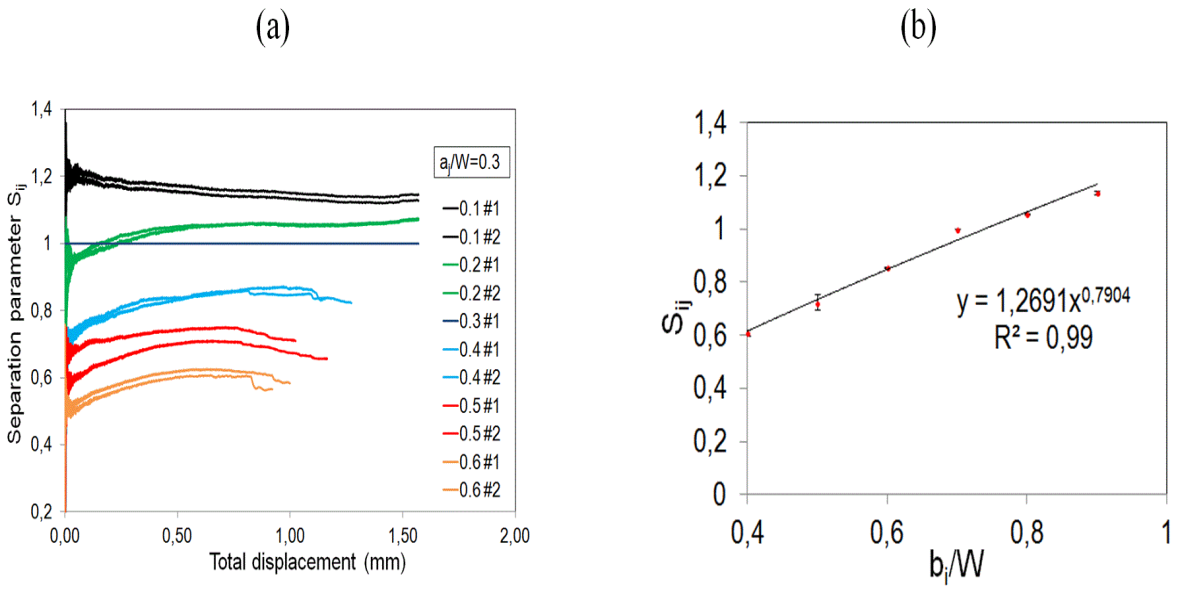

Figure 53. *S_{ij} vs total displacement plot and the corresponding power law fit (a_j/W =0.3 reference record)*

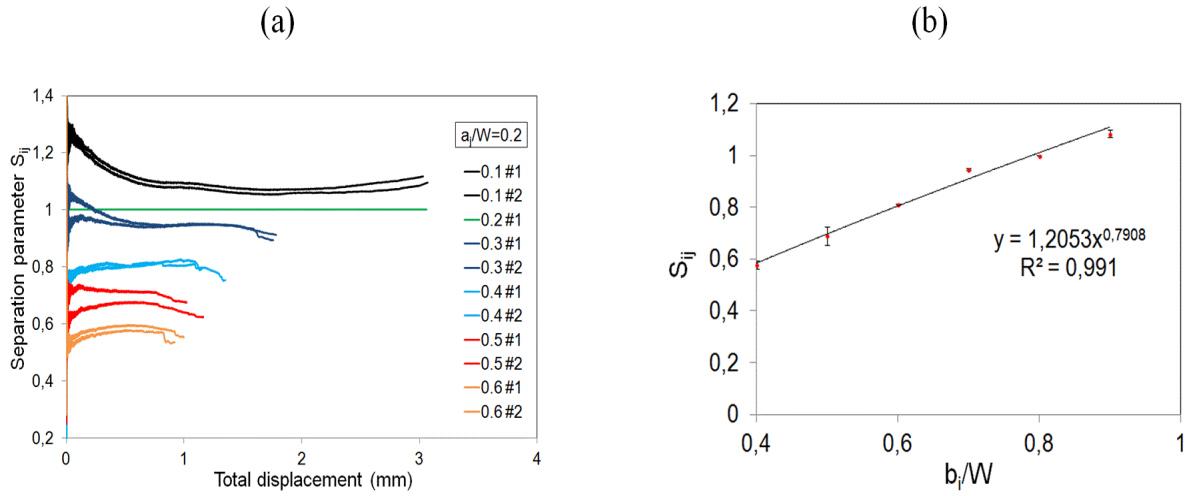

Figure 54. *S_{ij} vs total displacement plot and the corresponding power law fit (a_j/W =0.2 reference record)*

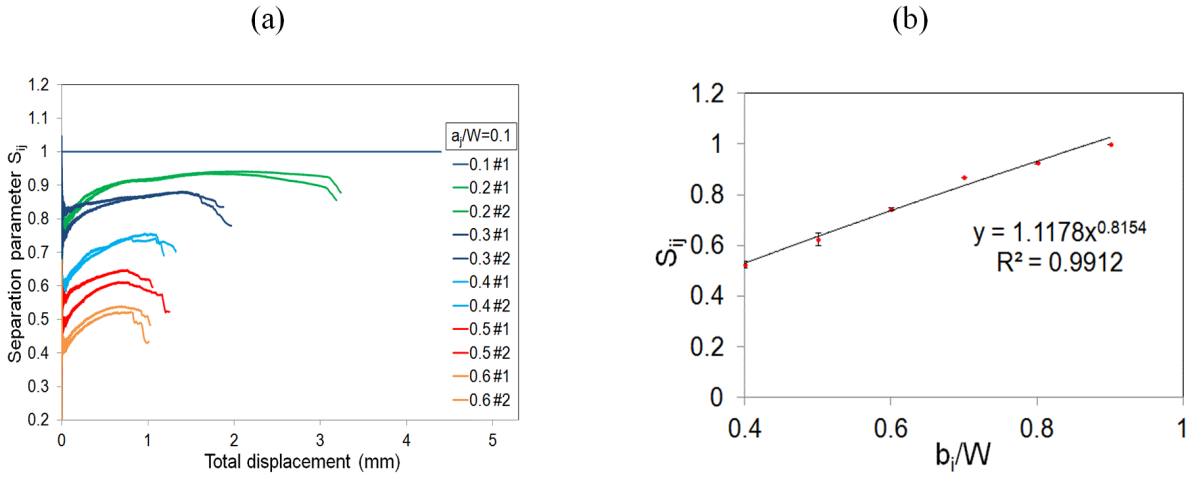

Figure 55. *S_{ij} vs total displacement plot and the corresponding power law fit (a_j/W =0.1 reference record)*

Table 5. *η_{pl}-factors obtained for different reference records*

Reference record	η_{pl}	$\eta_{pl_{mean}}$
0.1	0.8154	0.8037±0.0110
0.2	0.7908	
0.3	0.7904	
0.4	0.8141	
0.5	0.8028	
0.6	0.8086	

II.4.2.4 Determination of J-R curves

From Eq. (19) and based on the η-factors computed in section II.4.2.3, the strain energy release rate J_{tot} was determined. Figure 56 shows the total strain energy release rate J_{tot} and the elastic strain energy release rate J_{elast} according to the total displacement. One can notice that, for a constant displacement, the value of J_{tot} is virtually independent of the initial notch

length. In addition, the elastic strain energy release rate J_{elast} appears to be negligible comparing to the total strain energy release rate J_{tot}.

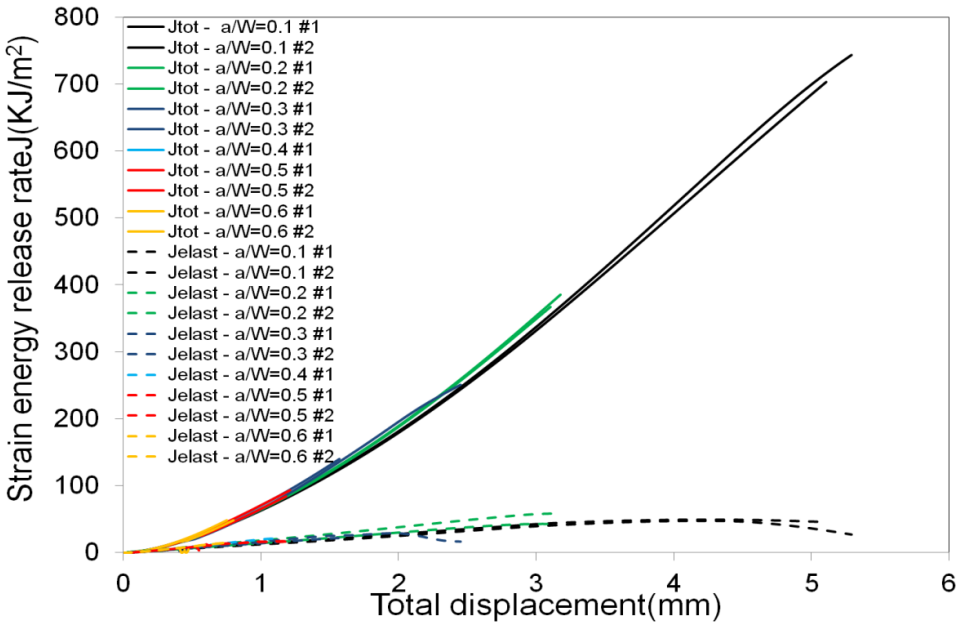

Figure 56. *J_{total} and $J_{elastic}$ vs total displacement in AP SEN specimens*

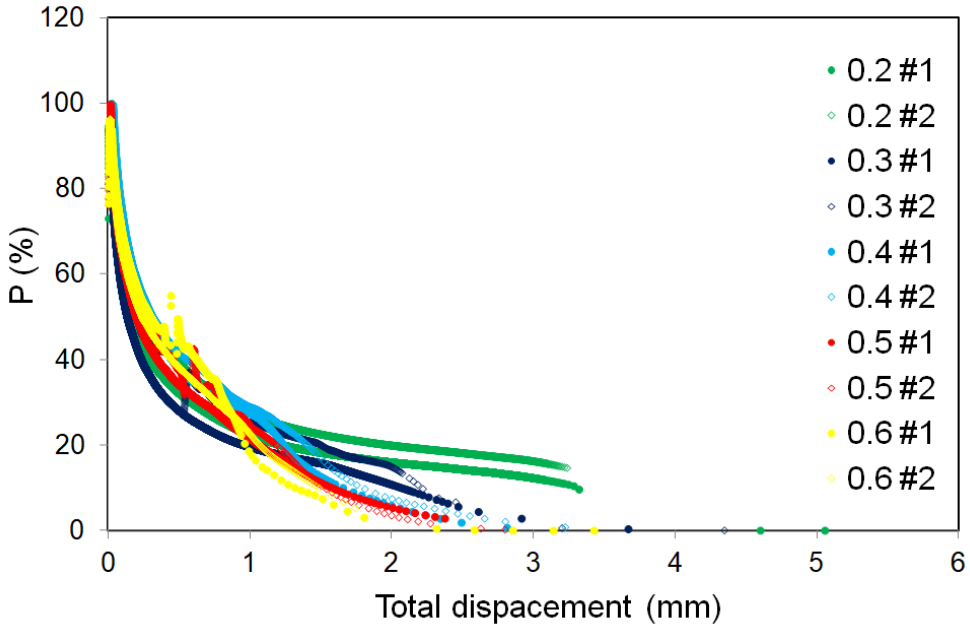

Figure 57. *Evolution of P according to the total displacement*

The elaboration of J-R curves requires knowing the growth of the transverse crack as a function of the applied tensile load. Such crack growth can be obtained from (Eq. 33) provided that a notched specimen with a blunt notch (with constant crack length during loading) is used as a reference record.

For a ratio $a/W = 0.1$, the notch is gradually opened and blunted without crack propagation prior to peak load. These phenomena are associated with significant strain energy storage during loading to maximum load. Once the maximum load is reached, the blunted notch can no longer resist and fails brutally (see Figure 58).

In this section, the first portion curve corresponding to the specimen with $a/W = 0.1$ is defined from zero load to the peak load. It is used as a reference record as the crack can be considered as stationary (see Figure 58).

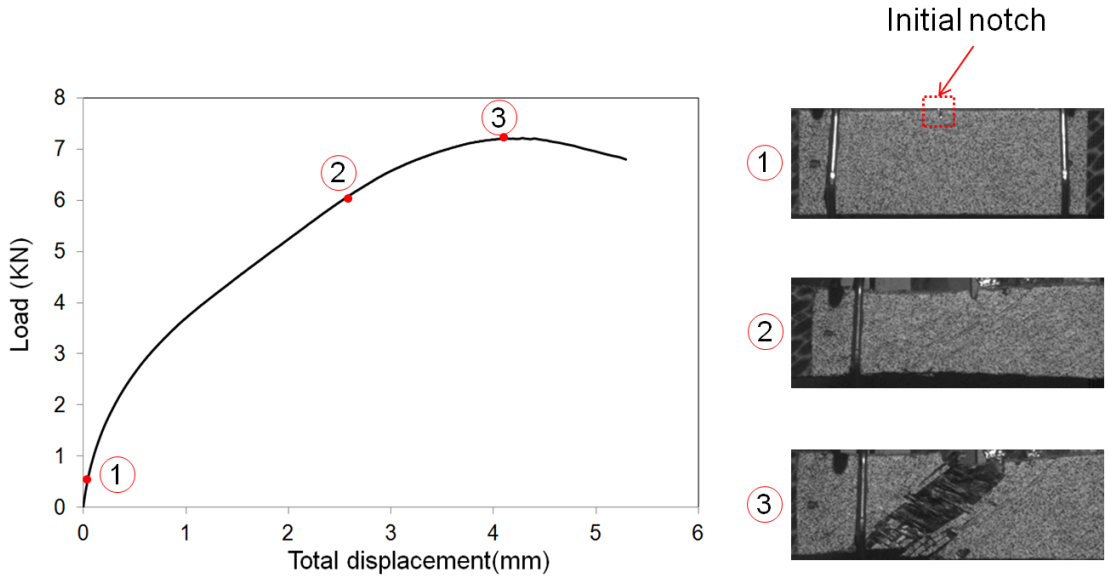

Figure 58. *Evolution of the notch in SEN laminates with a/W=0.1 subjected to tensile loading at T>T_g*

From Eq. 33, it is therefore possible to compute the crack growth in the separable zone and the growing crack zone. It is assumed that there is no significant crack growth during the whole crack tip blunting process. Thus, in the unseparable zone, the crack length can be considered as the initial crack length.

Figure 59 shows the J-R curves as well as the elastic stain energy release rate J_{elast} according to the crack growth for ratios $a/W = 0.2 - 0.3 - 0.4 - 0.5 - 0.6$.

In order to study the interest to take into account the plastic part in strain energy release rate calculation, the parameter *P* is introduced as: $P(\%) = \frac{J_{elast} \times 100}{J_{tot}}$

According to Figure 57 and Figure 60, the contribution of J_{elast} in the total strain energy release rate calculation is important at the beginning of the mechanical loading then it starts to decrease rapidly as plastic phenomena take place.

Figure 59 shows the J-R curves for ratios $a/W = 0.2 - 0.3 - 0.4 - 0.5 - 0.6$. It appears that the critical strain energy released J_c is more significant in specimens with small initial notches what seems to be relevant as the mechanical energy required to induce transverse cracking is larger as well. However, for larger initial notches, the initiation of cracking doesn't require important strain energy released as the crack propagates gradually without an important crack tip blunting (see Figure 61).

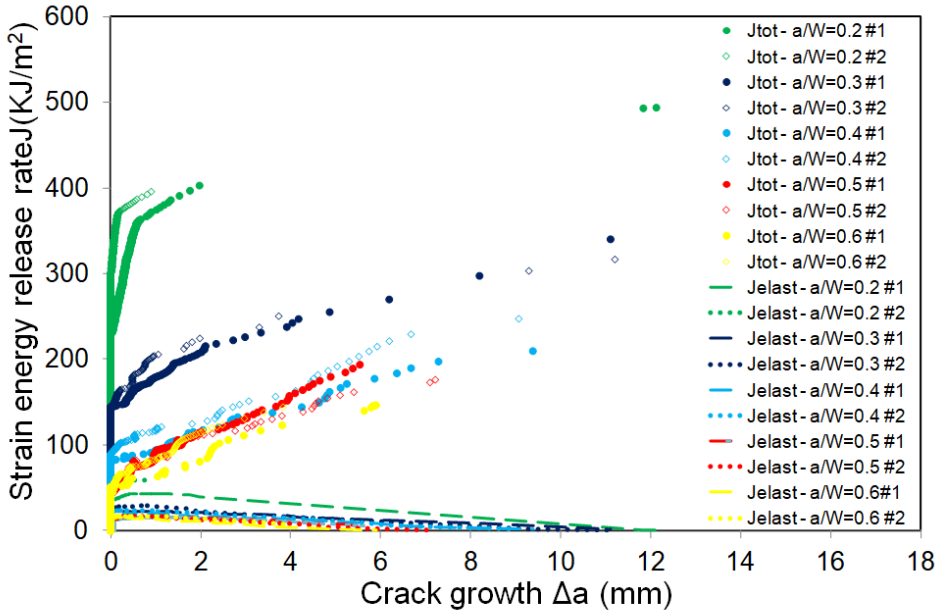

Figure 59. *J-R curves obtained using the load separation method and $J_{elastic}$ vs crack growth for different initial crack length over specimen width ratio a/W*

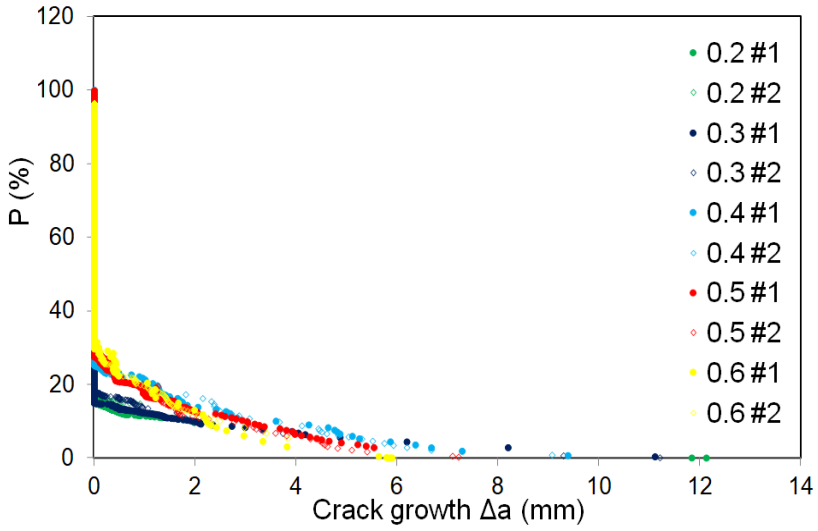

Figure 60. *Evolution of P according to the crack growth*

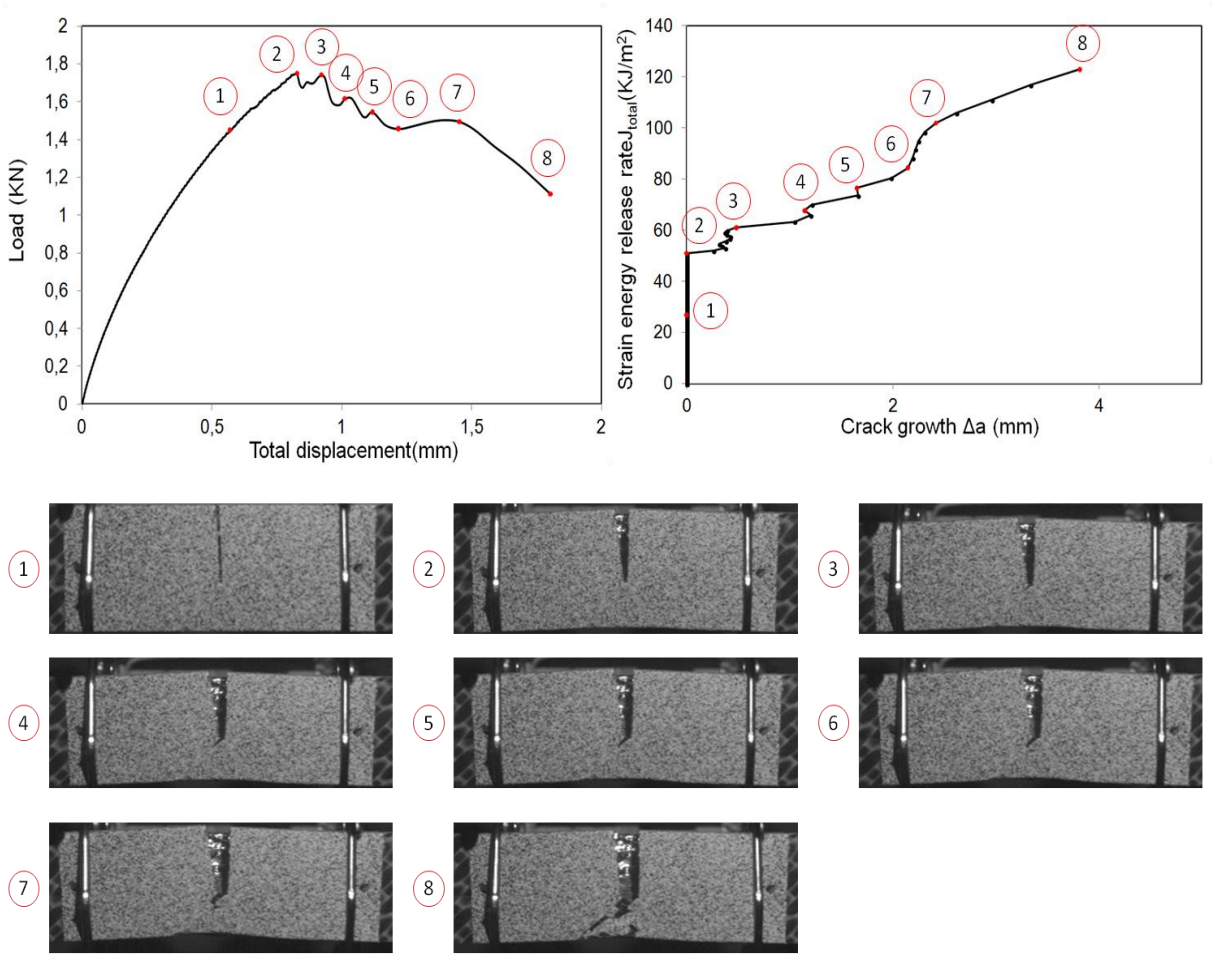

Figure 61. *Evolution of the notch in SEN laminates with a/W=0.6 subjected to tensile loading at $T>T_g$*

This result confirms that, for composite materials and contrary to isotropic ones, the critical strain energy released is not a material property but rather depends on geometry [Lin et al, 1976]. In other words, the strain energy released during fracture decreases when the surface to be changed ($b_i \times B$) decreases. Depending on the specimen geometry, different fracture mechanisms can be observed resulting in changing the fracture surface. In addition, this fracture surface is not limited to the transverse plane along the initial pre-crack. The different damage mechanisms contribute to the formation of the fracture surface between the plies of the laminates as well as at the fiber/matrix interface (debonding).

The comparison of J-R curves obtained from the separation parameter method and a DIC technique shows a good agreement for a/W=0.3 and 0.6 (see Figure 62). As a consequence, the load separation method appears to be efficient tool to compute J-R curves of highly ductile composite systems (e.g. C/PPS laminates) at $T > T_g$.

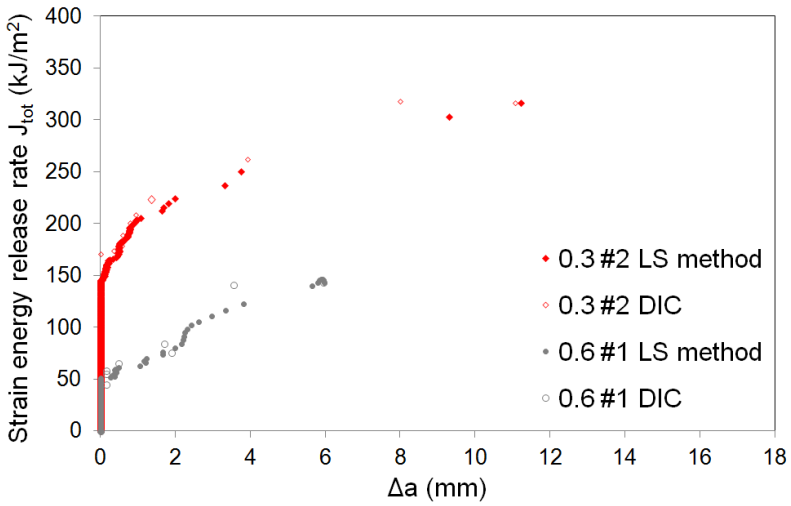

Figure 62. *Comparison between J-integral vs crack growth obtained using the load separation method and the DIC technique for a/W =0.6 and a/W =0.3*

II.5 Influence of matrix ductility and toughness on strain energy release rate and failure behavior [Vieille et al., 2017a]

In SEN specimens, the fracture toughness can obtained from analytical representation of the translaminar failure modes based on fracture mechanics concepts. Depending on laminates' stacking sequence, the contribution of matrix behavior to strain energy release can be

evaluated during damage in both brittle and ductile composite laminates subjected to high temperature conditions ($T > T_g$) when matrix ductility and toughness are enhanced. In SEN specimens subjected to tensile loadings, the cumulative acoustic energy can be correlated with the strain energy release rate. Depending on the initial notch orientation (0° or 45°), the failure mode is either a mode I or a mixed mode (I + II). A Digital Image Correlation technique is also used to observe the influence of matrix ductility on the Crack Tip Opening Displacement as applied stress increases.

Single-Edge Notch (SEN) specimens, having a given ratio $a/w = 0.3$, were subjected to monotonic tensile loadings at 120°C. Two types of initial notch were considered:

- 0° SEN specimens referred to as samples with a notch oriented at 0° along the $\vec{x}$ axis (see Figure 63),
- 45° SEN specimens referred to as samples with a notch oriented at 45° with respect to the $\vec{x}$ axis.

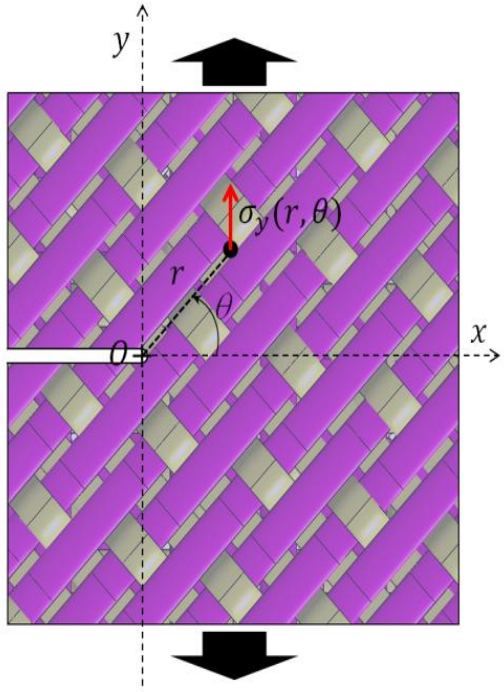

Figure 63. *Longitudinal stress in the vicinity of the crack tip in quasi-isotropic laminate loaded in opening mode.*

II.5.1 About the influence of temperature on energy dissipation

In the literature, the modes of energy dissipation are mainly affected by the matrix fracture mode (brittle or ductile) which is mainly determined by the loading rate or temperature conditions [Boccardi et al., 2016] [Lauke et al., 1986].

The energy dissipated during controlled crack propagation in carbon fibers reinforced composites is usually evaluated in terms of different source mechanisms: plastic deformation, fiber-snapping, matrix-cracking and fiber pull-out [Lauke et al., 1986] [Wells et al., 1985]. In a brittle resin matrix composite, the energies dissipated in crack initiation and propagation in the weakly-bonded composite are derived principally from the work of fiber pull-out (which is due to the frictional forces that hold a broken fiber in its matrix socket). If the composite contains ductile matrices, the local plastic deformation of the matrix must also be taken into account in the total fracture toughness (see Section I.4.3).

The mechanical behavior of polymer resins exhibits temperature dependence (viscoelastic and viscoplastic behaviors) not only above T_g but also below T_g. Kim et al. have studied the influence of temperature on interfacial debonding on composites with TP coated carbon fibers [Wells et al., 1987]. The TP coating reduced significantly the bond strength at the fiber-matrix interface at high temperature resulting in enhanced interlaminar fracture toughness. The influence of temperature on the fatigue behavior of TP-based composites has also been discussed in the literature to understand how matrix ductility modifies damage mechanisms [Kim et al., 1991] [Kawai et al., 1996] [Ma et al., 2016] [Ibáñez-Gutiérrez et al., 2017], particularly at high temperatures [Albouy et al., 2014] [Montesano et al., 2012] [Sendeckyj et al., 1977] [Sorrentino et al., 2017] [Gabrion et al., 2016]. Another approach to the characterization of crack resistance is given by the work-of-fracture measurement (for controlled crack propagation) corresponding to the energy absorbed by the creation of fracture surfaces of completely broken samples [García et al., 2016]. In their study on C/epoxy composites, Munro et al. have shown that the fracture energy significantly increased with temperature (from 124 to 200 kJ/m^2, at room temperature and 80 °C respectively). Carbon-fiber pull-out energy represents 25% of the total fracture energy [Lauke et al., 1986].

II.5.2 Influence of matrix ductility and toughness on thermomechanical behavior

The influence of matrix ductility on the thermomechanical behavior of SEN structures can be evaluated considering laminates with fiber-dominated behavior (quasi-isotropic stacking sequence) or matrix-dominated behavior (angle-ply stacking sequence). For comparison purposes, the tensile behavior of SEN specimens can be discussed with respect to unnotched specimens. In addition, the initial crack length over the specimen width is the same ($a/W = 0.3$) in 0° and 45° SEN specimens, and therefore the bearing cross sections are indeed different, denoted Sb_0 and Sb_{45} respectively. They are defined by:

$$S_{b0} = t.W\left(1 - \frac{a}{W}\right) = 0.7tW \text{ and } S_{b45} = t.W\left(1 - \frac{\sqrt{2}a}{2W}\right) \approx 0.788tW$$

Where t and W are the laminates' thickness and width, respectively. Thus, the macroscopic responses are drawn in terms of bearing stress σ_{b0} and σ_{b45} (see Figure 64a and Figure 64b):

$$\sigma_{b0} = \frac{F_0}{S_{b0}} \text{ and } \sigma_{b45} = \frac{F_0}{S_{b45}}$$

Regardless the stacking sequence, it appears that both 0° and 45° SEN samples have virtually the same behavior until failure occurs in 0° specimens. Most of the curves presented in this thesis are based on these definitions in order to ease the comparison.

In AP laminates, the comparison of tensile macroscopic responses (see Figure 64a) shows that both unnotched and 0° SEN specimens have a similar elastic-ductile thermomechanical behavior until tensile loading reaches the ultimate strength of SEN specimens which is about 30% lower due to stress concentration at the notch tip (see Table 6). From the ultimate stress level in 0° specimens (about 121 MPa), a gradual failure (the load borne by the specimen decreases) can be observed on the stress-strain curves, and the reasons will be further explained in next section. With respect to the unnotched laminates, the strain at failure is about 30% lower in 0° SEN specimens, whereas the longitudinal stiffness is virtually unaffected by the presence of the 0° notch (see Table 6). In 45° SEN specimens subjected to tensile loading, the stress-strain tensile significantly differs from the response of 0° SEN specimens with the same ratio $a/w = 0.3$ (see Figure 64a), suggesting that a mixed failure mode is less critical (from the ultimate strength standpoint) than mode I. Though the strain at failure is virtually the same in 0° and 45° SEN specimens, both longitudinal stiffness and

strength are higher (about 11 to 23% - see Table 6) because fiber bundles tend to rotate during tensile loading as the initial notch gradually opens (see stages 3 and 4 on Figure 64a). The comparison of crack tip opening displacement (CTOD) vs bearing stress shows that the CTOD is the same in 0° and 45° SEN specimens until the value at failure is reached in the 0° SEN specimens (see Figure 65a). In both SEN specimens subjected to bearing stresses lower than 50 MPa (equivalent to remote tensile stresses equal to 35-40 MPa), the CTOD linearly increases suggesting that crack growth is stable. For bearing stresses higher than 50 MPa, the CTOD suddenly increases, suggesting that crack propagation becomes instable. This bearing stress level (about 50 MPa) can be considered as the threshold corresponding to the onset of macroscopic plastic deformation (onset of non-linearity - see Figure 64a) coming along with the rotation of fiber bundles at the crack tip and the crack opening displacement. In mixed-mode, the rotation of fibers comes along with the shearing of PPS matrix leading to a more ductile tensile response (see Figure 64a). Such rotation implies that fibers better contribute to bear the tensile load therefore justifying higher stiffness and strength. The load borne by fibers also results in stabilizing the crack growth. Contrary to the gradual failure observed in 0° SEN specimens, when fibers reach their ultimate strength, failure occurs in brittle fashion in 45° SEN specimens.

Table 6. *Mechanical properties of angle-ply C/PPS laminates subjected to tensile loadings at 120°C*

	E_x (GPa)	σ_x^u (MPa)	ε_x^u (%)
Unnotched	6.50±0.46	192±2	19.87±3.09
SEN 0°	6.42±0.49	121±4	13.31±2.24
SEN 45°	7.25±0.32	149±4	11.73±1.29

(a)

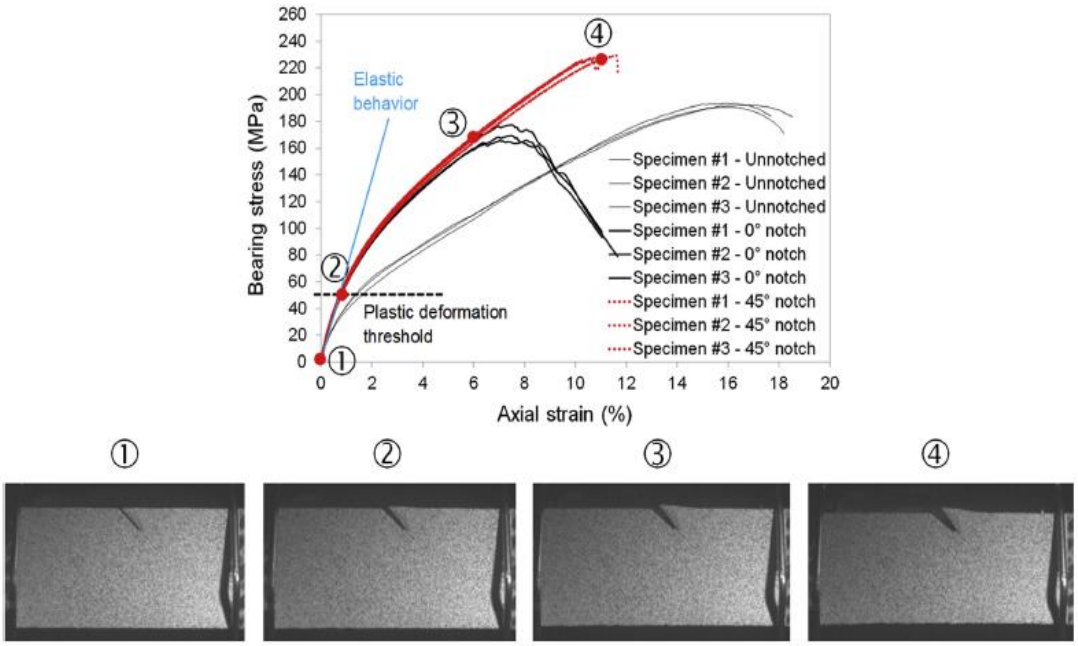

(b)

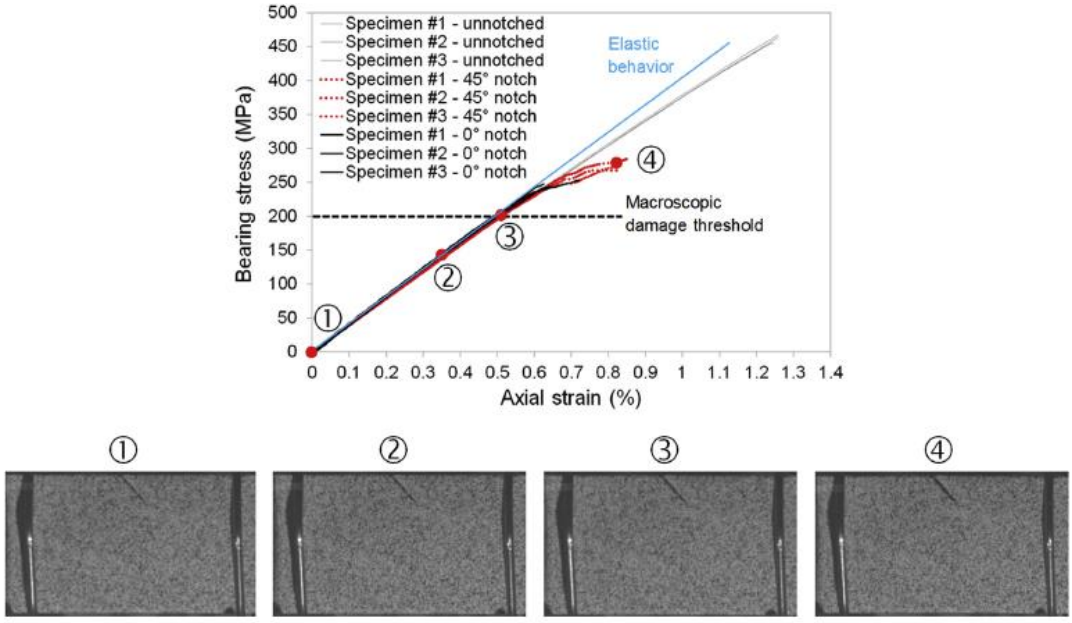

Figure 64. *Influence of the notch orientation on the macroscopic response of SEN C/PPS laminates subjected to tensile loadings at 120°C: (a) Angle-ply – (b) Quasi-isotropic*

In QI laminates, all specimens are characterized by elastic-brittle tensile responses (see Figure 64b), and the mechanical properties are adversely influenced by the stress concentration due to the notch (see Table 7). With respect to the unnotched laminates, the longitudinal stiffness is about 25% lower in SEN specimens, whereas the longitudinal strength is 53 to 63% lower in 45° and 0° SEN specimens respectively. The effect is all the more significant in 0° SEN

specimens with a mode I failure. In 45° SEN specimens experiencing mixed failure mode, as observed in AP SEN laminates there is also a slight rotation of fibers at the crack tip resulting in an increase in the longitudinal strength (about 30%) with respect to 0° SEN specimens. From the macroscopic tensile response of SEN specimens, it appears that failure occurs gradually from stage 3 where the onset of non-linearity is observed on Figure 64b. The corresponding threshold (about 140-160 MPa equivalent to a bearing stress of 200 MPa) is identified as the onset of the macroscopic damage. This threshold corresponds to the stress level from which the longitudinal overstressed fibers at the crack tip start breaking. The observation of CTOD vs applied stress shows that the evolution of CTOD is virtually linear (see Figure 65b). The values of CTOD in QI laminates are ten times as low as in AP laminates, because the tensile load is primarily borne the longitudinal fibers whose mechanical response is elastic-brittle. From the macroscopic damage threshold identified on the tensile response (about 140MPa – see Figure 64b), there is no visible change in the CTOD. It therefore suggests that the gradual breakage of overstressed longitudinal fibers at the crack tip is not associated with an observable change in the opening of the crack. As the CTOD is very small in QI laminates, it is also worth noticing that the accuracy of the full-field measurements to evaluate CTOD significantly depends on the fineness of the patterns at the crack tip. In addition, as the growth of the transverse crack is very rapid in QI laminates, the sudden increase of the CTOD cannot be captured and estimated.

Table 7. *Mechanical properties of quasi-isotropic C/PPS laminates subjected to tensile loadings at 120°C*

	E_x (GPa)	σ_x^u (MPa)	ε_x^u (%)
Unnotched	40.49±0.30	472±6	1.25±0.03
SEN 0°	29.36±0.75	174±3	0.68±0.07
SEN 45°	31.72±1.38	226±6	0.86±0.06

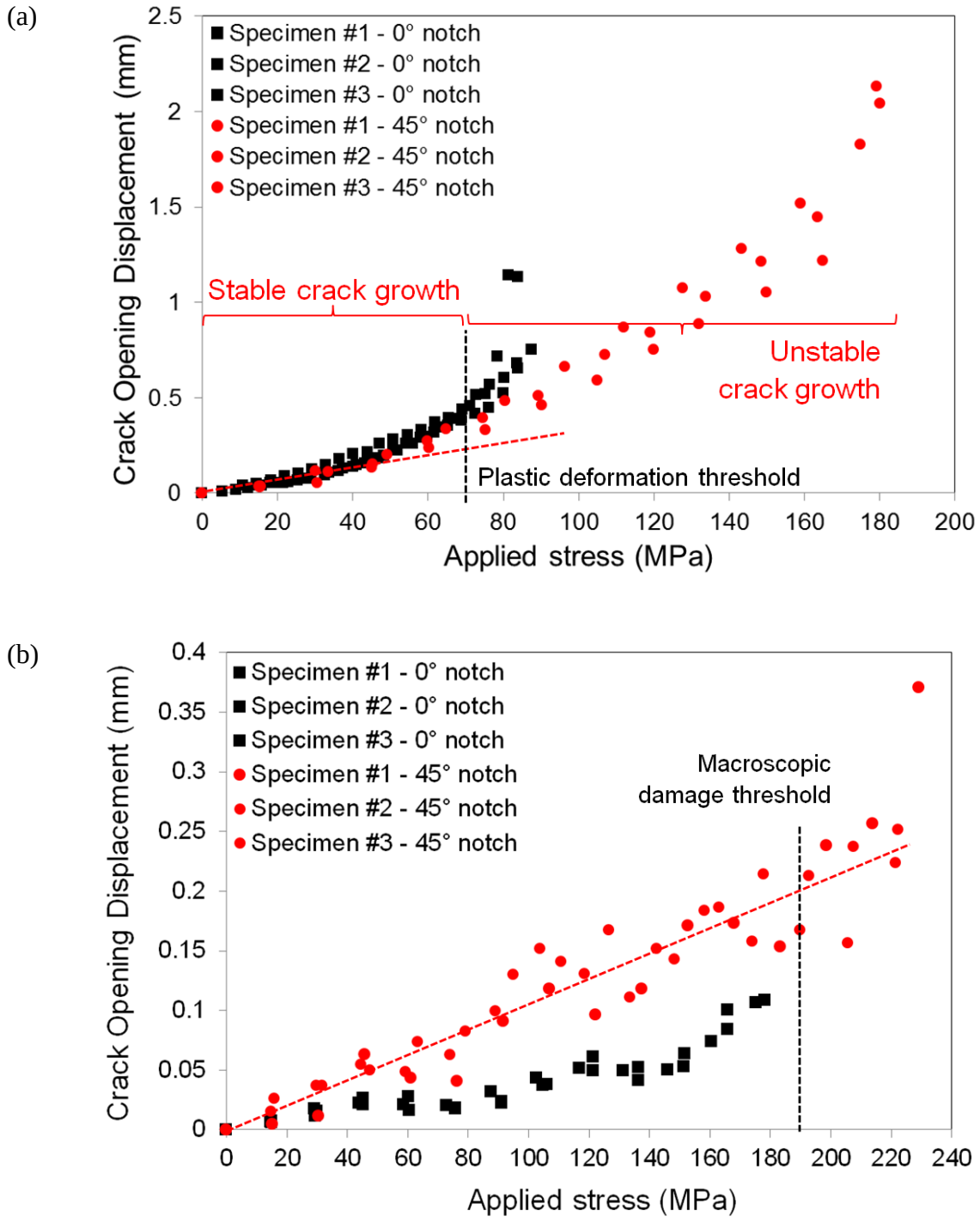

Figure 65. *Influence of the notch orientation on the evolution of the Crack Tip Opening Displacement in SEN C/PPS laminates subjected to tensile loadings at 120°C: (a) Angle-ply - (b) Quasi-isotropic*

II.5.3 Influence of matrix ductility and toughness on fracture mechanisms

The crack arrest or blunting by longitudinal splitting or matrix plastic deformation along the fiber direction gives a substantial reduction in the stress concentration ahead of the crack, enabling the fibers to sustain higher levels of load prior to fracture. It is therefore expected that the influence of matrix ductility and toughness on the fracture mechanisms will significantly depend on fibers orientation (hence laminates lay-up) with respect to the orientation of the initial notch. From previous studies conducted on the same composite materials subjected to impact loadings, it was concluded that the weft fibers undulation over the warp fibers cause local stress concentration under uniaxial tension at the crimp in woven-ply laminates [Vieille et al., 2013]. These local overstresses may result in early damage initiation in the form of fiber/matrix interface debonding or matrix cracking. In addition to the fracture toughness at the fiber/matrix interface, the fabric thickness and the weaving patterns introduce some "structural" macroscopic toughness associated with the deviation of fabric surface from planarity.

II.5.3.1 Angle-ply laminates

In AP laminates, both 0° and 45° SEN specimens are characterized by a highly ductile and gradual failure, what is promoted by the enhanced ductility of PPS matrix at temperatures higher than T_g. The observation of fracture surfaces clearly indicate that, regardless of the orientation of the initial notch, the fracture surface is oriented at 45° along the warp direction, suggesting that fibers breakage preferentially occurs in weft fibers which are overstressed due to fabric weaving pattern (see Figure 66a). Important splitting of the warp and weft fibers can be observed on laminates' surface (see Figure 67a), as well as pull-out of fibers bundles and extensive delamination along the laminates' edges. Pull-out results from the stress concentration at the crimp as fiber-matrix debonding is primarily initiated in this area. Delamination is classically associated with edge effects, and is more specifically due to the rotation of fiber bundles coming along with the large plastic deformation of the PPS matrix (highly ductile at $T > T_g$). These damage mechanisms are schematically illustrated on Figure 68a, and the scissoring effect at the crimps is instrumental in concentrating stresses in weft fiber bundles whose failure rules the macroscopic crack growth. Depending on the orientation of the initial notch, a mixed-mode (opening and shearing) failure is observed in 45° SEN specimens. As shearing is promoted by the 45° oriented notch, the local plastic deformation of PPS matrix in matrix-rich areas contribute to delay matrix cracking which is usually the

earliest damage mechanism in carbon fiber-reinforced laminates. Thus, the strain energy release rate resulting from the translaminar failure is expected to be significantly higher in AP laminates experiencing mixed-mode failure (e.g. with 45° initial notch).

(a)

(b)

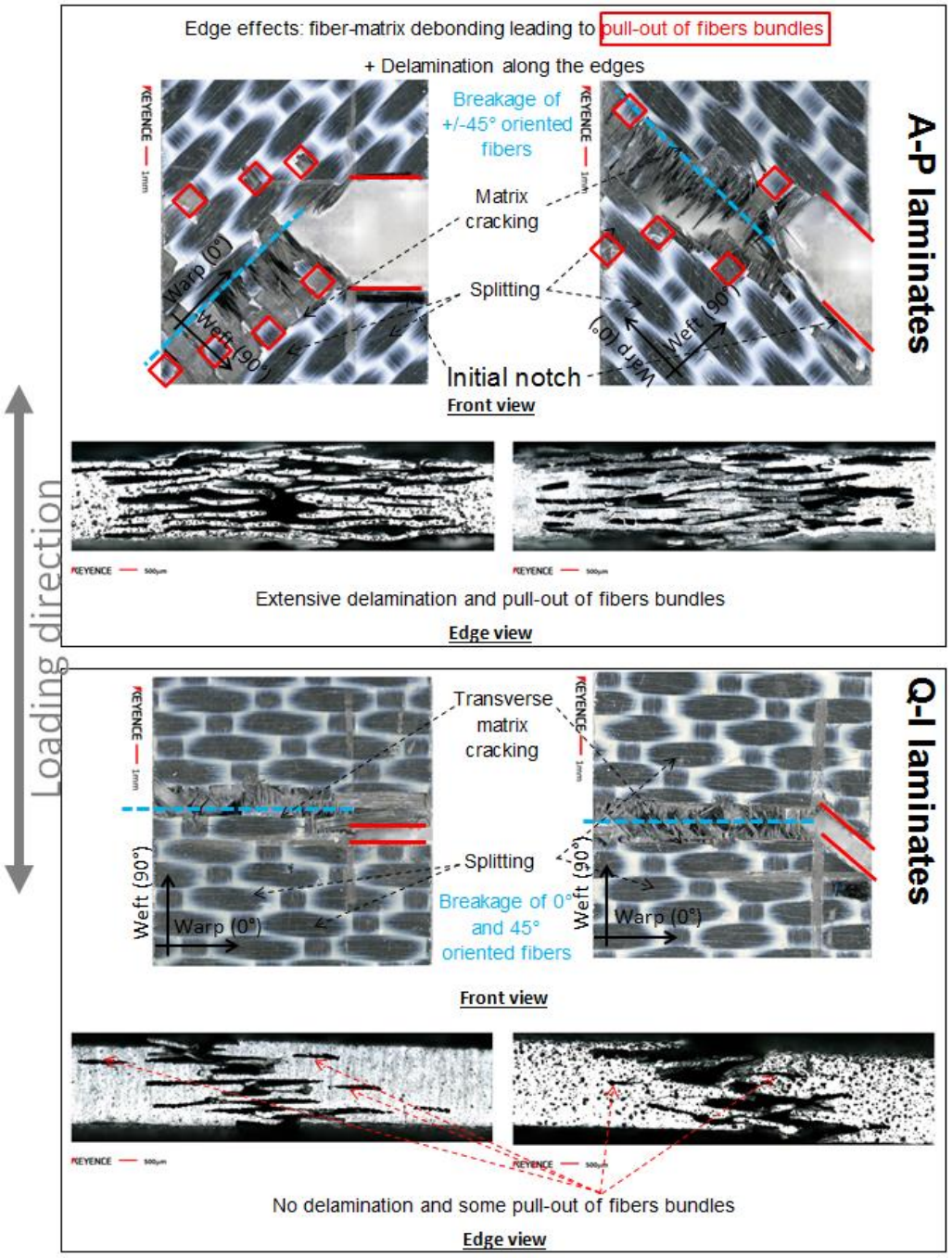

Figure 66. *Observations of failed specimens and analysis of damage mechanisms depending on notch orientation and stacking sequences in SEN C/PPS laminates subjected to tensile loadings at 120°C: (a) Angle-ply - (b) Quasi-isotropic*

(a)

(b)

Figure 67. *Observation of fracture surfaces in 45° oriented SEN specimens subjected to mixed-mode loading: (a) Angle-ply - (b) Quasi-isotropic*

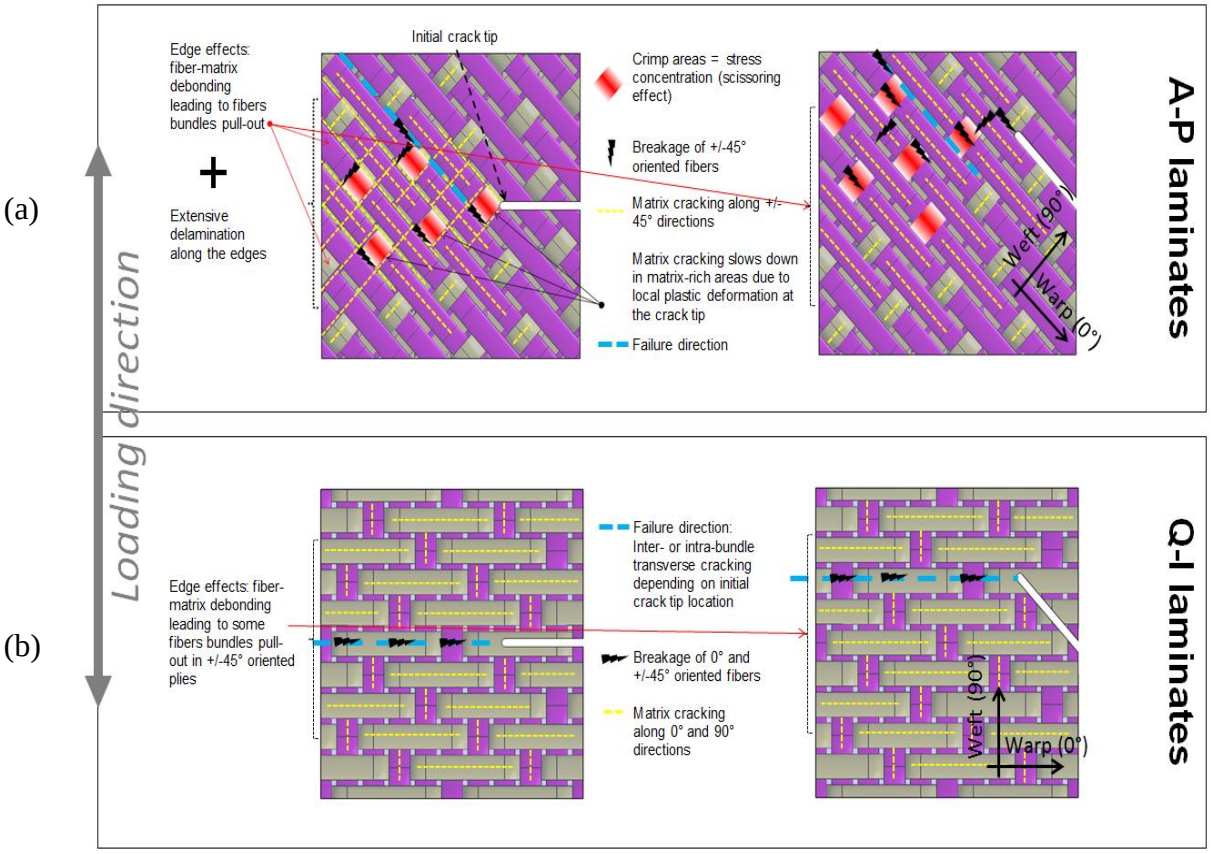

Figure 68. *Schematic interpretation of damage mechanisms in SEN C/PPS woven-ply laminates: (a) Angle-ply - (b) Quasi-isotropic*

II.5.3.2 Quasi-isotropic laminates

In QI laminates, as was discussed in [Vieille et al., 2016] [Vieille et al., 2016], the elastic-brittle mechanical response (see Figure 64b) primarily results from the transverse matrix cracking and the breakage of weft fibers along the warp direction (see Figure 66b). In quasi-isotropic specimens, transverse crack initiation and propagation virtually occur at the same time corresponding to ultimate failure. The observation of fracture surfaces also shows a few bare fiber bundles in the ±45° direction along specimens' free edges, due to fiber–matrix debonding and some fibers pull-out. In the present case, no delamination can be observed along laminates' edges. Regardless of the orientation of the initial notch, the failure direction is transverse in both 0° and 45° oriented notches. Fracture mechanisms appear to be very

similar in cases, therefore suggesting that the effect of shearing induced by a mixed-mode loading is not prominent to rule failure. These damage mechanisms are schematically illustrated on Figure 68b. The mechanical load is primarily borne by the longitudinal (weft) fibers, and when they fail in the vicinity of the crack tip, the load is transferred to the neighboring longitudinal and 45° oriented fibers which cannot bear a significant portion of the tensile load. As a result, most of the load being borne by the longitudinal fiber bundles, the failure of the overstressed fibers at the crack tip leads to a rapid growth of the transverse crack (see Figure 64b and Figure 66b). In addition, the macroscopic responses reveal that the crack growth is more gradual in laminates subjected to mixed-mode loading. Indeed as shown by the observation of the fracture surface on Figure 67b, the broken +/-45° oriented fibers loaded in shear are clearly visible, therefore suggesting that these fibers may momentarily take up the load and the local matrix-rich areas may plastically deform during load transfer. Such mechanism is also expected to reflect on the strain energy release rate during transverse cracking, as it should be more significant in QI laminates subjected to mixed-mode loading.

II.5.4 Influence of matrix ductility and toughness on Acoustic Emission activity

Monitoring the Acoustic Emission activity is a real-time indicator of damage chronology within laminates. Prior knowledge of the primary damage mechanisms taking place within the laminates (see section II.5.3) is therefore required to discuss the evolution of both cumulated events and acoustic energy depending on PPS matrix ductility (see Figure 69).

In AP laminates, the evolution of cumulated AE energy vs cumulated events does not significantly depend on the failure mode (see Figure 69a). In both 0° and 45° SEN specimens, the cumulated energy reaches an asymptotic value (about 1e7 aJ) as cumulative events increase. The most energetic phase of loading occurs with a few thousands of cumulated events (about 1500 to 2000 events) between free stress-state and 70 MPa, whereas most of the

events are lowly energetic for stresses ranging from 70MPa to ultimate strength (see Figure 70). The plastic deformation threshold is identified as the limit between stable and unstable crack growth in 45° SEN specimens (see Figure 65a). At mesoscopic scale (in matrix-rich areas preferentially localized at the crimp), as long as plastic deformation is restricted to a local area around the crack tip, crack tip blunting can be observed along with a linear evolution of the CTOD as a function of applied stress (stable crack growth). From the Eq.(12) introduced in section I.4.3, the changes in the total strain energy release rate $J_{tot} = J_I + J_{II}$ (mode I + mode II) as a function of the cumulative AE energy can be computed from the energy E_i absorbed during the elastic-plastic deformation (see Figure 72a). For applied stresses lower than the plastic deformation threshold, it clearly appears that the total strain energy release rate remains low (J_{tot}<30 kJ/m²) when crack growth is stable and during which crack blunting is prominent. When crack growth becomes instable, the total strain energy release rate increases suddenly and significantly ($J_{tot} \approx 420$ kJ/m²). From the values drawn from this formulation, it also appears that the critical strain energy release rate resulting from failure is significantly higher in 45° SEN laminates experiencing mixed-mode failure (about twice as high as the value obtained with 0° SEN specimens – See Table 8a).

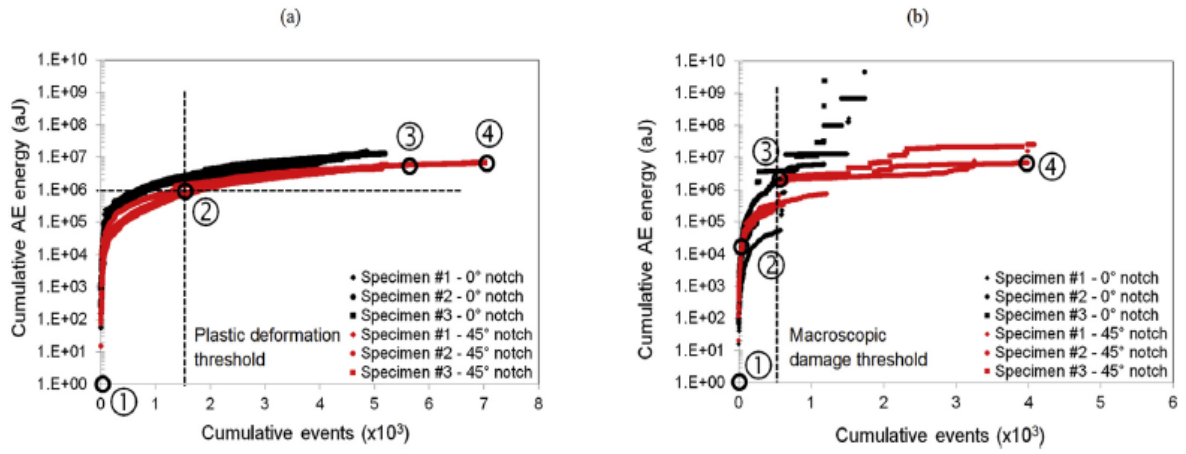

Figure 69. *Influence of the notch orientation on the AE activity in C/PPS laminates subjected to tensile loadings at 120°C: (a) Angle-ply - (b) Quasi-isotropic*

Contrary to AP laminates, the delaying effect of plastic deformation on crack growth in QI laminates occurs at the mesoscopic scale (in matrix-rich areas of the woven-plies) and does not directly reflect on the macroscopic response (see Figure 64b). In addition, the evolution of cumulated AE energy vs cumulated events significantly depends on the loading mode (see Figure 69b). In 45° SEN specimens, the cumulated energy reaches an asymptotic value (about 1e7 aJ) as cumulative events increase. Similarly to AP laminates, the most energetic phase of loading occurs with a few hundreds of cumulated events (about 500 events) between free stress-state and 180 MPa, whereas most of the events are lowly energetic for stresses ranging from 180MPa to ultimate strength (see Figure 71b). For applied stresses higher than the macroscopic damage threshold, a gap in cumulative AE energy clearly appears whereas the cumulative AE events suddenly increase (see Figure 71). According to the evolution of the CTOD vs applied stress (cf. Figure 65b), it is assumed that the failure of the longitudinal fibers results in an unstable growth of the transverse crack which cannot be captured by the Digital Image Correlation technique, as the growth is sudden and very rapid. From the macroscopic damage threshold identified on the tensile response (see Figure 64b), the gradual failure also suggests that a portion of the strain energy released during translaminar failure can be associated with a local plastic deformation of PPS matrix in matrix-rich areas coming along with some crack blunting. In addition, from the equations (3-7) introduced in section I.4.3, the changes in the total strain energy release rate $G_{tot} = G_I + G_{II}$ (mode I + mode II) as a function of the cumulative AE energy can be computed from the applied stress and the length of the initial notch (see Figure 72b). From the values drawn from this formulation, it also appears that the critical strain energy release rate resulting from failure is significantly higher in 45° SEN laminates experiencing mixed-mode failure about twice as high as the value obtained with 0° SEN specimens – (See Table 8b). In both 0° and 45° SEN QI laminates, the total strain energy release rate is 6 times as low as in AP laminates. This

difference suggests that large plastic deformation in AP laminates (due to a matrix-driven behavior and an enhanced matrix ductility at $T > T_g$) are instrumental in dissipating a great portion of the mechanical energy brought to the specimen. The "material" effect is combined with a structural one (rotation of the fibers) at the crack tip, and leads to ductile failure. Both effects contribute to high fracture toughness in AP laminates.

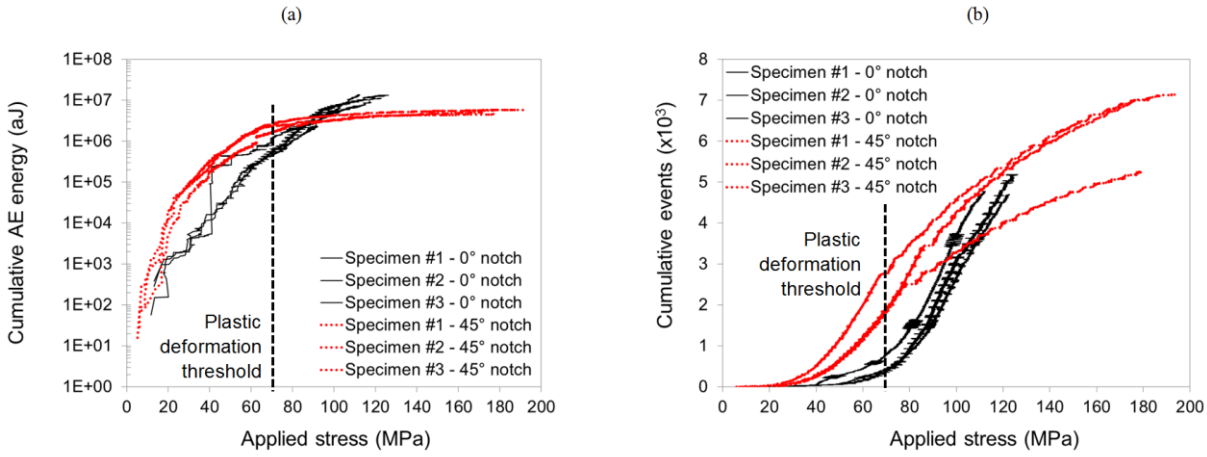

Figure 70. *Influence of the notch orientation on the AE activity in SEN C/PPS AP laminates subjected to tensile loadings at 120°C: (a) cumulative AE energy – (b) cumulative AE events*

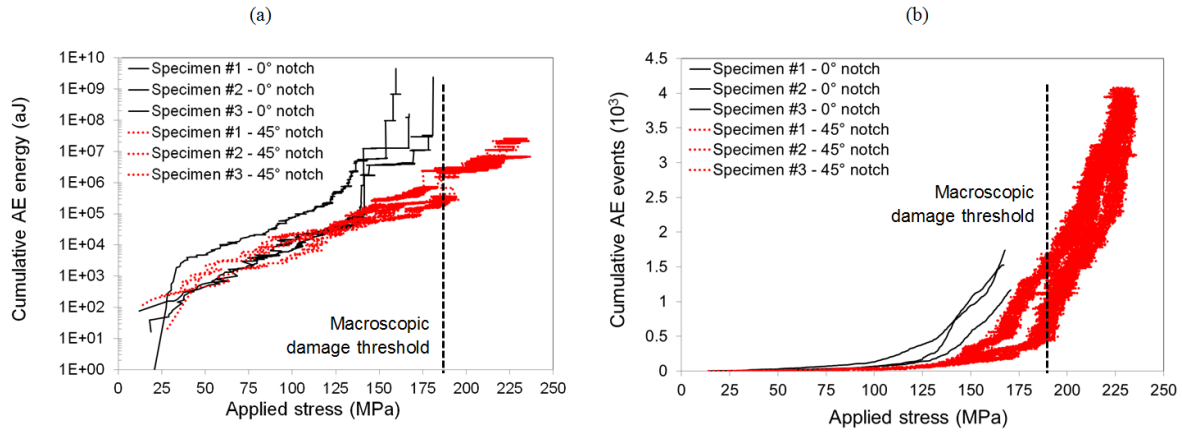

Figure 71. *Influence of the notch orientation on the AE activity in SEN C/PPS QI laminates subjected to tensile loadings at 120°C: (a) cumulative AE energy – (b) cumulative AE events*

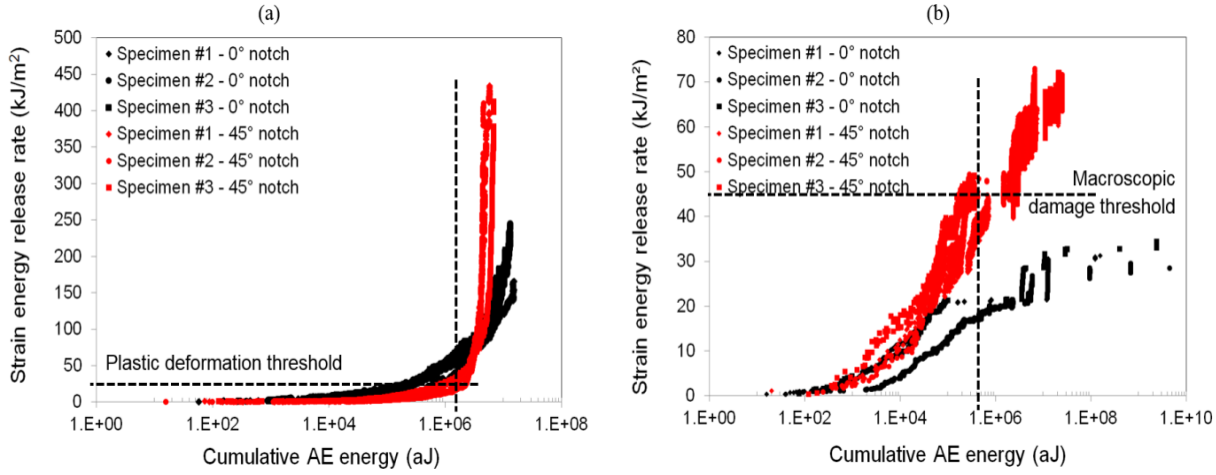

Figure 72. *Influence of the notch orientation on the evolution of the strain energy release rate in SEN C/PPS laminates subjected to tensile loadings at 120°C: (a) Angle-ply - (b) Quasi-isotropic*

Table 8. *Values of critical strain energy release rate in SEN C/PPS laminates subjected to tensile loadings at 120°C: (a) Angle-ply – (b) Quasi-isotropic*

	(a)	(b)
	J_{tot} (kJ/m^2)	G_{tot}(kJ/m^2)
0° notch	201±31	32±3
45° notch	419±13	70±5

II.6 Conclusion

The aim of this experimental chapter was to study the fracture behavior of woven-ply C/PPS laminates at high temperature. This work was carried out in 3 stages:

– Investigation of the fracture behavior of QI laminates characterized by an elastic brittle response.

- Investigation of the fracture behavior of AP laminates characterized by a time dependent behavior.
- Investigation of the matrix ductility and toughness on the strain energy release rate and failure behavior of C/PPS laminates.

In the first stage, based on the LEFM, the initiation and critical mode I fracture toughness K_{I_init} and critical K_{Ic} were determined in the case of QI laminates using different techniques. The AE technique is particularly relevant as it allows to detect not only the crack onset at the microscopic scale but also to quantify the critical strain energy release rate G_{Ic}. Then, the definition of a macroscopic damage variable based on stiffness measurements and the evolution of the cumulative AE events are used to investigate the fracture sequence. The correspondence in damage evolution given by the experimental AE data at microscopic scale and a cumulated damage variable at macroscopic scale validates the ability of both approaches to quantify the damage degree in fiber-reinforced PMCs, and to identify a critical threshold for damage initiation.

In the second stage, we were interested to the experimental determination of the strain energy release rate *J* in AP laminates characterized by a high ductile behavior at high temperature. The η_{el}-factor was determined using the compliance method. The η_{pl}-factor was calculated using the load separation method which appears to be an efficient tool to compute J-R curves of highly ductile composite systems (e.g. C/PPS laminates) at $T > T_g$. Finally, the increase of J_C as the initial crack length increases indicates that the energy released during fracture depends in particular on geometry and it is not a material property.

In the third stage, the damage evolution in carbon fibers woven-ply reinforced PolyPhenylene Sulphide (PPS) structures with different initial single edge notches was investigated. In SEN specimens, the fracture toughness can be obtained from analytical representation of the translaminar failure modes based on fracture mechanics concepts in order to understand how the physical properties of the constituents (e.g. matrix toughness and ductility) and the architecture of reinforcement (woven-ply) affect the fracture behavior of composite systems.

The influence of matrix ductility on the thermomechanical behavior of SEN structures can be evaluated considering laminates with fiber dominated behavior (quasi-isotropic stacking sequence) or matrix-dominated behavior (angle-ply stacking sequence). It is determined by the combination of loading (orientation of initial notch), location of defect and material

heterogeneity (presence of matrix-rich regions at the crimp area in woven-ply laminates). The total strain energy release rate resulting from translaminar failure is significantly higher in structures experiencing mixed-mode failure, with in AP and QI laminates respectively.

In AP laminates, a threshold (about 40 MPa) corresponding to the onset of macroscopic plastic deformation is identified from both the macroscopic responses and the AE activity. For applied stresses lower than this threshold, it clearly appears that the total strain energy release rate remains low ($J_{tot} < 30\ kJ/m^2$) when crack growth is stable and during which crack blunting is prominent. When crack growth becomes instable, the total strain energy release rate increases suddenly and significantly ($J_{tot} \approx 420\ kJ/m^2$).

In QI laminates, a threshold (about 140-160 MPa) corresponding to the onset of the macroscopic damage is also identified from both the macroscopic responses and the AE activity. The total strain energy release rate in QI laminates is 6 times as low as in AP laminates. This difference suggests that large plastic deformation in AP laminates (due to a matrix-driven behavior and an enhanced matrix ductility at $T > T_g$) are instrumental in dissipating a great portion of the mechanical energy brought to the specimen. The "material" effect is combined with a structural one (rotation of the fibers) at the crack tip, and leads to ductile failure. Both effects contribute to high fracture toughness in AP laminates.

The understanding of the influence of matrix ductility and toughness on strain energy release rate and fracture behavior of C/PPS laminates is of the utmost importance to develop numerical tools capable of capturing the deformation mechanisms in highly ductile materials. It is therefore possible to compute fracture mechanisms parameters (e.g. the critical stress intensity factor K_C or the strain energy release rate J_C) for design purposes.

Chapter III. Modeling of translaminar cracking at high temperature

Chapter III outline

III.1 Introduction

Firstly, this chapter presents the background on the numerical methods available in the literature for determining the strain energy release rate. A brief recall of the time dependent model used to take into account the highly ductile behavior of C/PPS laminates at HT is presented. Then, a mesh optimization in the case of quasi-isotropic stacking sequences is conducted through a comparison between two meshing types with different meshing refinement. The numerical overstress and overstrain profiles was validated through the comparison with theoretical stress fields and longitudinal overstrain fields obtained from experimental full-field measurements (by Digital Image Correlation technique). The selected meshing type was then used to simulate the numerical overstrain and overstress profiles for AP laminates. Finally, the strain energy release rate was evaluated using G_θ-integral method based on the mechanical fields at the crowns surrounding the crack tip. The independence path integral was checked by representing the evolution of the strain energy release rate versus each crown in laminates with a viscoelastic viscoplastic behavior at high temperature. Then, the strain energy release rate was plotted according to the applied load and crack growth. The results obtained were compared to those obtained experimentally. It's important to notice that the purpose is not to simulate the crack growth under mechanical loading but to evaluate the capability of this method to determine the strain energy release rate for different loading levels before crack initiation (where the crack growth can be considered as stable).

III.2 Modeling Background

The study of fracture mechanics in composite materials is not recent [Whitney et al., 1974] [Valentini, 1999] [Belmonte et al., 2004] [Pinho et al., 2006] [Shameli et al., 2016] [Fan et al., 2014]. When it comes to investigate numerically the crack propagation in TP-based composites at high temperature as matrix toughness and viscous behavior are significantly enhanced, there is virtually no reference in the literature. It is known that the comprehension and the prediction of both initiation and propagation of primary damage in TP composites is highly related to the presence of singular stress and strain fields [Pupurs, 2012] responsible for the accommodation of overstresses in high gradients zones (e.g. notches or holes). According to [Vieille et al., 2012] [Vieille et al., 2011], the overstress accommodation is highly temperature-dependent in high-performance TP-based composites mainly under off

axis loading. Hence, in order to account for the non-linear behavior (time-dependent and plastic behaviors) of TP-based laminates at high temperature, there is a need to develop a reliable model to capture their visco-elastic-plastic behaviors. The present work is based on a viscoelastic and viscoplastic model developed by [Albouy et al., 2013]. In the literature, many studies have been conducted to describe the time dependent behavior of Polymer Matrix Composites (PMCs). A comprehensive review of the main models is proposed by [Albouy et al., 2013]. Most of the viscoelastic models presented in the literature such as Schapery's model, were initially elaborated for polymer materials and was later extended to composites [Bonnet et al., 2004]. At higher loading levels, the viscoplastic behavior becomes prominent and not surprisingly, the viscoelastic models lose their accuracy. Finally, in the vicinity of T_g, it turns out that most of the viscoelastic models are unable to precisely predict the viscous behaviors [Al-Haik et al., 2006]. That's the reason why, a viscoelastic viscoplastic model has been developed for TP-based composites [Albouy et al., 2013] and implemented into a Finite Element code (cast3m®).

The study and the comprehension of fracture mechanics in high performance TP composite require the development of a numerical tool which is able to evaluate the energy release rate and predict the initiation and crack growth process. The main purpose of this part is then to determine the strain energy release rate G in high performance TP composite at $T > T_g$.

Many numerical tools have been developed to provide the mechanical field state in the vicinity of the crack tip. Among them, the energy methods, based on unvarying integrals, appear to be efficient to evaluate the energy release rate in accordance with a thermodynamic approach [Moutou Pitti et al., 2010]. Using such methods, it is possible to evaluate the fracture parameters far from the crack tip where the mechanical fields are largely disturbed by a strong singularity. However, some of these tools are mathematically limited to simple or global fracture modes for isotropic or orthotropic media [Moutou Pitti et al., 2010].

Using a contour integral related to energy in the vicinity of a crack, [Rice, 1968] proposed a method to solve 2D notch and crack problems in elastic-plastic materials. The J-integral can be seen as the amplitude of the stress and strain singularity; the latter is often referred to as the HRR (Hutchinson-Rice-Rosengren) singularity [Rice, 1968] [Hutchinson et al., 1968] [Rice et al., 1968] which is formally defined by the path-independent line integral:

$$J = \int_{\Gamma} \left(w(\varepsilon_{ij}).n_1 - \sigma_{ij}.n_j.\frac{\partial u_i}{\partial x} \right) d\Gamma \quad (34)$$

Where Γ is an arbitrary curve encircling the crack tip oriented by its normal n_j, u_i designates the displacement component and w is the strain energy density defined as:

$$w = \int_0^{\varepsilon} \sigma_{ij} d\varepsilon_{ij} \quad (35)$$

where σ_{ij} and ε_{ij} are the components of stress and strain, respectively.

According to [Dubois et al., 2005] and [Bouchard, 2000], the *J*-integral leads to difficulties in integrating fields at Gaussian points. Alternatively, the G_θ-integral method, applicable to materials whose behavior can be elastic, viscoelastic and viscoplastic [Dubois, Chazal, and Petit, 1999], provides a way to determine the strain energy release rate by using a surface integral. Initially developed by [Destuynder et al., 1981], the G_θ-integral is deduced from the *J*-Integral by operating, on the contour integral domain, a Gauss–Ostrogradsky transformation which changes the integration domain from a contour to a surface V. It is given by:

$$G_\theta = \int_V \left(-w.\theta_{k,k} + \sigma_{ij}.u_{i,k}.\theta_{k,j} \right) dV \quad (36)$$

where V is a surface bounded by two contours.

$\vec{\theta}\begin{pmatrix}\theta_1\\ \theta_2\end{pmatrix}$ is the virtual displacement field. It represents the virtual kinematics of the crack.

If J and G_θ integrals provide to determine an invariant leading at the mechanical state in the crack vicinity, they operate a global energy calculation independently to the mixed mode fractures. For this reason, these integrals are employed only for pure opening or pure shear fracture modes [Moutou Pitti et al., 2010].

In order to take into account the mixed mode separation, [Noether, 1971] proposed the conservative law method, based on an independent path integral. This method is characterized by an expensive finite element discretization. [Bui et al., 1985] have generalized the J-integral [Rice, 1968] by proposing a separation between symmetric and antisymetric displacement fields. This method requires a symmetric mesh in the vicinity of the crack tip. Then, initially

proposed by [Chen et al., 1977] for elastic and isotropic materials, [Moutou Pitti et al., 2007] have extended the M-integral to orthotropic materials based on virtual work principle.

[Chen el al., 1977] have introduced the M-integral adapted to isotropic and elastic material in order to separate mixed mode fracture:

$$M = \frac{1}{2} \cdot \int_{\Gamma} \left(\sigma_{ij,1}^{(v)} \cdot u_i - \sigma_{ij}^{(u)} \cdot v_{i,1} \right) \cdot n_j d\Gamma \tag{37}$$

where $(\sigma_{ij}^{(u)}, u)$ and $(\sigma_{ij}^{(v)}, v)$ are the real and virtual stresses and displacement field respectively.

Then, [Moutou Pitti, et al., 2007] have modified this integral from a curvilinear integral to a surface integral. Thus, for plane problems, M_θ-integral takes the following form:

$$M\theta = \frac{1}{2} \cdot \int_{V} \left(\sigma_{ij}^{(u)} \cdot v_{i,1} - \sigma_{ij,k}^{(v)} \cdot u_i \right) \cdot \theta_{k,j} dV \tag{38}$$

According to [Sih, 1974], in the case of orthotropic materials and for each fracture mode, the virtual displacements fields are expressed as follow:

$$\begin{aligned} v_1 = {} & 2 \cdot K_1^{(\sigma)} \cdot \sqrt{\frac{r}{2 \cdot \pi}} \cdot \Re e \left[\frac{1}{s_1 - s_2} \cdot \left(p_2 \cdot s_1 \cdot \sqrt{\rho_2} - p_1 \cdot s_2 \cdot \sqrt{\rho_1} \right) \right] \\ & + 2 \cdot K_2^{(\sigma)} \cdot \sqrt{\frac{r}{2 \cdot \pi}} \cdot \Re e \left[\frac{1}{s_1 - s_2} \cdot \left(p_2 \cdot \sqrt{\rho_2} - p_1 \cdot \sqrt{\rho_1} \right) \right] \\ v_2 = {} & 2 \cdot K_1^{(\sigma)} \cdot \sqrt{\frac{r}{2 \cdot \pi}} \cdot \Re e \left[\frac{1}{s_1 - s_2} \cdot \left(q_2 \cdot s_1 \cdot \sqrt{\rho_2} - q_1 \cdot s_2 \cdot \sqrt{\rho_1} \right) \right] \\ & + 2 \cdot K_2^{(\sigma)} \cdot \sqrt{\frac{r}{2 \cdot \pi}} \cdot \Re e \left[\frac{1}{s_1 - s_2} \cdot \left(q_2 \cdot \sqrt{\rho_2} - q_1 \cdot \sqrt{\rho_1} \right) \right] \end{aligned} \tag{39}$$

with $\rho_j = \cos(\theta) + i \cdot s_j \cdot \sin(\theta)$ avec $j \in \{1; 2\}$

and $p_j = S_{11} \cdot {s_j}^2 + S_{12}$ et $q_j = \frac{S_{22}}{s_j} + S_{12}$

s_j represent the roots of the following equation:

$$S_{11} \cdot {s_\beta}^4 + (2 \cdot S_{12} + S_{33}) \cdot {s_\beta}^2 + S_{22} = 0 \quad (40)$$

S_{11}, S_{12}, S_{22} and S_{33} are the components of the compliance tensor in an orthotropic body.

More recently, [Moutou Pitti et al., 2007] have generalized this approach into viscoelastic behavior by combining the generalized Kelvin Voigt model and M_θ-integral in the case of an elastic body. Eq. (38) becomes:

$$M\theta_v{}^{(k)} = \frac{1}{2} \cdot \int_V \left(\sigma_{ij}^{(k)}(u) \cdot {u_i}^{(k)} - \sigma_{ij,k}^{(v)}(v) \cdot {v_{i,k}}^{(k)}\right) \cdot \theta_{k,j} dV \quad (41)$$

with $k = (0,1, \ldots, N)$, where N is the number of springs.

$\left(\sigma_{ij}^{(k)}(u),\ {u_i}^{(k)}\right)$ and $\left(\sigma_{ij,k}^{(v)}(v),\ {v_i}^{(k)}\right)$ are the real and virtual stresses and displacements in the k^{th} spring.

This method is only applicable in the case of 2D configurations. In addition, although the viscoelastic behavior can be implicitly taken into account in the model through $M\theta_v$-integral, the mechanical fields are determined by considering an elastic behavior.

III.2.1 G_θ method

Destunyder et al. [1981, 1983] have introduced a vector field $\vec{\theta}$ allowing a virtual crown definition. This crown should be far enough from the crack tip in order to obtain good approximation of the solution.

The vector field $\vec{\theta}$ should verify the following properties:

- θ is parallel to the crack plan;
- θ is normal to the crack front;
- the support of θ is concentrated in the vicinity of the crack;
- $\|\theta\|$ is constant in a defined area around the crack tip

In 2D, two paths C_1 and C_2 can be considered around the crack tip. These paths divide the structure into three domains. For a given angle of inclination β, the vector field $\vec{\theta}$ can be expressed as follow [Bouchard, 2000]:

$$\begin{cases} \theta_1 = \left(1 - \frac{IM}{IJ}\right)\cos(\beta) \\ \theta_2 = \left(1 - \frac{IM}{IJ}\right)\sin(\beta) \end{cases}$$

where M is an integration point, I and J are the intersections between OM and C_1 and C_2 respectively.

Thus, θ is continuously differentiable and takes the following values in the three domains:

- in C_{int}, $\|\theta\| = 1$;
- in C_{ext}, $\|\theta\| = 0$;
- in C_{cour}, $\|\theta\|$ varies continuously from 1 to 0.

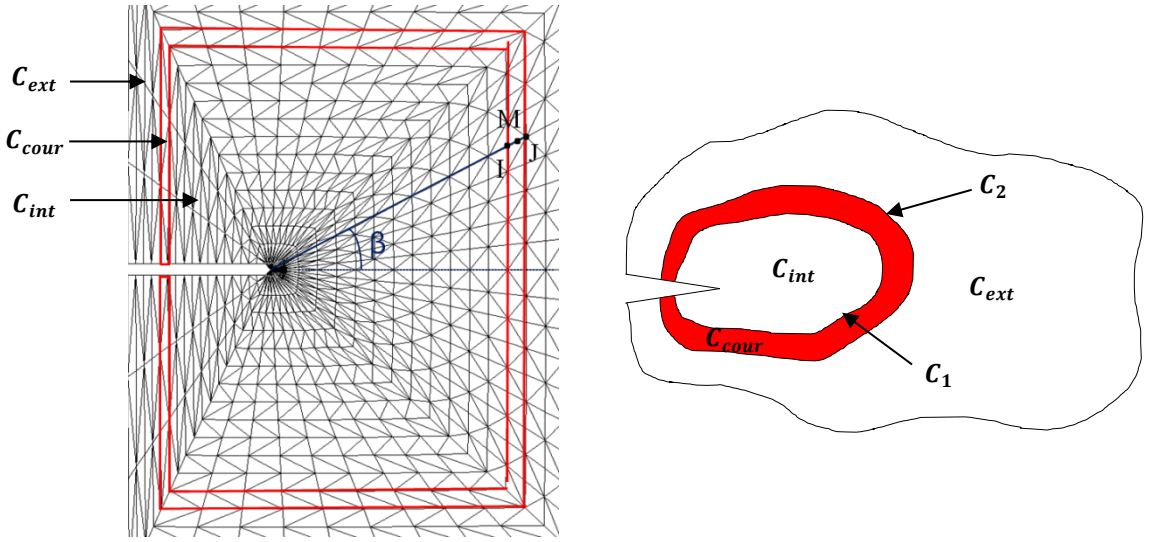

Figure 73. *Integration domain used for* Gθ*-method*

The $G\theta$-integral can be computed by means of the procedure G_THETA implemented in the finite element code cast3m®. This procedure can treat elastic, elasto-plastic and visco-plastic problems dealing with 2D, 3D or axisymmetry and can use homogenous, non-homogeneous or composite materials. It can also be used to separate the mixed modes for homogenous and isotropic materials. However, this procedure is complicated and it's very difficult to adapt it to external constitutive laws. In addition, by analyzing the analytical form of $G\theta$-integral, one can notice that it is expressed in term of displacement, strain and stress mechanical fields. In

this context, the idea was to apply directly the G_θ-integral form based on the CH-THETA procedure in order to create a θ field.

In order to accurately evaluate the G_θ-integral using G_θ-method, there is a need to develop reliable numerical tool able to predict accurate local mechanical fields in the vicinity of the crack tip.

III.3 Numerical modelling

The behavior of woven-ply thermoplastic laminates at temperature higher than their T_g was simulated using a time-dependent model. The purpose of this section was not to detail the model, but it is necessary to briefly recall its constitutive laws. For more details, the reader can refer to [Albouy et al., 2013].

III.3.1 Viscoelastic viscoplastic model constitutive laws

In order to predict accurately the time dependent behavior carbon fibers woven-ply reinforced PolyPhenylene Sulphide (PPS) laminates at temperature higher than their T_g, a linear spectral viscoelastic model and a generalized Norton-type viscoplastic formulation developed for TS-based composites have been considered [Albouy et al., 2013] [Boubakar et al., 2003]. As a first approximation, the small strain formulation is used. Thus, under an incremental formalism, the total stain can be divided into three parts as follow:

$$\underline{\Delta\varepsilon} = \underline{\Delta\varepsilon}^{e} + \underline{\Delta\varepsilon}^{ve} + \Delta\underline{\varepsilon}^{vp} \tag{42}$$

where $\underline{\varepsilon}^{e}$ is the elastic strain, $\underline{\varepsilon}^{ve}$ is the viscoelastic one and $\underline{\varepsilon}^{vp}$ is the viscoplastic one.

Viscoelastic spectral linear model

In order to simulate the viscoelastic behavior of Polymer Matrix Composites (PMCs) at high temperature, a viscoelastic spectral linear model was chosen [Albouy et al., 2013]. It consists in decomposing the viscoelastic strain rate $\underline{\dot{\varepsilon}}^{ve}$ into elementary mechanisms $\underline{\xi}_i$ which are associated with relaxation time spectrum such as:

$$\underline{\dot{\varepsilon}}^{ve} = \sum_{i=1}^{n_b} \underline{\xi}_i \tag{43}$$

where n_b is the total number of mechanisms.

The viscoelastic formulation assumes a normal distribution of the relaxation mechanisms weights μ_i according to the relaxation time of the i[th] mechanism $n(i) = \log(\tau_i)$ where τ_i is the relaxation time:

$$\mu_i = \frac{1}{n_0\sqrt{\pi}} \times exp\left(-\left(\frac{n(i) - n_c}{n_0}\right)^2\right) \tag{44}$$

with $n_i = n_c + n_0 + (i-1)\Delta$ is the ith relaxation mechanism and $\Delta = 2n_0/n_b - 1$ is the time interval separating two relaxation times.

The spectrum is described by two parameters: its standard deviation n_0 and its average value n_c.

$$\underline{\dot{\xi}}_i = \frac{1}{\tau_i}(\mu_i \underline{\underline{S}}^{\mathrm{ve}} \underline{\sigma} - \underline{\xi}_i) \tag{45}$$

where $\underline{\sigma}$ is the Cauchy stress tensor and $\underline{\underline{S}}^{ve}$ is the viscoelastic compliances tensor.

In the case of woven ply, under the assumption of a purely elastic behavior in fibers directions (direction 1 and 2 in the case of a woven-ply lamina) and a plane stress state (thin laminated plate), $\underline{\underline{S}}^{\mathrm{ve}}$ can be defined by:

$$\underline{\underline{S}}^{\mathrm{ve}} = \begin{vmatrix} 0 & 0 & 0 & 0 & 0 & 0 \\ 0 & 0 & 0 & 0 & 0 & 0 \\ 0 & 0 & 0 & 0 & 0 & 0 \\ 0 & 0 & 0 & \beta_{44}/G_{12} & 0 & 0 \\ 0 & 0 & 0 & 0 & 0 & 0 \\ 0 & 0 & 0 & 0 & 0 & 0 \end{vmatrix} \tag{46}$$

where G_{12} is the shear modulus and β_{44} is a material viscosity parameter.

Generalized Norton-type viscoplastic model

In order to develop a satisfactory modelling at high stress levels, a generalized Norton-type viscoplastic model [Boubakar et al., 2003] is added to the viscoelastic model:

$$f_{vp}(\underline{\sigma} - \underline{X}) = \overline{(\underline{\sigma} - \underline{X})} - \tau_y(T) \tag{47}$$

with $\overline{(\underline{\sigma} - \underline{X})} = \sqrt{{}^{T}(\underline{\sigma} - \underline{X})\underline{\underline{M}}(\underline{\sigma} - \underline{X})}$

$\underline{\underline{M}}$ describes the viscoplastic flow anisotropy associated with the PPS matrix in shear loading:

$$\underline{\underline{\mathrm{M}}} = \begin{vmatrix} 0 & 0 & 0 & 0 & 0 & 0 \\ 0 & 0 & 0 & 0 & 0 & 0 \\ 0 & 0 & 0 & 0 & 0 & 0 \\ 0 & 0 & 0 & 1 & 0 & 0 \\ 0 & 0 & 0 & 0 & 1 & 0 \\ 0 & 0 & 0 & 0 & 0 & 1 \end{vmatrix} \tag{48}$$

$\underline{X}$ is the thermodynamic force. In the case of a linear kinematics hardening, it is associated with $\underline{\alpha}$ such as $\underline{X} = \delta\underline{\alpha}$.

δ is a material parameter associated with the linear kinematic hardening.

The constitutive laws for the viscoplastic strain rate $\underline{\dot{\varepsilon}}^{vp}$ and the kinematic hardening rate $\underline{\dot{\alpha}}$ are derived from the thermodynamical potential f_{vp} such as:

$$\underline{\dot{\varepsilon}}^{vp} = K\langle f_{vp}\rangle^{N} \frac{\partial f_{vp}}{\partial \underline{\sigma}} \text{ and } \underline{\dot{\alpha}} = -K\langle f_{vp}\rangle^{N} \frac{\partial f_{vp}}{\partial \underline{X}} \tag{49}$$

with N represents the material rate sensitivity and K is a penalty coefficient. When $K \to \infty$, the classical time-independent plasticity expression is recovered. Therefore, the evolution laws can be expressed as follows:

$$\underline{\dot{\varepsilon}}^{vp} = \dot{\lambda}_{vp} \frac{\underline{\underline{M}}(\underline{\sigma} - \underline{X})}{\overline{(\underline{\sigma} - \underline{X})}} \text{ and } \underline{\dot{\alpha}} = \dot{\lambda}_{vp} \frac{\underline{\underline{M}}(\underline{\sigma} - \underline{X})}{\overline{(\underline{\sigma} - \underline{X})}} = \underline{\dot{\varepsilon}}^{vp} \tag{50}$$

where $\dot{\lambda}_{vp} = \sqrt{{}^{T}\underline{\dot{\varepsilon}}^{vp}\underline{\underline{M}}^{-1}\underline{\dot{\varepsilon}}^{vp}}$ is the Lagrange viscoplastic multiplier homogenous to a strain rate. Using a backward Euler method, the previous constitutive laws have been time-discretized, and the resulting incremental laws have been implemented into a Finite-Element code [Albouy et al., 2013].

Parameters identification

It is noteworthy that the main advantage of the present modelling compared to other models found in the literature is the reduced number of parameters to identify. The parameters of the viscoelastic and viscoplastic constitutive laws are summarized in Table 9. The mechanical tests carried out to identify the parameters of the models are detailed in [Albouy et al., 2013].

Table 9. *Parameters identification – mechanical properties, viscoelastic and viscoplastic parameters [Albouy et al., 2013]*

Mechanical properties					Viscoelastic parameters			Viscoplastic parameters		
E_1(GPa)	E_2(GPa)	G_{12}(GPa)	υ_{12}	τ_y(MPa)	n_c	n_0	B_{44}	δ(MPa)	K	N
56.5	56.6	1.35	0.04	10	4.05	6.9	0.6	400	$8.4e^{-12}$	9.5

III.4 Triaxility in ductile materials

The response of polymers is known to be sensitive to factors such as: temperature, plastic instability during the necking stage and the hardening, and the type of loading conditions, i.e. the loading rate and the stress triaxiality effect [Boisot et al., 2011] [Castagnet et al., 2007]. Under off-axis loading conditions, polymer-based composites also depend on these factors. More specifically, the stress triaxiality ratio TF is defined from the hydrostatic pressure and the Von Mises equivalent stress:

$$TF = \frac{p}{\overline{\sigma}} = \frac{1}{3}\frac{tr(\sigma)}{\overline{\sigma}} \tag{51}$$

Where the Von Mises equivalent stress is defined by $\overline{\sigma} = \sqrt{\sigma_1^2 + \sigma_2^2 - \sigma_1\sigma_2 + 3\sigma_{12}^2}$ in plane stress conditions, which is a reasonable assumption for thin laminates.

Stress triaxiality is known to be pronounced in the crack tip vicinity of edge crack and depends on notch geometry. According to [Boisot et al., 2011], by decreasing the notch root radius ρ, the peak stress increases (see Figure 74). It is a classical result related to the stress triaxiality ratio increase inversely to the notch radius of notched tensile specimens.

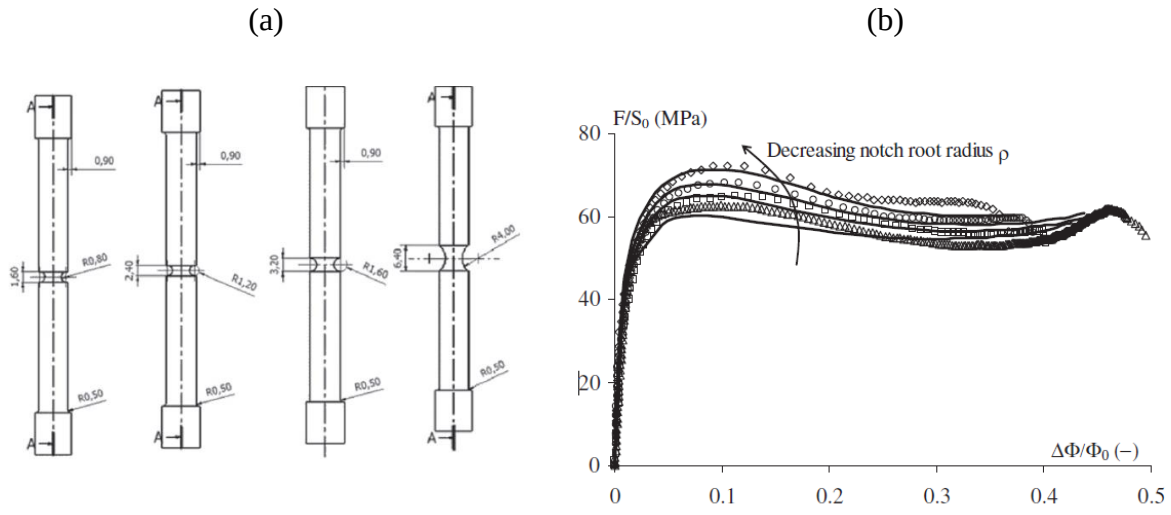

Figure 74. Influence of stress triaxiality ratio on tensile macroscopic response of PA polymers [Boisot et al., 2011]

The ductile failure of structures usually consists of three phases: (a) accumulation of damage; (b) initiation of fracture; and (c) crack propagation. One way to think of fracture initiation is to consider it as the result of the accumulation of ductile plastic damage [Xue, 2007] [Lemaître, 1985]. According to [Mou el al., 1996], among the factors influencing damage evolution in ductile materials, the stress triaxiality ratio has the greatest effects. Indeed, a faster rate of damage occurs at higher stress triaxiality ratios as it greatly influences the amount of plastic strain which a material may undergo before ductile failure occurs.

III.5 Meshing strategies [Chabchoub el al., 2016]

In order to test the capability of the numerical model to predict the response (overstress and overstrain profiles) of high-gradient structures [Vieille et al., 2016], simulations have been carried out on Single Edge Notched (SEN) specimens, characterized by a ratio=0.3 of the initial notch length over the specimen width. For symmetry reasons, only a half of the plate is

modelled. Although reduction in the mesh size leads to more accurate FE solution, the finer mesh refinement requires more computation time. That is the reason why, it is necessary to find a compromise between accuracy requirements and computation time. To this end, three-node triangular elements (Discrete Kirchhoff Triangles - DKT) have been used to mesh the crack tip with higher mesh density and two different types of meshing (radiant and concentric - see Figure 75) around the crack tip were tested, allowing us to generate crowns around the crack tip. Indeed, crowns, whose boundaries coincide with elements sides, have a crucial role when computing the strain energy release rate by means of the G_θ-method. In addition, the numerical integration is performed at Gauss integration points of elements belonging to the crown, giving therefore more accurate results.

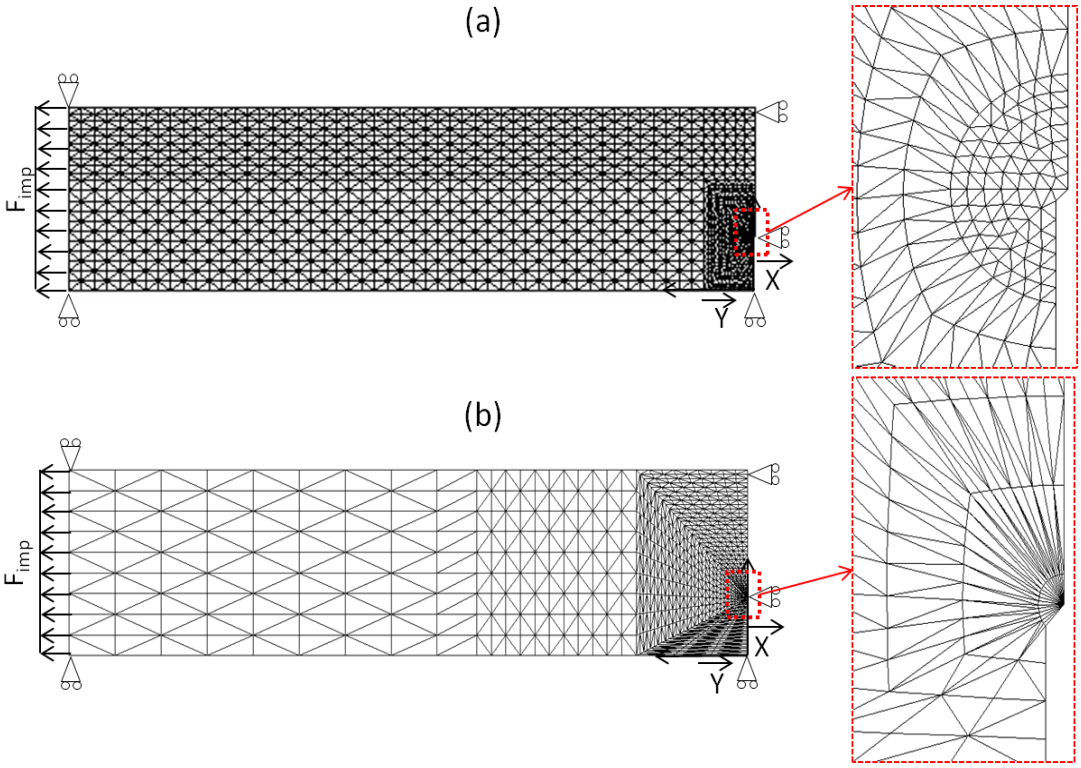

Figure 75. *Meshing of the notched specimens with zoom on the crack-tip area : (a) Concentric mesh (3933 elements) – (b) Radiant mesh (2061 elements)*

III.6 Results and discussion

One of the most important criteria for selecting an efficient mesh is its ability to generate accurate overstress and overstrain fields in high gradient zones. Indeed, the development and

the increase in stress concentration within composite materials [Tanet al., 1988] [Huang et al., 2015] has always been of great interest to researchers, and many studies have been conducted to investigate the effect of stress concentration zones (notches, holes…) on the mechanical properties of composites [Liu et al., 2010].

To account for the stress concentration near a singularity (namely at the crack tip), the stress concentration factor K_t is classically defined by:

$$K_t = \frac{\sigma_y(r,\theta)}{\sigma_{remote}} \tag{52}$$

where $\sigma_y(r,\theta)$ is the longitudinal stress in the vicinity of the crack tip (see Figure 63) and σ_{remote} is the remote stress applied at the specimen boundaries. More specifically, the expression of $\sigma_y(r,\theta)$ at the crack tip in mode I can be expressed as a function of the stress intensity factor K_I as follows:

$$\sigma_y(r,\theta) = \frac{K_I}{\sqrt{2\pi r}} \tag{53}$$

Substituting Eq. (53) into Eq. (52), one can obtain the expression of the stress concentration factor K_t in mode I type loading in the case of quasi-isotropic specimens:

$$K_t = \sqrt{\frac{a}{2r}} F(a/w) \tag{54}$$

III.6.1 Mesh optimization

From the macroscopic standpoint, the proposed model predicts suitably the tensile mechanical response of notched specimens consisting of angle-ply and quasi-isotropic stacking sequences (Figure 76). In QI specimens, a radiant meshing appears to be slightly more accurate than the concentric meshing (Figure 76b).

III.6.1.1 Quasi-isotropic laminates

As long as non-linear deformations are restricted to a small zone near the crack tip, LEFM stress intensity factors can be applied to a first approximation for quasi-isotropic laminates [Rice, 1968] [Sih et al., 1965]. The tested QI specimens are characterized by an elastic-brittle macroscopic response (Figure 76b) which results mainly from fiber tow fracture and

transverse matrix cracking adjacent to the notch [Albouy et al., 2013]. On the one hand, the comparison of overstresses profiles at 76.4 MPa (Figure 77 and Figure 78), before failure (155 MPa), shows that starting from 2061 elements for the radiant mesh and 3933 elements for the concentric mesh, the meshing refinement in the vicinity of the crack tip has virtually no influence on the overstress profiles. On the other hand, the evaluation of the intensity of overstrains at stress-concentration zones is also relevant in engineering design.

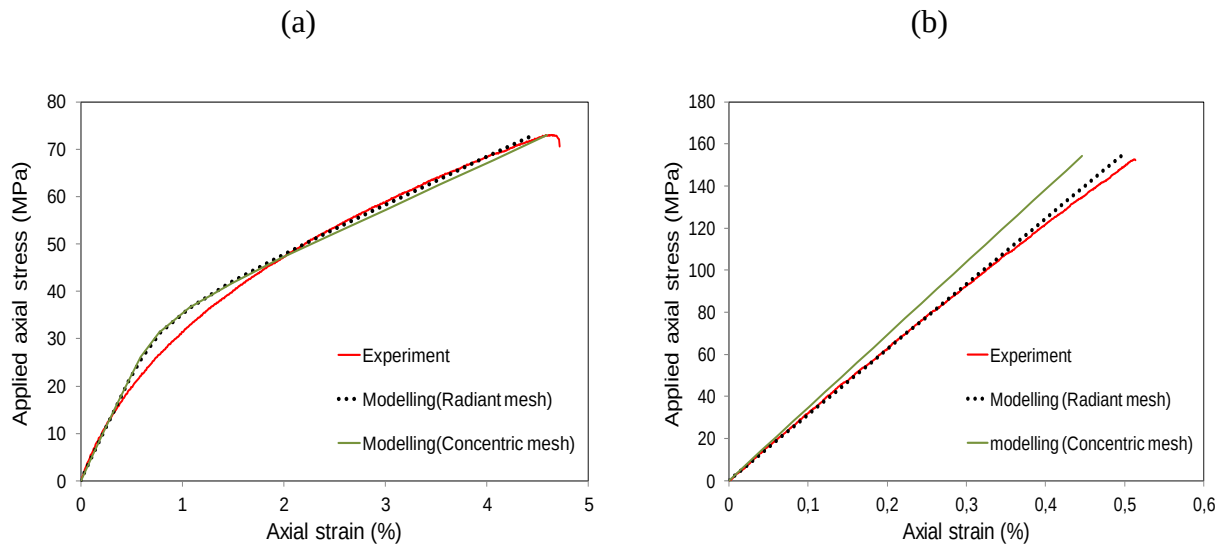

Figure 76. *Montonic tensile test on notched C/PPS laminates: experience vs numerical modelling (a) AP (b) QI*

In QI laminates, the comparison of the experimental overstrain profiles, obtained by DIC technique (Figure 79) at 76.4 MPa, shows that the radiant meshing provides more accurate profile than the concentric meshing with a lower number of elements. Knowledge of the CPU time computation is also important to choose the most effective meshing type. Table 10 shows that the concentric mesh requires higher CPU computation time using PC DELL Inspiron 15R with the processor Intel® Core™ 1.8GHz, 8GB RAM, hence one can conclude that radiant mesh with 2061 elements is more effective in terms of accuracy and computation time.

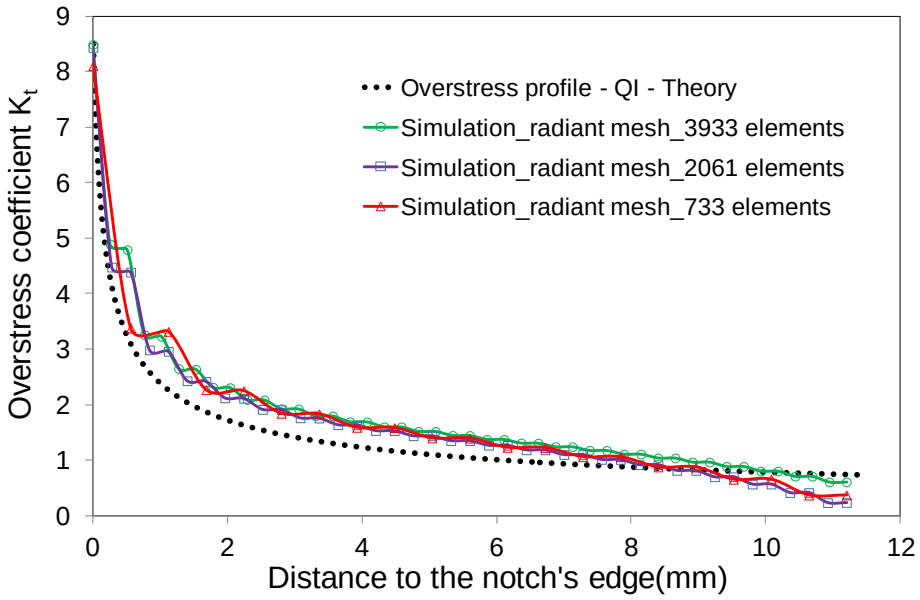

Figure 77. *Comparison of numerical and theoretical overstress profiles in notched QI C/PPS laminate at 120°C using a radiant meshing*

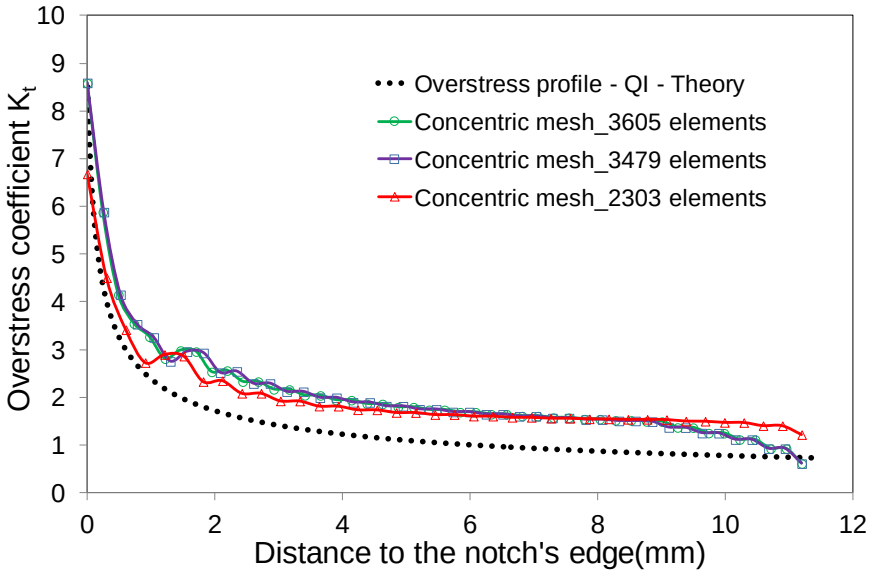

Figure 78. *Comparison of numerical and theoretical overstress profiles in notched QI C/PPS laminate at 120°C using a concentric meshing*

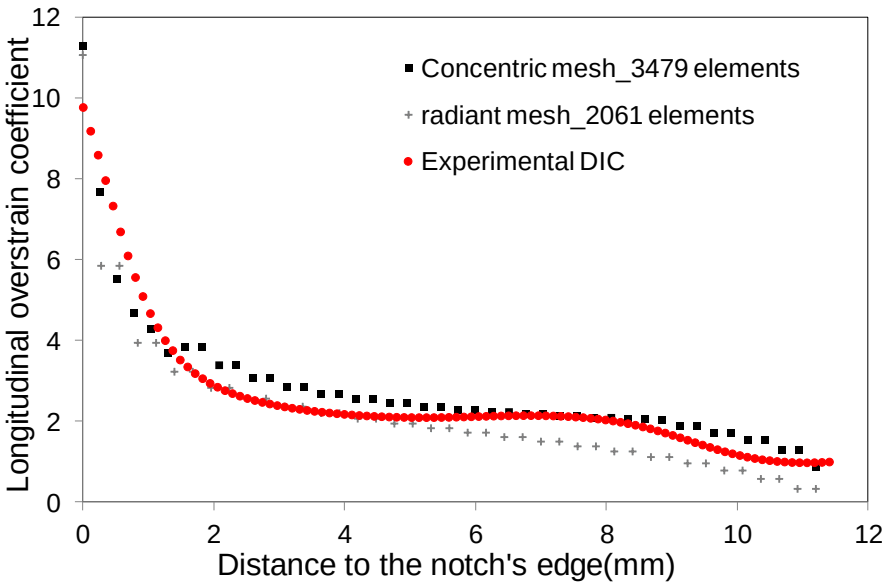

Figure 79. *Comparison of numerical and experimental overstrains profiles in notched QI C/PPS laminate at 120°C*

Table 10. *Comparison of CPU time computations*

Meshing type	*Radiant mesh*	*Concentric mesh*
Number of elements	2061	3479
CPU time	t	1.66t

To further investigate the relevance of the radiant mesh to predict accurate overstress or stress concentration factor at the crack tip, theoretical and numerical stress concentration factors have been compared for different initial length over width ratio (ranging from 0.1 to 0.6). Figure 80 illustrates the good accuracy of the proposed modelling. In addition, it appears that, as the ratio a/w increases, the stress concentration at the crack tip increases, hence confirming the high tensile strength dependence on the scale effects [Wisnom et al., 2010] [Carpinteri et al., 1998] [Green et al., 2007]. Comparing the overstress profiles at 76.4 MPa and 155 MPa, one can notice that K_t does not change resulting in similar overstress profiles (Figure 81a). At last, when comparing DIC and Finite Element (FE) results, the longitudinal Green-Lagrange strain fields at 76.4 MPa as well as at 155 MPa are in good agreement from qualitative and quantitative standpoints (Figure 82).

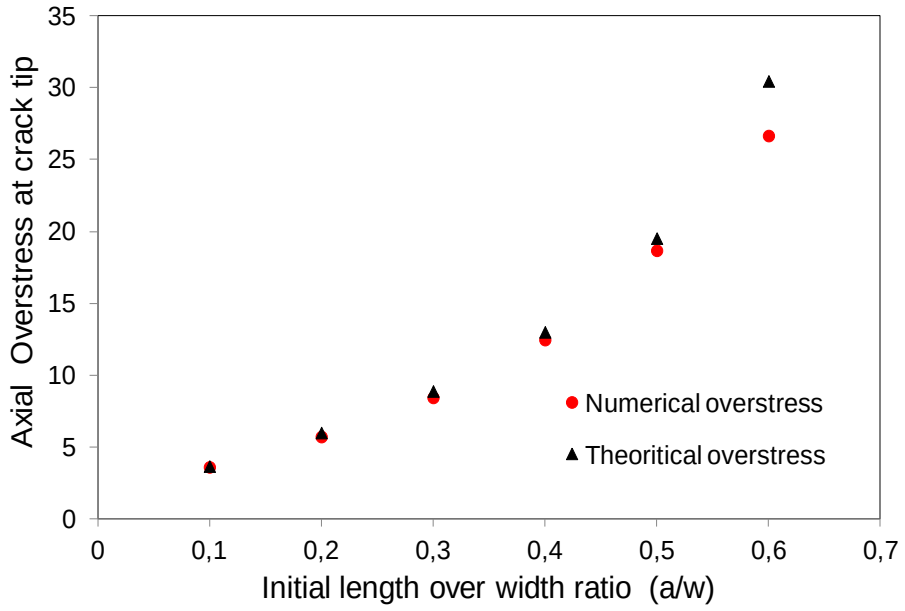

Figure 80. *Comparison of numerical and theoretical overstress at crack tip for different a/W in notched QI C/PPS laminate at 120°C*

(a) (b)

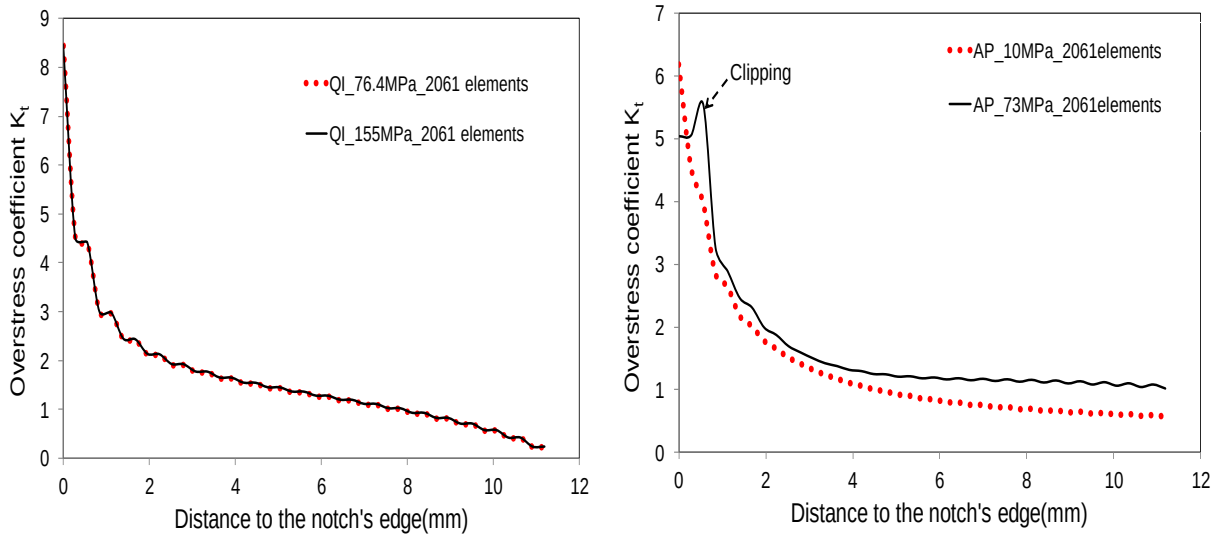

Figure 81. *Comparison of numerical overstress distribution for elastic and viscoelastoplastic behavior in notched C/PPS laminates at 120°C: (a) QI (b) AP*

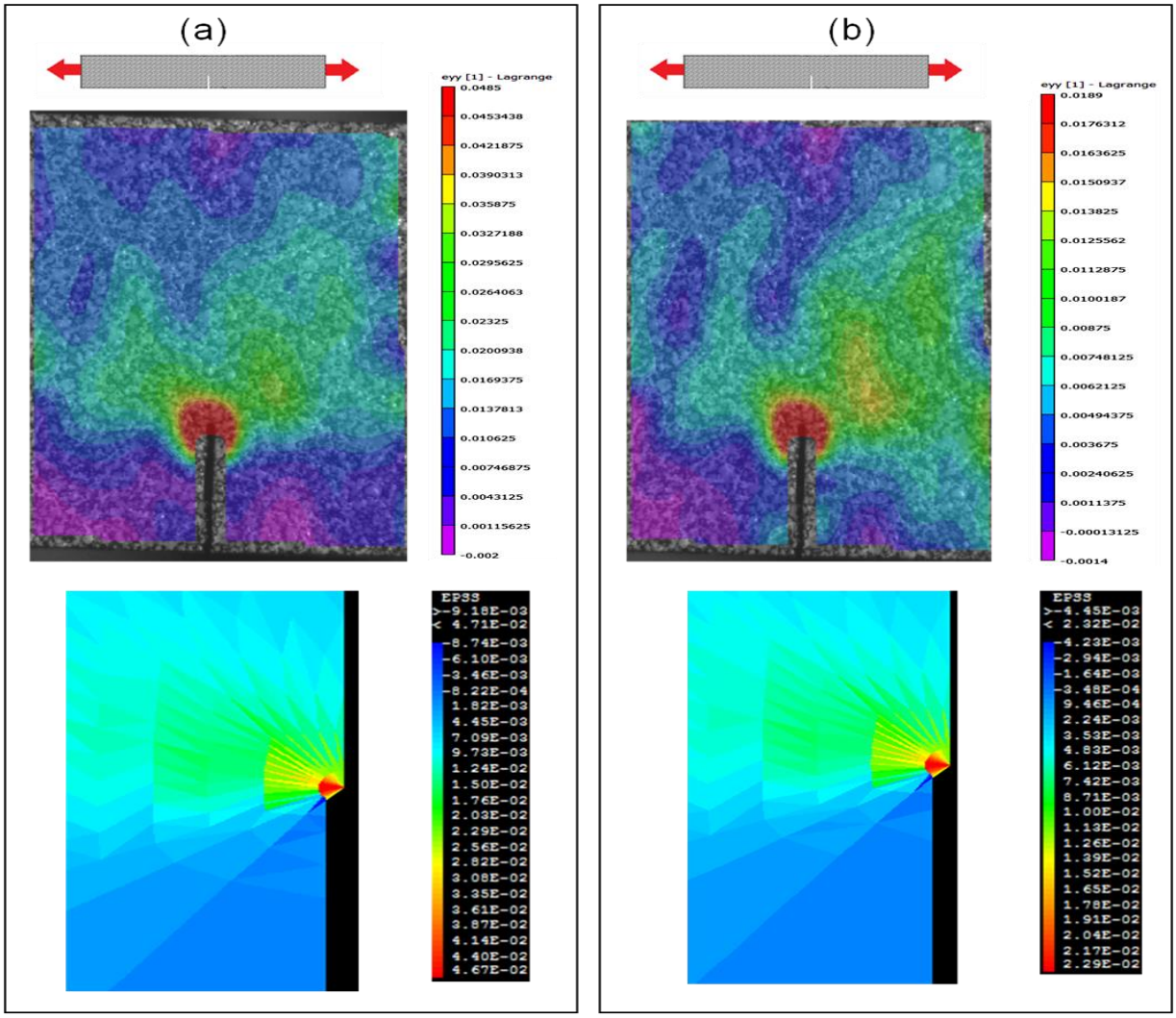

Figure 82. *Comparison of numerical and experimental longitudinal strain fields (obtained by Vic2D Digital Image Correlation) in quasi-isotropic C/PPS laminates at 120°C (a) 155 MPa (b) 76.4 MPa*

III.6.1.2 Angle-ply laminates

LEFM strictly applies only when the material behavior is dominantly elastic and the fracture response, brittle [Rice, 1968] [Sih et al., 1965] [Tada et al., 2000]. Therefore, the previous expression of K_t cannot be applied in the case of notched AP laminates whose behavior is strongly matrix-dependent (Figure 76). Indeed, the optimized mesh discussed in section III.6.1.1 virtually does not depend on the stacking sequence. Thus, it has been considered to simulate the overstress and overstrain profiles in notched AP laminates. At a stress level (e.g. 10MPa) lower than AP laminates' damage threshold (34MPa) [Vieille et al., 2012], the comparison of numerical and experimental overstrain profile (Figure 83) shows that the

modelling is in good agreement with the experience. From the strain distribution viewpoint, the comparison of Finite Element (FE) and DIC results reveals that the longitudinal Green-Lagrange strain fields at 10MPa are in good accordance (Figure 84b) as long as the mechanical response of AP laminates is elastic. However, at 73 MPa, one can notice that the numerical modelling relatively loses its accuracy comparing with DIC longitudinal strain distribution (Figure 84a). As it is shown in the literature [Cravero et al., 2007], it is usually explained by an important notch opening coming with large fiber rotation and displacement near the crack tip (Figure 85). Let's also recall that the proposed modelling is built within a small perturbations framework such as it is not adapted to account for these large deformation regimes.

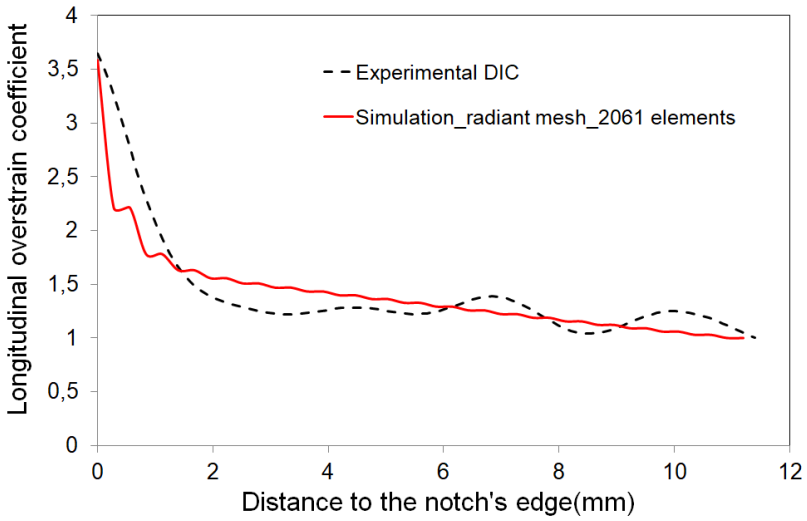

Figure 83. *Comparison of numerical and experimental overstrain profiles in notched AP C/PPS laminate at 120°C*

Finally, the obtained results also confirm the conclusion drawn in the literature on the influence of matrix plastic deformation on the distribution of overstresses near the singularity. Indeed, by increasing the applied tensile load to 73MPa, the enhanced ductility of C/PPS AP laminates at $T > T_g$ contributes to significant overstress accommodation at crack tip through an important plastic deformation along the ±45 fibers [Aidi et al., 2015] [Aidi et al., 2016] [Lagattu et al., 2005] [Vieille et al., 2011] [Vieille et al., 2012], resulting in a "clipping" of the overstress peak at the edge of the crack (Figure 81b).

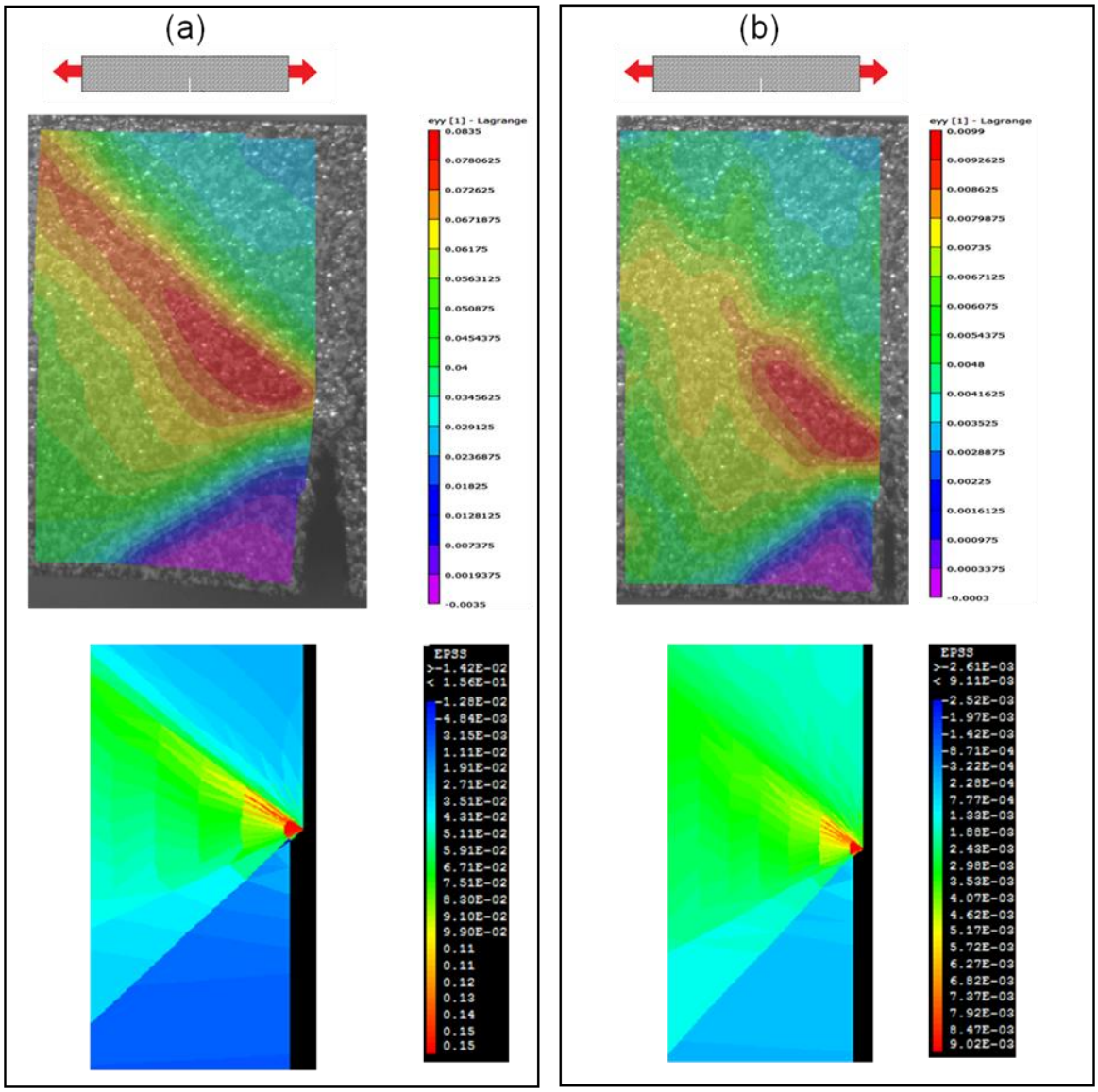

Figure 84. *Comparison of numerical and experimental (obtained by Vic2D Digital Image Correlation) longitudinal strain fields in angle-ply C/PPS laminates at 120°C: (a) 73 MPa (b) 10 MPa*

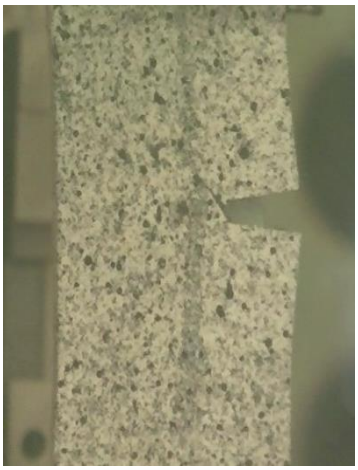

Figure 85. *Notch opening and AP specimen distortion at 73 MPa*

III.6.2 Stress triaxiality factor in SEN C/PPS laminates

The triaxiality of the stress state is known to greatly influence the amount of plastic strain which a material may undergo before failure occurs especially for high gradient structures. Figure 86 and Figure 87 show the evolution of the stress triaxiality factor for QI and AP laminates, respectively. In fact, the distribution of plastic deformation at the crack tip contributes to modify the local stress state and thus, the stress triaxiality near the singularity zone. The increase in triaxiality in the vicinity of crack tip highly influences the deformation mechanisms which can occur. Consequently, it affects the damage mechanisms initiation and propagation.

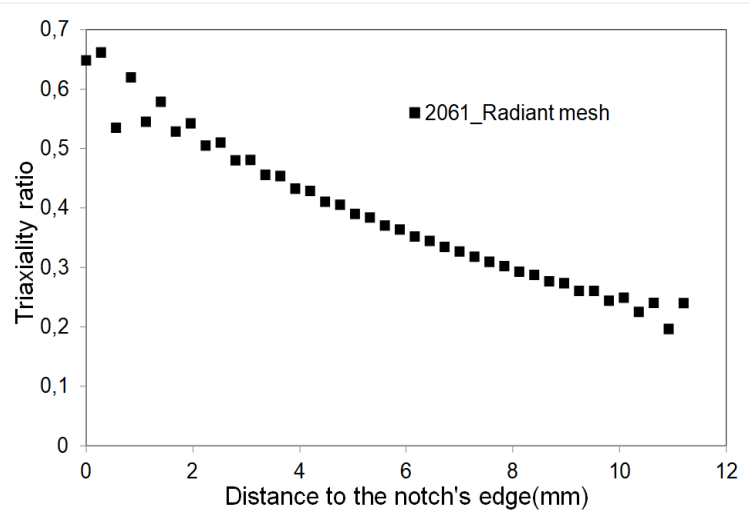

Figure 86. *Evolution of the stress triaxiality factor according to the distance to the notch' edge in notched QI laminates at 76.4 MPa*

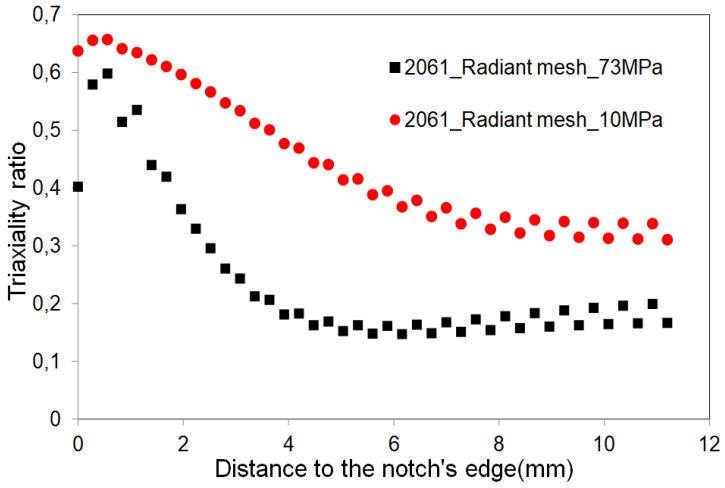

Figure 87. *Evolution of the stress triaxiality factor according to the distance to the notch' edge in notched AP laminates at 10 and 73 MPa*

III.6.3 Estimation of the strain energy release rate based on G_θ method

In this section, we are interested in the numerical determination of the initiation strain energy release rate evolution in AP and QI laminates. For the two stacking sequences, two ratios *a/W=0.2* and *0.3* were studied. These ratios were chosen so that to correctly apply the G_θ method. In other words, to obtain a strain energy release rate which stabilizes far from both the crack tip and the notch edge. In fact, it is necessary to choose an integration crown in such a way as to validate the path independence domain. Figure 88, Figure 89, Figure 90 and Figure 91 show the evolution of the strain energy release rate according to the i^{th} integration crown. It appears that G_θ highly depends on the integration crown. In both cases, G_θ increases gradually until a constant value is reached. It's the high singularity of the mechanical fields which disturbs the field integration around the crack tip.

(a) (b)

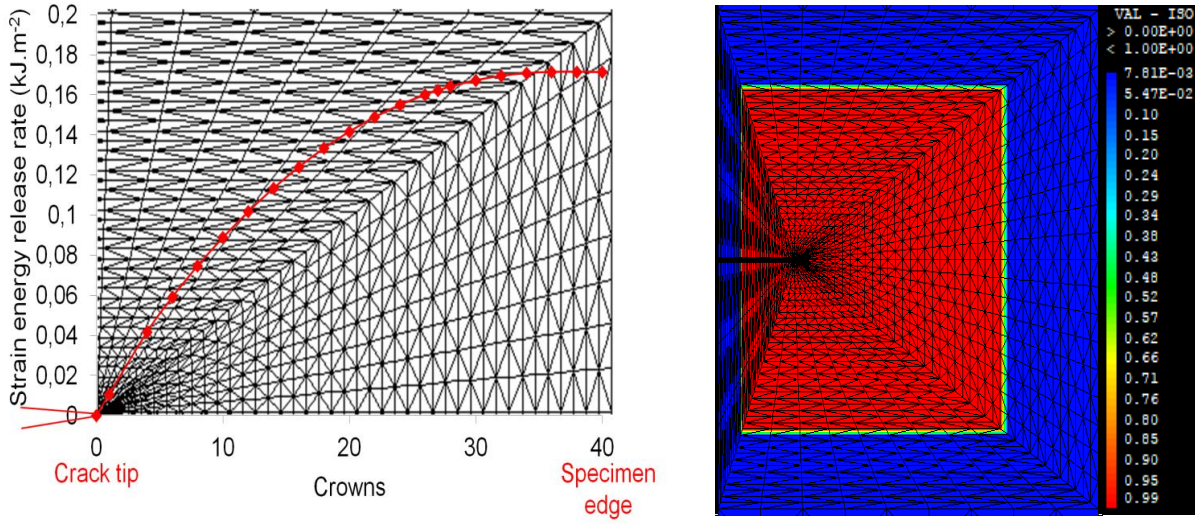

Figure 88. *Path independence domain for a/W=0.2 in notched QI laminates: (a) Evolution of the strain energy release rate according to each crown and (b)θ field in the 28th crown.*

(a) (b)

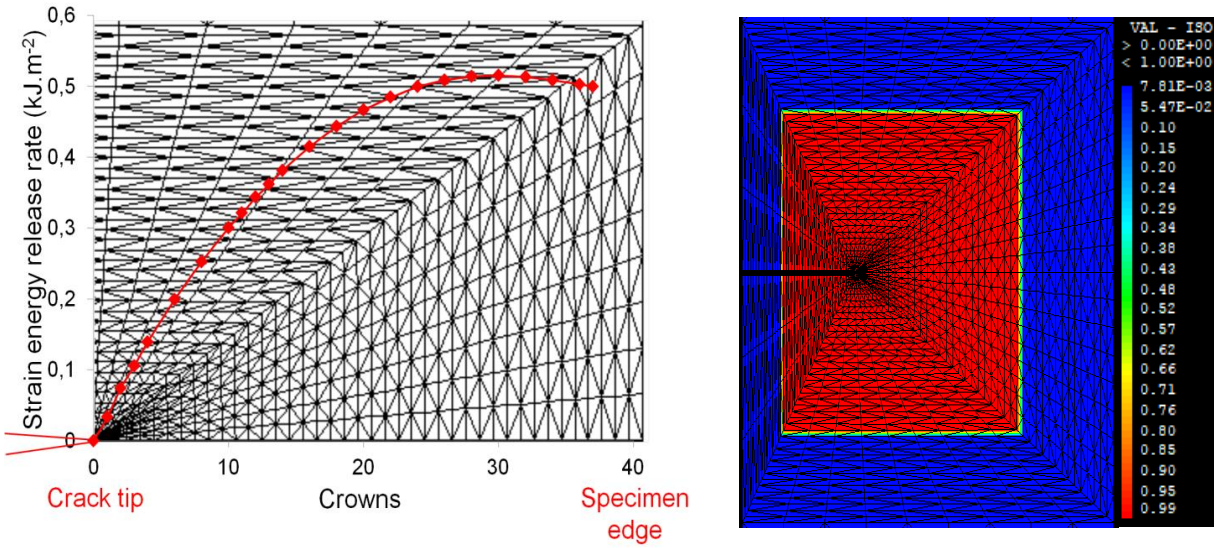

Figure 89. *Path independence domain for a/W=0.3 in notched QI laminates: (a) Evolution of the strain energy release rate according to each crown and (b)θ field in the 26th crown.*

(a) (b)

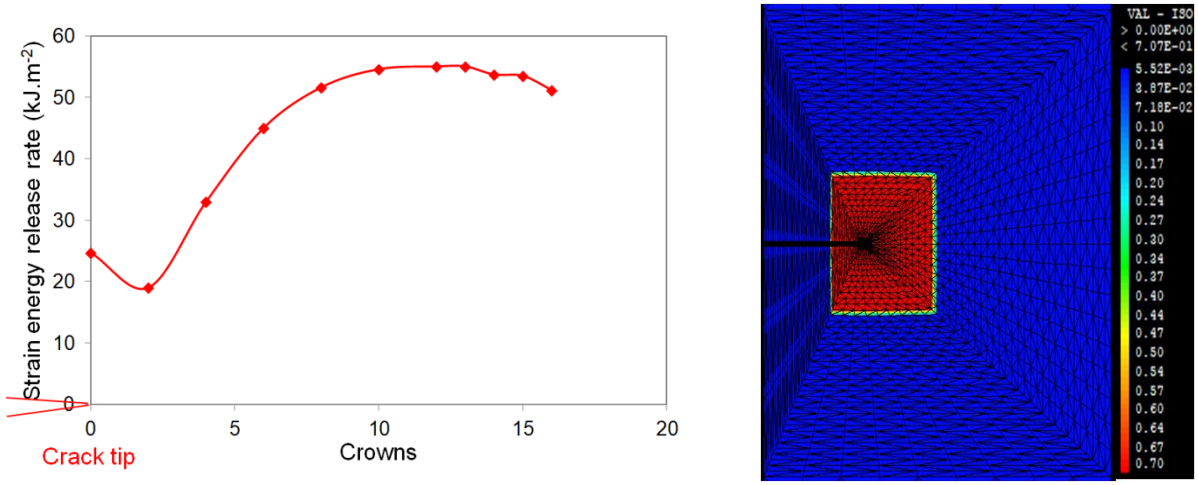

Figure 90. *Path independance domain for a/W=0.3 in notched AP laminates (a) Evolution of the strain energy release rate according to each crown (b)θ field in the 12th crown.*

(a) (b)

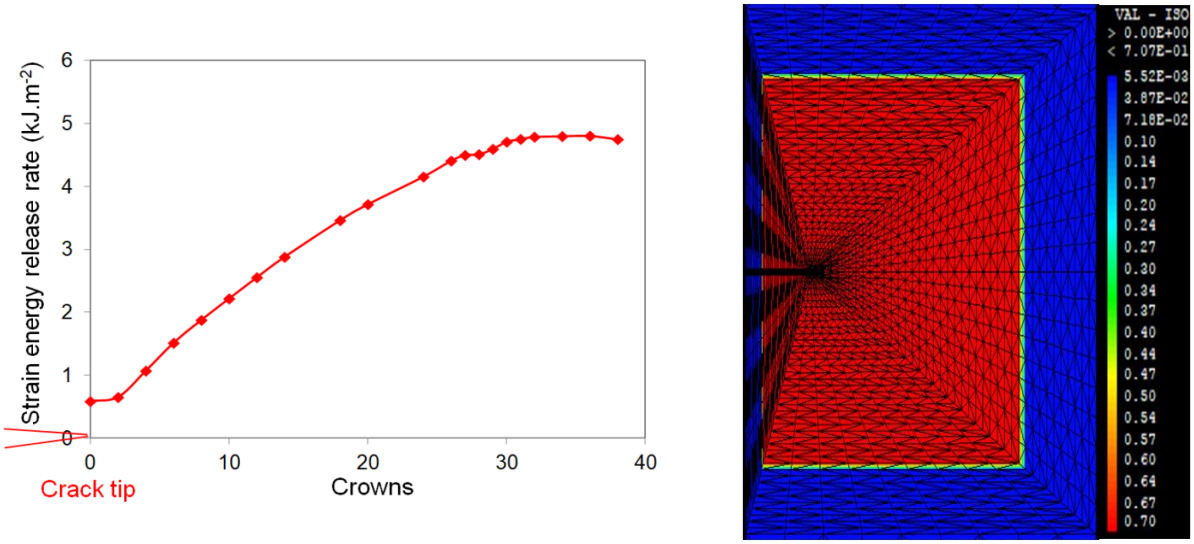

Figure 91. *Path independance domain for a/W=0.2 in notched AP laminates: (a) Evolution of the strain energy release rate according to each crown and (b)θ field in the 30th crown.*

Based on Eq.(36) and G_θ-method detailed in section III.2.1., the strain energy release rate was determined for different loading levels.

The behavior of QI laminates is almost elastic brittle and it's characterized by rapid crack extension until brittle failure. However, the material exhibits a stable crack growth before crack initiation. Thus, it is important to consider the gradual propagation of the crack in the model. Figure 92 represents a comparison between numerical and experimental evolution of the strain energy release rate according to the applied load by considering or not an artificial propagation. For *a/W=0.2*, the numerical results appear satisfactory by considering the artificial propagation. Whereas, for *a/W=0.3*, there is divergence between experimental and numerical results. Similarly for J-R curves in the case of QI laminates.

For AP laminates, a crack tip blunting is observed before reaching the critical strain energy release rate without important crack propagation mainly for small ratios. That's why, only crack opening was taking into account. Figure 93 represents the evolution of the strain energy release rate according to the applied load before the critical load. For *a/W=0.3*, the numerical result seems to be in accordance with the experimental result. However, a divergence is observed in the case of *a/W=0.2*. It's normal to find disparities between experimental and numerical results for AP and QI laminates. In fact, the model doesn't take account of damage at micro-meso scale. In addition, against the high instability of the crack, it appears essential to use an automatic remesher which takes into account the material state at each time step and the direction of the crack propagation. Finally, G_θ method operates a global energy calculation and cannot give an approximation of the strain energy release rate in mode II as AP laminates are characterized by a mixed failure mode.

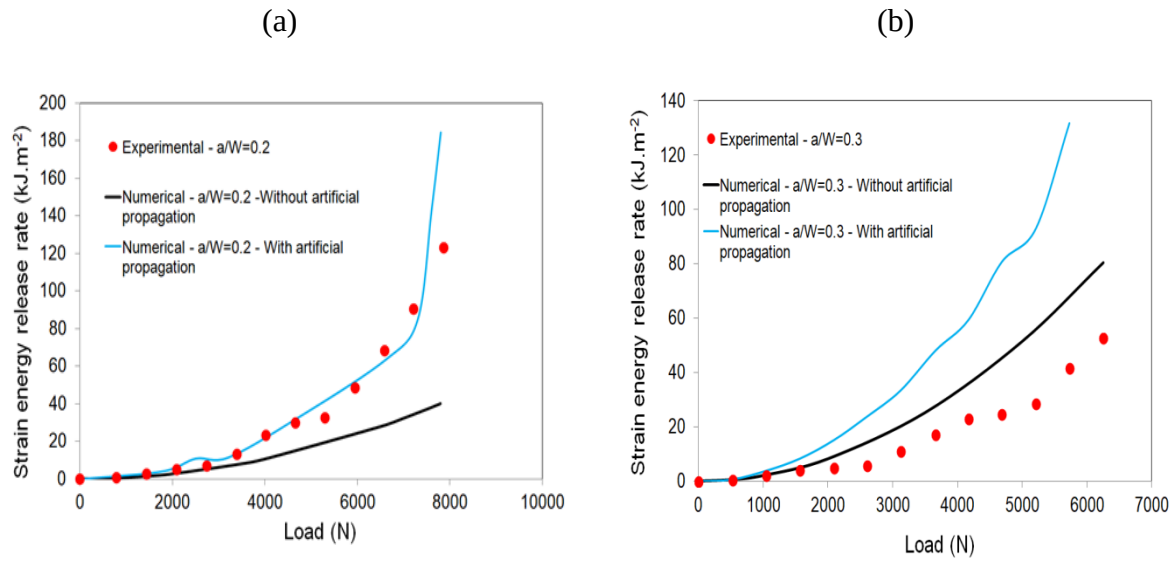

Figure 92. *Comparison between numerical and experimental strain energy release rate according to the applied load for QI laminates: (a) a/W=0.2 and (b) a/W=0.3.*

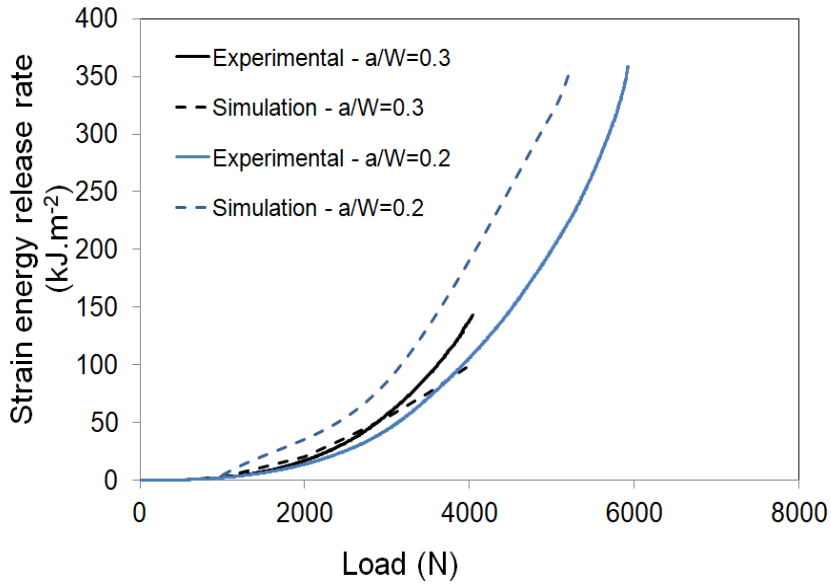

Figure 93. *Comparison between numerical and experimental evolution of the strain energy release rate according to the applied load for AP laminates for a/W=0.2 and 0.3.*

(a) (b)

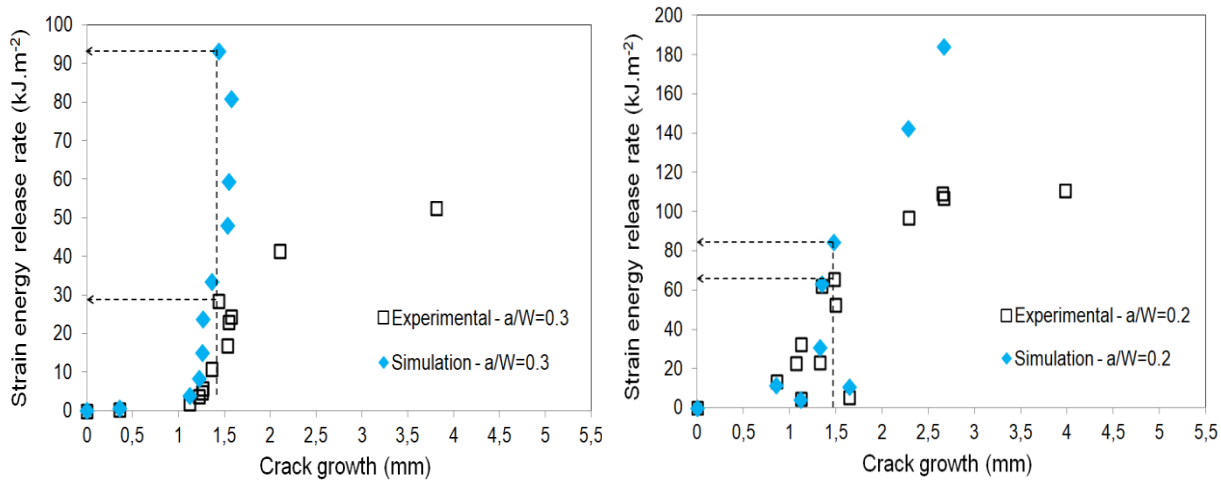

Figure 94. *Comparison between numerical and experimental J-R curves for QI laminates: (a) a/W=0.3 and (b) a/W=0.2.*

III.7 Conclusion

The ultimate goal of the research initiated in this chapter is to practice the G_θ-integral method, that's to say in the present case, to apply G_θ-integral in the case of orthotropic materials with high ductile behavior at high temperature and then, having an approximation of the strain energy release rate before crack initiation where the propagation can be considered as stable.

Firstly, a literature review of numerical methods for determining the strain energy release rate was presented. The high ductile behavior of TP based laminates at high temperature was taken into account using a time dependent model. Then, a mesh optimization was carried out in order to obtain accurate mechanical fields in the vicinity of the crack tip. A radiant mesh was selected to compute the strain energy release rate using G_θ method. Strain energy release rate according to both applied load and crack growth was obtained for AP and QI laminates having *a/W=0.2* and 0.3. Because of different phenomena which have not been taken into account in the model, such as damage and crack instability, some divergences between experimental and numerical results were obtained. However nevertheless the results seem to be promising and encouraging as it's a question of the first study that aims to determine numerically the strain energy release rate in 3D for composite orthotropic materials characterized by a visco-elasto-plastic behavior at high temperature.

Chapter IV. Application to the fracture of composite laminates with circular holes

Chapter IV outline

IV.1 Introduction

The design of composites materials for structural applications is very challenging, and that is why many models have been developed over the past 40 years available to predict the notched strength of Polymer Matrix Composites. Most of these models have been applied to quasi-isotropic laminates with central circular hole subjected to tensile loadings at room temperature when the contribution of matrix behavior to damage mechanisms is not prominent.

The purpose of this chapter is to predict the notched strength of C/PPS QI laminates at high temperature using a simple physically-based model derived from fracture mechanics criteria. First of all, a bibliographic review of some models used to predict the strength in notched polymer-based composites. Then, the critical damage growth model was applied. The following discussion is based on **[Vieille et al., 2016c]**.

IV.2 About the prediction of strength in notched polymer-based composites

When it comes to design composites materials for structural applications (e.g. perforated plates), many models have been developed to predict the notched strength of TS-based composite laminates [Awerbuch et al., 1985] [Tan et al., 1994], though they can be applied only to structures subjected to tensile loadings. More specifically, extensive research has been performed on the fracture behavior and toughness of composite systems containing holes or cracks. It is not question here to give a comprehensive review on the models commonly used for predicting the notched strength of composite laminates (the interested reader can refer to [Awerbuch et al., 1985]), but rather to consider a few common fracture models based on semi-empirical approaches which are operationally simple to implement. The well-known Point Stress Criterion developed by [Whitney et al., 1974] [Nuismer et al., 1975] has already been successfully adapted in the case of woven-ply epoxy composites [Naik et al., 1992] [Kim et al., 1995]. In the early seventies, in their equivalent flaw model, Waddoups et al. assumed the existence of intense energy (inherent flaw) regions whose size c is modelled as a through-crack of constant length [Waddoups et al., 1971], developing at the edges of the hole in a direction transverse to the loading direction (see Figure 95). For isotropic and homogeneous materials, the problem of symmetrical cracks emanating from a circular hole

has been solved by [Bowie, 1956]. Following an approach similar to the Waddoups-Eisenmann-Kaminski model, [Belmonte et al., 2004] proposed a Critical Damage Growth (CDG) model, which is derived from an effective crack growth model, for evaluating the residual strength of composite laminates with circular holes [Afaghi-Khatibi et al., 1996]. This model requires only the unnotched strength and the fracture toughness of the laminate as input parameters. In addition to its simplicity, this model represents the translaminar (fiber breaking and transverse matrix cracking) failure modes of fibers reinforced composites to account for the underlying physical phenomena [Belmonte et al., 2004]. In the case of quasi-isotropic laminates characterized by a translaminar failure mode [Kawai et al., 1996], the question is therefore to know whether this CDG model can be applied to carbon fibers thermoplastic (PPS) composites at temperatures higher than glass transition temperature (T_g).

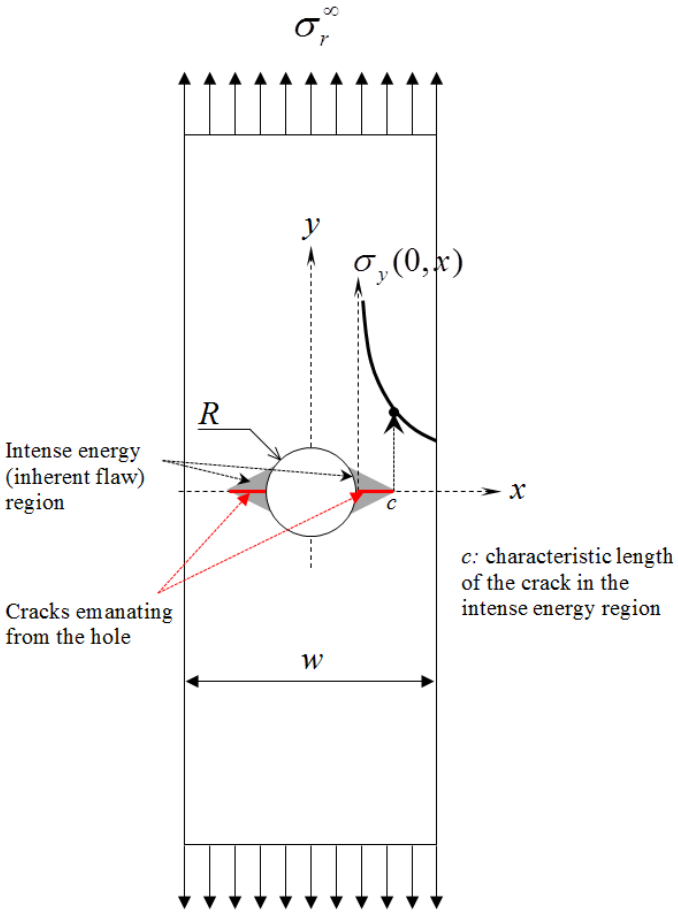

Figure 95. *Cracks emanating from the hole in laminates experiencing translaminar failure mode*

IV.3 Materials and experimental set-up

IV.3.1 Materials

In this chapter, the studied material is a quasi-isotropic C/PPS laminates. The central circular hole (CCH) specimens have different ratio d/w (ranging from 0.1 to 0.4) of the hole diameter over the specimen width. Single-Edge Notch (SEN) specimens have different ratio a/w (ranging from 0.1 to 0.6) of the initial crack length over the specimen width. The machining of the central circular holes may have a significant influence on potential damages near the hole. Using a twist drill can cause several types of defect in fiber-reinforced polymer-matrix composites [Lachaud et al., 2001]. In the present case, holes were drilled by means of a diamond tool (drill bit), which is known to minimize damage near the hole [Krishnaraj et al., 2013]. The machining of the single-edge notches was done by means of a precision endless diamond wire saw whose radius is 0.085mm. The average thickness (calculated from five measurements each) of consolidated specimens is virtually constant (2.22 ± 0.2mm).

IV.3.2 Methods and experimental set-up

All the tests were performed using a 100kN capacity load cell of a MTS 810 servo-hydraulic testing machine in displacement-controlled mode and with a temperature control system. Tensile loadings were applied to notched specimens at 120°C (see Figure 96): specimens with an central circular hole [Vieille et al., 2011] [Vieille et al., 2012] and SEN specimens [Woo et al., 2007]. The tensile mechanical properties were determined according to the European standards EN 6035. For both notched and unnotched laminates, the longitudinal modulus (E_X) and ultimate strength (σ^u) were calculated from the following definitions:

$$E_X = \frac{\Delta F}{S.\Delta\varepsilon_X} \tag{55}$$

and

$$\sigma^u = \frac{F^u}{S} \tag{56}$$

Where ΔF is the difference in the applied tensile loads at $(\varepsilon_X)_2 = 0.25\%$ and $(\varepsilon_X)_1 = 0.05\%$.

S is the specimen cross section.

$\Delta\varepsilon_X = (\varepsilon_X)_2 - (\varepsilon_X)_1$ is the difference in the longitudinal strains obtained from a blade-extensometer.

F^u is the maximum force borne by the specimen at failure.

The gage length (l_0 = 50mm) of the extensometer is large enough to provide an average strain $\Delta\varepsilon_X$ in the area, including the hole, such that an equivalent longitudinal stiffness can be measured. The mechanical properties were averaged from tests conducted on three specimens (See Table 11). The mechanical properties of the equivalent orthotropic material have been calculated from the Classical Laminates Theory (see Table 12). Finally, damage mechanisms have been discussed by means of fractographic analyses: macroscopic observations by means of an optical microscope and scanning electron microscope (SEM) observations with a Leo 1530 Gemini Zeiss microscope.

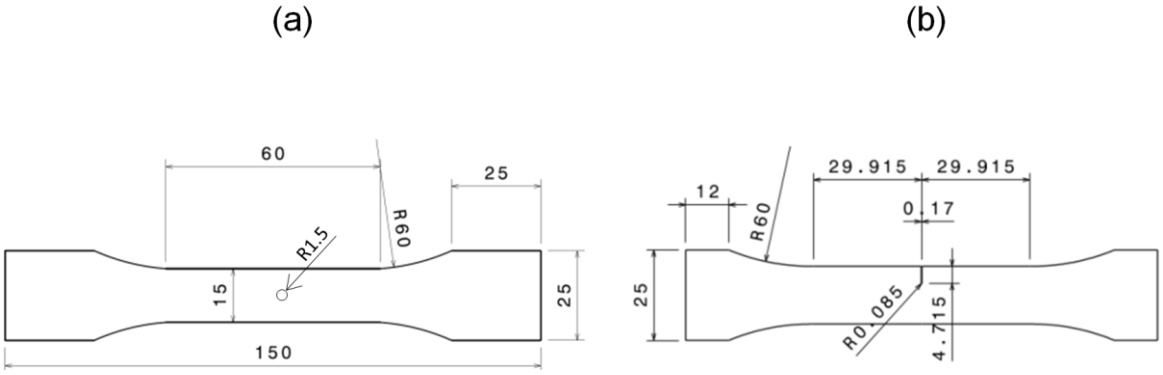

Figure 96. *Geometry of tested specimens: (a) Central Circular Hole – (b) Single-Edge Notch*

Table 11. *Tensile properties of quasi-isotropic C/PPS laminates at 120°C: (a) Unnotched – (b) Centrally notched (d/w=0.2)*

	(a) Unnotched	(b) Notched
E_x (GPa)	40.49 ±0.30	40.58 ±0.35
σ_x^u (MPa)	472 ±6.02	247 ±9.29
ε_x^u (%)	1.28 ±0.04	0.66 ±0.02

Table 12. *Mechanical properties of the equivalent orthotropic material calculated from the Classical Laminates Theory – Quasi-isotropic C/PPS specimens at 120°C*

E_x (GPa)	E_y (GPa)	G_{xy} (GPa)	ν_{xy}
41.31	41.31	12.19	0.3

IV.4 Results and discussion

IV.4.1 Influence of notch length on the mechanical behaviour of quasi-isotropic laminates

As seen in chapter 2, the tested notched specimens are characterized by an elastic-brittle response (see Figure 97 and Figure 98). With respect to unnotched specimens, it appears that the residual tensile strength of CCH and SEN specimens decreases with increasing notch

diameter (Figure 99). Scaling effects are known to significantly influence the tensile strength of notched laminates [Wisnom et al., 2010] [Green et al., 2007], as stress concentration strongly depends on notch characteristic length [Tan, 1994].

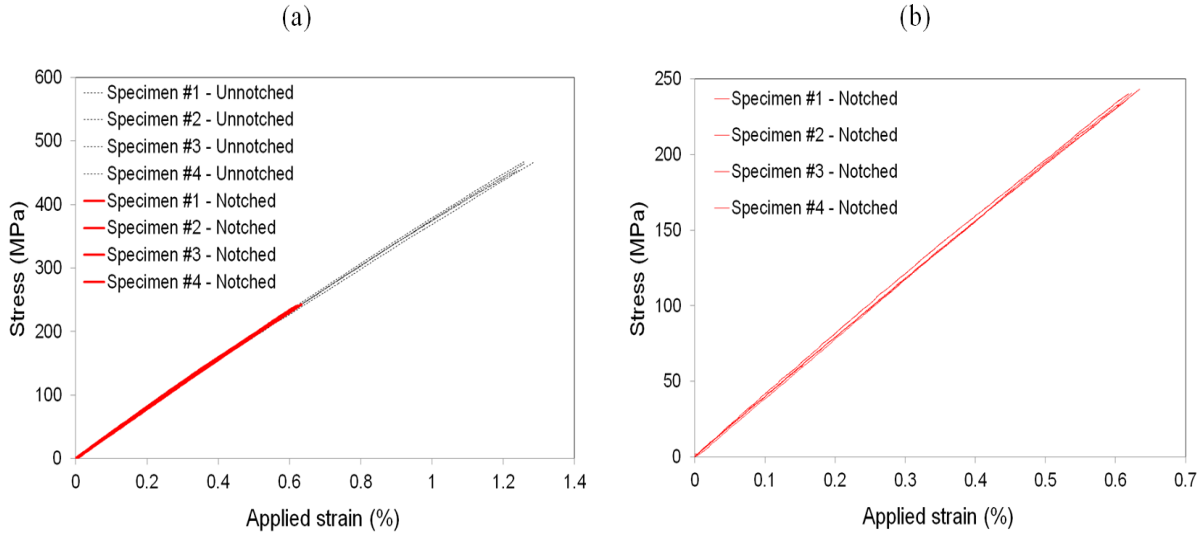

Figure 97. *Tensile responses of CCH quasi-isotropic C/PPS laminates at 120°C: (a) notched (d/w=0.2) vs unnotched laminates – (b) notched (d/w=0.2) laminates*

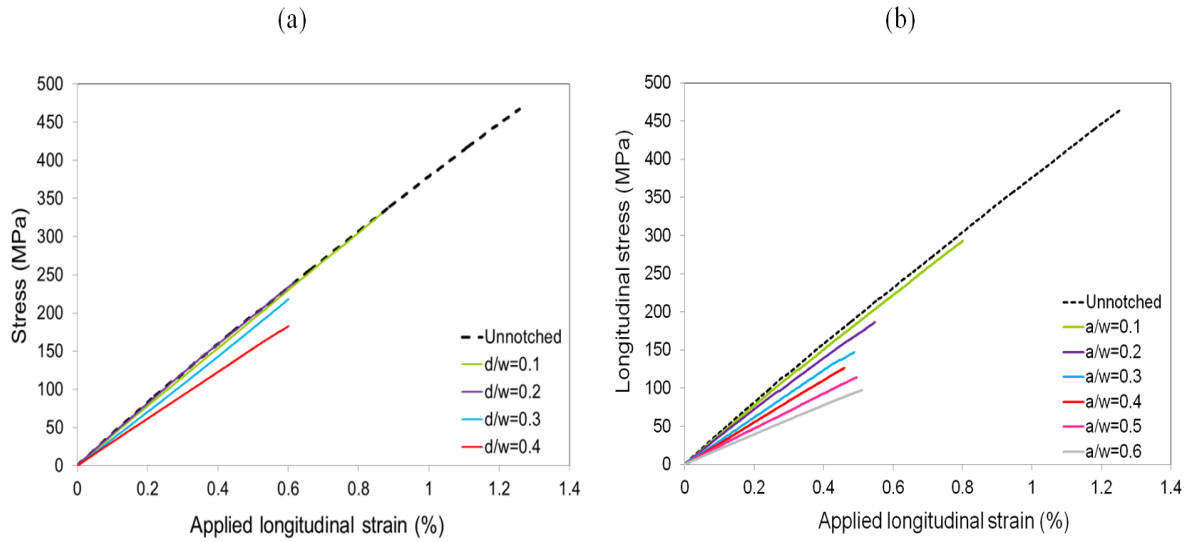

Figure 98. *Influence of the ratio of the initial notch length over the specimen width (d/w and a/W) on the tensile responses of quasi-isotropic C/PPS specimens at 120°C: (a) Central Circular Hole – (b) Single-Edge Notch*

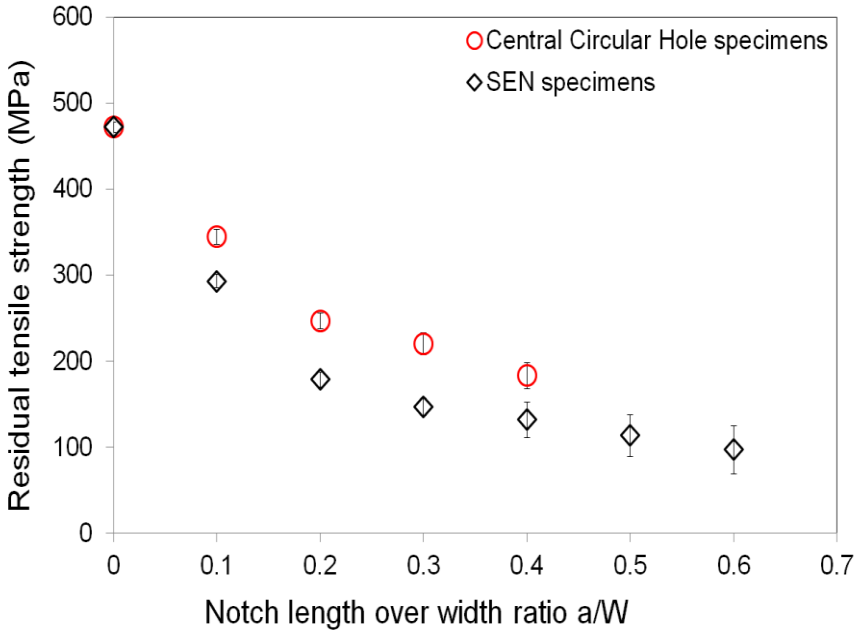

Figure 99. *Comparison of the residual tensile strength of notched quasi-isotropic C/PPS specimens at 120°C as a function of the ratio of the notch length over the specimen width: CCH vs SEN specimens*

It also worth noticing that CCH specimens have higher residual strengths than SEN specimens for a given ratio of the notch length over the specimen width, due to lower stress concentration. Indeed, the concentration factor K_T^∞ at the edge of a hole can be defined in orthotropic materials from the mechanical properties of the equivalent orthotropic material (see Table 12) as follows [Awerbuch et al., 1985] [Tan, 1994] [Whitney et al., 1974] [Nuismer et al., 1975] [Kim et al., 1995]:

$$K_T^\infty = 1 + \sqrt{2\left[\sqrt{\frac{E_y}{E_x}} - \nu_{xy}\right] + \frac{E_y}{G_{xy}}} \tag{57}$$

From the values given in Table 12, the stress concentration factor can be computed in QI laminates with a central hole, such that its value $K_T^\infty = 2.6$ does not depend on the hole diameter in infinite plates. The stress concentration factor can therefore be compared to the one obtained SEN isotropic specimens (see Figure 100).

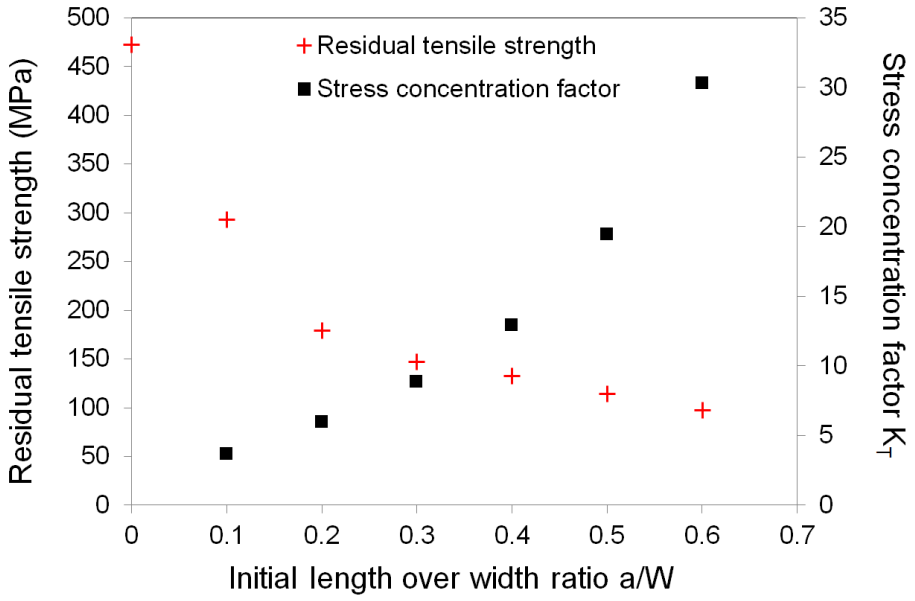

Figure 100. *Changes in the residual tensile strength of SEN specimens and the stress concentration factor K_T as a function of the ratio a/W of the initial crack length over the specimen width for quasi-isotropic C/PPS laminates at 120°C*

The stress concentration factor at the crack tip gradually increases as the ratio a/w increases, and not surprisingly, the residual tensile strength decreases at the same time (see Figure 100). Even for CCH specimens, the elastic-brittle mechanical response primarily results from the transverse matrix cracking and fiber breakage near the notch tip (see Figure 101). The damage mechanisms ruling the behavior of C/PPS laminates at $T > T_g$ have been investigated in a previous work [Vieille et al., 2011]. One may simply underline that cracks initiate at the edge of the hole and develop from the hole in the transverse direction.

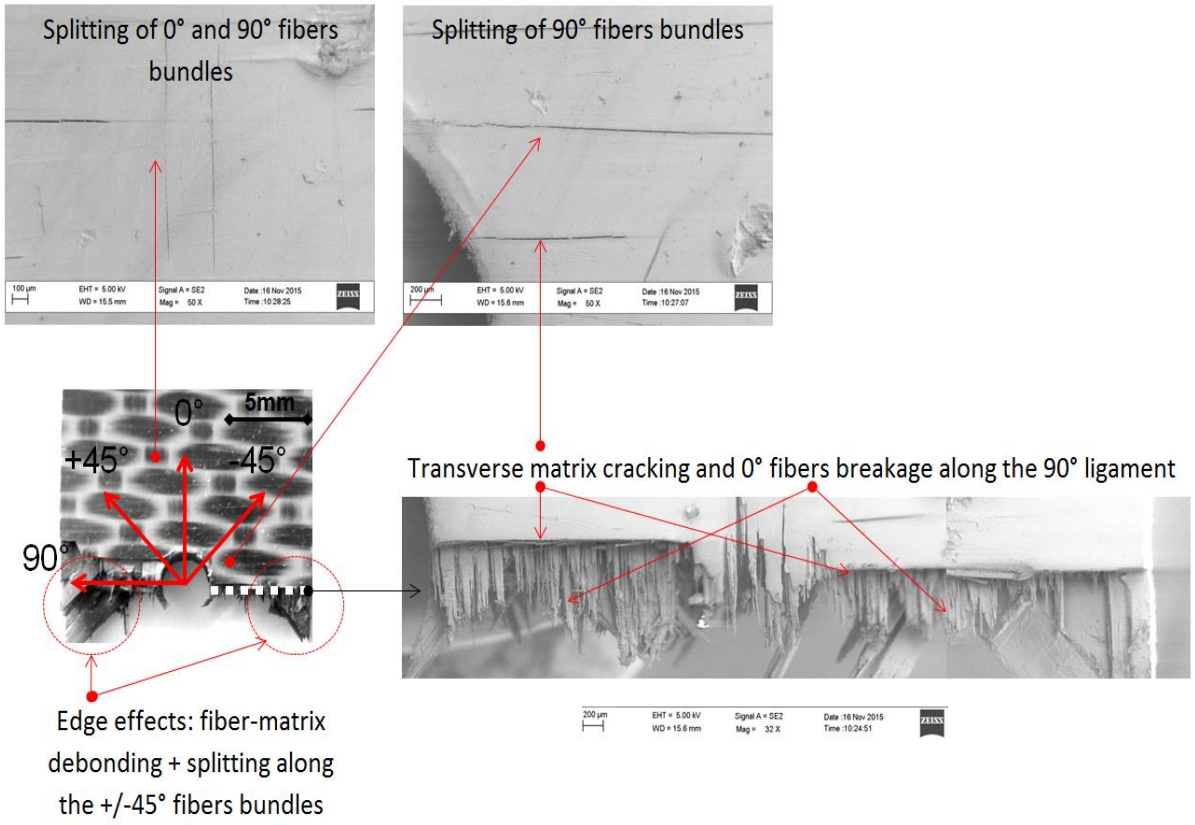

Figure 101. *Macroscopic and SEM observations of fracture surface for CCH quasi-isotropic C/PPS specimens subjected to tensile loadings at 120°C*

IV.4.2 Modelling

IV.4.2.1 Model principal

A simple physically-based model, known as Critical Damage Growth model, derived from a fracture mechanics criterion has been applied to quasi-isotropic laminates to predict the notched strength of carbon fibers woven-ply reinforced PPS laminates under high temperature conditions [Belmonte et al., 2004]. The CDG model proposed by Belmonte et al. is based upon the stable growth and subsequent catastrophic failure of a damage zone at the edge of CCH specimens. This model is interesting for many reasons: the failure criterion is based on LEFM principles and its parameters are physically meaningful. It is based on two competing mechanisms, which give both a prediction of the notched strength (remote applied stress), and the corresponding critical damage zone size c_0 (obtained from Average Stress Criterion). The average stress criterion (ASC) considers that the average stress over a characteristic length c_0 can be calculated from the average notch strength for a particular notch size [Tan, 1994]. This criterion assumes that failure occurs when the average stress, over a distance c_0, away from

the notch is equal or greater than the strength of the unnotched laminate. Furthermore, the characteristic distance c_0 is the same for a given reinforcement architecture and stacking-sequence [Whitney et al., 1974] [Nuismer et al., 1975]. For each laminate an average ASC characteristic distance was calculated for the 16 mm wide coupons; these average characteristic distance was then combined to the critical damage growth model to predict the notched strengths of quasi-isotropic C/PPS laminates at $T > T_g$. The applied laminate stress σ; required to grow a damage zone or crack to a length c; from the edge of the hole (of radius R) is defined using an average stress argument and is given by:

$$\sigma = \frac{1}{c}\int_{R}^{R+c} \sigma_y . Y_1 \, dx \tag{58}$$

σ_y is the longitudinal strength adjacent to the notch edge, and Y_1 is a FWC factor. In the case of orthotropic specimens with a finite width w containing a central circular hole with a diameter d, [Tan, 1994] has proposed the following approximate expressions of the FWC factor Y_1:

$$\frac{1}{Y_1} = \frac{3(1-d/w)}{2+(1-d/w)^3} + \frac{(K_T^{\infty}-3)}{2}\left[1-\left(\frac{d}{w}M\right)^2\right]\left(\frac{d}{w}M\right)^6 \tag{59}$$

where the stress concentration factor at the edge of the hole K_T^{∞} is defined in Section IV.4.1, and the coefficient M is obtained from the following equation:

$$M^2 = \frac{\sqrt{1-8\left[\frac{3(1-d/w)}{2+(1-d/w)^3}-1\right]}-1}{2(d/w)^2} \tag{60}$$

In the case of cracks emanating from a circular hole in isotropic materials, the remote stress σ required to observe a catastrophic failure is associated with the material fracture toughness K_C by the following equation [Tada et al., 2000]:

$$K_C = \sigma\sqrt{\pi a}.F_0.Y_2 \tag{61}$$

where F_0 is a correction factor determined by Bowie et al. in the case of isotropic materials for cracks [Bowie, 1956], whose length c is growing from a circular hole (see Figure 95):

$$F_0 = \frac{(3-s)}{2}[1 + 1.243 * (1-s)^3] \quad \text{with} \quad s = \frac{c}{c+R} \tag{62}$$

and the FWC factor Y_2 is given by:

$$Y_2 = \sqrt{sec\left(\frac{\pi R}{2w}\right) sec\left(\frac{\pi(R+c)}{2w}\right)} \tag{63}$$

IV.4.2.2 Comparison with experiment

In quasi-isotropic materials, the previous approach can be applied, and the CDG model requires only two input parameters (K_C and laminates unnotched strength) to predict the notched strength of quasi-isotropic laminates for various hole diameters. Table 13 presents average experimental values and corresponding standard deviation for the ultimate tensile strength of the CCH specimens, the values of damage zone length obtained from the average stress criterion, the value of the correction factor F_0 , the value of the FWC factor Y_2, and the value of the predicted strength for different hole diameters. It appears that the predicted values are in very good agreement with the experimental data (see Figure 102), as the relative error is low in most cases (see Table 13). It can be noted that the relative error is higher for small hole diameters (e.g. $d/w = 0.1$) probably due to lower stress concentration in the 0° oriented plies, resulting in a mixed failure mode (the edge effects are more noticeable with significant fiber-matrix debonding in the ±45° fibers bundles) rather than a translaminar failure mode. Finally, it can be concluded that the capabilities of the CDG model are very good to predict the notched strength of quasi-isotropic C/PPS laminates.

Table 13. *CDG model notched strength predictions for quasi-isotropic C/PPS specimens at 120°C*

d/w	σ_x^u (MPa)	Damage zone length c_0 (mm)	$F_0(c_0)$	$Y_2(c_0)$	Predicted strength (MPa)	Relative error (%)
0	472±6	0				
0.1	345±8	3.07	1.12	1.04	299.92	-12.98
0.2	247±9	3.95	1.18	1.09	239.19	-3.16
0.3	220±13	3.73	1.28	1.12	219.82	-0.31
0.4	183±15	4.40	1.32	1.20	183.53	0.14

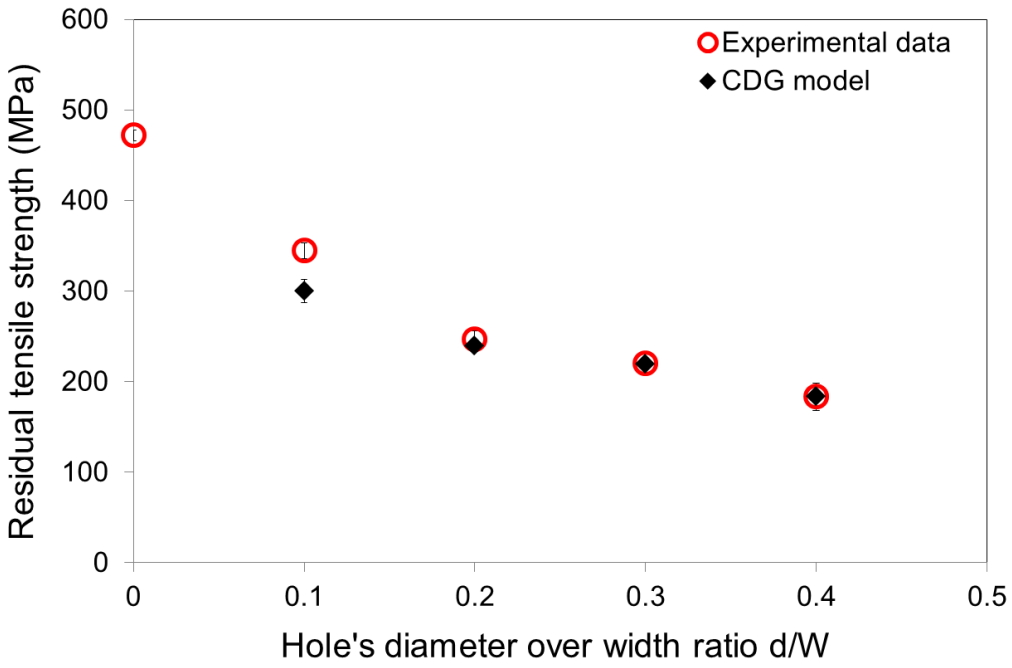

Figure 102. *Prediction of the residual tensile strength as a function of the ratio d/w of the hole diameter over the specimen width for CCH quasi-isotropic C/PPS specimens at 120°C*

IV.5 Conclusion

As an application of the fracture mechanics concepts (introduced in chapter 2) to thermoplastic-based composites, this chapter was aimed at studying the capability of a simple physically-based model, derived from fracture mechanics, to predict the notched strength of TP-based composites at temperature higher than their transition temperature when matrix ductility and toughness are enhanced. To this aim, the Critical Damage Growth Model was used to predict the notched strength of quasi-isotropic PPS-based laminates at high temperature. The CDG model proved to be well adapted to study the translaminar failure and accurately determine the notched strength of C/PPS laminates at high temperature.

Conclusions and future work

Recently, researchers have been increasingly interested in investigating the behavior of thermoplastic-based composites for aeronautical applications. When it comes to their fracture behavior at high temperature applications, there are lots of questions that should be asked and researchers' knowledge still requires further investigations. In this thesis, we focused on the investigation of fracture behavior of woven-ply thermoplastic based composites at temperature higher than their transition temperature when matrix ductility and toughness are enhanced.

This study proposed a literature review on composite materials and their mechanical behavior as well as some important concepts about fracture mechanics in heterogeneous (brittle or ductile) materials.

In chapter II, an experimental investigation of the fracture behavior of both QI and AP laminates has been carried out. For QI laminates, which are characterized by an elastic brittle response at high temperature, the results show that Acoustic Emission, Crack Tip Opening Displacement and cracking gage methods are efficient for predicting the strain energy release rate corresponding to crack initiation and the compliance method proved its capability to estimate the strain energy release rate corresponding to crack propagation for SEN specimens at high temperature. The AE showed to be particularly relevant as it allows to detect the crack onset at microscopic scale but also to quantify the critical strain energy release rate. In addition, the correlation between damage evolution given by the AE at microscopic scale and a macroscopic cumulated damage variable shows the ability of the two approaches to quantify the damage degree and identify a critical threshold for damage initiation.

AP laminates are characterized by a high ductile behavior at high temperature. To study their facture behavior, the J-integral was calculated using compliance and load separation methods. These methods proved to be able to compute J-R curves of highly ductile composite systems at $T > T_g$ for different initial crack length over specimen width ratios. Furthermore, it was observed that J_c increases as the initial crack length increases suggesting that the strain energy release rate depends on geometry and it's not a material property.

The influence of matrix ductility on the thermomechanical behavior of SEN structures was evaluated considering QI laminates (fiber-dominated behavior) or AP laminates (matrix-dominated behavior). It is determined by the combination of loading (orientation of initial notch), location of defect and material heterogeneity (presence of matrix-rich regions at the crimp area in woven-ply laminates. Regardless of the loading mode (opening or mixed-mode), the translaminar failure direction is oriented at 45° along the warp direction in AP laminates, and is transverse in QI laminates. The total strain energy release rate resulting from translaminar failure is significantly higher in structures experiencing mixed-mode failure, with in AP and QI laminates respectively and it's 6 times higher in AP laminates than in QI laminates suggesting that the plastic deformation in AP laminates is instrumental in dissipating a great portion of mechanical energy.

From the numerical standpoint, a brief background about numerical methods used for determining the strain energy release rate was presented. A time dependent model was used to account for the highly ductile behavior of TP based laminates at high temperature. Then, a mesh optimization was carried out in order to obtain accurate mechanical fields in the vicinity of the crack tip. A radiant mesh was selected to compute the strain energy release rate using G_θ method. Because of different phenomena which have not been taken into account in the model, such as damage and crack instability, some divergences between experimental and numerical results were obtained. However nevertheless the results seem to be promising and encouraging as it's a question of the first study that aims to determine numerically the strain energy release rate in 3D for composite orthotropic materials characterized by a visco-elasto-plastic behavior at high temperature.

Finally, the last chapter was aimed at studying the capability of a Critical Damage Growth model derived from fracture mechanics to predict the notched strength of QI laminates at high temperature. This model proved to be efficient to investigate the translaminar failure and determine the notch strength of C/PPS laminates at $T > T_g$.

Concerning the experimental aspect, this study proposed to investigate the behavior of C/PPS composite in the presence of a crack at high temperature subjected to quasi-static loading. It could be interesting to address an experimental study to investigate the fracture behavior of woven-ply thermoplastic based composites under fatigue loading and estimate the lifetime of the material in the presence of a crack.

Numerically, the results obtained are highly sensitive to crack stability as, once the crack starts propagating in instable manner, a divergence between numerical and experimental results is observed. To control the stability of the crack, the use of compact tension specimen can be relevant. In fact, the crack growth is inherently stable in compact tension specimens.

In addition, a remeshing technique to model the crack propagation can give more reliable results and allows improving its predictive capability.

For composite laminates, many damage mechanisms can occur such as fiber breakage, matrix cracking or delamination. In order to simulate the crack growth and obtain the J-R curves, damage mechanisms should be taken into account in the model. Moreover, for AP laminates, the crack propagates along 45° oriented fibers. Thus, an adequate radiant mesh should be proposed.

References

[Afaghi-Khatibi el al., 1996] Afaghi-Khatibi, A., Ye, L., and Mai, Y.W. (1996), An effective crack growth model for residual strength evaluation of composite laminates with circular holes, J Compos Mater, 30: 142–63.

[Agarwal el al., 1983] Agarwal B.D., Kumar P., Patro B.S. (1983) The *J*-Integral as a Fracture Criterion for Composite Materials. In: Marshall I.H. (eds) Composite Structures 2. Springer, Dordrecht.

[Aidi el al., 2015] Aidi, B., and Case, S.W. (2015), Experimental and numerical analysis of notched composites under tension loading, Applied Composite Materials, 22(6): 837-855.

[Aidi el al., 2016] Aidi, B., Philen, M.K., and Case, S.W. (2016), Progressive damage assessment of centrally notched composite specimens in fatigue, Composites Part A, 74: 47–59.

[Albouy el al., 2014] Albouy, W., Vieille, B., Taleb, L. (2014), Influence of plasticity and viscous effects on the high-temperature fatigue behaviour of off-axis woven-ply thermoplastic and thermoset laminates, International journal of fatigue, 63: 85-96.

[Albouy, 2013] Albouy, W. (2013), De la contribution de la visco-élasto-plasticité au comportement en fatigue de composites à matrice thermoplastique et thermodurcissable. Phd thesis, Institut National des Sciences Appliquées de Rouen, France.

[Albouy el al., 2014] Albouy, W., and Vieille, B. (2014), Determination of the damage threshold in woven-ply thermoplastic laminates at $T > T_g$: Acoustic emission and microscopic damage analysis, Composites Part B: Engineering, 64: 138-146.

[Albouy el al., 2013] Albouy, W., Vieille, B., and Taleb, L. (2013), Experimental and numerical investigations on the time-dependent behavior of woven-ply PPS thermoplastic laminates at temperatures higher than glass transition temperature, Composites Part A, 49: 165-178.

[Albouy el al., 2014] Albouy, W., Vieille, B., and Taleb, L. (2014), Influence of matrix ductility on the high temperature fatigue behaviour of quasi-isotropic woven-ply thermoplastic and thermoset laminates, Composite part A, 67: 22-36.

[Al-Haik el al., 2006] Al-Haik, M. S., Hussaini, M. Y., and Garmestani, H. (2006), Prediction of nonlinear viscoelastic behavior of polymeric composites using an artificial neural network, International Journal of Plasticity, 22(7): 1367-1392.

[Anderson el al., 2015] Anderson, D., Eberhardt, S. (2015), How airplanes fly: A physical description of lift. The Aviation History Online Museum.

[Apolinario Testoni, 2015] Apolinario Testoni, G. (2015), In situ long-term durability analysis of biocomposites in the marine environment. PhD thesis, Ecole Nationale Supérieure des Mines de Paris.

[Awerbuch el al., 1985] Awerbuch, J., and Madhukar, M.S. (1985), Notched strength of composite laminates: Predictions and experiments - A review, J Reinf Plast Comp, 4: 3-159.

[Baker el al., 2015] Baker, C., Morscher, G.N., Pujar, V.V., and Lemansk, J.R. (2015), Transverse cracking in carbon fiber reinforced polymer composites: Modal acoustic emission and peak frequency analysis, Composites Science and Technology, 116: 26-32.

[Baker el al., 2015] Baker, C., Morscher, G.N., Pujar, V.V., and Lemanski, J.R. (2015), Transverse cracking in carbon fiber reinforced polymer composites: Modal acoustic emission and peak frequency analysis, Composites Science and Technology, 116: 26-32.

[Begley el al., 1972] Begley, J.A and Landes, J.D. (1972), The J-integral as a fracture criterion. Fracture Toughness, Proceedings of the 1971 National Symposium on Fracture Mechanics, Part Ii.ASTMSTP 514, American Society for Testing and Materials, Philadelphia, PA, 1–20.

[Belmonte el al., 2004] Belmonte, H.M., Ogin, S.L., Smith, P.A., and Lewin, R. (2004), A physically-based model for the notched strength of woven quasi-isotropic CFRP laminates, Composites Part A, 35(7–8): 763-778.

[Ben Ammar el al., 2014] Ben Ammar, I., Karra, C., El Mahi, A., El Guerjouma, R., and Haddar, M. (2014), Mechanical behavior and acoustic emission technique for detecting damage in sandwich structures, Applied Acoustics, 86: 106-117.

[Bernal el al., 1995] Bernal, C.R., Cassanelli, A.N., and Frontini, P.M. (1995), A Simple Method for J-R Curve determination in ABS Polymers, Polymer Testing, 14: 85-96.

[Bernal el al., 1996] Bernal, C.R., Montemartini, P.E., and Frontini, P.M. (1996), The Use of Load Separation Criterion and Normalization Method in Ductile Fracture Characterization of Thermoplastic Polymers, Journal of Polymer Science: Part B Polymer Physics, 34: 1869-1880.

[Berthelot, 2005] Berthelot, J.M., (2005), Matériaux Composites - Comportement mécanique et analyse des structures, 4ème édition, Editions Tec&Doc, Lavoisier, Paris, 645p.

[Boccardi el al., 2016] Boccardi, S., Meola, C., Carlomagno, G.M., Sorrentino, L., Simeoli, G., and Russo, P. (2016), Effects of interface strength gradation on impact damage mechanisms in polypropylene/woven glass fabric composites, Composites Part B, 90: 179-187.

[Bohse, 2000] Bohse, J. (2000), Acoustic emission characteristics of micro-failure processes in polymer blends and composites, Composites Science and Technology, 60: 1213-1226.

[Boisot el al., 2011] Boisot, G., Laiarinandrasana, L., Besson, J., Fond, C., and Hochstetter, G. (2011), Experimental investigations and modeling of volume change inducedby void growth in polyamide, Int. J. Sol. Struct., 48(19): 2642-2654.

[Bonnet el al., 2004] Bonnet, B., Thionnet, A., Carrier, P., and Renard, J. (2004), Matériaux composites soumis à de grandes vitesses de sollicitation. Analyse expérimentale et modélisation, Revue des composites et des matériaux avancés, 14(1): 89-106.

[Boubakar el al., 2003] Boubakar, M.L., Vang, L., Trivaudey, F., and Perreux, D. (2003), A meso-macro finite element modelling of laminate structures: part II: time-dependent behaviour, Composite Structures, 60(3): 275-305.

[Bouchard, 2000] Bouchard, P. O. (2000), Contribution a la modélisation numérique en mécanique de la rupture et structures multi matériaux. Paris, France: Ph.D. thesis, Materials Science and Engineering, Ecole Nationale Supérieure des Mines.

[Bowie, 1956] Bowie, O. L. (1956), Analysis of an infinite plate containing radial cracks originating at the boundary of an internal circular hole, Journal of Mathematical Physics, 25(1): 60-71.

[Brocks, 2012] Brocks, W. (2012), Introduction to Fracture and Damage Mechanics. Five Lectures at Politecnico di Milano. Milano.

[Bui el al., 1985] Bui, H.D., Proix, J.M. (1985), Découplage des modes mixtes de rupture en thermo-élasticité par des intégrales indépendantes du contour. Actes du Troisième Colloque Tendances Actuelles en Calcul de Structure, Bastia, pp 631–643.

[Bussiba el al., 2008] Bussiba, A., Kupiec, M., Ifergane, S., Piat, R., and Böhlke, T. (2008), Damage evolution and fracture events sequence in various composites by acoustic emission technique, Composites Science and Technology, 68(5): 1144-1155.

[Carpinteri el al., 1998] Carpinteri, A., Chiaia, B., and Ferro, G. (1998), Scale dependence of tensile strength of concrete specimens: a multifractal approach. Magazine of Concrete Research, 50: 237-246.

[Cassanelli el al., 2003] Cassanelli, A. N., Cocco, R., and De Vedia, L. A. (2003), Separability property and η_{pl} factor in ASTM A387-Gr22 steel plate. Engineering Fracture Mechanics, 70: 1131–1142.

[Cassanelli el al., 2001] Cassanelli, A.N., Ortiz, H., Cocco, R., and De Vedia, L.A. (2001), A study for η_{pl} factor determination in AA 6061T6 alloy, Engineering Fracture Mechanics, 68: 501-511.

[Castagnet el al., 2007] Castagnet, S., and Deburck, Y. (2007), Relative influence of microstructure and macroscopic triaxiality on cavitation damage in a semi-crystalline polymer, Mat. Sci. Eng. A, 448(1-2): 56-66.

[Chabchoub el al., 2017a] Chabchoub, M. Vieille, B., Beyaoui, M., Taktak, M., Haddar, M., and Taleb, L. (2017), Determination of J-R curves by load separation criterion in highly ductile TP-based composites under high temperature conditions, Composite Structures, https://doi.org/10.1016/j.compstruct.2017.09.060.

[Chabchoub el al., 2017b] Chabchoub, M., Bouscarrat, D., Vieille, B., Gautrelet, C., Beyaoui, M., Taktak, M., Haddar, M., and Taleb, L (2017), Investigations on the mode I translaminar failure and determination of fracture toughness in woven-ply carbon fibers thermoplastic composites at high temperatures, Applied Acoustics, 128: 55-63.

[Chabchoub el al., 2016] Chabchoub, M., Vieille, B., Beyaoui, M., Taktak, M., Haddar, M., and Taleb, L. (2016), Investigations on crack propagation and strain energy release rate in notched woven-ply thermoplastic laminates at high-temperature, Int. Journal of Applied Mechanics, 8(6): 1–19.

[Chen el al., 1977] Chen, F., and Shield, R. (1977), Conservation laws in elasticity of the *J*-integral type, Journal of Applied Mechanics and Physics, 28(1): 1-22.

[Clarke el al., 1979] Clarke, G.A., and Landes, J.D. (1979), Evaluation of the *J*-integral for the compact specimen, J Test Evaluat, 7: 264–9.

[Cravero el al., 2007] Cravero, S., and Ruggieri, C. (2007), Estimation procedure of *J*-resistance curves for SE(T) fracture specimens using unloading compliance, Engineering Fracture Mechanics, 74(17): 2735-2757.

[Daggumati el al., 2011] Daggumati, S., Voet, E., Van Paepegem, W., Degrieck, J., Xu, J., Lomov, S.V., and Verpoest, I. (2011), Local strain in a 5-harness satin weave composite under static tension: Part I Experimental analysis, Composites Science and Technology, 71(8): 1171-1179.

[Davies el al., 2003] Davies, A.J., Qineti, U.K., Curtis, P.T. (2003), Fatigue in aerospace applications. In: Harris B, editor. Fatigue in composites: science and technology of the fatigue response of fiber-reinforced plastics. Chapter 26. Cambridge: Woodhead Publishing Ltd; p. 686-708.

[Davies el al., 1989] Davies, P, Benzeggagh, M.L. (1989), Chapter 3. Interlaminar mode-I fracture testing. In: Friedrich K, editor. Application of fracture mechanics to composite materials. Elsevier Science Publishers B.V.; p. 81-112.

[De Azevedo Soriano, 1999] De Azevedo Soriano, E.D.A. (1999), Notch sensitivity of C/epoxy fabric laminates, Compos Sci Technol, 59: 1143–51.

[Destuynder el al., 1981] Destuynder, P., and Djaoua, M. (1981), Sur une interprétation mathématique de l'intégrale de Rice en théorie de la rupture fragile, Mathematical Methods in the Applied Sciences, 3: 70-87.

[Dickinson el al., 2009] Dickinson, L.P., and Fletcher, N.H. (2009), Acoustic detection of invisible damage in aircraft composite panels, Applied Acoustics, 10(1): 110-119.

[Dowling el al., 1976] Dowling, N.E., and Begley, J.A. (1976), Fatigue crack growth during gross plasticity and the J-integral. ASTM STP, 590: 82-103.

[Dubois el al., 2005] Dubois, F., and Petit, C. (2005), Modelling of the crack growth initiation in viscoelastic media by the G_θ-integral, Engineering Fracture Mechanics, 72: 2821- 2836.

[Dubois el al., 1999] Dubois, F., Chazal, C., and Petit, C. (1999), A finite element analysis of creep-crack growth in viscoelastic media, Mechanics of Time-Dependent Materials, 2: 186-269.

[Durelli , 1981] Durelli A.J. (1981), Stress concentrations. In: Sih GC, editor. Experimental evaluation of stress concentration and intensity factors. Mechanics of Fracture, vol.7. Springer;. p. 1–162.

[Ernst el al., 1979] Ernst, H.A., Paris, P.C., Rossow, M., and Hutchinson, J.W., (1979) Analysis of Load-Displacement Relationship to Determine J-R Curve and Tearing Instability Material Properties, Fracture Mechanics, ASTM STP 677, American Society for Testing and Materials, Philadelphia, pp. 581-599

[Fan el al., 2014] Fan, M., Yi, D.K., and Xiao, Z.M. (2014), Elastic-plastic fracture behavior analysis on a Griffith crack in the cylindrical three-phase composites with generalized Irwin model, International Journal of Applied Mechanics, 06(04): 1450045.

[Fernando, 2003] Fernando, G. (2003), The effect of interleaving on the fatigue behavior of fiber composites. In: Harris Bryan, editor. Fatigue in composites - science and technology of the fatigue response of fiber-reinforced plastics. Woodhead Publishing; p. 189-238.

[Fotouhi el al., 2011] Fotouhi, M., Pashmforoush, F., Ahmadi, M., Refahi, Oskouei, A. (2011), Monitoring the initiation and growth of delamination in composite materials using acoustic emission under quasi-static three-point bending test. J Reinf Plast Compos, 30(17): 1481-93.

[Gabrion el al., 2016] Gabrion, X., Placet, V., Trivaudey, F., and Boubakar, L. (2016), About the thermomechanical behaviour of a carbon fibre reinforced high-temperature thermoplastic composite, Composites Part B, 95: 386-394.

[Gao el al., 1999] Gao, F., Boniface, L., Ogin, S.L., Smith, P.A., and Greaves, R.P. (1999), Damage accumulation in woven-fabric CFRP laminates under tensile loading: 2. Modelling the effect of damage on macro-mechanical properties, Composites Science and Technology, 59: 137-145.

[Gao el al., 1999] Gao, F., Boniface, L., Ogin, S.L., Smith, P.A., and Greaves, R.P. (1999), Damage accumulation in woven-fabric CFRP laminates under tensile loading: Part 1, Composites Science and Technology, 59(1): 123-136.

[García el al., 2016] García, I.G., Carter, B.J., Ingraffea, A.R., and Mantič, V. (2016), A numerical study of transverse cracking in cross-ply laminates by 3D finite fracture mechanics, Composites Part B, 95: 475-487.

[Giordano el al., 1998] Giordano, M., Calabro, A., Esposito, C., and D'Amore, A. (1998), An acoustic-emission characterization of the failure modes in polymer-composite materials, Composites Science and Technology, 58: 1923-1928.

[Green el al., 2007] Green, B.G., Wisnom, M.R., and Hallett, S.R. (2007), An experimental investigation into the tensile strength scaling of notched composites, Composites Part A, 38: 867–878.

[Gross el al., 1964] Gross, B., and Srawley, J.E. (1964), Stress intensity factors for Single-Edge-Notch Tension specimens by boundary collocation of a stress function, NASA TN D-2395.

[Hajikhani el al., 2011] Hajikhani, M., Ahmadi, M., Farjpour, M., and Oskouei, A. R. (2011), Strain energy release rate assessment in mode I delamination of foam core sandwich composites by acoustic emission, Journal of Composite Materials, 45(22): 2271–2277.

[Hamdi el al., 2013] Hamdi, S. E., Le Duff, A., Simon, L., and Plan, G. (2013), Acoustic emission pattern recognition approach based on Hilbert–Huang transform for structural health monitoring in polymer-composite materials, Applied Acoustics, 74(5): 746-757.

[Harris el al., 2003] Harris, B. (2003), A historical review of the fatigue behavior of fiber-reinforced plastics. In: Harris Bryan, editor. Fatigue in composites - science and technology of the fatigue response of fiber-reinforced plastics. Woodhead Publishing; p. 3-35.

[Harris el al., 2003] Harris, B. (2003), Fatigue in composites: science and technology of the fatigue response of fiber-reinforced plastics, Cambridge: Woodhead Publishing Ltd.

[Henaff-Gardin el al., 1996] Henaff-Gardin, C., Lafarie-Frenot, ,. M., and Gamby, D. (1996), Doubly periodic matrix cracking in composite laminates Part 1: General in-plane loading, Composite Structures, 36: 113-130.

[Hertzberg el al., 1996] Hertzberg, R.W., Vinci, R.P., Hertzberg, J.L. (1996), Element of fracture mechanics. In: Deformation and fracture mechanics of engineering materials. fifth ed. J. Wiley & Sons.

[Huang el al., 2015] Huang, Z.M., and Xin, L.M. (2015), Stress concentration factor in matrix of a composite subjected to transverse compression, International Journal of Applied Mechanics, 08(03): 1650034.

[Huguet el al., 2002] Huguet, S., Godin, N., Gaertner, R., Salmon, L., and Villard, D. (2002), Use of acoustic emission to identify damage modes in glass fibre reinforced polyester, Composites Science and Technology, 62: 1433-1444.

[Hutchinson, 1968] Hutchinson, J.W. (1968), Plastic stress and strain fields at a crack tip, Journal of the Mechanics and Physics of Solids, 16: 13-31.

[Hutchinson el al.,1979] Hutchinson, J.W., and Paris, P.C. (1979), Stability analysis of *J*-controlled crack growth. ASTM STP, 668, 37-64.

[Ibáñez-Gutiérrez el al., 2017] Ibáñez-Gutiérrez, F.T., and Cicero, S. (2017), Fracture assessment of notched short glass fibre reinforced polyamide 6: An approach from failure assessment diagrams and the theory of critical distances, Composites Part B, 111: 124-133.

[Irwin el al., 1954] Irwin, G.R., and Kies, J.A. (1954), Critical energy rate analysis of fracture strength, Welding J. Res. Suppl., 33: 193-198.

[Ivanov el al., 2017] Ivanov, S.G., Beyens, D., Gorbatikh, L., and Lomov, S.V. (2017), Damage development in woven carbon fibre thermoplastic laminates with PPS and PEEK matrices: A comparative study, Journal of Composite Materials, 51(5): 637-647.

[Jones, 1999] Jones, R.M. (1999), Mechanics of Composite Materials, 2nd Ed., Philadelphia: Taylor and Francis, Inc.

[Kassapoglou el al., 2015] Kassapoglou C. (2015), Modeling the effect of damage in composite structures: simplified approaches. first ed. John Wiley & Sons, Ltd; p. 41-56.

[Kawai el al., 1996] Kawai, M., Morishita, M., Fuzi, K., Sakurai, T., and Kemmochi, K. (1996), Effects of matrix ductility and progressive damage on fatigue strengths of unnotched /notched CF plain woven roving fabric laminates, Comp Part A, 27(6): 493-502.

[Kim el al., 1998] Kim, J.K., Mai, Y.W. (1998), Interface mechanics and fracture toughness theories. In: Kim Jang-Kyo, Mai Yiu-Wing, editors. Engineered interfaces in fiber reinforced composites. Elsevier Science.

[Kim el al., 1991] Kim, J.K., Baillie, C., and Mai, Y.W. (1991), The effect of interfacial coating and temperature on the fracture behaviors of unidirectional KFRP and CFRO, J Mater Sci, 26: 4701-4720.

[Kim el al., 1995] Kim, J.K., Kim, D.S., and Takeda, N. (1995), Notched strength and fracture criterion in fabric composite plates containing a circular hole, J Composite Material, 29: 982-998.

[Kim el al., 1992] Kim, S.J., and Cho, J.Y. (1992), Role of matrix in viscoplastic behavior of thermoplastic composites at elevated temperature, AIAA Am Inst Aeronaut Astronaut Journal, 30(10): 2571-2573.

[Kim el al., 2001] Kim, Y.J., and Budden, P.J. (2001), Plastic η factor solutions of homogeneous and bi-material SE(T) specimens for toughness and creep crack growth testing, Fatigue Fract Engng Mater Struct, 24: 751–760.

[Kirk el al., 1993] Kirk, M.T., and Dodds, R.H. (1993), *J* and CTOD estimation equations for shallow cracks in single edge notched bend specimens, J Test Evaluat, 21: 228–38.

[Krishnaraj el al., 2013] Krishnaraj, V., Zitoune, R., and Davim, J.P. (2013), Drilling of polymer-matrix composites. Dans J. Davim (Éd.), Springer briefs in applied sciences and technology, Manufacturing and surface engineering. Springer-Verlag Berlin and Heidelberg GmbH and Co. KG Publish.

[Kumar el al., 1984] Kumar, V., German, M.D., Shih, C.F. (1981), An engineering approach for elastic-plastic fracture analysis. General Electric Company, Corporate Research and Development; Research project 1237-1, Topical Report.

[Lachaud el al., 2001] Lachaud, F., Piquet, R., Collombet, F., and Surcin, L. (2001), Drilling of composite structures, Composite Structures, 52(3–4): 511-516.

[Ladevèze el al., 1992] Ladevèze, P., and Le Dantec, E. (1992), Damage modeling of the elementary ply for laminated composites, Comp Sc and Tech, 43: 257-267.

[Laffan el al., 2011] Laffan, M.J., Pinho, S.T., Robinson, P., and McMilla, A.J. (2011), Translaminar fracture toughness: The critical notch tip radius of 0° plies in CFRP, Composites Science and Technology, 72.

[Laffan el al., 2012] Laffan, M., Pinho, S., Robinson, P., and McMilla, A. (2012), Translaminar fracture toughness testing of composites. A review, Polymer Testing, 31(3): 481-489.

[Lagace, 1986] Lagace, P.A. (1986), Notch sensitivity of graphite/epoxy fabric laminates, Compos Sci Technol, 26: 95–117.

[Lagattu el al., 2005] Lagattu, F., Lafarie-Frenot, M.C., Lam, T.Q., and Brillaud, J. (2005), Experimental characterisation of overstress accommodation in notched CFRP composite laminates. Composite Structures, 67, 347-357.

[Lauke el al., 1986] Lauke, B., and Pompe, W. (1986), Fracture toughness of short-fibre reinforced thermoplastics, Composites Science and Technology, 26(1): 37-57.

[Lauke el al., 1986] Lauke, B., and Pompe, W. (1986), Fracture toughness of short-fibre reinforced thermoplastics, Composites Science and Technology, 26(1): 37-57.

[Lemaître, 1985] Lemaître, J. (1985), A continuous damage mechanics model for ductile fracture, Journal of Engineering Materials and Technology, 107: 83-89.

[Li el al., 2015] Li, L., Lomov, S.V., and Yan, X. (2015), Correlation of acoustic emission with optically observed damage in a glass/epoxy woven laminate under tensile loading, Composite Structures, 123: 45-53.

[Lin el al., 1976] Lin, K.Y., and Mar, J.W. (1976), Finite Element Analysis of Stress Intensity Factors for Cracks at a Bi-Material Interface, International Journal of Fracture, 2(2): 521-531.

[Liu el al., 2010] Liu, C.J., Nijhof, A.H., and Ernst, L.J. (2010), A new ultimate strength model of notched composite laminates including the effects of matrix, Journal of Composite Materials, 44: 1335–1349.

[Low el al., 2017] Low, M.J. (2017), The failure micromechanics and toughening mechanisms of materials, Materials: 1966-1944.

[Ma el al., 2016] Ma, Y., Yang, Y., Sugahara, T., and Hamada, H. (2016), A study on the failure behavior and mechanical properties of unidirectional fiber reinforced thermosetting and thermoplastic composites, Composites part B, 99: 162-172.

[Montesano el al., 2012] Montesano, J., Selezneva, M., Fawaz, Z., Poon, C., and Behdinan, K. (2012), Elevated temperature off-axis fatigue behavior of an eight-harness satin woven carbon-fiber/bismaleimide laminate, Composites part A, 43(9): 1454-1466.

[Mou el al., 1996] Mou, Y., and Han, R.P. (1996), Damage Evolution in Ductile Materials, International Journal of Damage Mechanics, 5(3): 241-258.

[Moutou Pitti el al., 2010] Moutou Pitti, R., Dubois, F., and Taazount, M. (2010), Finite element analysis and Fracture in viscoelastic materials by Mv integral-Part I: crack initiation. Finite Element Analysis, David Moratal (Ed.), ISBN: 978-953-307-123-7, InTech, Available from: http://www.intechopen.com/books/finite-element-analysis/finite-element-analysis and-fracture-in-viscoelastic-materials-by-m-v-integral.

[Moutou Pitti el al., 2007] Moutou Pitti, R., Dubois, F., Petit, C., and Sauvat, N. (2007), Mixed mode fracture separation in viscoelastic orthotropic media: numerical and analytical approach by the $M_{\theta v}$-integral, International Journal of Fracture, 145(3): 181-19.

[Naik el al., 1992] Naik, N.K., and Shembekar, P.S. (1992), Notched strength of fabric laminates I: prediction, Compos Sci Technol, 44: 1–12.

[Ndiaye el al., 2000] Ndiaye, I., Maslouhi, A., and Denault, J. (2000), Characterization of Interfacial Properties of Composite Materials by Acoustic Emission, Polymer Composites, 21(4): 595-604.

[Nevalainen el al., 1995] Nevalainen, M., and Dodds, R.H. (1995), Numerical investigation of 3-D constraint effect on brittle fracture in SE(B) and C(T) specimens, Int J Fract, 74: 131–61.

[Nguyen el al., 2007] Nguyen, T.H., and Gamby, D. (2007), Effects of nonlinear viscoelastic behaviour and loading rate on transverse cracking in CFRP laminates, Composites Science and Technology, 67: 438–452.

[Noether, 1971] Noether, E. (1971), Invariant variations problem., Transport Theory and Statistical Physics, 1(3): 183-207.

[Nuismer el al., 1975] Nuismer, R.J., and Whitney, J.M. (1975), Uniaxial failure of composite laminates containing stress concentration. ASTM STP, 593, 117-142.

[Osada el al., 2003] Osada, T., Nakai, A., and Hamada, H. (2003), Initial fracture behavior of satin woven fabric composites, Composite Structures, 61(4): 333-339.

[Oskouei el al., 2010] Oskouei, A. R., and Ahmadi, M. (2010), Acoustic Emission Characteristics of Mode I Delamination in Glass/Polyester Composites, Journal of Thermoplastic Composite Materials, 44(7): 793-807.

[Oskouei el al., 2012] Oskouei, A.R., Zucchelli, A., Ahmadi, M., Minak, G. (2012), Using acoustic emission to evaluate fracture toughness energy release rate (G_{I}) at mode I delamination of composite materials. In: Sikorski Dr Wojciech, editor. Acoustic emission. InTech Publisher; p. 151-72.

[Pandita el al., 2001] Pandita, S.D., Huysmans, G., Wevers, M., and Verpoest, I. (2001), Tensile fatigue behaviour, Composites Part, 32(10): 1533-1539.

[Perrot, 2006] Perrot, Y. (2006), Influence des propriétés de la matrice sur le comportement mécanique de. PhD thesis, Université de Bretagne sud.

[Pilkey el al., 2008] Pilkey, W., and Pilkey, D. (2008), Peterson's Stress Concentration Factors, 3d Edition, John wiley and sons, Inc.

[Pinho el al., 2006] Pinho, S.T., Robinson, P., and Iannucci, L. (2006), Fracture toughness of the tensile and compressive fibre failure modes in laminated composites, Composites Sciences and Technology, 66: 2069-2079.

[Poursartip el al., 1989] Poursartip A, Chinatambi N. (1989), Fatigue damage development in notched (02/±45)s laminates, Comp mat : fatigue and fracture. Philadelphia: ASTM STP 1012.

[Pupurs, 2012] Pupurs, A. (2012), Micro-crack Initiation and Propagation in Fiber Reinforced Composites. Lulea, Sweden: Ph.D. thesis, Department of Engineering Sciences and Mathematics, Lulea University of Technology.

[Reifsnider, 1990] Reifsnider, K.L. (1990), Damage and damage mechanics. In: Reifsnider KL, editor. Fatigue of composite materials. Elsevier Science Publishers B.V.; p. 11-78.

[Rice, 1968] Rice, J.R. (1968), A path independent integral and the approximate analysis of strain concentration by notches and cracks, Journal of Applied Mechanics, 35: 379-386.

[Rice el al., 1968] Rice, J.R., and Rosengren, G. F. (1968), Plane strain deformation near a crack tip in a power-law hardening material, Journal of the Mechanics and Physics of Solids, 16: 1-12.

[Rice el al., 1973] Rice, J.R., Paris, P.C., and Merkle, J.G. (1973), Some further results of *J*-integral analysis and estimates. Progress in flaws growth and fracture toughness testing, ASTM STP 536. American Society for Testing and Materials: 231–45.

[Roos el al., 1986] Roos, E., Eisele, U., and Silcher, H. (1986), A procedure for the experimental assessment of the *J*-integral by means of specimen of different geometries, Int J Press VesPip, 23: 81–93.

[Rotem, 1989] Rotem, A. (1989), Stiffness change of a graphite epoxy laminate under reverse fatigue loading. Philadelphia, PA, USA: ASTM 11.

[Ruggieri, 2012] Ruggieri, C. (2012), Further results in *J* and CTOD estimation procedures for SE(T) fracture specimens - Part I: Homogeneous materials, Engineering Fracture Mechanics, 79: 245–265.

[Sause el al., 2014] Sause, M.G., and Monden, A. (2014), Comparison of predicted onset of failure mechanisms by nonlinear theory and by acoustic emission measurements. In: Proceedings of the 16th European Conference on Composite Materials ECCM16. Sevilla, Spain.

[Sause el al., 2009] Sause, M.G., Haider, F., and Horn, S. (2009), Quantification of metallic coating failure on carbon fiber reinforced plastics using acoustic emission, Surface and Coatings Technology, 204(3): 300-308.

[Schijve, 2001] Schijve, J. (2001), Fatigue of Structures and Materials. Kluwer academic publishers.

[Sendeckyj el al., 1977] Sendeckyj, G.P., Stalnaker, H.D., Kleismit, R.A. (1977), Effect of temperature on fatigue response of surface-notches $[(0/\pm45/0)_s]_3$ graphite/epoxy laminate. In: Reifsnider KL, Lauraitis KN, editors. Fatigue of filamentary materials, ASTM STP 636; p. 73-88.

[Shameli el al., 2016] Shameli, M., and Choupani, N. (2016), Fracture criterion of woven Glass-Epoxy Composite using a new modified mixed-mode loading fixture, International Journal of Applied Mechanics, 08(02): 1650015.

[Sharobeam el al., 1991] Sharobeam, M.H., and Landes, J.D. (1991), The load separation criterion and methodology in ductile fracture mechanics, Int J Fract, 47: 81–104.

[Sharobeam el al., 1993] Sharobeam, M.H., and Landes, J.D. (1993), The load separation and η_{pl} development in precracked specimen test records, Int J Fract, 59: 213–26.

[Sih el al., 1974] Sih, G.C. (1974), Strain-energy-density factor applied to mixed mode crack problems, International Journal of Fracture, 10(3): 305–321.

[Sih, 1981] Sih, G.C. (1981), Failure of composites as predicted by the strain energy density theory. In: Sih G.C., editor. Cracks in composite materials. Mechanics of Fracture, vol. 6. Springer. p. 1–162.

[Sih el al., 1981] Sih, G.C., Chen, E.P. (1981), Cracks in composite materials. In: Sih G.C., editor. Mechanics of fracture, vol. 6. London: Martinus Nijoff Publishers. Sih, G. C., Paris, P.

C., and Irwin, G. R. (1965), On cracks in rectilinearly anisotropic bodies, International Journal of Fracture Mechanics, 1(3): 189-203.

[Simeoli el al., 2014] Simeoli, G., Acierno, D., Meola, C., Sorrentino, L., Iannace, S., and Russo, P. (2014), The role of interface strength on the low velocity impact behaviour of PP/glass fibre laminates, Composites part B, 62: 88-96.

[Sorrentino el al., 2017] Sorrentino, L., Sarasini, F., Tirillo, J., Touchard, F., Chocinski-Arnault, L., Mellier, D., and Russo, P. (2017), Damage tolerance assessment of the interface strength gradation in thermoplastic composites, Composites part B, 113: 111-122.

[Sorrentino el al., 2017] Sorrentino, L., Silva de Vasconcellos, D., D'Auria, M., Sarasini, F., and Tirillo, J. (2017), Effect of temperature on static and low velocity impact properties of thermoplastic composites, Composites Part B, 113: 100-110.

[Sorrentino el al., 2015] Sorrentino, L., Simeoli, G., Iannace, S., and Russo, P. (2015), Mechanical performance optimization through interface strength gradation in PP/glass fibre reinforced composites, Composites part B, 76: 201-208.

[Stinchcomb, 1986] Stinchcomb, W. (1986), Nondestructive evaluation of damage accumulation processes in composite laminates, Composites Science and Technology, 25: 103–118.

[Sumpter, 1987] Sumpter, J.D. (1987), J_C Determination for shallow notch welded bend specimens, Fatigue Fract Engng Mater Struct, 10: 479–93.

[Sumpter el al., 1976] Sumpter, J.D., and Turner, C.E. (1976), Method for laboratory determination of J_C. Cracks and fracture. ASTM STP 601. American Society for Testing and Materials, 3–18.

[Tada el al., 2000] Tada, H., Paris, P.C., and Irwin, G.R. (2000), The stress analysis of cracks handbook. ASME Press. Third Edition.

[Talreja, 2012] Talreja, R. (2012), Damage mechanics of composite materials. Summer School in advanced composite materials. Serres, Greece.

[Tan, 1988] Tan, S.C. (1988), Finite-width correction factors for anisotropic plate containing a central opening, Journal of Composite Materials, 22: 1080-1097.

[Tan, 1994] Tan, S.C. (1994), Stress concentration in laminated composites (éd. Lancaster, Pa.: Technomic Pub. Co.).

[Torres el al., 1986] Torres, M., and Plissonneau, B. (1986), Repair of Helicopter composite structure: Techniques and Substantiations. Teh Repair of Aircraft Structures Involving Composite Materials (pp. 6-1-6-21). Advisory group for aerospace research and development (AGARD) CP402.

[Turner, 1973] Turner, C.E. (1973), Fracture toughness and specific energy: a reanalysis of results. Mater Sci Engng, 11, 275–82.

[Turner, 1980] Turner, C.E. (1980), The ubiquitous η factor. Fracture mechanics: twelfth conference. ASTM STP 700. American Society for Testing and Materials, 314–37.

[Valentini el al., 1999] Valentini, M., Sekov, S.K., Bigoni, D., and Movcha, A.B. (1999), Crack propagation in a Brittle elastic material with defects, Journal of Applied Mechanics, 66(1): 79-86.

[Vieille el al., 2015] Vieille, B., and Albouy, W. (2015), Fatigue damage accumulation in notched woven-ply thermoplastic and thermoset laminates at high-temperature: influence of matrix ductility and fatigue life prediction, International Journal of Fatigue, 80: 1-9.

[Vieille el al., 2016a] Vieille, B., Albouy, W., and Taleb, L. (2016), Viscoelastic viscoplastic model for aeronautical thermoplastic laminates at high temperature: Validation on high stress gradient structures, Composites Part B, 90: 278-286.

[Vieille el al., 2016b] Vieille, B., Albouy, W., Bouscarrat, D., and Taleb, L. (2016), High-temperature fatigue behaviour of notched quasi-isotropic thermoplastic and thermoset laminates: Influence of matrix ductility on damage mechanisms and stress distribution, Composite structures, 153: 311-320.

[Vieille el al., 2011] Vieille, B., Aucher, J., and Taleb, L. (2011), About the influence of temperature and matrix ductility on the behaviour of carbon woven-ply PPS or epoxy laminates: notched and unnotched laminates, Comp Sc and Tech, 71: 998-1007.

[Vieille el al., 2012] Vieille, B., Aucher, J., and Taleb, L. (2012), Overstress accommodation in notched woven-ply thermoplastic laminates at high-temperature: numerical modeling and validation by digital image correlation, Composites Part B, 45(1): 290-302.

[Vieille el al., 2013] Vieille, B., Casado, V. M., and Bouvet, C. (2013), About the impact behavior of woven-ply carbon fiber-reinforced thermoplastic- and thermosetting-composites: a comparative study, Composite structures, 101: 9–21.

[Vieille el al., 2014] Vieille, B., Casado, V. M., and Bouvet, C. (2014), Influence of matrix toughness and ductility on the compression after-impact behavior of woven-ply thermoplastic- and thermosetting composites: a comparative study, Composite Structures, 110: 207–218.

[Vieille el al., 2017a] Vieille, B., Chabchoub, M., and Gautrelet, C. (2017), Influence of matrix ductility and toughness on strain energy release rate and failure behavior of woven-ply reinforced thermoplastic structures at high temperature, Composites Part B, 132: 125-140.

[Vieille el al., 2017b] Vieille, B., Chabchoub, M., Bouscarrat, D., and Gautrelet, C. (2017), A fracture mechanics approach using Acoustic Emission technique to investigate damage evolution in woven-ply thermoplastic structures at temperatures higher than glass transition temperature. Composites Part B, 116: 340-351.

[Vieille el al., 2016c] Vieille, B., Chabchoub, M., Bouscarrat, D., and Keller, C. (2016), Prediction of the notched strength of woven-ply Polyphenylene Sulfide thermoplastic composites at a constant high temperature by a physically-based model, Composite Structures, 153: 529-537.

[Viswanathan, 1993] Viswanathan, R. (1993), Damage mechanisms and life assessment of high temperature components. ASM international.

[Waddoups el al., 1971] Waddoups, M.E., Eisenmann, J.R., and Kaminski, B.E. (1971), Macroscopic fracture mechanics of advance composite material, J Composite Material, 5: 446 -454.

[Wainstein el al., 2003] Wainstein, J., De Vedia, L.A., and Cassanelli, A.N. (2003), A study to estimate crack length using the separability parameter S_{pb} in steels, Engineering Fracture Mechanics, 70: 2489–2496.

[Wainstein el al., 2004] Wainstein, J., Frontini, P. M., and Cassanelli, A. N. (2004), J-R curve determination using the load separation parameter S_{pb} method for ductile polymers, Polymer Testing, 23: 591–598.

[Wells el al., 1985] Wells, J. K., and Beaumont, P. W. (1985), Crack-tip energy absorption processes in fibre composites, Journal of Materials Science, 20(8): 2735–2749.

[Wells el al., 1987] Wells, J. K., and Beaumont, P. W. (1987), The prediction of R-curves and notched tensile strength for composite laminates, Journal of Materials Science, 22(4): 1457–1468.

[Whitney el al., 1974] Whitney, J. M., and Nuismer, R. J. (1974), Stress fracture criteria for laminated composites containing stress concentrations, Journal of Composite Materials, 8(3): 253-265.

[Wisnom el al., 2010] Wisnom, M. R., Hallett, S. R., and Soutis, C. (2010), Scaling effects in notched composites, Journal of Composite Materials, 44: 195–210.

[Woo el al., 2007] Woo, S. C., and Choi, N. S. (2007), Analysis of fracture process in single-edge notched laminated composites based on the high amplitude acoustic emission events, Comp Sci Tech, 67: 1451-1458.

[XUE, 2007] Xue, L. (2007), Damage accumulation and fracture initiation in uncracked ductile solids subject to triaxial loading, International Journal of Solids and Structures, 44(16): 5163-5181.

[Zhu X-K, 2012] Zhu X-K, J.J. (2012), Review of fracture toughness ($G, K, J, CTOD, CTOA$) testing and standardization, Eng Fract Mech, 85: 1–46.

Abstract

The present work was aimed at investigating the fracture mechanics in woven-ply TP (PPS) based laminates at $T > T_{g_{|C/PPS}}$.

A fractography analysis and microscopic observations of fracture surfaces were used to apprehend the damage mechanisms in C/PPS at high temperature (HT) in the presence of a crack. For quasi-isotropic laminates (elastic brittle behavior), several techniques were used to investigate the tenacity at initiation and propagation. In particular, the acoustic emission showed to be particularly relevant as it allows to detect the crack initiation, propagation but also to follow the evolution of the damage. For cross-ply laminates (ductile behavior), an approach based on the calculation of integral J using the load separation method was used. This method showed its capability to provide the J-R curves of composites with very ductile HT behavior for different crack length over specimen width ratios a/W.

Numerically, a linear spectral viscoelastic model and a generalized Norton viscoplastic model were used to account for the time-dependent behavior of C/PPS composite laminates at HT. To precisely evaluate the fracture parameters in TP-based laminates, a study on the mesh type and its refinement was carried out. Finally, based on the selected mesh and using the finite element code Cast3m, the G_θ method was applied in order to test its capability to determine J for different loading levels.

Keywords: Composite materials, Thermoplastic, Carbon/PPS, Temperature, Fracture, Tenacity, Damage, Numerical simulation.

Résumé

Ce travail vise à étudier le comportement à la rupture des composites tissés C/PPS à haute température $T > T_{g_{|C/PPS}}$.

Des analyses fractographiques et des observations microscopiques des faciès de rupture ont permis d'appréhender les mécanismes d'endommagement qui existent dans les stratifiés C/PPS à haute température (HT) en présence de fissure. Pour les stratifiés quasi-isotropes (comportement élastique fragile), plusieurs techniques ont été utilisées afin d'étudier la ténacité à l'initiation et à la propagation. En particulier, l'émission acoustique semble pertinente car elle permet de détecter l'initiation, la propagation de la fissure mais aussi de suivre l'évolution de l'endommagement. Pour les stratifiés à plis croisés (comportement ductile), une approche basée sur le calcul de l'intégrale J en utilisant la méthode de séparation de charge a été utilisée. Cette méthode a montré sa capacité à fournir les courbes J-R des composites à comportement très ductile à HT pour différents rapports longueur d'entaille initial sur la largeur de l'éprouvette a/W.

Numériquement, un modèle viscoélastique spectral linéaire et un modèle viscoplastique de Norton généralisé ont été utilisés pour tenir compte du comportement dépendant du temps des composites C/PPS à HT. Pour évaluer précisément les paramètres de rupture dans les stratifiés à base TP, une étude sur le type de maillage et son raffinement a été réalisée. Enfin, en se basant sur le maillage sélectionné et en utilisant le code de calcul aux éléments finis Cast3m, la méthode G_θ a été appliquée afin de tester sa capacité à déterminer J pour différents niveaux de chargement.

Mots clés : Matériaux composites, Thermoplastique, Carbone/PPS, Température, Rupture, Ténacité, Endommagement, Simulation Eléments Finis.